Modulators of Cellular and Biochemical PRC2 Activity

Modulators of Cellular and Biochemical PRC2 Activity

A dissertation presented

by

Joshiawa Lanair James Paulk

to

The Committee on Higher Degrees in Chemical Biology

in partial fulfillment of the requirements

for the degree of

Doctor of Philosophy

in the subject of

Chemical Biology

Harvard University

Cambridge, Massachusetts

September, 2014

Dissertation Advisor: Professor Stuart Schreiber Joshiawa Lanair James Paulk

Modulators of Cellular and Biochemical PRC2 Activity

Abstract

EZH2 is a SET domain-containing methyltransferase and the catalytic component of the multimeric Polycomb- group (PcG) protein complex, PRC2. When in complex with other PRC2 members (EED, SUZ12, AEBP2, and RBBP4), EZH2 catalyzes methylation of H3K27, a histone modification associated with transcriptional repression and developmental regulation. As several PRC2 components are upregulated or mutated in a variety of human cancers, efforts to discover small-molecule modulators of PRC2 and understand its regulation may yield therapeutic insights. Identification of small-molecule probes with distinct chemotypes, MOAs, and selectivity profiles are not only of great value, but necessary in establishing comprehensive probe sets capable of illuminating the various roles of EZH2 in oncogenesis.

Here we describe efforts to identify and characterize small-molecule modulators of PRC2 and further understand its regulation. Chapter II outlines the expression and purification of 5-component PRC2 (EZH2-EED-SUZ12-AEBP2-RBBP4) and the establishment of biochemical and cellular HTS assays. These assays were used to screen a diverse set of small molecules (>120,000), identifying biochemical PRC2 inhibitors and activators (described in Chapter III). One biochemical PRC2 inhibitor, BRD1835, appeared to inhibit PRC2 activity through a novel artifactual mechanism involving interaction with peptide substrate, leading to apparent peptide-competitive behavior and putative cellular activity (described in Chapter IV). The characterization of

novel biochemical PRC2 activators, BRD3934 and BRD8284, is discussed in Chapter V. Chapter VI describes the use of an HCS assay to identify known bioactive compounds that alter intracellular levels of H3K27me3 through modulating H3K27me3-connected regulatory nodes or by targeting PRC2 directly. These efforts led to the discovery that an antifungal agent, miconazole, is capable of *activating* PRC2 activity in vitro, while a mucolytic agent, bromhexine, selectively ablates cellular H3K27me3 levels through targeting an activity distinct from PRC2. Finally, Chapter VII discusses novel PRC2-connected crosstalk mechanisms identified through screening libraries of uniquely modified histone peptides for their ability to bind or support methylation by PRC2. These studies enhance our understanding of PRC2 regulation by revealing the effects of H3R26 and H3K23me1 modifications on enzymatic activity, implicating their respective methyltransferases in PRC2 regulation.

Table of Contents

Acknowledgements

First and foremost, I'd like to thank my advisor, Stuart Schreiber, for opening my eyes to the world of chemical biology and collaborative science at the Broad Institute. My time with Stuart has been remarkably transformative and has greatly inspired me to focus my future efforts towards impacting human health. Special thanks to my committee members, Andy Phillips, Todd Golub, Brad Bernstein, and Alan Saghatelian, for providing critical scientific guidance and helping me grow as a scientist. I'd like to give thanks to Aly Shamji for being a great guy and an amazing mentor throughout the years; I will never forget 'geeking out' in your office after hours. I'd like to give a HUGE thank you to Joanne Kotz for helping me with thesis writing and encouraging me to push forward during my weakest moments. Thanks to Drew Adams for being a great friend and providing a critical ear when I most needed one. Bridget Wagner, Paul Clemons, Damian Young, Jay Bradner, and Angela Koehler, thanks for being so incredibly kind and supportive during my time at the Broad. Vasanthi Viswanathan, you are one of the sweetest and most intelligent individuals I've ever had the pleasure of interacting with – thank you so much for your friendship over the years. Shrikanta Chattopadhyay, thanks for all the amazing conversations and reminding me of why I chose science as a career. Thanks to Enrique Garcia-Rivera, Hidehisa Iwata, Jason Law, Hiroshi Uehara, Fumika Yakushiji, Max Majireck, Sixun Chen, Bennett Meier, Cynthia Liu, Qiu Wang, Mengfei Zhang, Melissa Kemp, Clementine Feau, Amit Choudhary, Deepika Walpita, and Stefan Kubicek for all the scientific support and for being great people in general. And Amedeo Vetere, thanks for being my partner in the fight to preserve the art of traditional biochemistry and molecular biology.

Of course, I couldn't have done any of this without support from my family and friends. Aunt Pat, Aunt Karen, Uncle Bob, and Uncle Kenny, thanks for all the unconditional love and truly believing in me. To my mom, Antoinette Johnson, and sister, Brittney Paulk, we've been through hard times and made it through each one with love and smiles on our faces – thanks for being so strong and so amazing; I couldn't have made it through graduate school without your love and example. To my close friends, Jen Gautam, Jed Powell, Jake Carlson, Alexandra Cantley, Colin Sargent, Edmund Price, Shambhavi Singh, Sarah Kelley, and Nicole Maloof, thank you so much for putting up with my craziness and providing me the joy and support necessary to persevere. Lastly, I'd like to show my immense gratitude to Cardinal Warde, Shawna Young, and LaTese Briggs for introducing me to the MITES program—teaching those students was one of the most rewarding experiences of my graduate career.

Chapter I

Chromatin, histone methylation, and PRC2

1.1 Chromatin function and regulation

In eukaryotes, DNA exists as part of a nucleoprotein complex known as chromatin, a structure permitting over a meter of DNA to fit within a nucleus of less than 10 microns in diameter (1). The fundamental unit of chromatin, the nucleosome (Figure 1.1), consists of ~147 base pairs of DNA wrapped around an octamer of core histone proteins—an H3/H4 heterotetramer in complex with two H2A/H2B dimers (2)—enabling compaction of DNA into higher-order structures. These structures comprise euchromatin domains, marked by low levels of compaction and greater accessibility, and highly condensed heterochromatin domains (3) Given that underlying DNA must be accessible to various cellular machineries to perform key functions, such as DNA damage repair, replication, transcription, and recombination, regulation of chromatin structure is essential for basic cellular physiology (4,5). Moreover, beyond simply regulating DNA accessibility, nucleosomes act as signaling scaffolds, enabling coordination of activities at specific genomic loci through the recognition and binding of regulatory proteins to post-translational modifications occurring on DNA or histones (6).

To date, over 130 site-specific modifications have been identified on histones, present on both the globular domains and, most frequently, the unstructured N-terminal tails (7). These modifications, including acetylation, ubiquitination, phosphorylation, and methylation, are deposited and removed by distinct chromatin-modifying enzymes (CMEs) that are often recruited to specific genomic loci through interactions with sequence-specific DNA-binding proteins (e.g. transcription factors) (8). In a similar fashion, CME recruitment can be regulated by large intergenic non-coding RNAs (lincRNAs) –a mechanism recently attributed to transcriptional regulation by Xist and

HOTAIR, two lincRNAs found to facilitate heterochromatinization of target genes through interaction with CME complex PRC2 (9,10). In a sequence-independent manner, some CMEs can interact directly with RNA polymerase II and associated elongation factors (e.g. Set2 and Set1 in yeast, respectively) (11,12), while others recognize and bind pre-existing chromatin modifications enriched at specific genetic loci (13).

Genome-wide analysis of histone modifications (i.e. ChIP-seq) has revealed distinct localization of specific chromatin 'marks', connecting them to various regulatory activities at promoters, enhancers, and gene bodies (14). Consequently, many CMEs act as transcriptional co-activators or co-repressors, regulating transcriptional initiation and elongation or facilitating heterochromatin formation at a given gene (15). As described in further detail below, the roles of CMEs in controlling gene expression programs designate them as central players in organismal development, the maintenance of cell state, and disease pathogenesis.

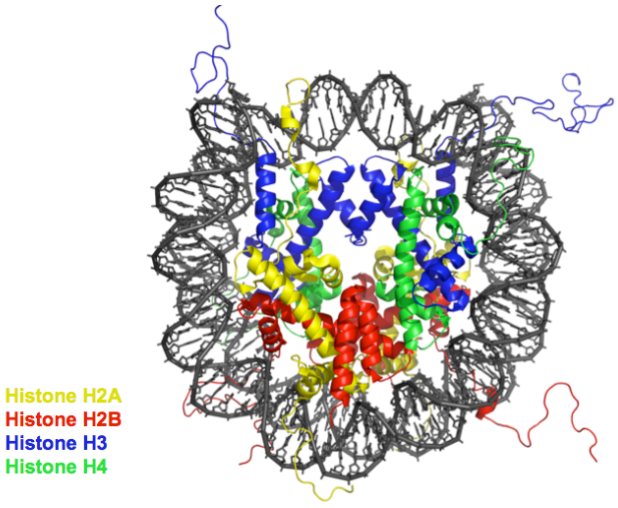

Figure 1.1 Structure of the nucleosome
147 base pairs of DNA wrapped around an octamer of histone proteins (H2A, H2B, H3, and H4). Each histone comprises an alpha-helical globular domain and an unstructured N-terminal tail that extends beyond the core particle.(1KX5: DOI:10.2210/pdb1kx5/pdb)

1.2 Histone methyltransferases (HMTs) and the roles of methylation

Methylation of specific histone residues regulates a diverse set of fundamental processes orchestrated on chromatin, from transcription to heterochromatin formation to DNA repair (14-16). Histone methyltransferases (or more appropriately, protein methyltransferases) are a family of enzymes (>60 in humans (17)) comprising three classes—arginine methyltransferases (PRMTs), SET domain-containing lysine methyltransferases (PKMTs), and non-SET domain-containing lysine methyltransferases, each of which binds and uses the cofactor S-adenosylmethionine (SAM) to transfer a methyl group to lysine or arginine residues on histone and non-histone proteins (18) (Figure 1.2). While lysine residues can be mono-, di-, or trimethylated, arginine methylation—given the chemical nature of the guanidino group—is more complex, with monomethylation occurring on either delta- or omega-N^G atoms and dimethylation occurring symmetrically (omega-N^G, N^G –dimethylarginine) or asymmetrically (omega-N^G-dimethylarginine) (19).

Histone methylation exhibits its effects primarily through the recruitment of effector proteins (termed ‘readers’) whose binding is dependent on the residue modified (e.g. H3R2, H3K4, H4K20, H126, etc.), degree of methylation (i.e. mono-, di-, or trimethylation), as well as the presence or absence of specific neighboring chromatin modifications (13,15,20-22). Known effector proteins contain one or more ‘reader domains’ that selectively bind their target PTMs using—in the case of methyl-lysine readers—an aromatic “cage” within their binding pockets (22). Methyl-lysine reader domains include PHD fingers, WD40 domains, and the Royal Family proteins, including Chromo, Tudor PWWP, and MBT domains (23), all of which have been found in several

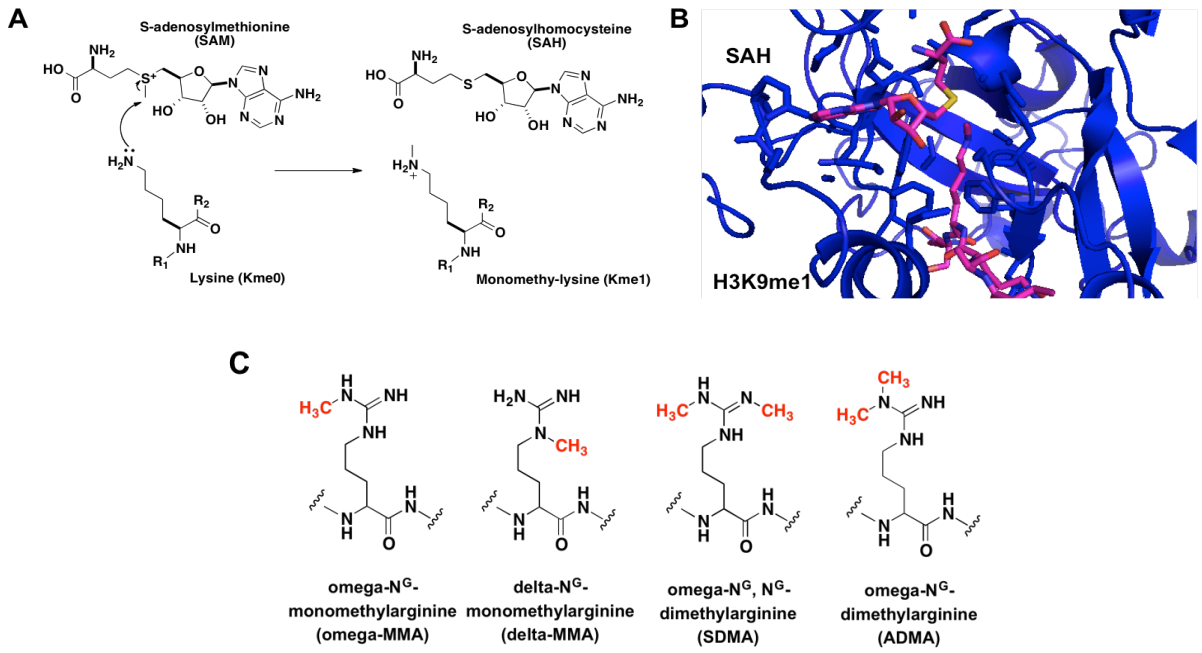

Figure 1.2 Histone methyltransferase mechanism and products
(A) Currently accepted mechanism for processive lysine methylation (18). SAH is released after each cycle of methylation. (B) Crystal structure of EHMT1 in complex with H3K9me1 and SAH (DOI:10.2210/pdb3HNA/pdb). (C) Structures of methylarginine residues.

hundred diverse human proteins to date (24). While a majority of reader proteins regulate transcriptional events, others are involved in maintaining higher-order chromatin structure (e.g. HP1 and L3MBTL1) (25-27), recruiting DNA damage response factors (e.g. MSH-6 and 53BP1) (28,29), or facilitating replication (e.g. LRWD1) (28).

As the roles of histone methylation in transcriptional regulation have been extensively studied, several methyl 'marks' have been broadly linked to activating or repressive transcriptional activities. For instance, H3K4, H3K36, and H3K79 methylation at a given genetic loci typically associates with transcriptional activation, while H3K9, H3K27, and H4K20 methylation often suggests transcriptional repression (15). However, a given mark can mediate several outcomes depending on its context. For example, H3K4me3 was recently found to recruit both transcriptional repressors (Sin3/HDAC corepressor complex via GATAD1) and activators (SAGA and NuRF

complexes), suggesting multiple transcriptional outputs (28,30,31). Similarly, H3K36me3, a mark typically associated with transcriptional activation and RNAP II elongation (32,33), mediates transcriptional silencing through PRC2 recruitment (via PHF19 binding) during ESC differentiation (34,35).

The localization of specific methyl marks corresponds to their overall function—those enriched at transcriptional start sites (TSSs) or distal enhancers typically regulate transcription initiation events, while those occurring on gene bodies often facilitate transcriptional elongation or regulate the general accessibility of various machineries to DNA (32,36-40). For instance, H3K4me3, present at the TSS of several actively transcribed genes, increases the rate of pre-initiation complex (PIC) formation through the recruitment of basal transcription factor TFIID via binding of TAF3—a PHD finger-containing protein (41,42). H379me2, localized throughout gene bodies, is thought to regulate elongation, as the only known H3K79 methyltransferase, hDOT1L, is found in complex with core elongation factors Paf1 (11) and p-TEFb (43). Enhancer chromatin is characteristically enriched in H3K4me1 and H3K27ac, providing a robust signature for genome-wide identification of enhancers across cell types (44). While the specific functional consequences of these marks are still under active investigation, it is speculated that H3K4me1 recruits TIP60/p400 complex (via its H3K4me1 reader domain) to facilitate H2A.Z incorporation at enhancer regions, thus promoting an open chromatin state that enables transcription factor binding (45,46).

As many important and diverse processes are mediated by histone methylation, HMTs—as well as all associated readers and erasers (histone demethlyases)— play central roles in their regulation. For this reason, it is not surprising that aberrant

expression, localization, or activity of HMTs has been linked to a variety of disease states, from neurodevelopmental disorders (47-50) to a large number of cancers (51-55). With this biological liability, however, comes opportunity, as small-molecule modulators of readers, writers, and erasers of these modifications provide a potential route for manipulating cellular states for therapeutic benefit in regenerative medicine (e.g. transdifferentiation, induced pluripotency, etc.) and targeted cancer treatment.

1.3 Polycomb repressive complex 2 (PRC2) and EZH2

EZH2 is a SET domain-containing methyltransferase and the catalytic component of the multimeric Polycomb- group (PcG) protein complex, PRC2 (Figure 1.3). When in complex with other PRC2 members (EED, SUZ12, AEBP2, and RBBP4), EZH2 catalyzes mono- and dimethylation of H3K27, requiring only EED and SUZ12 for basal enzymatic activity (56). To achieve efficient H3K27 trimethylation, PRC2 requires an additional component, PHF1/PCL1, which enables loci specific regulation of H3K27me3 deposition (57,58). Other PCL proteins (MTF2/PCL2 and PHF19/PCL3), as well as JARID2, have been shown to interact with PRC2, facilitating recruitment to target genes and further stimulating activity (35,59-63).

Beyond varying the composition of PRC2, EZH2 activity can be governed by direct phosphorylation (66-69), glycosylation (70), or allosterically regulated through its partner proteins. For example, as a consequence of binding H3K4me3 or histone H3 (within residues 35-42), SUZ12 adopts conformations that inhibit or activate EZH2, respectively (64,71), while WD40 domain-containing protein, EED, can activate PRC2 when bound to known repressive marks— H3K27me3 and, to a lesser degree, H3K9me3 (65,72). These regulatory mechanisms are thought to assist in the spreading

of H3K27me3 and initiation of heterochromatin formation, leading to transcriptional repression of target genes (56). Phosphorylation of EZH2 at T350 by CDK1 promotes PRC2 binding to lincRNAs , Xist and HOTAIR, facilitating recruitment to target loci (66). Conversely, phosphorylation of EZH2 at S21 (AKT) and T487 (CDK1) has been shown to disrupt the PRC2 complex and inhibit H3K27 methyltransferase activity (69,73).

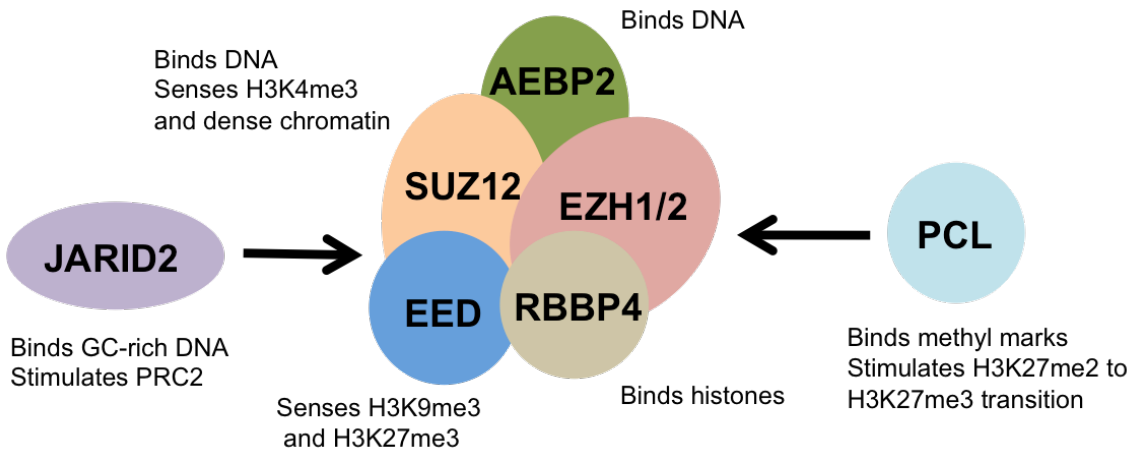

Figure 1.3 Composition of PRC2
PRC2 is a multimeric complex comprising three core components (EZH2, EED, and SUZ12) and two accessory components (AEBP2 and RBBP4) that further stimulate activity (56). JARID2 and PCL proteins are thought to enhance PRC2 activity in vivo and endow trimethylation activity, respectively (57,60). Core components, EED and SUZ12, have been found to regulate PRC2 activity through allosteric regulation involving interactions with chromatin and specific modifications thereof (64,65)

In mammals, there is an EZH2 paralog, EZH1, which harbors a nearly identical SET domain (96% identity) and shares 76% identity with EZH2 overall. EZH1 can form PRC2-type complexes in place of EZH2 (PRC2-EZH1), endowing the complex with H3K27 methyltransferase activity (albeit weaker) (74,75). In fact, PRC2-EZH1 targets a large subset of EZH2-regulated genes (75) and is able to maintain embryonic stem cell pluripotency in EZH2(-/-) ESCs (76), suggesting that EZH1 plays a redundant role. However, EZH1 is reciprocally expressed during development, with some tissues

expressing high levels of EZH2 (low EZH1) and others (e.g. skeletal, kidney, and brain) expressing high levels of EZH1 (low EZH2) (75,77-80). Moreover, PRC2-EZH1 co-localizes with H3K4me3 at transcriptionally active genes in differentiating myocytes, interacting with RNA Pol II complex to promote elongation (81). As these studies revealed distinct genomic localization, EZH1 and EZH2 paralogs may have specific functions depending on the cellular context**.**

Like many HMTs, PRC2 plays an essential role in several biological processes. Through methylation of promoter histones, PRC2 supports development by silencing lineage-specification genes and key developmental regulators (e.g. the HOX gene cluster) (36). H3K27me3 is found at enhancer regions upstream of early developmental genes, further implicating PRC2 in developmental regulation (82). Moreover, EZH2 is required for IgH rearrangement in pre-B cells, a key step in B-cell maturation (80). Since many PcG-regulated genes must be stably repressed through cell division, PRC2 is also thought to contribute to the transmission of repressive marks during cell division, maintaining cell fate (83). Thus, while some methyl marks (e.g. H3K79me2) are lost through cell division—primarily those that regulate housekeeping functions occurring on the level of chromatin—H3K27me3 appears to be truly ‘epigenetic’ in nature, setting EZH2 apart from most methyltransferases.

1.4 The emerging role of PRC2 in cancer

Several PRC2 components are upregulated or mutated in a variety of human cancers. Overexpression of EZH2 has been observed in cancers of the lung, skin, colon, and bladder and thought to contribute to their progression (84). In breast and prostate cancer, EZH2 has emerged as a biomarker for tumor aggressiveness, with

high expression levels correlating with increased proliferation rates and invasiveness (85,86). In follicular lymphoma (FL) and germinal center B-cell-like diffuse large B-cell lymphoma (GCB DLBCL), EZH2 activating mutations, involving substitution of Y641 in the SET domain, have been found in 7% and 22% of cases, respectively (87). These EZH2 mutants, while essentially incapable of methylating unmodified H3K27, are hyperactive on mono- and dimethylated H3K27 compared with the wild-type enzyme, suggesting an oncogenic role (88,89), at least in certain contexts (see below). This notion is further supported by the occurrence of cancer-associated inactivating mutations in UTX (an H3K27me3 demethylase) (90).

Whether EZH2 acts as an oncogenic or a tumor suppressor appears to be context dependent, as several inactivating mutations have been identified in both myeloid disorders (i.e. MDS/MPN; ref. 55) and T-cell acute lymphoblastic leukemia (T-ALL) (91). These mutations are not only limited to EZH2, but can span other PRC2 components, such as SUZ12 and EED, and known positive regulators, such as JARID2 (91,92). Moreover, it has recently been reported that in T-ALL, H3K27 demethylases can function as a tumor suppressor (UTX) or oncogene (JMJD3) in the same disease context (93). This dichotomy of EZH2 (and opposing demethylases) in supporting oncogenesis raises concerns about the potential effects of prolonged use of EZH2 inhibitor therapies; however, it is unknown whether loss of EZH2 HMTase activity is sufficient to support tumorigenesis.

1.5 Small-molecule probes for EZH2 and other HMTs.

In contrast to the large number of distinct histone deacetylases inhibitors, reports of small-molecule modulators of HMTs have only recently emerged (94). G9a and

Su(var)3-9 inhibitors, BIX-01294 (95) and chaetocin (96), were among the first probes to be identified, followed by DZNep, an indirect pan-methyltransferase inhibitor that lowers global histone methylation through the reduction of available SAM levels (97).

As evidence for the roles of HMTs in disease accumulated, so did their potential as promising drug targets, prompting several pharmaceutical companies to initiate probe development efforts (Figure 1.4). Inhibitors of DOT1L, developed by Epizyme, were the first in a wave of highly potent SAM-competitive HMT inhibitors recently reported (98). Shortly following, Epizyme, GSK, and others disclosed small-molecule probes for EZH2 (74,99-102). While immensely useful, these compounds are structurally similar, share the same mechanism of action (competition with the SAM cofactor), and inhibit both the WT and hyperactive mutant forms of EZH2. To date, no direct substrate-competitive or mutant-selective inhibitors of EZH2 have been reported or small-molecule probes of other PRC2 components. However, Orkin and colleagues recently described a stabilized alpha-helical peptide (SAH) capable of inhibiting PRC2 through disruption of EZH2-EED interaction (103).

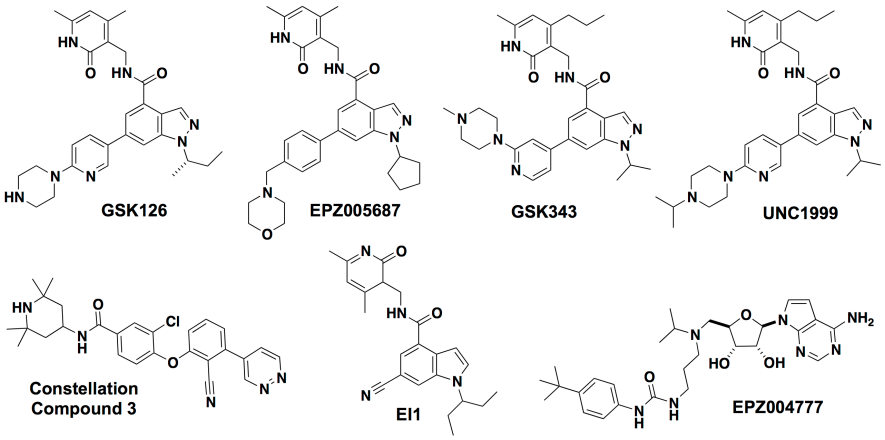

Figure 1.4 Structures of newly discovered HMT inhibitors
GSK (GSK343, GSK126), Epizyme (EPZ005687), Constellation (Cpd 3), Novartis (EI1), and SGC (UNC1999) inhibitors for EZH2 are structurally similar, with the exception of Constellation compound 3. Epizyme's hDOT1L inhibitor (EPZ004777) is also shown above.

The emergence of first-in-class EZH2 inhibitors has enabled evaluation of the target in DLBCL (104), MLL-AF9 leukemia (103), and aggressive rhabdoid sarcomas (105), revealing high therapeutic potential in animals studies. Clinical studies are currently underway, but early observations suggest anti-lymphoma activity of Epizyme's clinical candidate, E7438, in NHL patients (106). Whether this currently dominating EZH2i chemotype presents specific pharmacodynamic (PD) or pharmacokinetic (PK) liabilities, is yet to be determined.

Further studies are needed to gauge the effectiveness of EZH2 inhibitors in cancers dependent on Polycomb-independent EZH2 activity (69,73,107) and to determine whether these compounds increase the likelihood of myeloid disorders (55)—or have other unforeseen side-effects via disruption of cytosolic EZH2 function (108). More importantly, additional studies are needed to investigate the impact of EZH2i in other cancer contexts, given the aforementioned dichotomy of EZH2 and UTX in supporting tumorigenesis (51,93). Furthermore, dependencies on PRC2 functions beyond its methyltransferase activity may require probes that disrupt localization in addition to enzymatic activity (75,81).

1.6 Concluding remarks

Identification of small-molecule probes with distinct chemotypes, MOAs, and selectivity profiles are not only of great value, but necessary in establishing comprehensive probe sets capable of illuminating the various roles of EZH2 in oncogenesis. Towards this aim, we sought to recombinantly express and purify 5-component PRC2 (EZH2-EED-SUZ12-AEBP2-RBBP4), establish biochemical and cellular HTS assays (**Chapter II**), and screen a diverse set of compounds to discover

modulators of PRC2 activity (**Chapter III**). My doctoral thesis describes these efforts as well as the characterization of inhibitors (BRD1835; **Chapter IV**) and activators (BRD3934 and BRD8284; **Chapter V**) of PRC2 biochemical activity identified in our primary HTS campaign. **Chapter VI** describes the use of an HCS assay to identify known bioactive compounds that alter intracellular levels of H3K27me3 through modulating H3K27me3-connected regulatory nodes or by targeting PRC2 directly. This screen ultimately led to the discovery of an antifungal agent, miconazole, capable of *activating* PRC2 activity in vitro, as well as a mucolytic agent, bromhexine, that selectively ablates cellular H3K27me3 levels through targeting an activity distinct from PRC2. Lastly, **Chapter VII** discusses novel PRC2-connected crosstalk mechanisms identified through screening libraries of uniquely modified histone peptides for their ability to bind or support methylation by PRC2.

1.7 References

1. Alberts B, Johnson A, Lewis J, Raff M, Roberts K, Walter P. Chromosomal DNA and Its Packaging in the Chromatin Fiber. Garland Science; 2002.

2. Luger K, Mäder AW, Richmond RK, Sargent DF, Richmond TJ. Crystal structure of the nucleosome core particle at 2.8 A resolution. Nature. 1997 Sep 18;389(6648):251–60.

3. Huisinga KL, Brower-Toland B, Elgin SCR. The contradictory definitions of heterochromatin: transcription and silencing. Chromosoma. Springer-Verlag; 2006 Apr;115(2):110–22.

4. Li G, Reinberg D. Chromatin higher-order structures and gene regulation. Curr Opin Genet Dev. 2011 Apr;21(2):175–86.

5. Lavelle C, Foray N. Chromatin structure and radiation-induced DNA damage: From structural biology to radiobiology. Int J Biochem Cell Biol. 2014 Jan 29;49C:84–97.

6. Schreiber SL, Bernstein BE. Signaling network model of chromatin. Cell. 2002 Dec 13;111(6):771–8.

7. Tan M, Luo H, Lee S, Jin F, Yang JS, Montellier E, et al. Identification of 67 histone marks and histone lysine crotonylation as a new type of histone modification. Cell. 2011 Sep 16;146(6):1016–28.

8. Smith E, Shilatifard A. The Chromatin Signaling Pathway: Diverse Mechanisms of Recruitment of Histone-Modifying Enzymes and Varied Biological Outcomes. Molecular Cell. Elsevier Inc; 2010 Dec 10;40(5):689–701.

9. Zhao J, Sun BK, Erwin JA, Song JJ, Lee JT. Polycomb proteins targeted by a short repeat RNA to the mouse X chromosome. Science. 2008 Oct 31;322(5902):750–6.

10. Rinn JL, Kertesz M, Wang JK, Squazzo SL, Xu X, Brugmann SA, et al. Functional demarcation of active and silent chromatin domains in human HOX loci by noncoding RNAs. Cell. 2007 Jun 29;129(7):1311–23.

11. Krogan NJ, Dover J, Wood A, Schneider J, Heidt J, Boateng MA, et al. The Paf1 complex is required for histone H3 methylation by COMPASS and Dot1p: linking transcriptional elongation to histone methylation. Molecular Cell. 2003 Mar;11(3):721–9.

12. Xiao T, Hall H, Kizer KO, Shibata Y, Hall MC, Borchers CH, et al. Phosphorylation of RNA polymerase II CTD regulates H3 methylation in yeast. Genes & Development. Cold Spring Harbor Lab; 2003 Mar 1;17(5):654–63.

13. Lee J-S, Smith E, Shilatifard A. The language of histone crosstalk. Cell. 2010 Sep 3;142(5):682–5.

14. Bernstein BE, Meissner A, Lander ES. The mammalian epigenome. Cell. 2007 Feb 23;128(4):669–81.

15. Kouzarides T. Chromatin modifications and their function. Cell. 2007 Feb 23;128(4):693–705.

16. Roukos DH. Chromatin: a key player in complex gene regulation and future cancer therapeutics. Epigenomics. 2011 Aug;3(4):395–9.

17. Binda O. On your histone mark, SET, methylate! Epigenetics. 2013 May;8(5):457–63.

18. Smith BC, Denu JM. Chemical mechanisms of histone lysine and arginine modifications. Biochim Biophys Acta. 2009 Jan;1789(1):45–57.

19. Bedford MT, Clarke SG. Protein arginine methylation in mammals: who, what, and why. Molecular Cell. 2009 Jan 16;33(1):1–13.

20. Lan F, Shi Y. Epigenetic regulation: methylation of histone and non-histone proteins. Sci China, C, Life Sci. 2009 Apr;52(4):311–22.

21. Molina-Serrano D, Schiza V, Kirmizis A. Cross-talk among epigenetic modifications: lessons from histone arginine methylation. Biochem Soc Trans. 2013 Jun;41(3):751–9.

22. Yun M, Wu J, Workman JL, Li B. Readers of histone modifications. Cell Res. 2011 Apr;21(4):564–78.

23. Maurer-Stroh S, Dickens NJ, Hughes-Davies L, Kouzarides T, Eisenhaber F, Ponting CP. The Tudor domain “Royal Family”: Tudor, plant Agenet, Chromo, PWWP and MBT domains. Trends Biochem Sci. 2003 Feb;28(2):69–74.

24. Herold JM, Ingerman LA, Gao C, Frye SV. Drug discovery toward antagonists of methyl-lysine binding proteins. Curr Chem Genomics. 2011;5(Suppl 1):51–61.

25. Trojer P, Li G, Sims RJ, Vaquero A, Kalakonda N, Boccuni P, et al. L3MBTL1, a histone-methylation-dependent chromatin lock. Cell. 2007 Jun 1;129(5):915–28.

26. Margueron R, Trojer P, Reinberg D. The key to development: interpreting the histone code? Curr Opin Genet Dev. 2005 Apr;15(2):163–76.

27. Verschure PJ, van der Kraan I, de Leeuw W, van der Vlag J, Carpenter AE, Belmont AS, et al. In vivo HP1 targeting causes large-scale chromatin condensation and enhanced histone lysine methylation. Molecular and Cellular Biology. 2005 Jun;25(11):4552–64.

28. Vermeulen M, Eberl HC, Matarese F, Marks H, Denissov S, Butter F, et al. Quantitative interaction proteomics and genome-wide profiling of epigenetic histone marks and their readers. Cell. 2010 Sep 17;142(6):967–80.

29. Huyen Y, Zgheib O, Ditullio RA, Gorgoulis VG, Zacharatos P, Petty TJ, et al. Methylated lysine 79 of histone H3 targets 53BP1 to DNA double-strand breaks. Nature. 2004 Nov 18;432(7015):406–11.

30. Wysocka J, Swigut T, Xiao H, Milne TA, Kwon SY, Landry J, et al. A PHD finger of NURF couples histone H3 lysine 4 trimethylation with chromatin remodelling. Nature. 2006 Jul 6;442(7098):86–90.

31. Nagy Z, Riss A, Fujiyama S, Krebs A, Orpinell M, Jansen P, et al. The metazoan ATAC and SAGA coactivator HAT complexes regulate different sets of inducible target genes. Cell Mol Life Sci. SP Birkhäuser Verlag Basel; 2010 Feb;67(4):611–28.

32. Barski A, Cuddapah S, Cui K, Roh T-Y, Schones DE, Wang Z, et al. High-resolution profiling of histone methylations in the human genome. Cell. 2007 May 18;129(4):823–37.

33. Kizer KO, Phatnani HP, Shibata Y, Hall H, Greenleaf AL, Strahl BD. A novel domain in Set2 mediates RNA polymerase II interaction and couples histone H3 K36 methylation with transcript elongation. Molecular and Cellular Biology. American Society for Microbiology; 2005 Apr;25(8):3305–16.

34. Brien GL, Gambero G, O'Connell DJ, Jerman E, Turner SA, Egan CM, et al. Polycomb PHF19 binds H3K36me3 and recruits PRC2 and demethylase NO66 to embryonic stem cell genes during differentiation. Nat Struct Mol Biol. 2012 Dec;19(12):1273–81.

35. Qin S, Guo Y, Xu C, Bian C, Fu M, Gong S, et al. Tudor domains of the PRC2 components PHF1 and PHF19 selectively bind to histone H3K36me3. Biochem Biophys Res Commun. 2013 Jan 11;430(2):547–53.

36. Bernstein BE, Mikkelsen TS, Xie X, Kamal M, Huebert DJ, Cuff J, et al. A bivalent chromatin structure marks key developmental genes in embryonic stem cells. Cell. 2006 Apr 21;125(2):315–26.

37. Bernstein BE, Humphrey EL, Erlich RL, Schneider R, Bouman P, Liu JS, et al. Methylation of histone H3 Lys 4 in coding regions of active genes. Proc Natl Acad Sci USA. 2002 Jun 25;99(13):8695–700.

38. Mikkelsen TS, Ku M, Jaffe DB, Issac B, Lieberman E, Giannoukos G, et al. Genome-wide maps of chromatin state in pluripotent and lineage-committed cells. Nature. 2007 Aug 2;448(7153):553–60.

39. Kouskouti A, Talianidis I. Histone modifications defining active genes persist after transcriptional and mitotic inactivation. EMBO J. 2005 Jan 26;24(2):347–57.

40. Ghisletti S, Barozzi I, Mietton F, Polletti S, De Santa F, Venturini E, et al. Identification and characterization of enhancers controlling the inflammatory gene expression program in macrophages. Immunity. 2010 Mar 26;32(3):317–28.

41. Lauberth SM, Nakayama T, Wu X, Ferris AL, Tang Z, Hughes SH, et al. H3K4me3 interactions with TAF3 regulate preinitiation complex assembly and selective gene activation. Cell. 2013 Feb 28;152(5):1021–36.

42. Vermeulen M, Mulder KW, Denissov S, Pijnappel WWMP, van Schaik FMA, Varier RA, et al. Selective anchoring of TFIID to nucleosomes by trimethylation of histone H3 lysine 4. Cell. 2007 Oct 5;131(1):58–69.

43. Mueller D, Bach C, Zeisig D, Garcia-Cuellar M-P, Monroe S, Sreekumar A, et al. A role for the MLL fusion partner ENL in transcriptional elongation and chromatin modification. Blood. 2007 Dec 15;110(13):4445–54.

44. Heintzman ND, Stuart RK, Hon G, Fu Y, Ching CW, Hawkins RD, et al. Distinct and predictive chromatin signatures of transcriptional promoters and enhancers in the human genome. Nat Genet. 2007 Mar;39(3):311–8.

45. Calo E, Wysocka J. Modification of enhancer chromatin: what, how, and why? Molecular Cell. 2013 Mar 7;49(5):825–37.

46. Jeong KW, Kim K, Situ AJ, Ulmer TS, An W, Stallcup MR. Recognition of enhancer element-specific histone methylation by TIP60 in transcriptional activation. Nat Struct Mol Biol. 2011 Dec;18(12):1358–65.

47. Tatton-Brown K, Hanks S, Ruark E, Zachariou A, Duarte SDV, Ramsay E, et al. Germline mutations in the oncogene EZH2 cause Weaver syndrome and increased human height. Oncotarget. 2011 Dec;2(12):1127–33.

48. Gibson WT, Hood RL, Zhan SH, Bulman DE, Fejes AP, Moore R, et al. Mutations in EZH2 cause Weaver syndrome. Am J Hum Genet. 2012 Jan 13;90(1):110–8.

49. Jensen LR, Amende M, Gurok U, Moser B, Gimmel V, Tzschach A, et al. Mutations in the JARID1C gene, which is involved in transcriptional regulation and chromatin remodeling, cause X-linked mental retardation. Am J Hum Genet. 2005 Feb;76(2):227–36.

50. Kleefstra T, Kramer JM, Neveling K, Willemsen MH, Koemans TS, Vissers LELM, et al. Disruption of an EHMT1-associated chromatin-modification module causes intellectual disability. Am J Hum Genet. 2012 Jul 13;91(1):73–82.

51. Chase A, Cross NCP. Aberrations of EZH2 in cancer. Clin Cancer Res. American Association for Cancer Research; 2011 May 1;17(9):2613–8.

52. Spannhoff A, Sippl W, Jung M. Cancer treatment of the future: inhibitors of histone methyltransferases. Int J Biochem Cell Biol. 2009 Jan;41(1):4–11.

53. Prinjha R, Tarakhovsky A. Chromatin targeting drugs in cancer and immunity. Genes & Development. Cold Spring Harbor Lab; 2013 Aug 15;27(16):1731–8.

54. Bojang P, Ramos KS. The promise and failures of epigenetic therapies for cancer treatment. Cancer Treat Rev. 2014 Feb;40(1):153–69.

55. Ernst T, Chase AJ, Score J, Hidalgo-Curtis CE, Bryant C, Jones AV, et al. Inactivating mutations of the histone methyltransferase gene EZH2 in myeloid disorders. Nat Genet. 2010 Aug;42(8):722–6.

56. Cao R, Zhang Y. SUZ12 is required for both the histone methyltransferase activity and the silencing function of the EED-EZH2 complex. Molecular Cell. 2004 Jul 2;15(1):57–67.

57. Sarma K, Margueron R, Ivanov A, Pirrotta V, Reinberg D. Ezh2 requires PHF1 to efficiently catalyze H3 lysine 27 trimethylation in vivo. Molecular and Cellular Biology. 2008 Apr;28(8):2718–31.

58. Nekrasov M, Klymenko T, Fraterman S, Papp B, Oktaba K, Köcher T, et al. Pcl-PRC2 is needed to generate high levels of H3-K27 trimethylation at Polycomb target genes. EMBO J. 2007 Sep 19;26(18):4078–88.

59. Li X, Isono KI, Yamada D, Endo TA, Endoh M, Shinga J, et al. Mammalian Polycomb-Like Pcl2/Mtf2 Is a Novel Regulatory Component of PRC2 That Can Differentially Modulate Polycomb Activity both at the Hox Gene Cluster and at Cdkn2a Genes. Molecular and Cellular Biology. 2010 Dec 24;31(2):351–64.

60. Li G, Margueron R, Ku M, Chambon P, Bernstein BE, Reinberg D. Jarid2 and PRC2, partners in regulating gene expression. Genes & Development. 2010 Feb 15;24(4):368–80.

61. Walker E, Chang WY, Hunkapiller J, Cagney G, Garcha K, Torchia J, et al. Polycomb-like 2 associates with PRC2 and regulates transcriptional networks during mouse embryonic stem cell self-renewal and differentiation. Cell Stem Cell. 2010 Feb 5;6(2):153–66.

62. Caganova M, Carrisi C, Varano G, Mainoldi F, Zanardi F, Germain P-L, et al. Germinal center dysregulation by histone methyltransferase EZH2 promotes lymphomagenesis. J Clin Invest. American Society for Clinical Investigation; 2013 Dec 2;123(12):5009–22.

63. Savla U, Benes J, Zhang J, Jones RS. Recruitment of Drosophila Polycomb-group proteins by Polycomblike, a component of a novel protein complex in larvae. Development. 2008 Mar;135(5):813–7.

64. Yuan W, Wu T, Fu H, Dai C, Wu H, Liu N, et al. Dense chromatin activates Polycomb repressive complex 2 to regulate H3 lysine 27 methylation. Science. American Association for the Advancement of Science; 2012 Aug 24;337(6097):971–5.

65. Margueron R, Justin N, Ohno K, Sharpe ML, Son J, DruryIII WJ, et al. Role of the polycomb protein EED in the propagation of repressive histone marks. Nature. Nature Publishing Group; 2009 Aug 10;461(7265):762–7.

66. Kaneko S, Li G, Son J, Xu CF, Margueron R, Neubert TA, et al. Phosphorylation of the PRC2 component Ezh2 is cell cycle-regulated and up-regulates its binding to ncRNA. Genes & Development. 2010 Dec 1;24(23):2615–20.

67. Chen S, Bohrer LR, Rai AN, Pan Y, Gan L, Zhou X, et al. Cyclin-dependent kinases regulate epigenetic gene silencing through phosphorylation of EZH2. Nature Publishing Group. Nature Publishing Group; 2010 Oct 10;12(11):1108–14.

68. Wei Y, Chen Y-H, Li L-Y, Lang J, Yeh S-P, Bin Shi, et al. CDK1-dependent phosphorylation of EZH2 suppresses methylation of H3K27 and promotes osteogenic differentiation of human mesenchymal stem cells. Nature Publishing Group. Nature Publishing Group; 2010 Dec 5;13(1):87–94.

69. Kim E, Kim M, Woo D-H, Shin Y, Shin J, Chang N, et al. Phosphorylation of EZH2 activates STAT3 signaling via STAT3 methylation and promotes tumorigenicity of glioblastoma stem-like cells. Cancer Cell. 2013 Jun 10;23(6):839–52.

70. Chu C-S, Lo P-W, Yeh Y-H, Hsu P-H, Peng S-H, Teng Y-C, et al. O-GlcNAcylation regulates EZH2 protein stability and function. Proc Natl Acad Sci USA. 2014 Jan 28;111(4):1355–60.

71. Schmitges FW, Prusty AB, Faty M, Stützer A, Lingaraju GM, Aiwazian J, et al. Histone methylation by PRC2 is inhibited by active chromatin marks. Molecular Cell. 2011 May 6;42(3):330–41.

72. Xu C, Bian C, Yang W, Galka M, Ouyang H, Chen C, et al. Binding of different histone marks differentially regulates the activity and specificity of polycomb repressive complex 2 (PRC2). Proc Natl Acad Sci USA. National Acad Sciences; 2010 Nov 9;107(45):19266–71.

73. Xu K, Wu ZJ, Groner AC, He HH, Cai C, Lis RT, et al. EZH2 oncogenic activity in castration-resistant prostate cancer cells is Polycomb-independent. Science. 2012 Dec 14;338(6113):1465–9.

74. McCabe MT, Ott HM, Ganji G, Korenchuk S. EZH2 inhibition as a therapeutic strategy for lymphoma with EZH2-activating mutations. Nature. 2012.

75. Margueron R, Li G, Sarma K, Blais A, Zavadil J, Woodcock CL, et al. Ezh1 and Ezh2 Maintain Repressive Chromatin through Different Mechanisms. Molecular Cell. Elsevier Inc; 2008 Nov 21;32(4):503–18.

76. EZH1 mediates methylation on histone H3 lysine 27 and complements EZH2 in maintaining stem cell identity and executing pluripotency. 2008 Nov 21;32(4):491–502.

77. Laible G, Wolf A, Dorn R, Reuter G, Nislow C, Lebersorger A, et al. Mammalian homologues of the Polycomb-group gene Enhancer of zeste mediate gene silencing in Drosophila heterochromatin and at S. cerevisiae telomeres. EMBO J. 1997 Jun 2;16(11):3219–32.

78. Caretti G, Di Padova M, Micales B, Lyons GE, Sartorelli V. The Polycomb Ezh2 methyltransferase regulates muscle gene expression and skeletal muscle differentiation. Genes & Development. Cold Spring Harbor Lab; 2004 Nov 1;18(21):2627–38.

79. Ezhkova E, Lien WH, Stokes N, Pasolli HA, Silva JM, Fuchs E. EZH1 and EZH2 cogovern histone H3K27 trimethylation and are essential for hair follicle homeostasis and wound repair. Genes & Development. 2011 Mar 1;25(5):485–98.

80. Su I-H, Basavaraj A, Krutchinsky AN, Hobert O, Ullrich A, Chait BT, et al. Ezh2 controls B cell development through histone H3 methylation and Igh rearrangement. Nat Immunol. 2003 Feb;4(2):124–31.

81. Mousavi K, Zare H, Wang AH, Sartorelli V. Polycomb protein Ezh1 promotes RNA polymerase II elongation. Molecular Cell. 2012 Jan 27;45(2):255–62.

82. Rada-Iglesias A, Bajpai R, Swigut T, Brugmann SA, Flynn RA, Wysocka J. A unique chromatin signature uncovers early developmental enhancers in humans. Nature. 2011 Feb 10;470(7333):279–83.

83. Schuettengruber B, Chourrout D, Vervoort M, Leblanc B, Cavalli G. Genome regulation by polycomb and trithorax proteins. Cell. 2007 Feb 23;128(4):735–45.

84. Spannhoff A, Hauser A-T, Heinke R, Sippl W, Jung M. The emerging therapeutic potential of histone methyltransferase and demethylase inhibitors. ChemMedChem. 2009 Oct;4(10):1568–82.

85. Collett K, Eide GE, Arnes J, Stefansson IM, Eide J, Braaten A, et al. Expression of enhancer of zeste homologue 2 is significantly associated with increased tumor cell proliferation and is a marker of aggressive breast cancer. Clin Cancer Res. 2006 Feb 15;12(4):1168–74.

86. Cooper CS, Campbell C, Jhavar S. Mechanisms of Disease: biomarkers and molecular targets from microarray gene expression studies in prostate cancer. Nat Clin Pract Urol. 2007 Dec;4(12):677–87.

87. Morin RD, Johnson NA, Severson TM, Mungall AJ, An J, Goya R, et al. Somatic mutations altering EZH2 (Tyr641) in follicular and diffuse large B-cell lymphomas of germinal-center origin. Nat Genet. 2010 Feb;42(2):181–5.

88. Sneeringer CJ, Scott MP, Kuntz KW, Knutson SK, Pollock RM, Richon VM, et al. Coordinated activities of wild-type plus mutant EZH2 drive tumor-associated hypertrimethylation of lysine 27 on histone H3 (H3K27) in human B-cell lymphomas. Proc Natl Acad Sci USA. National Acad Sciences; 2010 Dec 7;107(49):20980–5.

89. Yap DB, Chu J, Berg T, Schapira M, Cheng S-WG, Moradian A, et al. Somatic mutations at EZH2 Y641 act dominantly through a mechanism of selectively altered PRC2 catalytic activity, to increase H3K27 trimethylation. Blood. 2011 Feb 24;117(8):2451–9.

90. van Haaften G, Dalgliesh GL, Davies H, Chen L, Bignell G, Greenman C, et al. Somatic mutations of the histone H3K27 demethylase gene UTX in human cancer. Nat Genet. 2009 May;41(5):521–3.

91. Ntziachristos P, Tsirigos A, Van Vlierberghe P, Nedjic J, Trimarchi T, Flaherty MS, et al. Genetic inactivation of the polycomb repressive complex 2 in T cell acute lymphoblastic leukemia. Nat Med. 2012 Feb;18(2):298–301.

92. Score J, Hidalgo-Curtis C, Jones AV, Winkelmann N, Skinner A, Ward D, et al. Inactivation of polycomb repressive complex 2 components in myeloproliferative and myelodysplastic/myeloproliferative neoplasms. Blood. 2012 Feb 2;119(5):1208–13.

93. Ntziachristos P, Tsirigos A, Welstead GG, Trimarchi T, Bakogianni S, Xu L, et al. Contrasting roles of histone 3 lysine 27 demethylases in acute lymphoblastic leukaemia. Nature. 2014 Aug 17.

94. Helin K, Dhanak D. Chromatin proteins and modifications as drug targets. Nature. 2013 Oct 24;502(7472):480–8.

95. Kubicek S, O'Sullivan RJ, August EM, Hickey ER, Zhang Q, Teodoro ML, et al. Reversal of H3K9me2 by a small-molecule inhibitor for the G9a histone methyltransferase. Molecular Cell. 2007 Feb 9;25(3):473–81.

96. Greiner D, Bonaldi T, Eskeland R, Roemer E, Imhof A. Identification of a specific inhibitor of the histone methyltransferase SU(VAR)3-9. Nat Chem Biol. 2005 Aug;1(3):143–5.

97. Miranda TB, Cortez CC, Yoo CB, Liang G, Abe M, Kelly TK, et al. DZNep is a global histone methylation inhibitor that reactivates developmental genes not silenced by DNA methylation. Mol Cancer Ther. 2009 Jun;8(6):1579–88.

98. Daigle SR, Olhava EJ, Therkelsen CA, Majer CR, Sneeringer CJ, Song J, et al. Selective killing of mixed lineage leukemia cells by a potent small-molecule DOT1L inhibitor. Cancer Cell. 2011 Jul 12;20(1):53–65.

99. Knutson SK, Wigle TJ, Warholic NM, Sneeringer CJ, Allain CJ, Klaus CR, et al. A selective inhibitor of EZH2 blocks H3K27 methylation and kills mutant lymphoma cells. Nat Chem Biol. 2012 Nov;8(11):890–6.

100. Konze KD, Ma A, Li F, Barsyte-Lovejoy D, Parton T, Macnevin CJ, et al. An orally bioavailable chemical probe of the Lysine Methyltransferases EZH2 and EZH1. ACS Chem Biol. 2013 Jun 21;8(6):1324–34.

101. Qi W, Chan H, Teng L, Li L, Chuai S, Zhang R, et al. Selective inhibition of Ezh2 by a small molecule inhibitor blocks tumor cells proliferation. Proc Natl Acad Sci USA. 2012 Dec 26;109(52):21360–5.

102. Garapaty-Rao S, Nasveschuk C, Gagnon A, Chan EY, Sandy P, Busby J, et al. Identification of EZH2 and EZH1 small molecule inhibitors with selective impact on diffuse large B cell lymphoma cell growth. Chem Biol. 2013 Nov 21;20(11):1329–39.

103. Kim W, Bird GH, Neff T, Guo G, Kerenyi MA, Walensky LD, et al. Targeted disruption of the EZH2-EED complex inhibits EZH2-dependent cancer. Nat Chem Biol. 2013 Oct;9(10):643–50.

104. McCabe MT, Ott HM, Ganji G, Korenchuk S, Thompson C, Van Aller GS, et al. EZH2 inhibition as a therapeutic strategy for lymphoma with EZH2-activating mutations. Nature. 2012 Dec 6;492(7427):108–12.

105. Knutson SK, Warholic NM, Wigle TJ, Klaus CR, Allain CJ, Raimondi A, et al. Durable tumor regression in genetically altered malignant rhabdoid tumors by inhibition of methyltransferase EZH2. Proc Natl Acad Sci USA. 2013 May 7;110(19):7922–7.

106. Copeland RA. EZH2 Inhibitor EPZ-6438 (E7438) in Non-Hodgkin Lymphoma: Pre-Clinical Models and Early Clinical Observations. Available from: http://www.epizyme.com/wp-content/uploads/2014/08/ASH-Lymphoma-Conference-Copeland-FINAL.pdf

107. Cavalli G. Molecular biology. EZH2 goes solo. Science. American Association for the Advancement of Science; 2012 Dec 14;338(6113):1430–1.

108. Su I-H, Dobenecker M-W, Dickinson E, Oser M, Basavaraj A, Marqueron R, et al. Polycomb group protein ezh2 controls actin polymerization and cell signaling. Cell. 2005 May 6;121(3):425–36.

Chapter II

PRC2 purification and assay development for high-throughput screening

Collaborator Contributions

- **Dr. Qiu Wang** assisted in PRC2 biochemical assay (DELFIA) development.
- **Dr. Russell Ryan** provided the 1XFLAG-EZH2 Gateway® Entry vector for downstream cloning and PRC2 expression in Sf9 cells.

2.1 Introduction

2.1.1 Biochemical approaches to measuring HMTase activity

While there is no widely accepted standard for measuring HMT activity, numerous methods have been developed. Some assays measure SAH production, in coupled-enzyme (1-3) and competitive fluorescence polarization (4) formats, while others measure levels of methylated substrate, by way of radiometric detection (5-8), immunodetection (9-11), mass spectrometry (9), or capillary electrophoresis (12). Depending on the HMT of interest and application (i.e. kinetic studies, HTS, etc.), each approach has its advantages and limitations.

Most coupled-enzyme assays detect methyltransferase activity by enzymatically converting the byproduct of methylation, SAH, into homocysteine which can then be quantified using ThioGlo (2) or Ellman's reagent (1)—both thiol-reactive fluorescent probes. While these assays have proven useful for kinetic characterization and small-molecule discovery for some HMTs (13-15), the requirement of additional enzymes to produce signal complicates optimization of key assay parameters (e.g. buffer conditions) and can increase the false positive rate when screening for inhibitors; moreover, the use of thiol-reactive probes can alter HMT activity and negatively impact the signal-to-background ratio when surface cysteines are present.

Radiometric HMT assays quantify ^{3}H or ^{14}C incorporation into target substrate (by scintillation counting or autoradiography) following incubation with labeled cofactor, S-[methyl-^{3}H]- or S-[methyl-^{14}C]-adenosyl-methionine. Radiolabeled product is typically purified via small-scale chromatography (e.g. ZipTip®) (16), SDS-PAGE (17), or filter-binding methods (7,18) to remove excess labeled cofactor; however, the development

of scintillation proximity assays (SPA) has obviated this step, provided that the product can be immobilized (usually by means of biotin) (8). While these methods afford high sensitivity and are generally less prone to artifacts (19), safety concerns and the practical considerations of handling radiological waste limit their use in high-throughput screening.

In contrast to radiometric assays, immunodetection of specific methylated products has proven to be a valuable approach in the realm of high-throughput assay development. In 2007, Kubicek et al. reported the discovery of BIX-01294, a substrate-competitive G9a inhibitor found in a screen of 125,000 compounds using a dissociation-enhanced lanthanide fluoroimmunoassay (DELFIA). In DELFIA, biotinylated product is captured on a streptavidin-coated surface, incubated with a methylation-specific antibody bound to a europium-conjugated secondary antibody, and then detected via time-resolved fluorescence (9,20). Chemiluminecence-based detection has also been reported, using an HRP-linked secondary antibody in place of lanthanide-conjugates (10). HMT profiling services provided by BPS Bioscience has demonstrated the utility of this approach, as >20 distinct, validated HMT assays are commercially available for small-molecule characterization.

Due to the requirement of several wash steps and extensive liquid handling in DELFIA, several HMT-adapted homogenous immunoassays have also been developed. These include AlphaLISA (11) and LANCE (21), both of which require use of biotinylated substrates and selective antibodies to generate a FRET-like (AlphaLISA) or FRET-based (LANCE) signal upon ternary complex formation. While these assays remove the need for wash steps, the cost of reagents can be prohibitive to scale-up,

limiting the scope of high-throughput screening campaigns. Furthermore, compared with DELFIA, assay artifacts are more prominent, as compounds that disrupt singlet oxygen transfer (in the case of AlphaLISA) or display autofluorescence (LANCE) will emerge as low-signal outliers.

While versatile and amenable to HTS, antibody-based HMT assays are limited by the quality, consistency, and availability of selective antibodies. Fortunately, in response to the growing activity in chromatin research, many companies, such as AbCam and Cell Signaling Technology, have developed several products with proven selectivity and low lot-to-lot variability, meeting the increased need for reliable antibodies against histone marks. As a result, these products have enabled antibody-based assay development for a number of histone methyltransferases (11,21).

2.1.2 Assay development for small-molecule screening

Small-molecule screening has become a major source for starting points in the development of chemical probes and drugs. At the heart of a successful screening campaign, lies a robust and well validated, high-throughput assay. Development of such assays requires careful optimization of several key parameters to ensure reproducibility and statistically-significant signal over background (22,23). As screens of >100,000 compounds are often required to cover sufficient chemical space, cost and automation compatibility must also be considered. Failure to establish a proper workflow and assay prior to a high-throughput screening campaign can lead to unmanageable false-positive and false-negative rates, hindering identification of worthy lead compounds.

Most HTS assays fall into two major categories – biochemical assays, using purified target protein to measure direct binding (NMR, small-molecule microarray, etc)

or activity modulation by small molecules, and phenotypic assays, measuring the effect of compounds on cellular features (ATP levels, reporter gene activity, morphology, etc.). Each approach has its unique set of considerations in terms of proper assay development. For biochemical assays measuring enzymatic activity, it is important to obtain quality protein preparations and have an understanding of target biochemistry; for example, enzyme kinetic parameters (K_M, V_{MAX}) under established buffer conditions. Defining appropriate buffer conditions is also a key step, requiring evaluation of enzyme activity in the presence of different additives (salts, reducing agents, etc.) and buffers at varying pH. Optimal enzyme, substrate, and cofactor concentrations are often determined based on measured K_M and V_{MAX} values, but can be influenced by their cost and stability. Product detection systems must be adaptable to miniaturization (96-, 384-,or 1536-well formats) and automation, allowing sensitive and reproducible measurement of activity. Lastly, to prevent high false-negative rates, reaction time and detection is optimized to ensure measurement in the linear range (24).

If imaged-based phenotypic screening (HCA/HCS) is employed, other factors are taken into account, with proper selection of representative, validated cellular phenotypes—robustly detected by automated microscopy—being the most critical. Use of consistent cell lines and growth/treatment conditions is required to ensure detection of the given phenotype with low variability between assay plates and wells. Parameters such as compound incubation time, cell number/density, growth media, and any necessary staining procedures must be carefully optimized prior to screening. Furthermore, establishment of appropriate imaging and image analysis protocols should also be considered (25).

In order to screen for and validate small–molecule modulators of PRC2, we developed both biochemical (primary; DELFIA) and cell-based (secondary; H3K27me3 HCA) assays suitable for HTS. Described in detail below, these efforts required expression and purification of active PRC2 (EZH2-EED-SUZ12-RBBP4-AEBP2 complex), identification of a suitable substrate, determination of kinetic parameters, and optimization of an HTS-ready DELFIA. As a secondary assay, we developed an immunofluorescence-based HCA protocol to detect changes in cellular H3K27me3 levels, which we validated using siRNA against EZH2 and EED.

2.2 Results and discussion

2.2.1 Expression and purification of recombinant PRC2

Expression and purification of recombinant five-component PRC2 (EZH2, EED, SUZ12, AEBP2, and RBBP4; 5C-PRC2) was first developed by Cao and Zhang in an effort to dissect the function of individual subunits found in isolated PRC2 complexes (26). Due to the difficulty in expressing full-length EZH2 in *E.coli* (26,27), Cao employed a baculovirus expression strategy to ensure proper folding and enable co-expression of PRC2 components, generating an active complex (26). In order to produce large quantities of highly active PRC2 for high-throughput screening and subsequent follow-up studies, we applied a similar strategy with minor modifications.

After cloning each component cDNA into Gateway-compatible bacmid-transfer vectors containing an N-terminal 6XHIS tag (for RBBP4, AEBP2, and SUZ12) or no tag (EED and 1xFLAG-EZH2), we generated bacmid constructs through amplification of transformed DH10BAC *E. coli* harboring recombined transgenes, purifying large bacmid DNA via anion-exchange chromatography. Bacmids were then transfected into

Spodoptera frugiperda (Sf9) cells to generate baculovirus stocks (denoted P1) that were amplified through infection of large-scale Sf9 suspension cultures to yield high-titer viral stocks (P2) suitable for subsequent amplification or immediate protein expression.

To optimize expression of each PRC2 component, we infected log-phase Sf9 cells with each component baculovirus individually at multiple MOIs and allowed expression to proceed for 48, 72, or 96 hrs. After infected cells were harvested and lysed, the levels of transgene expression under these varying conditions were determined for each component by western blot. For all components, expression was greatest at 96hrs, while the MOI required to achieve maximum expression varied for each component (Figure 2.1).

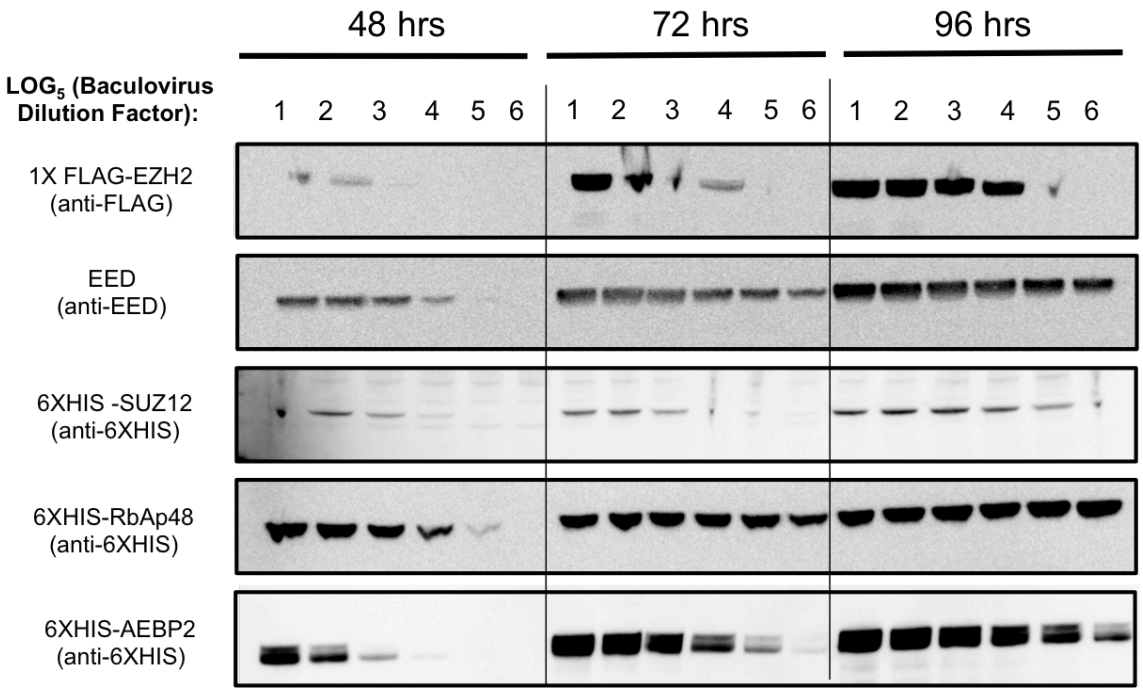

Figure 2.1 Expression optimization for PRC2 components
Log-phase Sf9 cells were infected with varying dilutions of PRC2 component baculoviruses for 48, 72, or 96 hours. Total protein was resolved via SDS-PAGE and recombinant protein was detected via western blot to estimate relative expression levels.

We expressed 5C-PRC2 by infecting Sf9 cells with each component baculovirus simultaneously (at their respective, optimal MOIs), allowing co-expression to proceed for 96 hours. To isolate recombinant complex, we harvested cells post-infection and lysed via sonication. Lysates were cleared by centrifugation and incubated with anti-FLAG M2 agarose beads, capturing all 1XEZH2-containing complexes—including 5C-PRC2. These complexes were then eluted with 3XFLAG peptide and the resulting eluate was separated through a gel filtration column (Superdex 200) to isolate 5C-PRC2 based on its predicted molecular weight (~325 kDa).

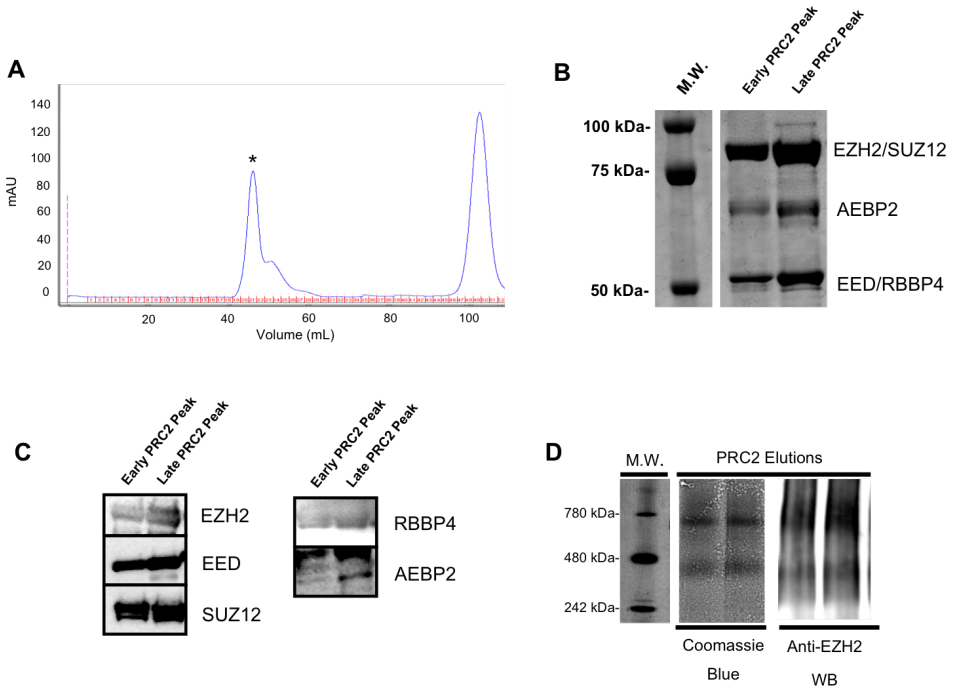

Figure 2.2 Characterization of recombinant 5C-PRC2
(A) Superdex 200 16/600 SEC separation of PRC2 elutions. Peaks eluting around 40 mL ("Early PRC2 Peak"; ~660 kDa) and 55 mL ("Late PRC2 Peak; ~300 ka) were collected. (B) SDS-PAGE of "Early" and "Late" PRC2 peaks. (C) Western blots for each PRC2 component within PRC2 fractions. (D) Native PAGE of PRC2 elutions and EZH2 western blot.

2.2.2 Characterization of recombinant PRC2

After purification, we confirmed incorporation of each component into PRC2 by western blot and verified homogeneity of the five-component complex by native PAGE

(Figure 2.2). Native PAGE revealed two prominent bands, one in the 480 kDa range and another around 780 kDa (as estimated by molecular weight standards). Anti-EZH2 western blots confirmed that these bands contained EZH2 and were likely monomeric (~325 kDa) and dimeric (~650 kDa) forms of the PRC2 complex. The existence of distinct complexes had been previously speculated, but they have only recently been characterized and reported (28). While these forms have not been shown to differ in enzymatic activity, dimeric and monomeric PRC2 bind lincRNA (e.g. HOTAIR) with varying affinities in vitro (28).

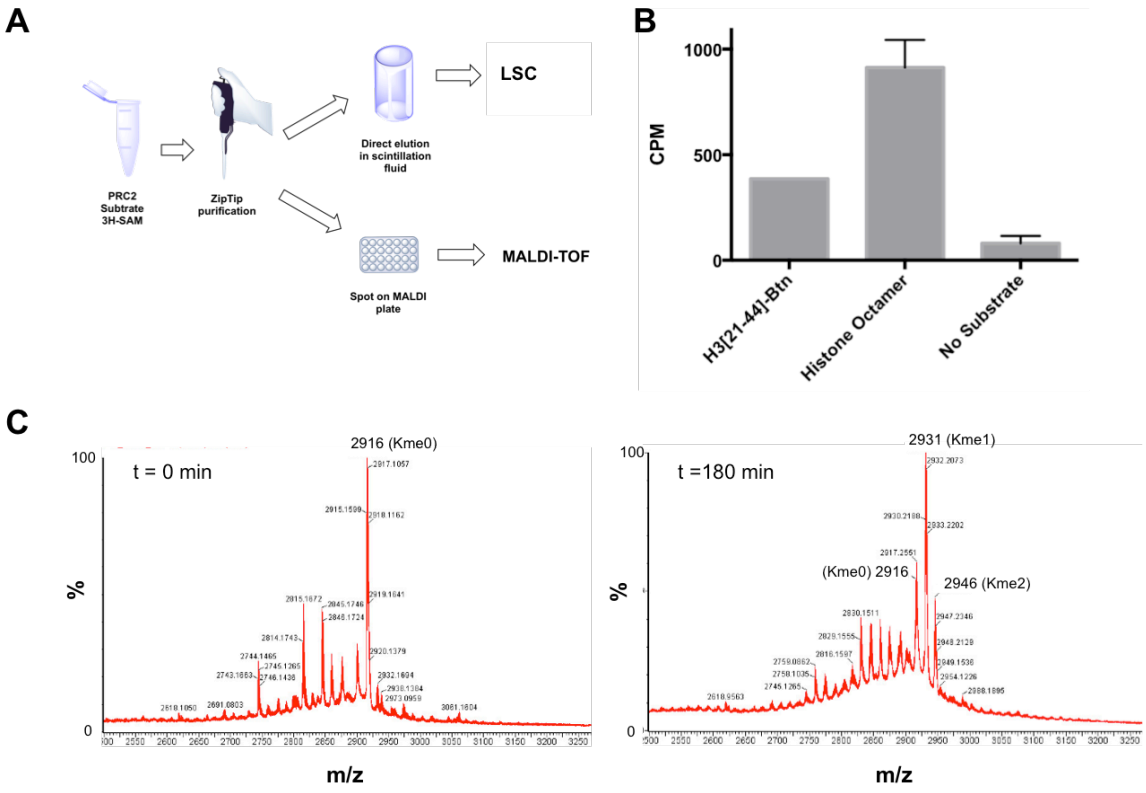

Figure 2.3 Confirmation of recombinant 5C-PRC2 activity
(A) Workflow of radiometric PRC2 assays. (B) Activity of recombinant PRC2 on histone octamer (1 ug) and peptide (1 uM) substrates as measured by LSC. Data represent the mean and standard error of triplicate measurements. (C) MALDI-TOF spectra of H3[21-44]-GK-biotin peptide isolated from PRC2 reaction at time 0 min (*left*) and 180 min (*right)*.

We initially measured activity of recombinant PRC2 using a radiometric assay (16), incubating purified enzyme with histone octamer or an H3-derived peptide (H3[21-44]) in the presence of ^{3}H-SAM for 2 hrs at RT. In comparison to the "no enzyme" controls, our recombinant PRC2 displayed activity on both substrates (with higher activity on octamer) (Figure 2.3B). To further confirm this activity and determine the degree of substrate methylation (i.e. mono-, di-, or trimethylation), we repeated our reaction in the presence of peptide and cold SAM, measuring peptide mass via MALDI-TOF mass spectrometry. These experiments revealed significant levels of monomethylation, modest levels of dimethylation, and no detectable trimethylation (Figure 2.3C)—results consistent with the finding that 5C-PRC2 is deficient in its ability to methylate H3K27me2-modified substrates in vitro (18).

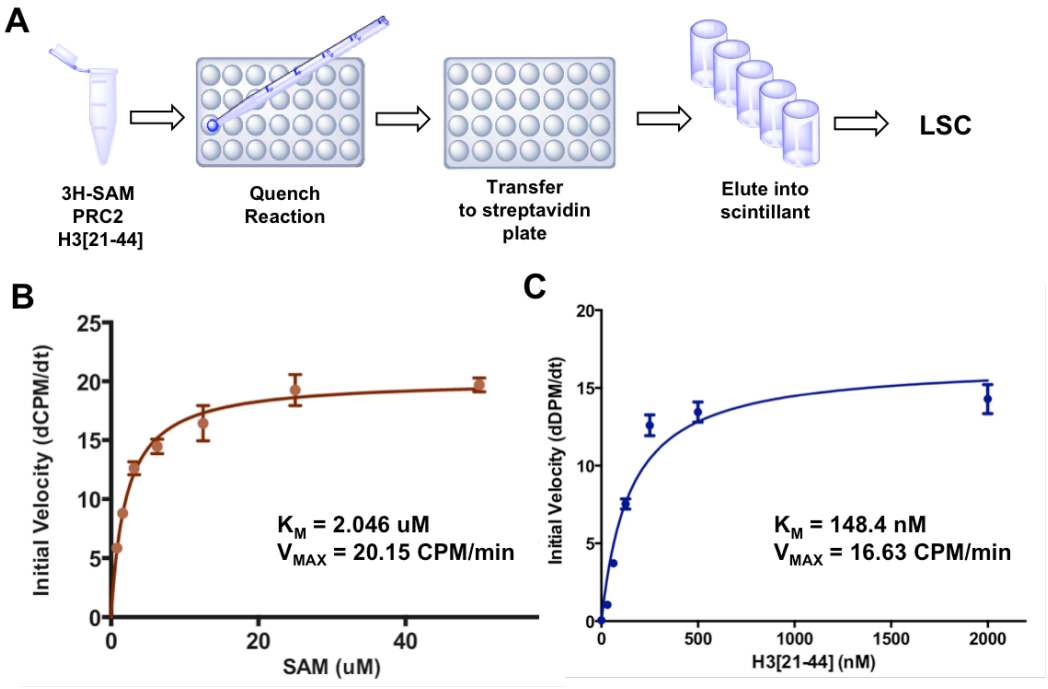

Figure 2.4 Kinetic characterization of recombinant 5C-PRC2
(A) Workflow for plate-based LSC assay. (B,C) Michaelis- Menten plots for SAM and H3[21-44]-GK-biotin peptide, respectively. Mean and SEM for initial velocities were generated from linear regression fits (PRISM 6.0) of triplicate measurements over six time points (0,15, 30, 45, 60, and 75 min). K_M and V_{MAX} values were determined using the Michaelis-Menten analysis module in PRISM 6.0.

For the purpose of downstream assay development, we next aimed to kinetically characterize our recombinant PRC2, measuring its kinetic parameters (K_M and V_{MAX}) for SAM and H3[21-44] peptide. Using an LSC protocol adapted for higher throughput (Figure 2.4A), we performed time-course measurements of PRC2 activity under varying concentrations of cofactor (Figure 2.4B) and substrate (Figure 2.4C). Our recombinant PRC2 was found to have K_M values for SAM in the 2 uM range, while the K_M for H3[21-44] was around 150 nM. As IC_{50} values (as opposed to K_i) are typically measured when assessing compound activity, it is important to establish assay conditions (namely, cofactor and peptide concentration) that take kinetic parameters into consideration. Depending on the mechanism of action, strong deviations between a compound's Ki (true potency) and IC_{50} (apparent potency) occur when cofactor or substrate concentrations exceed their respective K_M values (29,30).

2.2.3 Development of DELFIA for PRC2 HTS

With an established source of validated PRC2, we next aimed to develop a biochemical assay suitable for high-throughput screening. DELFIA (Figure 2.5A) was chosen as our primary assay detection method due to its versatility, relatively low cost, and reported success in similar HTS campaigns (9). As we had previously confirmed PRC2 activity on a biotinylated H3-derived peptide, our first challenge was to identify an antibody capable of detecting the methylated product (H3K27me1/2) selectively over the unmodified substrate. Using our former conditions, we set-up 40 uL reactions in 384-well DELFIA plates (streptavidin-coated) and screened a panel of H3K27me-selective antibodies (Figure 2.5B). While most of the antibodies failed to generate significant signal over background (no-enzyme control), three showed promising S/B

(>20) at a wide range of dilutions. Ultimately, an H3K27me2-selective antibody, CS#9728, was selected for its ability to deliver high signal at a reasonable dilution; moreover, this lot was available from Cell Signaling Technology in quantities that met our estimated needs for high-throughput screening.

Next, we optimized SAM, H3[21-44] peptide, and enzyme concentrations to minimize material requirements, yet maintain high signal (Figure 2.6). Using our H3K27me2-selective antibody for detection, we first titrated peptide (from 50- 800 nM) and then SAM (2.5 – 20 uM), selecting final concentrations based on K_M values and overall signal. For our assay, we aimed to maximize signal, yet prevent significant Ki versus IC_{50} discrepancies by using final concentrations at 2X K_M for peptide (300 nM) and 2.5X K_M for SAM (5 uM). Once optimal substrate and cofactor concentrations were determined, we titrated enzyme to find the minimum concentration that would produce high signal and behave linearly over the reaction course (Figure 2.6C,D). Under our optimized SAM and peptide conditions, 30 ng PRC2 (2.3 nM) was sufficient for detection (>20 S/B) and subsequent time course experiments confirmed linearity.

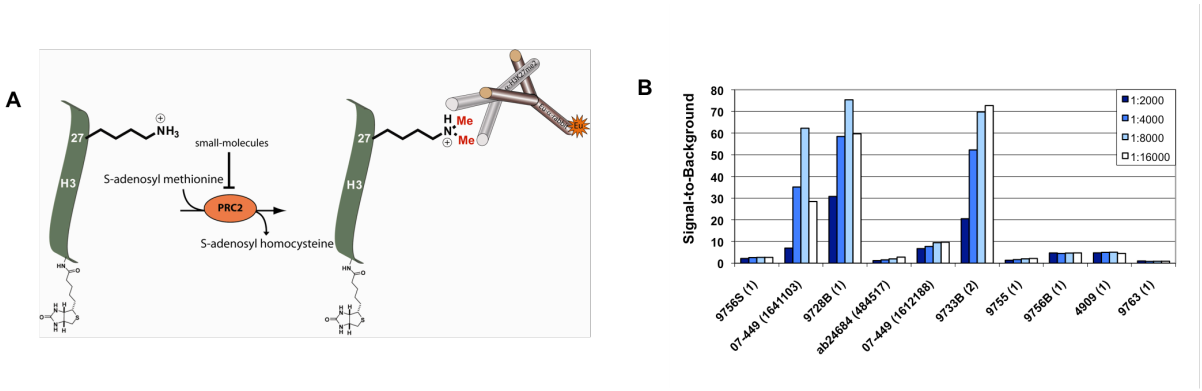

Figure 2.5 Antibody selection for PRC2 DELFIA
(A) Overview of DELFIA. (B) Signal-to-background measured for 10 methylation-specific antibodies at various dilutions in PRC2 DELFIA. Data represent the mean of four replicate wells.

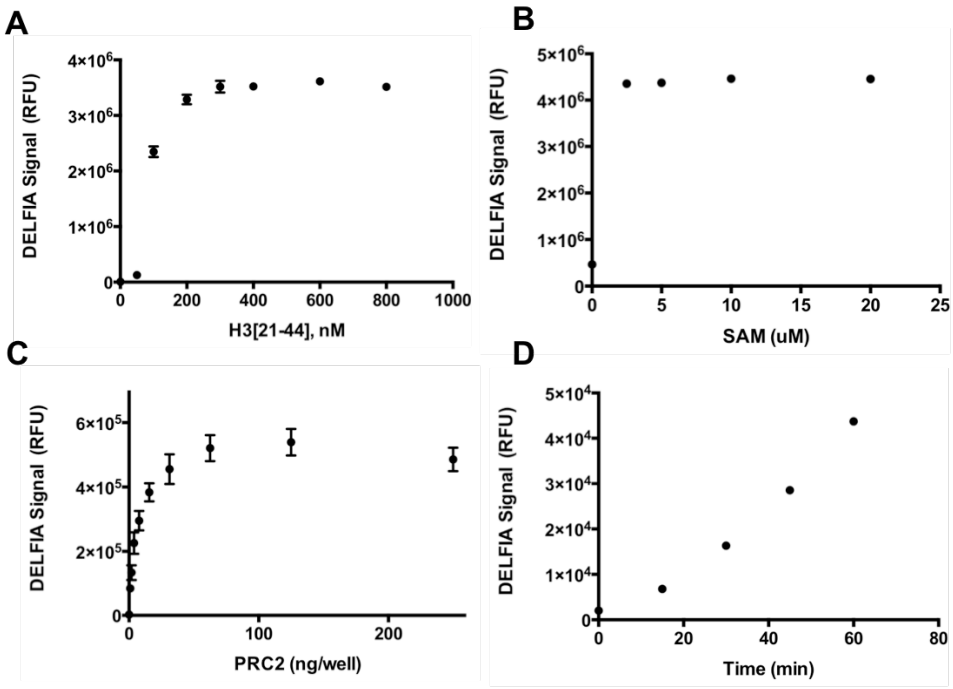

Figure 2.6 Optimization of substrate, SAM, and PRC2 concentrations
Resulting DELFIA signal (RFU) from titration of (A) H3[21-44] peptide, (B) SAM, and (C) PRC2. Reaction time was optimized by time course experiment (D), verifying linear progression over 60 minutes. Data points represent mean and SEM of four replicate wells.

2.2.4 Development of a Cellular H3K27me HCS assay

In anticipation of compound triaging, we next aimed to develop an assay capable of assessing the cellular activity of putative PRC2 modulators. As the number of initial screening hits (or lead analogs) could be large, we limited ourselves to assays that could be adapted to high throughput. Since many PRC2 target genes are known (and repressed by H3K27 methyltransferase activity), we considered HTS-compatible gene-expression assays (GE-HTS) using TurboCapture (31) or Cells-to-CT™ (32) methods for RT-qPCR readout; however, the cost of reagents and variability associated with these measurements persuaded us to consider other approaches.

Since disruption of PRC2 alters global H3K27me levels (33,34), we reasoned that measuring this mark may be an appropriate gauge of intracellular PRC2 activity.

Western blotting and mass spec approaches are effective (9,35), but lack the necessary throughput; ELISAs can be adapted to high-throughput, but require histone purification prior to readout. For these reasons, we pursued development of a high-content assay (HCA) using high-throughput microscopy to detect intracellular H3K27me2/3 via immunofluorescence (IF).

Using HeLa cells, we first screened a panel of H3K27me2/3-specific antibodies for their ability to generate a nuclear signal. While several antibodies nonspecifically stained the cytoplasm, we found three that selectively stained the nucleus with high intensity (Figure 2.7). Selectively of these antibodies towards H3K27 methylation was then determined through use of MODified™ Histone Peptide Arrays, a miniaturized panel of 384 uniquely-modified histone peptides immobilized on cellulose spots affixed to a glass slide. Of the three antibodies tested, two demonstrated absolute selectivity to H3K27 methylation (CS#9728 and CS#9733), while the other bound a wide range of modified H3 peptides (CS#9755). Interestingly, both CS#9728 and CS#9733 were

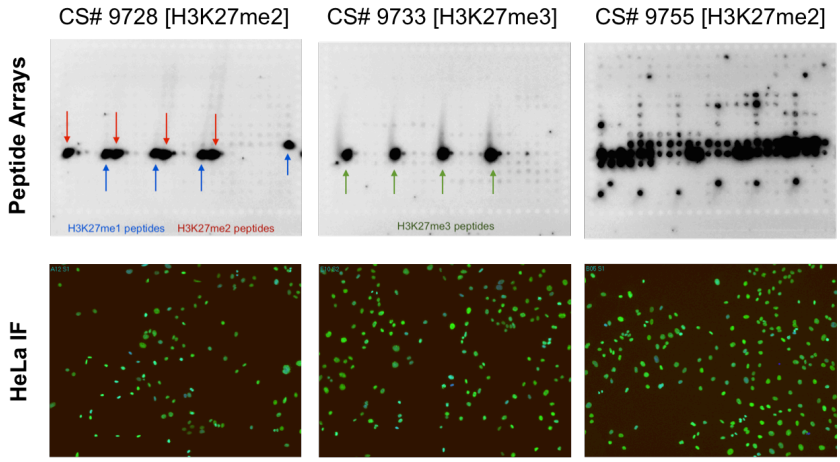

Figure 2.7 Profiling selectivity of H3K27me antibodies
(Top) Binding of H3K27me2/3 antibodies to MODified Histone Peptide Array containing 384 uniquely modified histone peptides. With the exception of those phosphorylated at S28, CS# 9728 binds H3K27me1 and H3K27me2-modified peptides, while CS# 9733 binds only H3K27me3-modified peptides. CS#9755 binds non-selectively to several methylated H3 peptides. (Bottom) IF staining demonstrates nuclear localization of antibodies in HeLa cells.

unable to bind H3K27me peptides harboring H3S28 phosphorylation (H3S28ph). Since H3S28ph is not a suitable substrate for PRC2 (36, **Chapter VII**), this phenomenon was deemed unlikely to severely impact estimation of global H3K27me levels.

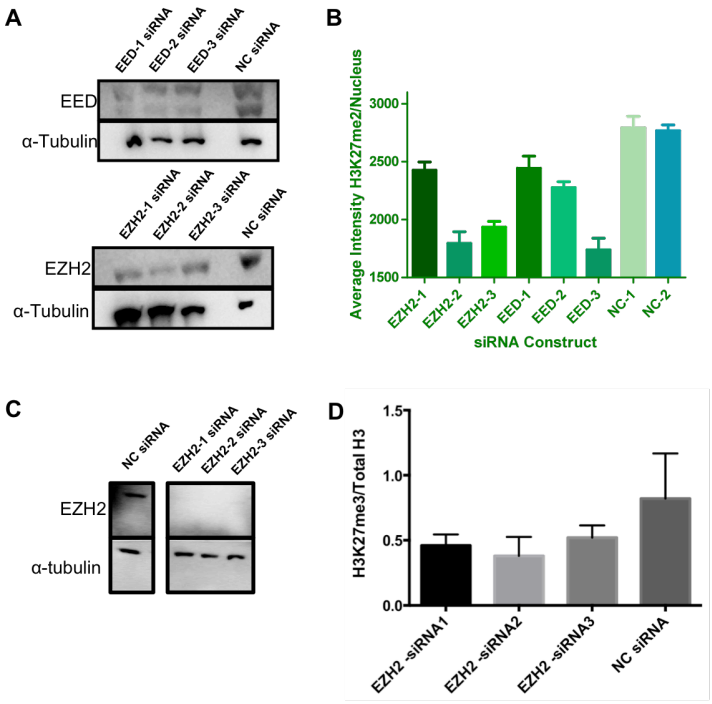

Figure 2.8 H3K27me HCS Assay Development
(A) Western blot confirming knockdown of EED (*top*) and EZH2 (*bottom*) in HeLa cells after 72 hrs (using 3 distinct siRNAs) compared to negative control (NC). (B) Average nuclear intensity of cells stained with H3K27me2 antib**o**dy (CS#9728) post-knockdown. Data represent mean and SEM of eight replicate wells (C) Western blot confirming knockdown of EZH2 prior to histone extraction and (D) H3K27me3 ELISA. Data represent mean and SEM of six replicate wells.

To assess whether this staining was dependent on H3K27me2/3 levels, we used siRNA to knockdown EZH2 and EED, measuring average nuclear fluorescence after staining with our H3K27me-selective antibodies (Figure 2.8A,B). Perturbation of both EZH2 and EED significantly lowered nuclear signal after 72 hrs, suggesting that intracellular H3K27me2/3 levels could be measured reliably by immunofluorescence. To further confirm that 72 hr knockdown of EZH2 resulted in lowered H3K27me levels, we extracted histones and performed an H3K27me3 ELISA (Figure 2.8C,D). Consistent

with IF data, knockdown of EZH2 resulted in a significant reduction (>40%) of H3K27me3.

2.2.5 Discussion and Conclusion

To date, all known selective HMT probes have originated from molecules identified in high-throughput screening campaigns, highlighting screening as a major source of chemical starting points for selective small-molecule probes (9,22). As we aimed to identify small-molecule probes with chemotypes and MOAs distinct from the current set of EZH2 inhibitors, we developed both biochemical (primary; DELFIA) and cell-based (secondary; H3K27me3 HCA) assays suitable for HTS. In order to establish a protein source for screening, we established a platform to express and purify 5-component PRC2 (EZH2-EED-SUZ12-AEBP2-RBBP4), verifying its composition (by western blot and native PAGE) and enzymatic activity by radiometric assay and MALDI-TOF. We then developed a PRC2 DELFIA, following substrate selection, kinetic characterization of PRC2, and identification of a reliable detection antibody. As proper assay development is key to HTS success, we optimized assay parameters through titration of each assay component, confirming assay reproducibility and linearity in the process. Development and siRNA-based validation of an HCA for cellular H3K27me3 levels then followed. These assays were used to screen and triage over 120,000 compounds assayed over two rounds (>60,000 compounds each), identifying several putative PRC2 inhibitors and activators (as described in **Chapter III**).

2.3 Experimental Methods

Cloning PRC2 components and bacmid purification. PRC2 component cDNAs were obtained from Harvard DF/HCC DNA resource core, with the exception of SUZ12 (Origene) and 1XFLAG-EZH2 (kind gift from Bradley Bernstein). Briefly, 1XFLAG-EZH2 (NM_004456), and EED (NM_003797) were sub-cloned into pDEST8, while SUZ12 (NM_015355), AEBP2 (NM_153207), and RbAp48 (NM_005610) were sub-cloned into pDEST10 using the Gateway® LIC (Life Technologies). These constructs were transformed into MAX Efficiency DH10Bac competent cells (Life Technologies) and bacmid DNA was purified using Qiagen's Large-Construct Kit.

PRC2 expression and purification. Sf9 cells cultured in Sf-900 SFM III (Life Technologies) were transfected with bacmid DNA to obtain a viral stock which was subsequently amplified as described in the Bac-to-Bac Baculovirus Expression System Manual (MAN0000414; Life Technologies). Sf9 cells were co-infected with PRC2 component baculoviruses and harvested 96 hrs post-infection. Cells were then lysed via sonication in lysis buffer (20 mM Tris pH 8, 500 mM NaCl, 4 mM MgCl2, 0.4 mM EDTA, 2 mM DTT, 20% glycerol, 0.1% IGEPAL CA-630). Lysates were incubated for 3 hrs with anti-FLAG M2 agarose (Sigma, A2220) at 4°C. After incubation, beads were washed three times with wash buffer (20 mM Tris pH 8, 150 mM NaCl, 2 mM MgCl2, 0.2 mM EDTA, 1 mM DTT, 15% glycerol, 0.01% IGEPAL CA-630) and bound PRC2 was eluted with 3X FLAG peptide (Sigma, F4799) diluted to 200 ug/mL in wash buffer. Eluate was then concentrated and loaded onto a Hi-Load 16/60 Superdex 200 pg column (GE Heathcare). Fractions containing full complex were pooled, concentrated, and stored at -80°C until further use.

Cell lysis, western blotting, nativePAGE, and antibodies. Total protein was isolated from cells via M-PER Extraction Reagent (Pierce) or, for Sf9 expression optimization, 1X-LDS Sample Buffer (Life Technologies). For detection of PRC2 components and confirmation of EED and EZH2 knockdown, purified protein or cell lysate was diluted in 1X LDS Sample Buffer containing 1X Reducing Agent (Life Technologies) and separated on 4-12% Bis-Tris NuPAGE gels (Life Technologies) prior to 1 hr transfer (30V at RT) onto Immobilon PVDF membranes (Bio-Rad). For NativePAGE, purified protein was separated on 4-16% NativePAGE gels (Life Technologies), in the absence of loading buffer or additives, following manufacturer's protocol for separation and western blotting of detergent-containing samples. Anti-EZH2 (CST; #3147), anti-EED (Abcam: ab4469), anti-SUZ12 (Abcam; ab12073), anti-AEBP2 (Abcam; ab107892), anti-RBBP4 (Abcam; ab117746), anti-FLAG M2 (Sigma; F1804), and anti-6XHIS (Abcam; ab18184) antibodies were diluted in 5% non-fat milk or 5% BSA in TBST to manufacturer's specification for overnight primary antibody incubations. Anti-mouse IgG or anti-rabbit IgG HRP conjugates (GE) diluted 1:2500 in primary antibody diluent (incubated at RT for 1hr) was used for chemiluminescence detection with SuperSignal West Pico Chemiluminescent Substrate (Pierce) following TBST washes.

PRC2 radiometric assays. PRC2 was diluted to final concentration in 2X enzyme buffer (50mM Tris HCl pH 8.5, 10 mM DTT). Reactions were initiated with an equal volume of an SAM solution (NEB) containing ^{3}H-SAM (at 25% total SAM concentration; NET155001MC; PerkinElmer) and H3[21-44]-GK-biotin (AnaSpec) or histone octamer (BPS Biosciences) and incubated at room temperature. For initial validation studies, reactions were quenched with 7.5 M guanidium HCl and processed via C4 (histone

octamer) or C18 (peptide) ZipTip® for LSC as described in (16). For kinetic analysis, 100 uL aliquots were quenched in an equal volume of 3.2 mM SAM at various time points in a 96-well plate. After all time points were collected, quenched reactions were transferred to a streptavidin-coated 96-well DELFIA plates (PerkinElmer) and incubated at RT for 1 hr. Unreacted ^{3}H-SAM was removed by washing plates three times with 200 uL of wash buffer (50mM Tris pH 7.4, 150 mM NaCl, 0.05% Tween 20, 0.2% BSA) per well. Modified peptide was then eluted by a 1 hr RT incubation with 100 uL/ well elution buffer (70% ACN, 5% formic acid, 1 mM biotin) and ^{3}H incorporation was measured by LSC (TriCarb 2910; PerkinElmer).

PRC2 MALDI-TOF. PRC2 was diluted to 40 nM in 2X enzyme buffer (50mM Tris HCl pH 8.5, 10 mM DTT). Reactions were initiated with an equal volume of an SAM solution (NEB) containing 2 uM H3[21-44]-GK-biotin (AnaSpec) and incubated at room temperature. Reactions were quenched at various time points with 7.5 M guanidium HCl and processed via C18 (peptide) ZipTip® as described in ref(16). Eluate was dried by GeneVac evaporation and resuspended in 10 uL of 70% ACN with 0.1% TFA. 0.5 uL of resulting solution was combined with an equal volume of 20 mg/mL CHCA matrix (Thermo) and spotted on a Waters 96-sample target plate. After drying, samples were analyzed using MALDI MicroMX mass spectrometer (Waters).

PRC2 DELFIA. PRC2 activity was measured using DELFIA performed on 384-well, white, streptavidin-coated plates (PerkinElmer). Briefly, PRC2 was diluted in 20 uL 2X Enzyme Buffer (50mM Tris HCl pH 8.5, 10 mM DTT) and reactions were initiated with 20 uL of a SAM (NEB) solution containing H3[21-44]-GK-biotin (Anaspec). Plates were incubated at room temperature for 1 hr and then washed three times with 100 uL of

wash buffer (50mM Tris pH 7.4, 150 mM NaCl, 0.05% Tween 20, 0.2% BSA). Fluoroimmunoassay (FI) Buffer (50 mM Tris HCl pH 7.8, 150 mM NaCl, 0.05% Tween 40, 25 μM DTPA, 0.2% BSA, 0.05% BGG) containing a anti-H3K27me2 rabbit IgG (Cell Signaling, #9728) with 691 ng/mL Eu-N1-anti-rabbit IgG (PerkinElmer) was added at 50 uL per well. Following 1 hr incubation at room temperature, the plates were washed three times with wash buffer and 50 uL of Enhancement Solution (PerkinElmer) was added to each well. Plates were incubated for 30 min at room temperature and time-resolved fluorescence (TRF) was measured on Wallac Envision 2104 Multilabel Reader (400 us window, 400 us delay, 320 excitation, 615 emission).

Immunofluorescence. HeLa cells (ATCC) were cultured in DMEM supplemented 10%(v/v) FBS, 1 mM sodium pyruvate, and 100 U mL-1 penicillin-streptomycin. Cells were diluted in culture medium at 5e4 cells/mL and plated in black clear-bottom 96-well plates (Corning, 3904) at 100 uL/well. After 24 hr incubation at 37°C/5% CO2, 100 nL of compound or DMSO vehicle was pinned into each well and cells were incubated for an additional 48 hrs. Treated cells were fixed with 4% paraformaldhyde for 10 min, permeabilized with 0.3% Triton X-100 in PBS for 20 min, and blocked with 3% BSA in PBST for 1 hr at room temperature. Cells were then incubated with primary antibody (anti-H3K27me3 or anti-H3K27me2 antibody; Cell Signaling, #9733 and #9728, respectively) diluted in blocking buffer overnight at 4°C. A mixture of 1 nM Hoechst 33342 (Life Technologies) and 2 ug/mL Alexa Fluor 488 goat anti-rabbit IgG (Life Technologies, A11008) in blocking buffer was then added. Following 1 hr incubation at RT, cells were then imaged on an ImageXpress Micro automated microscope (Molecular Devices) using a 10X objective with laser-based focusing. Image analysis

was performed using the Cell Scoring module in the MetaXpress software (Molecular Devices) to determine average nuclear fluorescence per well.

MODified™ Histone Peptide Array. Histone peptide arrays (ActiveMotif) were blocked with %5 non-fat milk in TBST for 1 hr at RT prior to antibody incubation. Anti-H3K27me2 (CST; #9755), anti-H3K27me2 (CST; #9728), and anti-H3K27me3 (CST; #9733) antibodies were diluted 1:500, 1:2000, and 1:2000, respectively, in blocking buffer and incubated on individual arrays for 1 hr at RT. Arrays were washed with TBST and incubated with anti-rabbit IgG-HRP (GE) diluted 1:2500 in blocking buffer for 1 hr at RT and washed in TBST prior to chemiluminescence detection with SuperSignal West Pico Chemiluminescent Substrate (Pierce).

EZH2 and EED knockdown. HeLa cells (ATCC) were cultured as described above. Cells were plated at 2e5 cells/well in 6-well dishes and transfected with Silencer® Select siRNA (Ambion) for EZH2 (EZH2-1 siRNA, s61343; EZH2-2 siRNA, s61426; EZH2-3 siRNA, s157425) and EED (EED-1 siRNA, s76035; EED-2 siRNA, s159465; EED-3 siRNA, s159467) using X-tremeGENE siRNA transfection reagent according to manufacturer's protocol.

Histone extraction and ELISA. Cells were rinsed with PBS, scraped into ice-cold PBS, and collected via centrifugation at 200 x g for 10 minutes. Pellets were resuspended in 0.2 volumes of 0.4 N HCl and incubated for at least 30 minutes on ice to extract histones. Cellular debris was then cleared by centrifugation at 10,000 x g for 10 minutes. Supernatant containing extracted histones was then neutralized with 0.4 volumes of 1 M sodium phosphate (pH 12.5) and concentration was determined via Bradford assay. H3K27me3 ELISA was performed using Histone H3 trimethyl Lys27

ELISA and, for normalization, Total Histone H3 ELISA kits from ActiveMotif, following manufacturer's protocols.

2.4 References

1. Hendricks CL, Ross JR, Pichersky E, Noel JP, Zhou ZS. An enzyme-coupled colorimetric assay for S-adenosylmethionine-dependent methyltransferases. Analytical Biochemistry. 2004 Mar 1;326(1):100–5.

2. Collazo E, Couture J-F, Bulfer S, Trievel RC. A coupled fluorescent assay for histone methyltransferases. Analytical Biochemistry. 2005 Jul 1;342(1):86–92.

3. Dorgan KM, Wooderchak WL, Wynn DP, Karschner EL, Alfaro JF, Cui Y, et al. An enzyme-coupled continuous spectrophotometric assay for S-adenosylmethionine-dependent methyltransferases. Analytical Biochemistry. 2006 Mar 15;350(2):249–55.

4. Graves TL, Zhang Y, Scott JE. A universal competitive fluorescence polarization activity assay for S-adenosylmethionine utilizing methyltransferases. Analytical Biochemistry. 2008 Feb 15;373(2):296–306.

5. Rathert P, Cheng X, Jeltsch A. Continuous enzymatic assay for histone lysine methyltransferases. BioTechniques. 2007 Nov;43(5):602–604–606passim.

6. Sneeringer CJ, Scott MP, Kuntz KW, Knutson SK, Pollock RM, Richon VM, et al. Coordinated activities of wild-type plus mutant EZH2 drive tumor-associated hypertrimethylation of lysine 27 on histone H3 (H3K27) in human B-cell lymphomas. Proc Natl Acad Sci USA. National Acad Sciences; 2010 Dec 7;107(49):20980–5.

7. Horiuchi KY, Eason MM, Ferry JJ, Planck JL, Walsh CP, Smith RF, et al. Assay development for histone methyltransferases. Assay Drug Dev Technol. 2013 May;11(4):227–36.

8. Diaz E, Machutta CA, Chen S, Jiang Y, Nixon C, Hofmann G, et al. Development and validation of reagents and assays for EZH2 peptide and nucleosome high-throughput screens. J Biomol Screen. 2012 Dec;17(10):1279–92.

9. Kubicek S, O'Sullivan RJ, August EM, Hickey ER, Zhang Q, Teodoro ML, et al. Reversal of H3K9me2 by a small-molecule inhibitor for the G9a histone methyltransferase. Molecular Cell. 2007 Feb 9;25(3):473–81.

10. Quinn AM, Allali-Hassani A, Vedadi M, Simeonov A. A chemiluminescence-based method for identification of histone lysine methyltransferase inhibitors. Mol Biosyst. 2010 May;6(5):782–8.

11. Simard JR, Plant M, Emkey R, Yu V. Development and implementation of a high-throughput AlphaLISA assay for identifying inhibitors of EZH2 methyltransferase. Assay Drug Dev Technol. 2013 Apr;11(3):152–62.

12. Wigle TJ, Provencher LM, Norris JL, Jin J, Brown PJ, Frye SV, et al. Accessing protein methyltransferase and demethylase enzymology using microfluidic capillary electrophoresis. Chem Biol. 2010 Jul 30;17(7):695–704.

13. Vedadi M, Barsyte-Lovejoy D, Liu F, Rival-Gervier S, Allali-Hassani A, Labrie V, et al. A chemical probe selectively inhibits G9a and GLP methyltransferase activity in cells. Nat Chem Biol. 2011 Aug;7(8):566–74.

14. Palmer NA, Sattler SE, Saathoff AJ, Sarath G. A continuous, quantitative fluorescent assay for plant caffeic acid O-methyltransferases. J Agric Food Chem. 2010 May 12;58(9):5220–6.

15. Allali-Hassani A, Wasney GA, Siarheyeva A, Hajian T, Arrowsmith CH, Vedadi M. Fluorescence-based methods for screening writers and readers of histone methyl marks. J Biomol Screen. SAGE Publications; 2012 Jan;17(1):71–84.

16. Suh-Lailam BB, Hevel JM. A fast and efficient method for quantitative measurement of S-adenosyl-l-methionine-dependent methyltransferase activity with protein substrates. Analytical Biochemistry. Elsevier Inc; 2010 Mar 15;398(2):218–24.

17. Li Y, Trojer P, Xu C-F, Cheung P, Kuo A, Drury WJ, et al. The target of the NSD family of histone lysine methyltransferases depends on the nature of the substrate. Journal of Biological Chemistry. American Society for Biochemistry and Molecular Biology; 2009 Dec 4;284(49):34283–95.

18. Sneeringer CJ, Scott MP, Kuntz KW, Knutson SK, Pollock RM, Richon VM, et al. Coordinated activities of wild-type plus mutant EZH2 drive tumor-associated hypertrimethylation of lysine 27 on histone H3 (H3K27) in human B-cell lymphomas. Proc Natl Acad Sci USA. 2010 Dec 7;107(49):20980–5.

19. Glickman JF, Schmid A, Ferrand S. Scintillation proximity assays in high-throughput screening. Assay Drug Dev Technol. 2008 Jun;6(3):433–55.

20. Eskola JU, Näntö V, Meurling L, Lövgren TN. Direct solid-phase time-resolved immunofluorometric assay of cortisol in serum. Clin Chem. 1985 Oct;31(10):1731–4.

21. Gauthier N, Caron M, Pedro L, Arcand M, Blouin J, Labonté A, et al. Development of homogeneous nonradioactive methyltransferase and demethylase assays targeting histone H3 lysine 4. J Biomol Screen. SAGE Publications; 2012 Jan;17(1):49–58.

22. Mayr LM, Bojanic D. Novel trends in high-throughput screening. Curr Opin Pharmacol. 2009 Oct;9(5):580–8.

23. Sundberg SA. High-throughput and ultra-high-throughput screening: solution- and cell-based approaches. Curr Opin Biotechnol. 2000 Feb;11(1):47–53.

24. Brooks HB, Geeganage S, Kahl SD, Montrose C, Sittampalam S, Smith MC, et al. Basics of Enzymatic Assays for HTS. Eli Lilly & Company and the National Center for Advancing Translational Sciences; 2012 Oct 1.

25. Buchser W, Collins M, Garyantes T, Guha R, Haney S, Lemmon V, et al. Assay Development Guidelines for Image-Based High Content Screening, High Content Analysis and High Content Imaging. Eli Lilly & Company and the National Center for Advancing Translational Sciences; 2012 Oct 1.

26. Cao R, Zhang Y. SUZ12 is required for both the histone methyltransferase activity and the silencing function of the EED-EZH2 complex. Molecular Cell. 2004 Jul 2;15(1):57–67.

27. Rea S, Eisenhaber F, O'Carroll D, Strahl BD, Sun ZW, Schmid M, et al. Regulation of chromatin structure by site-specific histone H3 methyltransferases. Nature. 2000 Aug 10;406(6796):593–9.

28. Davidovich C, Goodrich KJ, Gooding AR, Cech TR. A dimeric state for PRC2. Nucleic Acids Research. 2014 Jul 3.

29. Yang J, Copeland RA, Lai Z. Defining balanced conditions for inhibitor screening assays that target bisubstrate enzymes. J Biomol Screen. SAGE Publications; 2009 Feb;14(2):111–20.

30. Cheng Y, Prusoff WH. Relationship between the inhibition constant (K1) and the concentration of inhibitor which causes 50 per cent inhibition (I50) of an enzymatic reaction. Biochemical Pharmacology. 1973 Dec 1;22(23):3099–108.

31. Arany Z, Wagner BK, Ma Y, Chinsomboon J, Laznik D, Spiegelman BM. Gene expression-based screening identifies microtubule inhibitors as inducers of PGC-1alpha and oxidative phosphorylation. Proc Natl Acad Sci USA. National Acad Sciences; 2008 Mar 25;105(12):4721–6.

32. Yuan Y, Hartland K, Boskovic Z, Wang Y, Walpita D, Lysy PA, et al. A small-molecule inducer of PDX1 expression identified by high-throughput screening. Chem Biol. 2013 Dec 19;20(12):1513–22.

33. EZH1 mediates methylation on histone H3 lysine 27 and complements EZH2 in maintaining stem cell identity and executing pluripotency. 2008 Nov 21;32(4):491–502.

34. Pasini D, Bracken AP, Jensen MR, Lazzerini Denchi E, Helin K. Suz12 is essential for mouse development and for EZH2 histone methyltransferase activity. EMBO J. 2004 Oct 13;23(20):4061–71.

35. Jaffe JD, Wang Y, Chan HM, Zhang J, Huether R, Kryukov GV, et al. Global chromatin profiling reveals NSD2 mutations in pediatric acute lymphoblastic leukemia. Nat Genet. 2013 Nov;45(11):1386–91.

36. Lau PNI, Cheung P. Histone code pathway involving H3 S28 phosphorylation and K27 acetylation activates transcription and antagonizes polycomb silencing. Proc Natl Acad Sci USA. 2011 Feb 15;108(7):2801–6.

Chapter III

Screening and identification of PRC2 modulators

Collaborator Contributions

- **Dr. Qiu Wang, Marc Hickey, and Dr. Zarko Boskovic** offered technical assistance for the first round of PRC2 HTS.
- **Dr. Max Majireck, Mengfei Zhang, Dr. Hiroshi Uehara, Enrique Garcia-Rivera, and Dr. James Spoonamore** offered technical assistance for the second round of PRC2 HTS.
- **Dr. Max Majireck and Dr. James Spoonamore** assisted in the selection of PRC2 HTS hit compounds for follow-up studies.

3.1 Introduction

As small-molecule screening has become a major source for starting points in the development of chemical probes and drugs, we aimed to use a suite of HTS-compatible PRC2 assays to screen a diverse set of small molecules, aspiring to identify novel PRC2 inhibitors that could be developed into impactful chemical tools. Toward this goal, we established a critical path for hit selection and compound triaging prior to screening (Figure 3.1), taking into account several aspects that would be desirable for bona fide chemical probes, including sufficient *in vitro* potency, selectivity over related HMTs, and cellular activity that associates well with its biochemical profile (1,2). Final selection of lead compounds would also depend on chemical tractability (for medicinal chemistry optimization), structural novelty, and mechanism of action– with priority given to hit compounds inhibiting in a substrate-competitive or allosteric manner. Given the large number of SAM-dependent enzymes encoded by the human genome (~0.9% of all genes) (3), we speculated that SAM-competitive probes would be more likely to induce off-target cellular effects, depending on the potency and in-class selectivity of the compound.

One significant challenge associated with screening large collections of diverse molecules is distinguishing true modulators (those exhibiting classical target engagement) from those exhibiting artifacts specific to the assay. As a high incidence (>90% in some cases) (4) of these false-positive hits are typically identified through HTS, we included several assays designed to eliminate compounds inhibiting through various nonspecific mechanisms. Compounds that inhibit by such means are known as pan-assay interference compounds or PAINS, as they often arise as frequent hitters in a

large number of primary HTS campaigns against diverse targets (5). Although many PAINS interfere with assay readout by modulation of fluorescence signal (6), or inhibition of signal-generating reporter enzymes (7), a majority of these compounds can directly disrupt the target enzyme through irreversible modification (8), redox effects (9), or, most commonly, sequestration by compound aggregation (10-12).

Nonspecific aggregate-forming compounds are highly sensitive to assay buffer conditions and are often disrupted in the presence of small amounts of detergent (such as Tween 20 or Triton X-100) providing a basis for high-throughput detection (13). As part of our workflow to identify artifacts, we included a detergent-based assay, removing compounds that lost significant activity (>10-fold reduction in IC_{50}) in the presence of Tween 20 (0.1% v/v). To rule out other mechanisms, primary hits were assayed in counterscreens against related HMTs (G9a and NSD2), as many nonspecific compounds are promiscuous in their inhibitory activity. In addition, we implemented a secondary filter, using alternative substrates (full-length histone H3) and an orthogonal detection method (^{3}H-radiolabeling and liquid scintillation counting), to remove false-positives dependent on use of peptide substrates and DELFIA.

This chapter describes the implementation of a PRC2 DELFIA to identify small-molecule modulators within a collection of over 120,000 compounds. After two rounds of screening, 294 confirmed hits were identified and subsequently profiled against G9a and NSD2 to assess selectivity and included in assay interference screens to identify potential false-positives as mentioned above. As PRC2 disruption alters global H3K27me3 levels (14,15), cellular activity was assessed using an H3K27me3 HCS assay to prioritize compounds with putative on-target engagement in cells. In the end,

one apparent PRC2 inhibitor (BRD-K97550475) and one putative activator (BRD-K51079083) were selected for resynthesis and extensive follow-up studies.

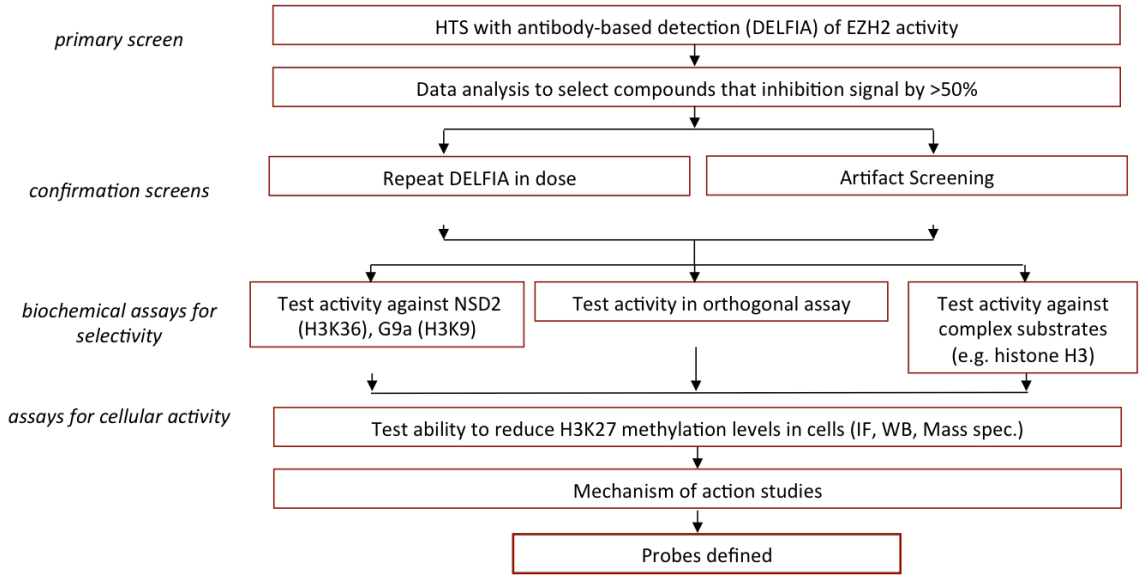

Figure 3.1 Critical path to PRC2 probe discovery

3.2 Results and discussion

3.2.1 Initial screening of 65,333 compounds and hit retest in PRC2 DELFIA

Using PRC2 DELFIA, we conducted an initial screen of over 65,000 compounds. These compounds included ~47,000 compounds derived from diversity-oriented synthesis (DOS) and ~18,000 compounds from standard GPCR, kinase, bioactive, natural product, and other commercial screening decks. To limit reagent costs, we conducted our 384-well primary assay in singlicate, as we would later confirm hits in dose. To measure assay performance and quality for each assay plate, we used a Z-factor statistic (16), assessing the degree of separation between DELFIA signal distributions of negative control (DMSO) and positive control (PosCon) wells. Since no potent small-molecule inhibitors for PRC2 were known at the time of the screen, options

for positive controls were limited to SAH and sinefungin, two non-selective SAM-competitive compounds that exhibited prohibitively weak activity in our assay. Furthermore, the inclusion of wells lacking a key reagent (such as enzyme or SAM) was technically challenging given available automation. To address this problem, we used 3 uM biotin as a control, as it would compete with biotinylated-product immobilization on streptavidin-coated DELFIA plates and effectively lower signal. While limited in its utility, this positive control allowed us to account for high-background generating events occurring with detection. Lastly, to correct for systematic variations in signal within our assay plates (due to temperature, evaporation, or instrumentation), we included 'base plates' in which only DMSO (no compound) was added to assay wells. Throughout the screen, two 'base plates' were added to each batch of assay plates (typically ~30)—one plate at the beginning and end of each run.

For a majority of assay plates, we were able to maintain high S/B with strong separation between PosCon and DMSO wells (average Z' Factor >0.5; Figure 3.2A,C). Using a normalized activity cutoff of <50%, 327 compounds showing apparent inhibition of PRC2 were called, yielding a 0.5% hit rate (Figure 3.2B). While enriched in compounds originating from the natural products library (~30%), hit compounds from each major screening deck were identified— including Bioactives (14%), DOS (8%), HDAC-biased (5%), GPCR (16%), Kinase (15%), Structurally Diverse (5%), and Commercial (10%) collections.

Of the identified hits, we were able to obtain 305 compounds for retest in 8-point dose, as several were unavailable from our compound management service. After two rounds of retest assays, 270 hits were confirmed (89% retest rate), showing does-

responsive inhibition with varying potencies in the high nM to high uM range. The statistical screening and retest summary is included in Table 3-1 below.

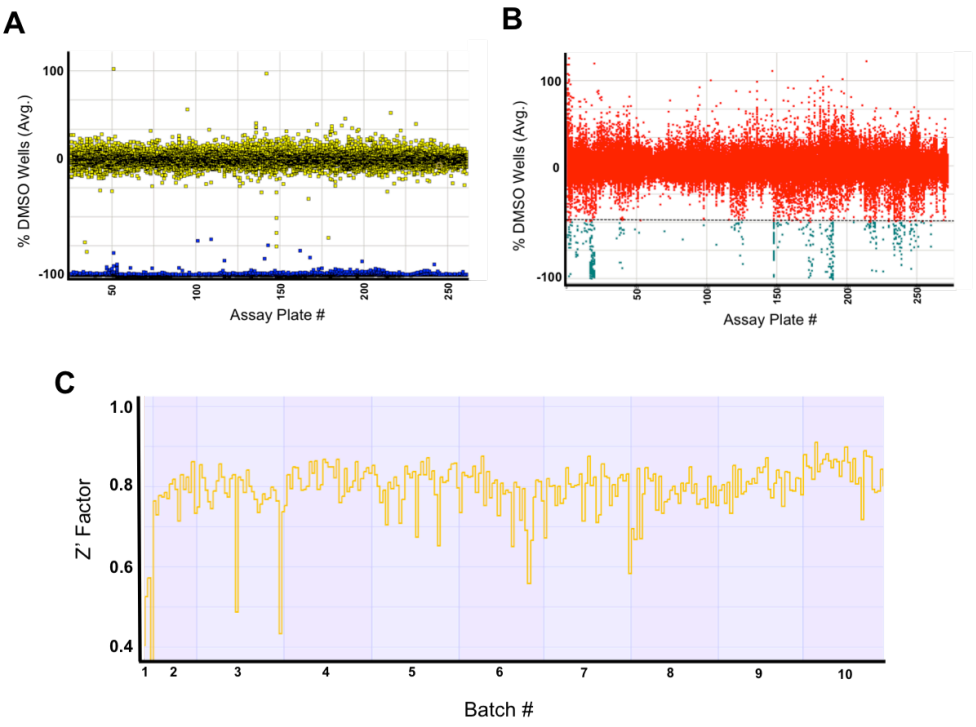

Figure 3.2 First round of primary screening using DELFIA
(A) Scatter plot showing distribution of normalized DELFIA signal from DMSO wells (yellow) and positive control (PosCon) wells (3 uM biotin; blue) across all assay plates. (B) Distribution of normalized DELFIA signal from compound wells across all assay plates. Compounds lowering signal by >50% were called hits (shown in teal) (C) Z' factor (comparing PosCon wells to DMSO) for each assay plate across batches.

Table 3-1 Summary statistics for first round of HTS

Primary Screening Summary (Round 1)	
Total compounds screened	65,333
Hit rate	0.50%
Number of assay plates	227
Average Z' Factor	>0.5
Number of hits (>50% inhibition)	327
Number of hits for retest	305
Confirmed hits	270
Retest rate	89%
Potency range (IC50)	
>10 uM	128
<10 uM	129
<1 uM	8

3.2.2 Artifact elimination and counterscreening against G9a and NSD2

We next aimed to triage our hits by eliminating artifact compounds and assessing compound selectivity for PRC2 over two related HMTs, G9a and NSD2. As discussed earlier, many false positives arise as a result of direct interference with assay signal (e.g. fluorescence, luminescence, etc.). To identify compounds lowering signal through disruption DELFIA detection, we performed a PRC2 DELFIA, pinning hit compounds into assay plates *after* reaction and proceeding immediately to antibody incubation and detection. In an alternative version of this assay, compounds were pinned in the absence of enzyme, but in the presence of biotinylated product peptide (H3[21-44], K27me2). No compounds were found to lower signal in either control assay, suggesting that all hit compounds lowered signal, specifically or nonspecifically, through disruption of PRC2 activity.

Since G9a DELFIA had been previously reported (17) and an HTS–ready NSD2 DELFIA was developed in our lab (18), we aimed to prioritize hits based on selectivity for PRC2 over these two methyltransferases. Using these DELFIAs, we counterscreened all 270 confirmed hits in 8-point dose, identifying 14 compounds that inhibited both G9a and NSD2, 54 compounds that inhibited only NSD2, 56 compounds that inhibited only G9a, and 146 compounds that showed no detectable activity on either HMT at the highest concentrations tested (Figure 3.3). We chose 92 compounds that had at least 5-fold selectivity over G9a and/or NSD2 and an IC_{50} of less than 10 uM against PRC2 for further study. The potency (IC_{50}) and PRC2 selectivity values (ratio of PRC2 IC_{50} over G9a or NSD IC_{50}) for compounds inhibiting G9a and NSD2 are summarized Table S3-1 and Table S3-2, respectively.

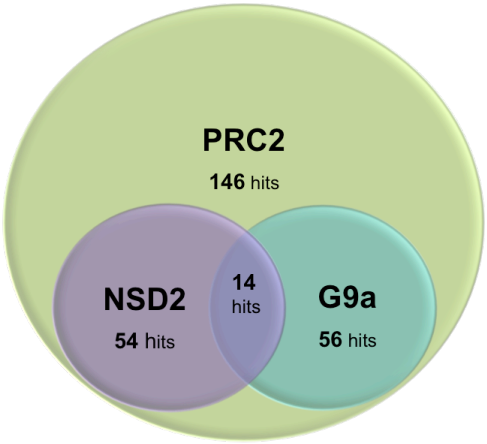

Figure 3.3 Summary of HMT counterscreen
All 270 of the confirmed PRC2 hits were screened against NSD2 and G9a using established DELFIAs. The diagram above illustrates the selectivity of PRC2 hits, showing that nearly half of compounds inhibit other HMTs to varying degrees. Compounds exhibiting >50% activity at the highest tested dose were deemed hits.

3.2.3 Detergent-based assay for identification of aggregator compounds

As mentioned previously, artifactual inhibition can occur through a variety of mechanisms, but one most challenging to predict based on structure alone, is aggregation (10). Depending on the buffer conditions, some molecules can form large colloidal aggregates in solution, leading to nonspecific inhibition through sequestration of target enzyme (10). One such method to identify these compounds is to evaluate their sensitivity to detergent, as many aggregators will lose activity in the presence of small concentrations of Tween 20 or Triton-X100—presumably through colloidal disruption (13).

As our assay buffer lacked detergent, we assayed the 92 prioritized compounds in the presence and absence of 0.01% Tween 20, noting any significant changes in activity against PRC2 (IC_{50}). Of the compounds tested, several exhibited significant attenuation of activity (>0.5 logIC50 shift) in the presence of detergent, with many losing activity entirely. As they were likely inhibiting through aggregation-based mechanism,

these compounds were de-prioritized and not considered for further study. A total of 51 compounds were deemed insensitive to detergent addition, showing little (<0.5 logIC_{50} shift) or no loss of activity, and further evaluated in downstream assays (e.g. H3K27me3 HCA). Examples of putative inhibitors exhibiting differential detergent sensitivity are illustrated in Figure 3.4 below; the results of this assay are summarized in their entirety in Table S3-3.

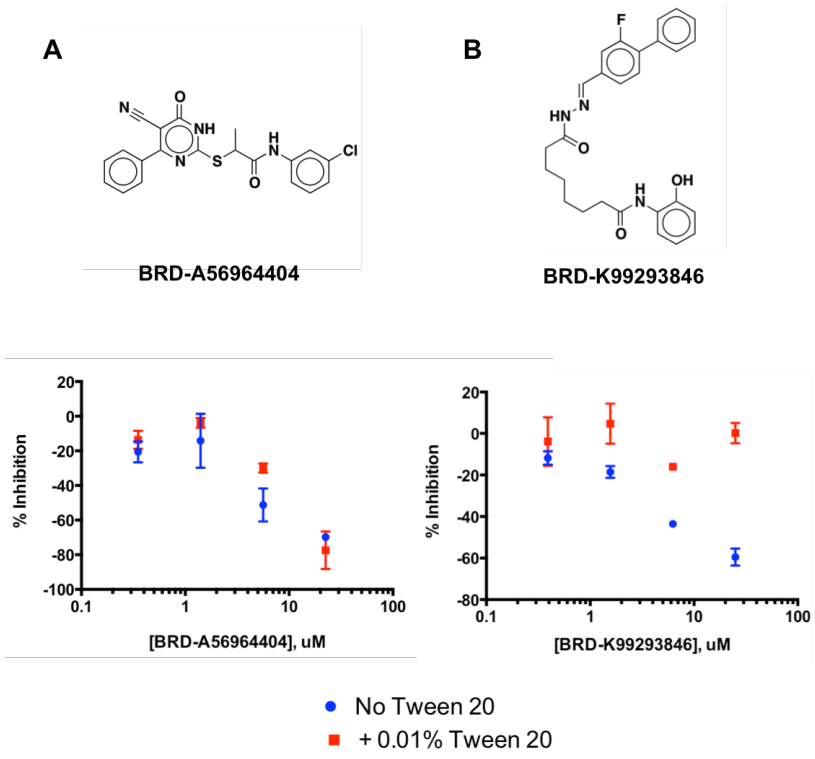

Figure 3.4 Examples of detergent-sensitive and -insensitive compounds
(A) BRD-A56964404 (*top)* potency shifts slightly in the presence of detergent (*bottom*), while (B) BRD-K99293846 (*top*) loses complete activity in the presence of detergent (*bottom*). Data points represent the mean and standard error of triplicate measurements.

3.2.4 Assessing cell-based activity with an H3K27me3 HCS assay

To further triage our list of prioritized compounds, we evaluated the top 51 inhibitors in an H3K27me3 HCA, treating HeLa cells with DMSO vehicle or various concentrations of compound. Following 48 hr incubation, cells were stained for

H3K27me3 and imaged by automated microscope (IX Micro), using an optimized immunofluorescence protocol (described in the previous chapter). Average nuclear

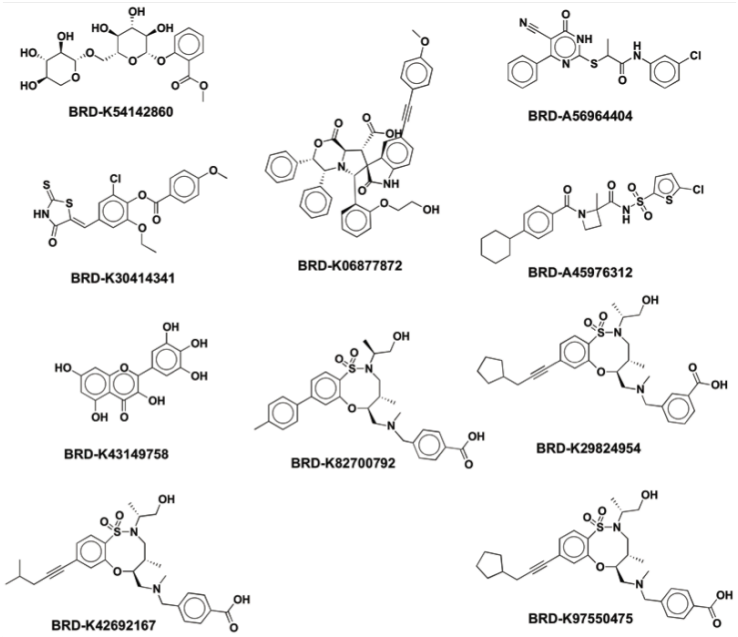

Compound Name	Z-Score (H3K27me3)
BRD-K43149758	-1.09
BRD-A25705184	-1.23
BRD-A56964404	-1.68
BRD-K06877872	-1.71
BRD-K29824954	-1.75
BRD-K82700792	-1.89
BRD-K54142860	-2.00
BRD-K42692167	-2.28
BRD-K30414341	-2.43
BRD-A45976312	-2.99
BRD-K97550475	-4.30

Figure 3.5 Compounds scoring in the H3K27me3 HCA
Structures of compounds lowering average nuclear fluorescence with a Z-score < -1.0 in an H3K27me3 HCS assay. Over-represented in this list are 8-membered ring sultams. See **Experimental Methods** for details on Z score calculation.

fluorescence and total cell number were determined for each treatment condition by image analysis –using the Multi Wavelength Cell Scoring in MetaXpress. Since background fluorescence (attributed to nonspecific antibody interactions, autofluorescence, etc) could not be assessed, we used a Z-score metric (see Experimental Methods) to identify compounds that, compared to the signal distribution of DMSO wells, significantly lowered average nuclear fluorescence signal. Of the 51 compounds evaluate, only 10 were found to lower H3K27me3 signal by at least one standard deviation. Over-represented in this list was a cluster of four 8-membered ring sultams—members of the SNAr SO_2 DOS library (Figure 3.5). BRD-K97550475, the top hit in this assay and a member of the SNAr library, appeared to lower average nuclear

fluorescence, while not significantly affecting cell number (Figure 3.6). Given its apparent activity in both cellular and biochemical assays (and the number of related compounds exhibiting presumed cellular activity), BRD-K97220475 was selected for resynthesis and further study. These efforts are described in detail in **Chapter IV**.

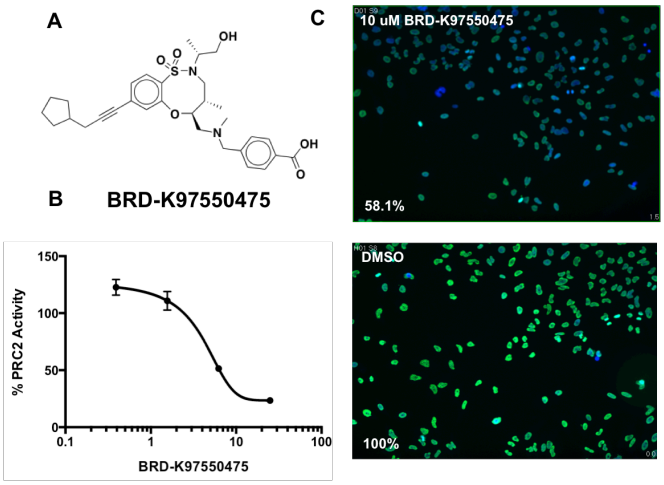

Figure 3.6 BRD-K97550475 activity in PRC2 DELFIA and H3K27me3 HCA
(A) Structure of BRD-K97550475. (B) Activity in PRC2 DELFIA. Data points represent the mean and standard error of triplicate measurements. (C) Raw image of H3K27me3 staining in the presence of 10 uM BRD-K97550475 (*top*) versus DMSO (*bottom*) suggests cell-based activity.

3.2.5 Screening of an additional 58,917 DOS compounds in PRC2 DELFIA

In hopes of uncovering more potent PRC2 modulators and additional starting points for probe development, we used a modified PRC2 DELFIA to screen an additional 58,917 DOS compounds. As the available compound libraries had been reorganized with the addition of new DOS compounds, we screened a total of 66,203 DOS compounds, assaying 7,286 DOS compounds included in the previous screen. Represented in the set of non-overlapping DOS molecules were novel scaffolds—including members of Pyridone, THQ, Oxazocane, and Tricyclic glycal libraries—as well as new analogs of previously explored scaffolds (e.g. RCM, Azetidine, and SO2 SnAR).

Aiming to lower the number of potential aggregator hits and further bias for identification peptide-competitive modulators, we included 0.01% Tween 20 in the assay buffer and lowered peptide concentration from 300 nM to 62.5 nM H3[21-44] (or 0.5X K_M). Substrate methylation appeared linear over the course of an hour, so previous reaction time and SAM concentration (2X K_M) were maintained. Given the reduced signal (~10 S/B) resulting from the new substrate concentration, we performed our assay in duplicate to compensate for potential increases in plate-to-plate variation. As before, 3 uM biotin was used as a positive control for Z' Factor calculations and DMSO base plates were employed to correct for variations within each assay plate. Comparable to the initial PRC2 DELFIA screen, we noted good separation between signal distributions for biotin and DMSO wells within assay plates, maintaining an average Z' Factor of 0.55 (Figure 3.7).

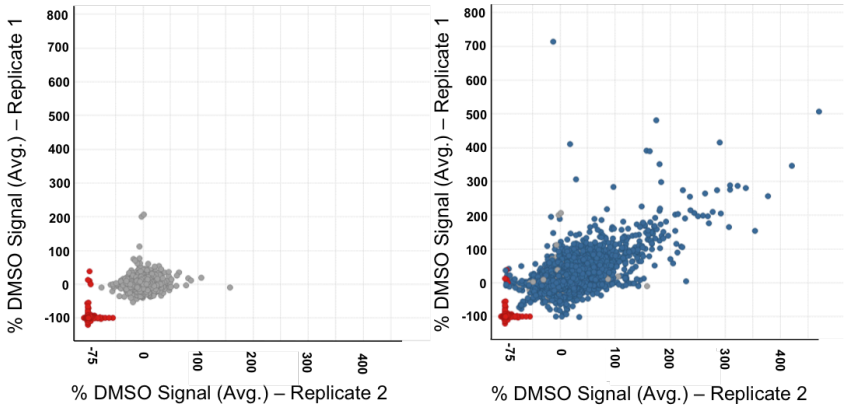

Figure 3.7 Second round of primary screening using PRC2 DELFIA
(*Left)* Scatter plot showing the distribution of normalized DELFIA signal across replicates for DMSO (shown in grey) and poscon (3 uM biotin; showing in red) wells across assay plates. (*Right*) Scatter plot showing the distribution of normalized DELFIA signal across replicate test wells (shown in blue) overlaying DMSO and poscon distributions.

A total of 191 primary hits were called, each of which lowered PRC2 DELFIA signal by >50% in a single replicate and/or >30% in both replicates. Interestingly, a large number of high signal outliers (potential PRC2 activators) were identified among

this collection of DOS molecules. Compounds that increased DELFIA signal by >50% relative to DMSO were deemed hits (274 total compounds) and ordered for retest. All primary hits (both activators and inhibitors) were retested in 8-point dose. Of the putative inhibitors, we identified 60 compounds that lowered signal by >30% at the screening dose (25 uM), but only 24 compounds exhibited reproducible dose-responsive inhibition with IC_{50} values <20 uM. Notably, over half (13/24) of these compounds were structurally related to the previously identified 8-membered ring sultams (e.g. BRD-K97550475), while the remainder clustered into various other structural categories (e.g. Pyridone, RCM, THQ/Povarov). Of the potential activators, 235 of the 274 hits retested (>50% increase in signal) at the screening dose; however, only 23 compounds could increase DELFIA signal in a dose-responsive manner. These putative activators clustered into five major structural categories, all with AC_{50} values (assuming maximum activation of 10-fold) in the 3-25 uM range. Screening statistics and retest summary are included in Table 3-2 below**,** while example structures for all clustered inhibitors and activators, along with measured activity (IC_{50} values), are included in Figure 3.8.

Table 3-2 Summary statistics for second round of screening

Primary Screening Summary (Round 2)	
Total compounds screening	66,203
Hit rate (putative activators + inhibitors)	0.70%
Number of assay plates	407
Average Z' Factor	>0.55
Number of hits (>50% inhibition in singlicate, >30% both reps)	194
Number hits (>50% activation in both replicates)	274
Number of hits for retest	468
Confirmed hits (inhibitors)	60
Confirmed hits (activators)	235
Retest rate (Inhibitors/activators)	31% / 87%
Potency range of inhibitors (IC50)	
>10 uM	42
<10 uM	17
<1 uM	1

A

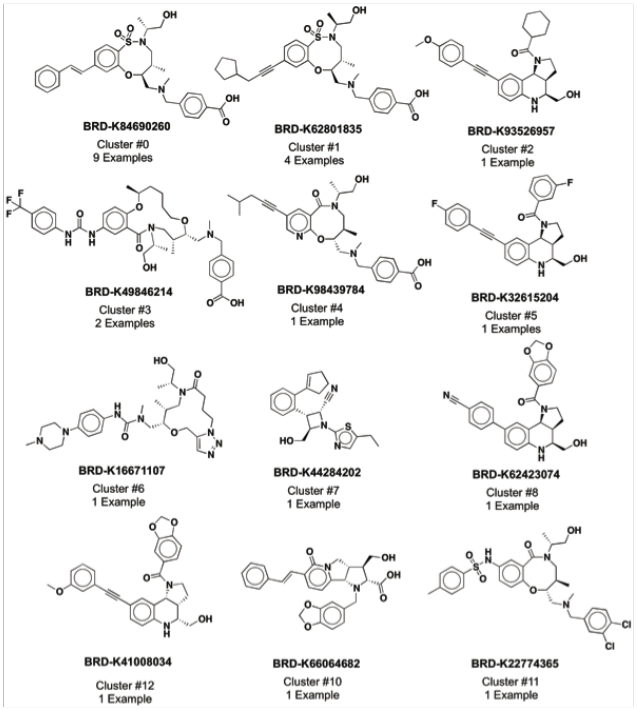

Coumpound Name	Cluster #	IC50 (M)
BRD-K17110283	0	5.493E-06
BRD-K97316517	0	6.796E-06
BRD-K41488990	0	1.395E-06
BRD-K84690260	0	1.638E-06
BRD-K18448590	0	1.192E-05
BRD-K17545487	0	3.578E-06
BRD-K18228465	0	1.807E-06
BRD-K19784967	0	1.903E-06
BRD-K17545487	0	3.578E-06
BRD-K30288623	1	2.754E-06
BRD-K62801835	1	4.891E-07
BRD-K90287226	1	1.687E-06
BRD-K97550475	1	1.387E-06
BRD-K93526957	2	1.497E-05
BRD-K49846214	3	3.438E-06
BRD-K55066668	3	2.818E-06
BRD-K98439784	4	2.007E-05
BRD-K79998087	5	6.446E-06
BRD-K16671107	6	2.253E-06
BRD-K44284202	7	1.215E-05
BRD-K62423074	8	1.23E-05
BRD-K66064682	10	6.532E-06
BRD-K22774365	11	4.482E-05
BRD-K41008034	12	4.474E-06

B

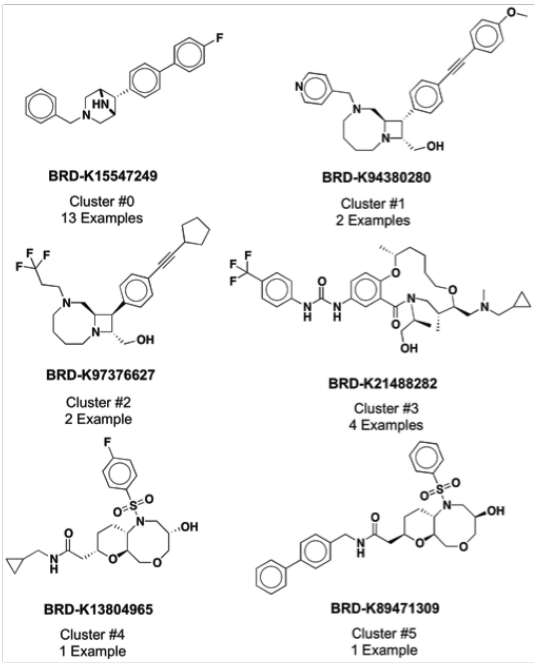

Compound Name	Cluster #	AC50 (M)
BRD-K29779756	0	7.640E-06
BRD-K88851479	0	3.125E-05
BRD-K25024116	0	2.978E-05
BRD-K91224798	0	7.175E-06
BRD-K88803419	0	2.461E-05
BRD-K41879705	0	2.495E-05
BRD-K58461886	0	4.287E-06
BRD-K74663820	0	1.682E-05
BRD-K83118423	0	1.079E-05
BRD-K89317027	0	3.125E-05
BRD-K15547249	0	1.871E-05
BRD-K76211354	0	1.352E-05
BRD-K51079083	0	3.456E-06
BRD-K94380280	1	5.058E-05
BRD-K98855854	1	5.485E-06
BRD-K97376627	2	6.291E-05
BRD-K99959381	2	5.081E-05
BRD-K21488282	3	3.105E-05
BRD-K82862028	3	1.842E-05
BRD-K23999919	3	4.232E-05
BRD-K02569795	3	3.139E-05
BRD-K13804965	4	4.095E-05
BRD-K89471309	5	3.125E-05

Figure 3.8 Potency (IC_{50} or AC_{50}) and representative structures of clustered activators and inhibitors identified in the second iteration of PRC2 HTS.
Along with complete lists of potency values (IC_{50} or AC_{50}), representative structures for each cluster of identified (A) inhibitors and (B) activators are shown above. For AC_{50} determination, S_0 was set to 100% activity and S_{inf} to 500% activity for all activators. See **Experimental methods** for details on AC_{50} and IC_{50} calculations and compound clustering.

We next aimed to determine whether these additional hit compounds displayed apparent PRC2 modulation through assay disruption or aggregation-based mechanisms. Given the small number of activators and inhibitors identified, we used low-throughput dynamic light scattering (DLS) to determine if our compounds aggregated near IC_{50} concentrations in PRC2 assay buffer. Even up to 100 uM, no particle formation was detected for any compounds tested, suggesting that they were inhibiting or activating by mechanisms distinct from aggregation. Furthermore, detection-interference counterscreens also confirmed that our selected inhibitors and activators were not artifacts of DELFIA readout. Encouraged by these results, we selected the top three novel and most potent clusters of inhibitors—representing RCM (Cluster #3), Pyridone (Cluster #10), and Povarov (Cluster #12) chemical series—for further study. As mechanistic studies on BRD1835, an 8-membered ring sultam, were underway at the time of their identification, newly identified SNAr SO_2 members were not explored further. Characterization of the largest cluster of activators (Cluster #0; Figure 3.8B) is described in detail in **Chapter V.**

3.2.6 Initial characterization of RCM, Pyridone, and Povarov series inhibitors

Strong stereochemical preferences in regard to compound activity are typically suggestive of true target engagement, as small-molecule binding occurs in the context of a chiral protein environment. The DOS compound libraries available at the Broad Institute are designed to enable rapid identification of stereochemical structure-activity relationships (SSAR) (19), containing a large number of stereoisomers (if not all) for any given DOS molecule. In order to establish preliminary SSAR for the RCM, Pyridone, and Povarov series compounds, we obtained and assayed (in 8-point dose) all available

stereoisomers of the most potent compounds represented in each of the top three inhibitor clusters identified. Overall, we evaluated the activity 14 stereoisomers of BRD-K55066668 (RCM) as well as the corresponding enantiomers of BRD-K66064682 (Pyridone) and BRD-K41008034 (Povarov).

For all chemical series tested, no striking SSAR (i.e. absolute stereoselectivity) could be established. Pyridone enantiomers exhibited similar activity against PRC2, with BRD-K66064682 and its enantiomer, BRD-K57393707, inhibiting at 7 and 3.2 uM, respectively (Figure S3.1). Both Povarov compounds tested were found to have significant issues with purity—a phenomenon later confirmed to be a common issue with members of this library. Only the enantiomer of the initial hit compound was active against PRC2 (BRD-K34245999; 4.7 uM IC_{50} at 33% purity) due to the remarkably low purity (2%) of BRD-K41008034 (Figure S3.2). Lastly, while stereoisomers of the hit RCM compound (BRD-K55066668) were found to inhibit PRC2 over a wider range of potencies (1-30uM), no clear SSAR patterns emerged (Figure S3.3).

While efforts to establish SSAR failed to deliver evidence supporting clear PRC2 engagement, we continued to characterize these compounds on the basis of HMT selectivity and MOA. For these studies, we focused on the most potent compounds resulting from SSAR studies (RCM- BRD-K55066668, Pyridone- BRD-K57393707, and Povarov-BRD-K34245999). Using a G9a DELFIA, we found that all compounds inihibited PRC2 with absolute selectivity over this HMT, as they had no activity on G9a at concentrations up to 100 uM (Figure 3.9B). To determine whether PRC2 inhibition was competitive for peptide or cofactor, we tested the activity of each compound in PRC2 DELFIA, measuring IC_{50} under varying SAM and peptide concentrations. While

the K_i (true potency) for competitive inhibitors should be invariant under differing substrate and cofactor conditions, the IC_{50} is known to change in a manner proportional to the ratio of substrate or cofactor concentration to its respective K_M (20). While all compounds

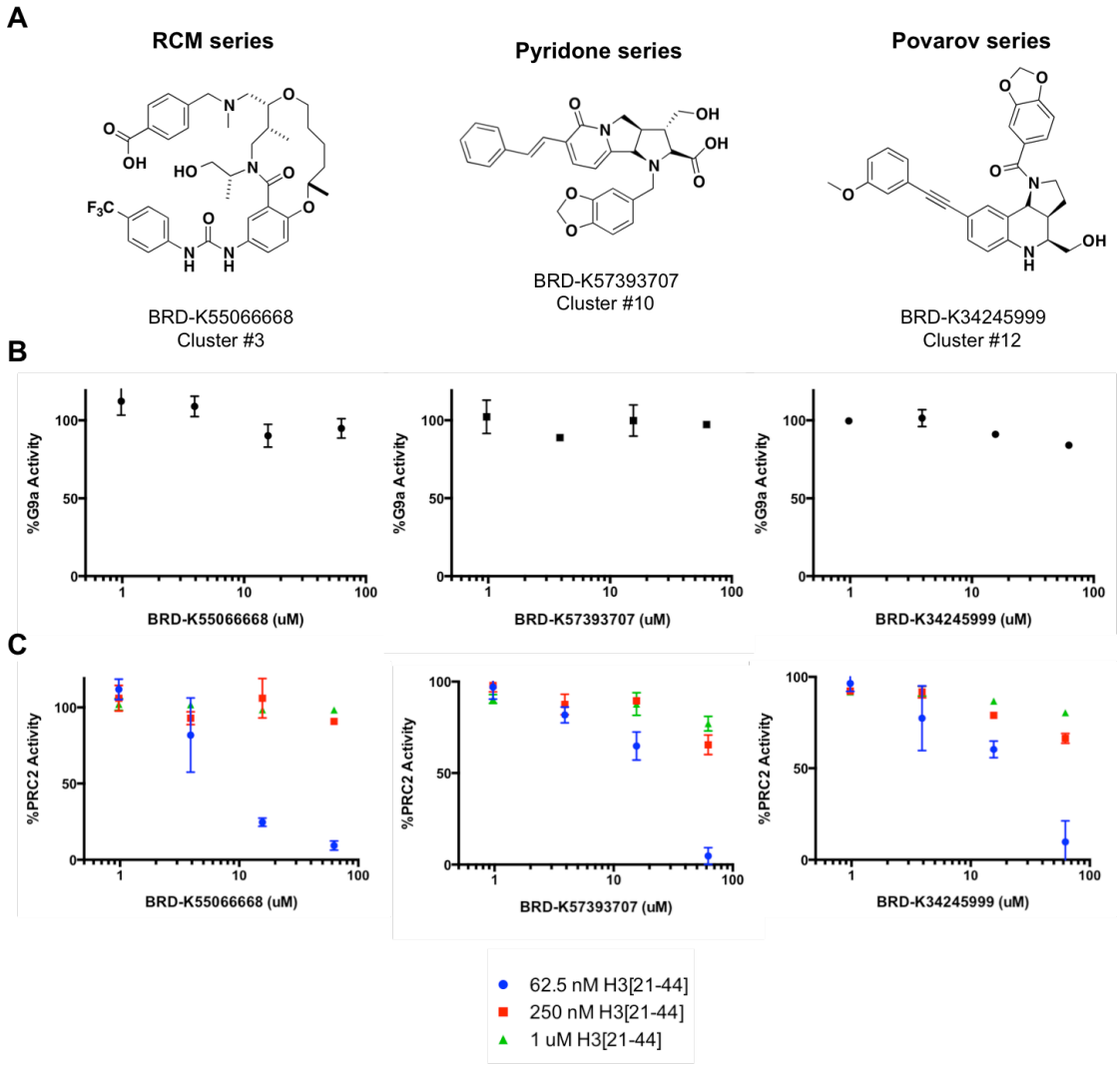

Figure 3.9 G9a DELFIA and initial MOA studies of representative members of top PRC2 inhibitor clusters identified in second iteration of screening.
(A) Structures of BRD-K55066668 (RCM), BRD-K57393707 (Pyridone), and BRD-K34245999 (Povarov) and their associated activities in (B) G9a DELFIA. (C) Initial MOA studies measuring the activity of each compound in PRC2 DELFIA under different substrate (H3[21-44]) concentrations. Data points represent the mean and standard error of triplicate measurements in all assays.

retained similar potency in the presence of up to 50 uM SAM (25X K_M), each one of our top hits appeared to be highly sensitive to the addition of peptide, losing activity completely in the presence of 250 nM (~1.5X K_M) peptide (Figure 3.9C). These results suggested that all compounds identified might inhibit through a peptide-competitive mechanism.

We next explored whether these compounds could lower H3K27me3 levels in HeLa cells using the previously described HCA assay, testing compounds in 12-point dose. Results for two of the hit compounds are shown in Figure 3.10. While global H3K27me3 levels appeared to decrease in the case of BRD-K55066668 and *increase* in the case of BRD-K55066668, cell number appeared to drop at all active concentrations of compound, suggesting that these alterations in average nuclear fluorescent signal were mere artifacts of immunostaining and imaging dead or dying cells.

Given their lack of cellular activity, flat SSAR, and remarkable sensitivity to the addition of peptide, we next explored whether these compounds could be behaving through peptide-binding or peptide–sequestration mechanisms. Detailed studies into BRD1835 found that some compounds able to inhibit PRC2 exhibit this behavior, endowing them with *apparent* substrate-competitive activity. Using a fluorescently labeled version of the peptide substrate, we explored whether high concentrations of each of these compounds could generate a detectable FP signal. As suspected, each of these compounds, to varying degrees, could increase FP signal over DMSO (Figure 3.11), suggesting the formation of peptide-compound complexes (of presumably high molecular weight). While these compounds could be engaging PRC2, the current data

support a novel, potentially artifactual mechanism undesirable of a chemical probe. This mechanism is further discussed in **Chapter IV.**

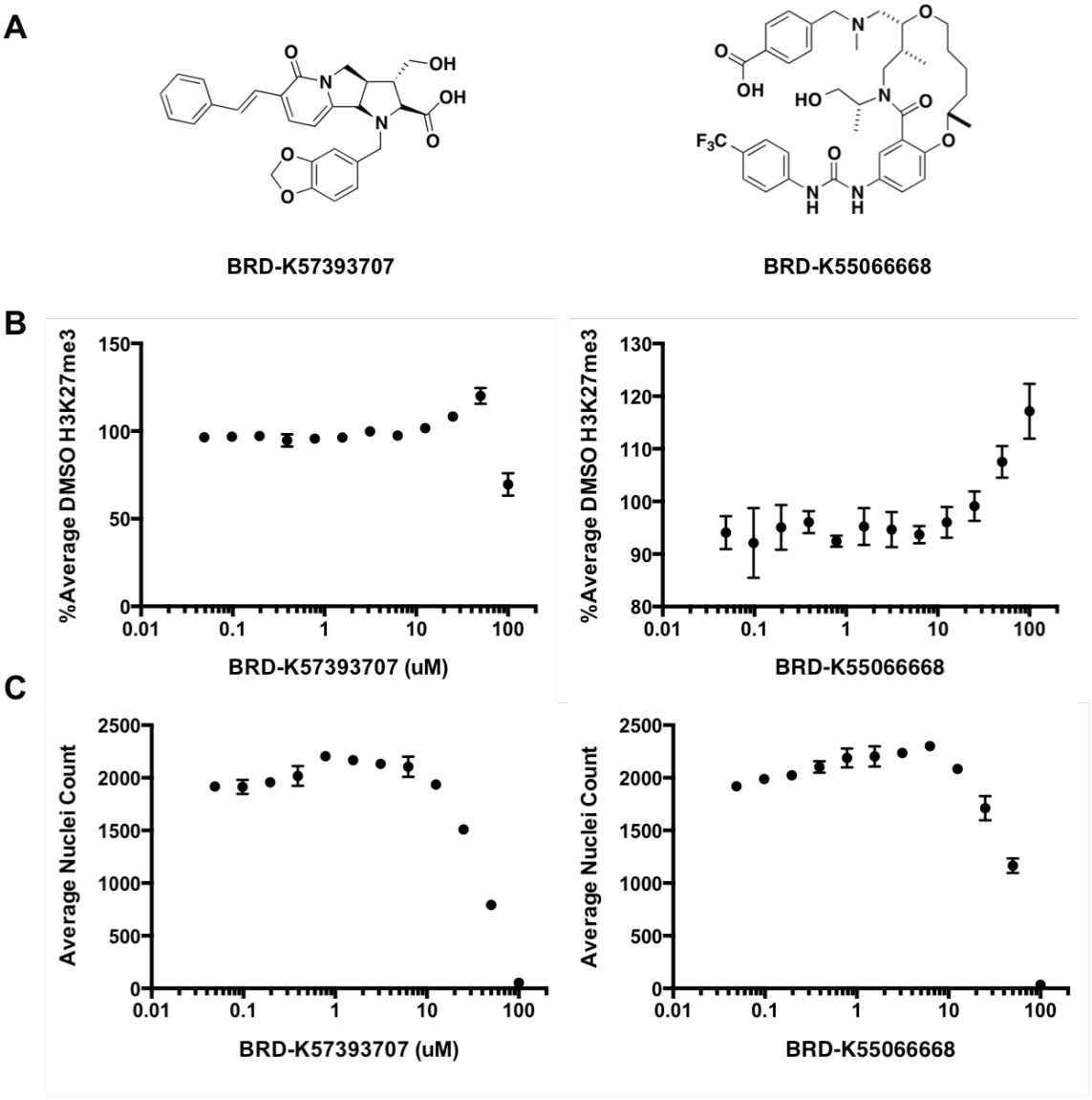

Figure 3.10 Activity of top Pyridone and RCM inhibitor analogs in H3K27me3 HCA
(A) Structures of top Pyridone (BRD-K57393707) and RCM (BRD-K55066668) compounds arising from SSAR studies of selected PRC2 inhibitor candidates. (B) Effect of various concentrations of BRD-K57393707 and BRD-K55066668 on DMSO-normalized average nuclear fluorescence (%Average DMSO H3K27me3) and (C) cell number in H3K27me3 HCA. Data points represent the mean and standard error of triplicate measurements in all assays.

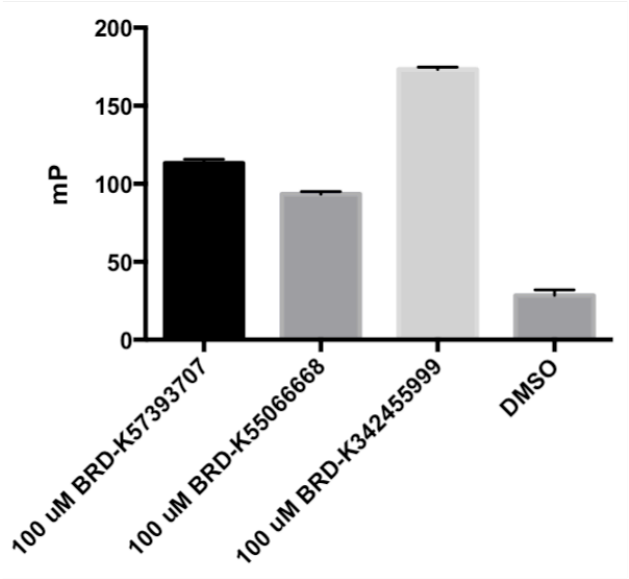

Figure 3.11 HiLyte™ Fluor 488-H3[21-44] FP assay on top RCM, Pyridone, and Povarov PRC2 inhibitors. Activity of RCM (BRD-K55066668), Pyridone (BRD-K57393707), and Povarov (BRD-K342455999) PRC2 inhibitor candidates (100 uM) in peptide-binding FP assay using 31.25 nM HiLyte™ Fluor 488-H3[21-44]. Compared with DMSO, all compounds substantially increased mP signal, suggesting an interaction with peptide. Data points represent the mean and standard error of four replicate measurements.

3.3 Experimental methods

PRC2 HTS DELFIA. PRC2 activity was measured using DELFIA performed on 384-well, white, streptavidin-coated plates (PerkinElmer). In short, PRC2 was diluted in 20 uL 2X Enzyme Buffer (50mM Tris HCl pH 8.5, 10 mM DTT) with (second HTS) or without (first HTS) 0.02% Tween 20, 100 nL compound was pinned, and reactions were initiated with 20 uL of a SAM (NEB) solution containing (600 nM for initial HTS and 125 nM for second HTS) H3[21-44]-GK-biotin (Anaspec). Plates were incubated at room temperature for 1 hr and then washed three times with 100 uL of wash buffer (50mM Tris pH 7.4, 150 mM NaCl, 0.05% Tween 20, 0.2% BSA). Fluoroimmunoassay (FI) Buffer (50 mM Tris HCl pH 7.8, 150 mM NaCl, 0.05% Tween 40, 25 μM DTPA, 0.2% BSA, 0.05% BGG) containing a anti-H3K27me2 rabbit IgG (Cell Signaling, #9728) with 691 ng/mL Eu-N1-anti-rabbit IgG (PerkinElmer) was added at 50 uL per well. Following 1 hr incubation at room temperature, the plates were washed three times with wash buffer and 50 uL of Enhancement Solution (PerkinElmer) was added to each well. Plates were incubated for 30 min at room temperature and time-resolved fluorescence (TRF) was measured on Wallac Envision 2104 Multilabel Reader (400 us window, 400 us delay, 320 excitation, 615 emission).

G9a and NSD2 purification and DELFIAs. GST-G9a (amino acids 685-1000) and NSD2-SET were prepared as previously described—(17) and (21), respectively. Biochemical activity of G9a was measured as described in (17). NSD2 activity was measured by DELFIA using the PRC2 protocol described above with few modifications. NSD2-SET was diluted to 3 ng per well in 2X Enzyme Buffer (50mM Tris HCl pH 8.5, 5 mM DTT) and reactions were initiated with 20 uL of a 10 uM SAM (NEB) solution

containing 600 nM biotin-H3[21-40] following compound addition. For product detection, FI buffer containing a 1:24,000 dilution of anti-H3K36me1 rabbit IgG (Abcam, Ab9048) with 22ng/mL Eu-N1-anti-rabbit IgG was used.

Detergent and DELFIA-interference assays DELFIA assays were conducted as above with the following modifications. Detergent screening was performed using assay buffer with and without 0.01% Tween 20. For DELFIA-disruption assays, compounds were either pinned 1 hr post-reaction initiation and washed after 10 min or pinned into 2X Enzyme Buffer without enzyme, substituting H3K27me2-modified H3[21-44]-GK-biotin (AnaSpec) for unmodified H3[21-44]-GK-biotin

Fluorescence polarization. Compound or DMSO was diluted to 2X final concentration in 1X Enzyme Buffer and added at 20 uL per well in black 384-well plates. H3[21-44] -HiLyte488 peptide was then diluted to 62.5 nM in 1X Enyzme Buffer and added at 20 uL per well. Following 10 min incubation, fluorescence polarization (mP) was measured using Wallac Envision 2104 Multilabel Reader (FP FITC dual optical module; Excitation: 480 nm, Emission: 535 nm for both S- and P-channels).

Immunofluorescence. HeLa cells (ATCC) were cultured in DMEM supplemented 10%(v/v) FBS, 1 mM sodium pyruvate, and 100 U mL-1 penicillin-streptomycin. Cells were diluted in culture medium at 5e4 cells/mL and plated in black clear-bottom 96-well plates (Corning, 3904) at 100 uL/well. After 24 hr incubation at 37°C/5% CO2, 100 nL of compound or DMSO vehicle was pinned into each well and cells were incubated for an additional 48 hrs. Treated cells were fixed with 4% paraformaldhyde for 10 min, permeabilized with 0.3% Triton X-100 in PBS for 20 min, and blocked with 3% BSA in PBST for 1 hr at room temperature. Cells were then incubated with primary antibody

(anti-H3K27me3; Cell Signaling, #9733) diluted in blocking buffer overnight at 4°C. A mixture of 1 nM Hoechst 33342 (Life Technologies) and 2 ug/mL Alexa Fluor 488 goat anti-rabbit IgG (Life Technologies, A11008) in blocking buffer was then added. Following a 1 hr incubation at RT, cells were then imaged on an ImageXpress Micro automated microscope (Molecular Devices) using a 10X objective with laser-based focusing. Image analysis was performed using the Multi Wavelength Cell Scoring module in MetaXpress (Molecular Devices) to determine average nuclear fluorescence and nuclei counts per well. Z-scores were calculated as indicated below. Mean and standard deviation (STDEV) were calculated for all DMSO wells within each assay plate.

$$Z-score = \frac{Average\ Nuclear\ Fluorescence_{Compound} - MEAN(Average\ Nuclear\ Fluorescence_{DMSO\ Wells})}{STDEV(Average\ Nuclear\ Fluorescence_{DMSO\ Wells})}$$

Data analysis and curve fitting (IC_{50}, AC_{50}). For IC_{50} and AC_{50} determination, DMSO-normalized, background-subtracted activity values (see equation below) for each compound at varying concentration were fit using Condoseo GeneData Screener (Smart Fit Strategy using default settings with no restrictions and no requirement for convergence).

$$\%Activity = 100 \times \frac{Signal_{Compound} - MEAN(Signal_{PosCon\ wells})}{MEAN(Signal_{DMSO\ wells}) - MEAN(Signal_{PosCon\ wells})}$$

Compound clustering. All compound clustering was performed using ChemMine-Binning Clustering (0.6 Tanimoto Coefficient) online tool (22)

3.4 References

1. Frye SV. The art of the chemical probe. Nat Chem Biol. 2010 Mar;6(3):159–61.

2. Perfecting probes. Nat Chem Biol. 2009 Jul;5(7):435–5.

3. Petrossian TC, Clarke SG. Uncovering the human methyltransferasome. Mol Cell Proteomics. American Society for Biochemistry and Molecular Biology; 2011 Jan;10(1):M110.000976–6.

4. Thorne N, Auld DS, Inglese J. Apparent activity in high-throughput screening: origins of compound-dependent assay interference. Curr Opin Chem Biol. 2010 Jun;14(3):315–24.

5. Baell JB, Holloway GA. New substructure filters for removal of pan assay interference compounds (PAINS) from screening libraries and for their exclusion in bioassays. J Med Chem. 2010 Apr 8;53(7):2719–40.

6. Simeonov A, Jadhav A, Thomas CJ, Wang Y, Huang R, Southall NT, et al. Fluorescence spectroscopic profiling of compound libraries. J Med Chem. 2008 Apr 24;51(8):2363–71.

7. Auld DS, Southall NT, Jadhav A, Johnson RL, Diller DJ, Simeonov A, et al. Characterization of chemical libraries for luciferase inhibitory activity. J Med Chem. 2008 Apr 24;51(8):2372–86.

8. Rishton GM. Reactive compounds and in vitro false positives in HTS. Drug Discov Today. 1997 Sep;2(9):382–4.

9. Johnston PA, Soares KM, Shinde SN, Foster CA, Shun TY, Takyi HK, et al. Development of a 384-well colorimetric assay to quantify hydrogen peroxide generated by the redox cycling of compounds in the presence of reducing agents. Assay Drug Dev Technol. 2008 Aug;6(4):505–18.

10. Shoichet BK. Screening in a spirit haunted world. Drug Discov Today. 2006 Jul;11(13-14):607–15.

11. Seidler J, McGovern SL, Doman TN, Shoichet BK. Identification and prediction of promiscuous aggregating inhibitors among known drugs. J Med Chem. 2003 Oct 9;46(21):4477–86.

12. Coan KED, Maltby DA, Burlingame AL, Shoichet BK. Promiscuous aggregate-based inhibitors promote enzyme unfolding. J Med Chem. 2009 Apr 9;52(7):2067–75.

13. Feng BY, Shoichet BK. A detergent-based assay for the detection of promiscuous inhibitors. Nat Protoc. 2006;1(2):550–3.

14. EZH1 mediates methylation on histone H3 lysine 27 and complements EZH2 in maintaining stem cell identity and executing pluripotency. 2008 Nov 21;32(4):491–502.

15. Pasini D, Bracken AP, Jensen MR, Lazzerini Denchi E, Helin K. Suz12 is essential for mouse development and for EZH2 histone methyltransferase activity. EMBO J. 2004 Oct 13;23(20):4061–71.

16. Zhang J, Chung T, Oldenburg K. A Simple Statistical Parameter for Use in Evaluation and Validation of High Throughput Screening Assays. J Biomol Screen. 1999;4(2):67–73.

17. Kubicek S, O'Sullivan RJ, August EM, Hickey ER, Zhang Q, Teodoro ML, et al. Reversal of H3K9me2 by a small-molecule inhibitor for the G9a histone methyltransferase. Molecular Cell. 2007 Feb 9;25(3):473–81.

18. National Center for Biotechnology Information. PubChem BioAssay Database. AID 624260, Source = Broad Institute; http://pubchem.ncbi.nlm.nih.gov/assay/assay.cgi?aid=624260 (accessed 6/6/2012).

19. Heidebrecht RW, Mulrooney C, Austin CP, Barker RH, Beaudoin JA, Cheng KC-C, et al. Diversity-Oriented Synthesis Yields a Novel Lead for the Treatment of Malaria. ACS Med Chem Lett. 2012 Feb 9;3(2):112–7.

20. Cheng Y, Prusoff WH. Relationship between the inhibition constant (K1) and the concentration of inhibitor which causes 50 per cent inhibition (I50) of an enzymatic reaction. Biochemical Pharmacology. 1973 Dec 1;22(23):3099–108.

21. Li Y, Trojer P, Xu C-F, Cheung P, Kuo A, Drury WJ, et al. The target of the NSD family of histone lysine methyltransferases depends on the nature of the substrate. Journal of Biological Chemistry. American Society for Biochemistry and Molecular Biology; 2009 Dec 4;284(49):34283–95.

22. Backman TWH, Cao Y, Girke T. ChemMine tools: an online service for analyzing and clustering small molecules. Nucleic Acids Research. 2011 Jul;39(Web Server issue):W486–91.

Chapter IV

BRD1835 characterization and mechanism-of-action studies

Collaborator Contributions

- **Dr. Hidehisa Iwata** assisted in performing HU172 photo-crosslinking experiments and developing the protocol.
- **Dr. Max Majireck** synthesized GSK-2d1, BRD1835 (and associated stereoisomers), and various BRD1835 analogs (e.g. BRD5100 and BRD7301).
- **Dr. Hiroshi Uehara** synthesized HU172.
- **Cynthia Liu** performed initial PRC2 radiometric assays with BRD1835
- **Enrique Garcia-Rivera** developed GST-EED[78-441]-H3K9me3 AlphaLISA and assisted in both GST-EED[78-441] purification and GST-EED[78-441] SPR.
- **Professor Andy Phillips and Michal Hallside** performed all ^{1}H-NMR CAC determination experiments.

4.1 Introduction

In the previous chapter, we described the identification of BRD-K97550475 (BRD0475), an 8-membered ring sultam from SO_2 DOS library and confirmed hit emerging from an HTS campaign for PRC2 modulators. This compound exhibited low uM range potency against PRC2, high selectivity (over NSD2 and G9a), and putative cellular activity in an HCS assay—lowering global H3K27me3 levels in HeLa cells. Given these findings, we nominated BRD0475 for further investigation, resynthesizing all 8 associated stereoisomers for initial SSAR studies. While no absolute stereochemical preference was observed, one stereoisomer, BRD1835, demonstrated consistently higher potency over BRD04750 and other stereoisomers tested. BRD1835 exhibited apparent cellular activity on global H3K37me3 levels and initial mechanistic studies revealed that it inhibited PRC2 in a peptide-competitive manner. As no peptide-competitive probes had been disclosed, we pursued further development and characterization of BRD1835, exploring the molecular basis of its inhibition of PRC2 activity. This chapter describes these efforts to determine the mechanism of action (MOA) of BRD1835 and evaluate its cellular activity.

4.2 Results and discussion

4.2.1 BRD0475 SSAR studies and the Identification of BRD1835

The skeletal and stereochemical diversity yielded by DOS enables construction of compound libraries designed to facilitate establishment of not only structure-activity relationships (SAR), but also sterochemical structure-activity relationships (SSAR) (1,2). As we aimed to understand these relationships for future compound optimization, we

obtained each BRD0475 stereoisomer, measuring activity against PRC2 in DELFIA (Figure 4.1A). All stereoisomers inhibited PRC2 activity, with IC_{50} values between 6- 30 uM, suggesting no strong stereochemical preference (i.e. 'flat' SSAR). We rationalized that the variation in 8-membered ring conformation between stereoisomers was likely small (an assumption later verified by crystallography), leading to similar spatial arrangements in key bonding functionalities. Inhibiting PRC2 with ~7 uM IC_{50}, BRD1835 was found to be the most potent stereoisomer (2-fold more potent than BRD0475). To verify that BRD1835 maintained PRC2 selectivity, we tested its activity on NSD2 and G9a as before, measuring little activity of this compound against either of these distinct HMTs (Figure 4.1B).

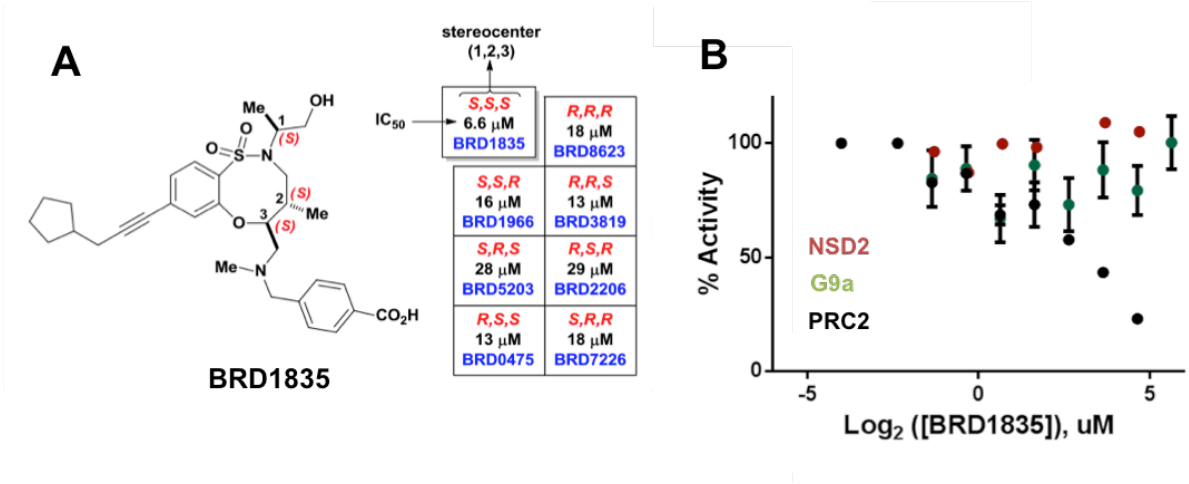

Figure 4.1 BRD0475 SSAR studies identify BRD1835
(A) Structure of BRD1835 and PRC2 DELFIA IC_{50} values for stereoisomers. (B) Activity of BRD1835 in PRC2, G9a, and NSD2 assays. IC_{50} values were determined by fitting methods described in **Experimental Methods**. Data points represent the mean and standard error of duplicate measurements in each assay.

As differing stereochemical configurations could alter aggregation properties, we measured BRD1835 activity in the presence of detergent (0.01% Tween 20) and used dynamic light scattering (DLS) to detect any potential particle formation under our buffer conditions (Figure S4.1A). DLS has been used in several studies and is the gold

standard for identifying small-molecule aggregators (3-5). To avoid errors in particle size estimations by incorrect model selection, we examined DLS autocorrelation functions, comparing those of DMSO, BRD1835, and a known aggregator—Nile red (Figure S4.1B,C). While Nile red exhibited stronger intensity autocorrelation over longer decay times—a hallmark of large particles, BRD1835 (up to 250 uM) and DMSO shared similar low intensity autocorrelation with rapid decay. Furthermore, BRD1835 retained potency (<10uM) in the presence of 0.01% Tween 20 and exhibited similar activity under high and low enzyme concentrations (Figure 4.2), suggesting that this compound was unlikely inhibiting PRC2 through an aggregation–based mechanism.

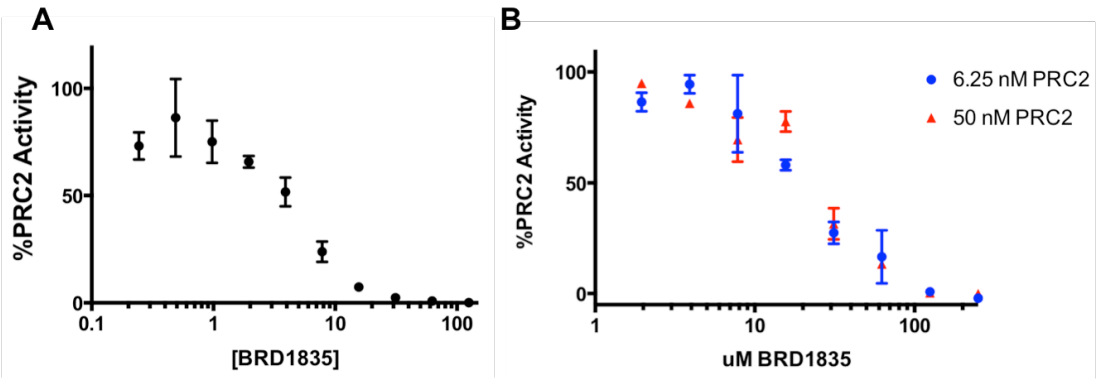

Figure 4.2 BRD1835 detergent sensitivity assay and enzyme titration
(A) Activity of BRD1835 on PRC2 in the presence of 0.01% Tween 20. (B) Activity of BRD1835 under high (50 nM) and low (6.25 nM) PRC2 conditions. Data points represent the mean and standard error of triplicate measurements in each assay

We next aimed to explore whether PRC2 inhibition by BRD1835 was specific to DELFIA, using an orthogonal readout for product formation. Reactions were carried out in the presence of DMSO or 25 uM BRD1835 in a radiometric time-course assay. Using biotinylated peptide and ^{3}H-SAM cofactor, reactions were quenched at 30 min intervals and product was detected with LSC (Figure 4.3A). Compared to DMSO, BRD1835 was able to reduce apparent reaction velocity, suggesting that its activity against PRC2 was

not a DELFIA-dependent artifact. Since this assay, like DELFIA, used a peptide substrate and was dependent on a streptavidin-biotin interaction for product purification, we performed a filter-binding assay (6-8) using histone H3.1 as a substrate. In this assay, product was captured by filtration of reaction mixtures through a high-protein-binding membrane (HA or PVDF) and the levels of ^{3}H-incorporation were measured via LSC. Measuring BRD1835 activity in 8-point dose, we confirmed that its inhibition was unlikely an artifact of detection methods dependent on biotin pull-down or use of peptide substrate, as similar potency (~10 uM) was observed (Figure 4.3B).

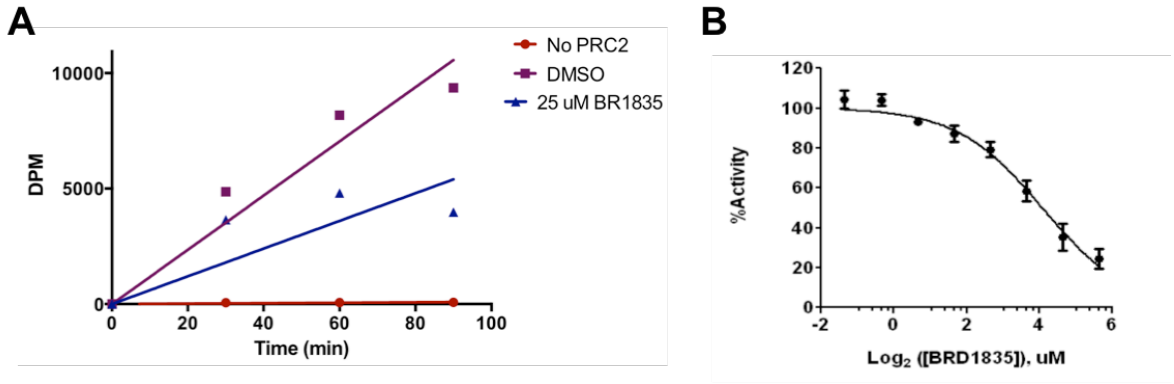

Figure 4.3 BRD1835 activity in orthogonal radiometric assays
(A) PRC2 time course using peptide substrate in the presence of DMSO or 25 uM BRD1835. A 'No PRC2' control was added to measure background. (B) BRD1835 activity in a filter-binding assay using histone H3.1 as a substrate. Data points represent the mean and standard error of triplicate measurements in filter-binding assay and single measurements in the time course assay.

As EZH2 activity is dependant on interactions between PRC2 partner proteins and only the monomeric catalytic domains of G9a and NSD2 were used in counterscreening, we speculated that PRC2 might be uniquely sensitive to compounds that could disrupt protein-protein interactions. To determine whether inhibition by BRD1835 was due to nonspecific complex disruption, we incubated PRC2 with varying concentrations of compound for 1 hr and assessed complex integrity by NativePAGE. At all

concentrations tested (up to 100 uM BRD1835), neither dimeric nor monomeric forms of PRC2 were disrupted (Figure 4.4).

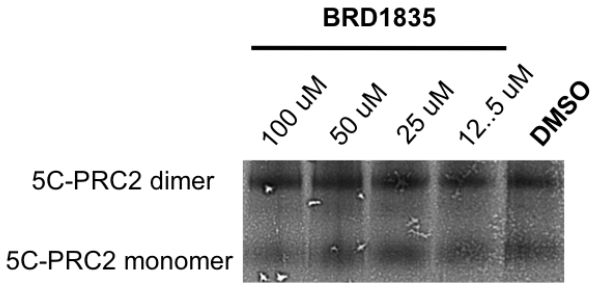

Figure 4.4 NativePAGE of PRC2 in the presence of BRD1835
PRC2 was incubated with 100 uM, 50 uM, 25 uM, and 12.5 uM BRD1835 or DMSO and separated by native PAGE. Bands corresponding to monomeric (~325 kDa) and dimeric (~650 kDa) forms of 5-component PRC2 could be detected.

Encouraged by these results, we next aimed to confirm the cellular activity of BRD1835 and its stereoisomers by measuring their ability to lower H3K27me3 levels in HeLa cells. Since our H3K27me3 HCS assay initially suggested BRD0475 to be active in cells, we chose to verify this finding and explore BRD1835 cellular activity by way of histone extraction and western blot analysis. After 48 hr treatment, each stereoisomer appeared to lower levels of both di- and trimethylated H3K27 at 10 uM in a manner correlated to their in vitro potency (Figure 4.5). Moreover, this activity appeared to be selective for H3K27 methylation, as no effect on H3K36me2 or H3K9me2 was detected. Using HEK293T, we repeated this experiment, measuring the levels of additional histone marks and treating cells for 96 hrs with varying concentrations of BRD1835. At high concentrations (20 and 40 uM), BRD1835 was able to selectively reduce H3K27me2 and H3K27me3 levels and *increase* the levels of H3K27me1 and H3K27ac (Figure 4.6A). This behavior is consistent with previous reports demonstrating that inhibition of EZH2 (7,11), given the processive nature of histone methyltransferases,

leads to accumulation of monomethylation and rapid acetylation of unmodified H3K27 residues.

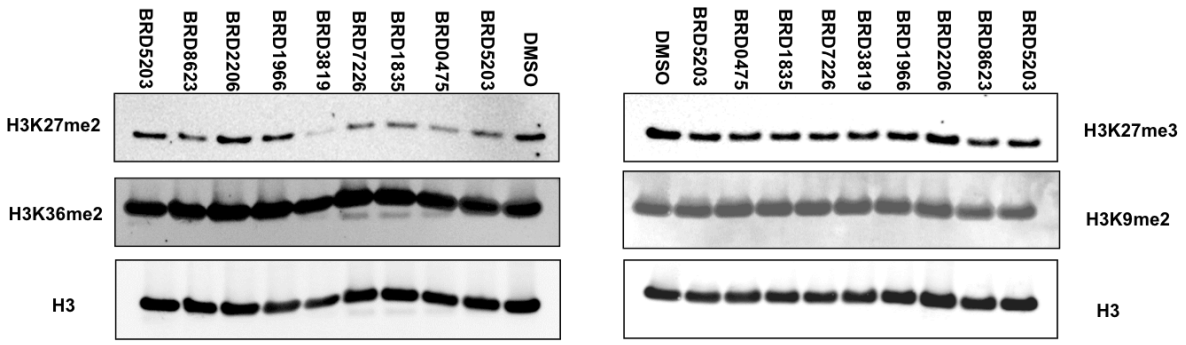

Figure 4.5 Effects of BRD0475 stereoisomers on global histone methylation levels in HeLa
Western blot detection of global H3K27me2/3, H3K9me2, and H3K36me2 levels in HeLa cells following treatment with BRD0475 or given stereoisomer at 10 um,

We next examined whether BRD1835 could induce other cellular phenotypes suggestive of PRC2 inhibition. Since PRC2 trimethylation of H3K27 results in the silencing of target genes, inhibition of PRC2 through siRNA-mediated knockdown or small-molecule treatment leads to concomitant derepression and activation of their expression. For example, EZH2 inhibition by GSK126 had been shown to markedly increase transcript levels of PRC2 target genes, TXNIP and TNFSR21, in DLBCL cell lines (7). To evaluate BRD1835's ability to induce gene expression changes suggestive of EZH2 inhibition, we measured the levels of TXNIP and TNFSR21 expression in four DLBCL lines (Pfeiffer, WUS-DLCL2, HT, and OCI-LY-19) by RT-qPCR after 96 hr treatment with BRD1835 or GSK-2d1 (an active GSK126 analog synthesized in our lab). In a dose-responsive fashion, both BRD1835 and GSK-2d1 were able to activate TXNIP and TNFRS21 expression—further suggesting that BRD1835 may be inhibiting PRC2 in cells (Figure 4.6B). However, as always, caution must be taken when interpreting any cellular change occurring as a result of treatment with high concentrations of compound,

as these changes could be results off-target effects generated through nonspecific interactions.

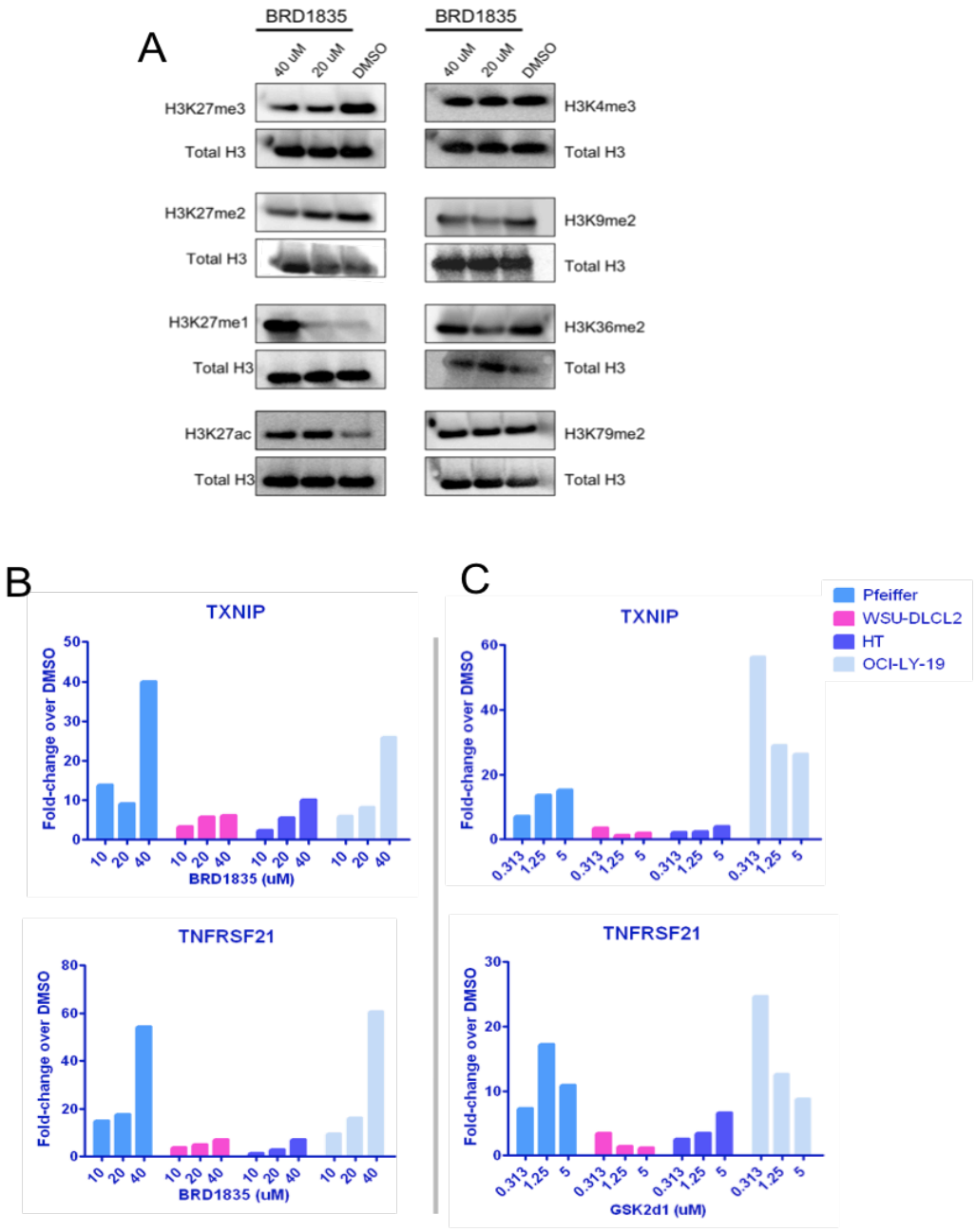

Figure 4.6 Global histone methylation and PRC2- target gene expression changes induced by BRD1835
(A) Western blot detection of global H3K27me2/3/1/ac, H3K9me2, H3K4me3, H3K79me2, and H3K36me2 levels in HEK293T cells following 96 hr treatment with BRD1835. (B and C) RT-qPCR analysis of TXNIP and TNFRS21 expression in four DLBCL lines (Pfeiffer, WSU-DLCL2, HT, and OCI-LY-19) upon 96 hr treatment with BRD1835 or GSK126 analog (GSK-2d1), respectively. Fold-change data represent the mean and standard error of four normalized replicates.

4.2.2 Cofactor and peptide competition studies

While the K_i (true potency) for competitive inhibitors should be invariant under differing substrate and cofactor conditions, the IC_{50} is known to change in a manner proportional to the ratio of substrate concentration to K_M, a relationship described by the Cheng-Prusoff equation (see Equation 4-1) (9). With interest in assigning a specific mechanism of action to BRD1835, we speculated whether we could use PRC2 DELFIA—an assay not amenable to kinetic studies—to quickly assess whether our compound was inhibiting through a competitive mechanism, varying concentrations of substrate or cofactor and measuring BRD1835 activity (IC_{50}) under each of these conditions. Using an active GSK126 analog, GSK-2d1 (synthesized by a member of our lab), we explored whether we could confirm SAM-competitive inhibitors using this method, as the parent compound was reported to be cofactor-competitive (10). As expected, varying concentrations of peptide (up to 7X K_M) had no effect on GSK-2d1 activity, while high levels of SAM (up to 70X K_M) decrease potency in a linear fashion (Figure 4.7**,** top).

We next performed a similar analysis on BRD1835, varying peptide and substrate across a wide range of concentrations and measuring its activity (IC_{50}) against PRC2. Interestingly, BRD1835 demonstrated near opposite behavior to that of GSK-2d1, with potency being unchanged at various SAM concentrations and highly attenuated in the presence of micromolar concentrations of peptide (Figure 4.7**,** bottom). These results suggested BRD1835 to be a peptide-competitive inhibitor, distinct from the many reported SAM-competitive inhibitors (10-13). Despite exhibiting modest

potency, this novel MOA encouraged us to continue probe development efforts and further characterize BRD1835.

Equation 4-1 Cheng-Prusoff equation for competitive inhibition (9)

$$IC_{50} = K_i \bullet (1 + \frac{[S]}{K_M})$$

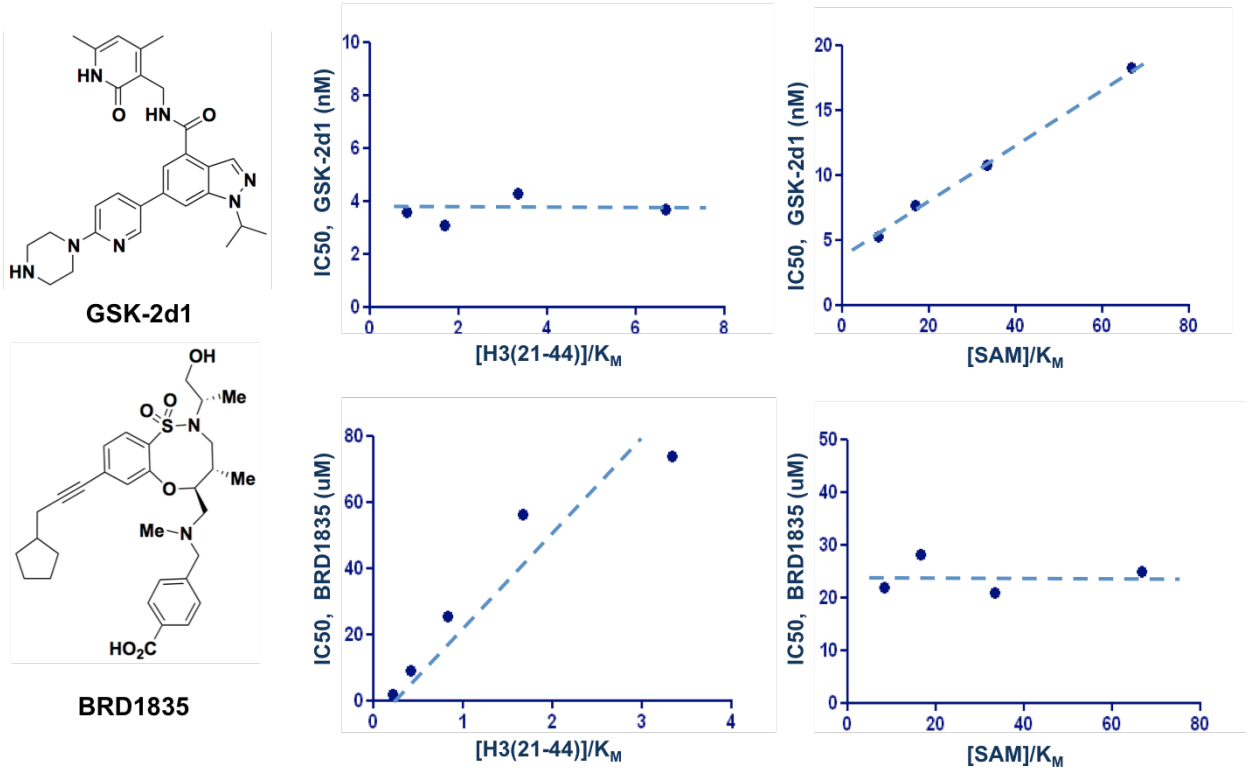

Figure 4.7 SAM and H3[21-44] competition experiments in PRC2 DELFIA
(*Top*) GSK-2d1, an active GSK126 analog, inhibits PRC2 with similar IC_{50} across varying peptide concentrations; while IC_{50} is altered by increasing concentrations of SAM, consistent with the finding that GSK126 is cofactor-competitive (7). (*Bottom*) BRD1835 retains the same potency at varying concentrations of SAM, but its IC_{50} is altered at increasing peptide concentrations, suggestive of a peptide-competitive mechanism. IC_{50} values were determined as described in **Experimental methods**.

4.2.3 SPR studies on BRD1835 and PRC2

Although previous data suggest that BRD1835 inhibits PRC2 in a manner independent of assay format and competitive for peptide, it was essential to confirm 1:1 target engagement. Isothermal titration calorimetry (ITC) is a widely used approach for

determining stoichiometry and affinity (K_a) of ligand-protein interactions since these properties can be determined through the measurement of heat released upon ligand binding (14). Due to the low apparent affinity between BRD1835 and PRC2, as well as the difficulty in achieving high concentrations of soluble protein complex in solution, ITC was not pursued, as the concentrations for both compound and protein required to characterize binding proved to be a barrier. Surface plasmon resonance (SPR) is another technique used to determine kinetic constants, such as K_D and associated on- and off-rates. SPR biosensors measure the change in mass of a surface functionalized with a ligand of interest or immobilized target (15,16). Since measured responses (RU) have a theoretical maximum (RU_{MAX}) dependent on the molecular weight of surface bound ($MW_{immobilized}$) and unbound interactants (i.e. ligand; MW_{Ligand}), stoichiometry of binding (n) can be determined by measuring responses achieved upon surface saturation (16). Since this method can been used to confirm binding of low-affinity compounds and requires little protein (ng-ug scale), we chose to determine stoichiometry of BRD1835-PRC2 binding by SPR.

Equation 4-2 Maximum RU equation

$$RU_{MAX} = RU_{immobilized} \bullet \left(\frac{MW_{Ligand}}{MW_{immobilized}} \right) \bullet n$$

Given that our recombinant PRC2 harbored FLAG-EZH2, we used a Biacore T200- compatible CM5 chip to covalently attach anti-FLAG M2 antibody to its surface, enabling immobilization of PRC2. Initial studies revealed that 5-component complex could be captured on the surface, but only to a maximal level of ~2000 RU. As the molecular weight of PRC2-antibody complex is quite large (~475 kDa) compared to that

of BRD1835 (~569 Da), the resulting theoretical maximum response (~2.4 RU) was determined to be insufficient for accurate determination of binding stoichiometry given the baseline noise (>0.5 RU). In addition to these baseline fluctuations, a >3 RU/min drift was measured—likely the result of PRC2 or its components dissociating from the surface under chosen assay conditions (Figure S4.2). To address this issue, we considered purification of EZH2 (solo) and EZH2-EED complex; however, their lack of catalytic competency was thought to be a complicating factors in interpreting the relevance of any associated binding data. For these reasons, we pursued other means to confirm target engagement.

4.2.4 Activity of BRD1835 in peptide-displacement assays

We next aimed to explore whether the apparent peptide-competitive behavior of BRD1835 was occurring through a *truly* competitive mechanism—involving direct binding of the inhibitor to the EZH2 substrate pocket. Towards this aim, we developed a fluorescence polarization (FP) assay using a HiLyte™ Fluor 488-conjugated derivative of the H3[21-44] peptide to determine whether BRD1835 could disrupt the interaction between PRC2 and substrate. In the presence of 31.25 nM tracer peptide, we titrated PRC2 from 1.6 to 100 nM to confirm PRC2-substrate binding and to determine an appropriate concentration for subsequent competition assays. As expected, we measured dose-dependent increases in FP signal with increasing concentrations of PRC2, confirming interaction with the tracer peptide. Furthermore, we identified a concentration of PRC2 that would achieve 80% tracer binding for competition experiments (Figure 4.8A).

Under optimized FP conditions, we examined whether BRD1835 could lower FP signal, including unlabeled H3[21-44] as a positive control. While the positive control peptide was able to reduce FP signal to background levels, BRD1835 failed to lower signal at the highest concentration tested (25 uM), suggesting that it is unable to directly compete with substrate binding or displace bound substrate from PRC2 (Figure 4.8B). From these results, we concluded that BRD1835 is likely inhibiting PRC2 through either a nonspecific or allosteric mechanism influenced by peptide concentration.

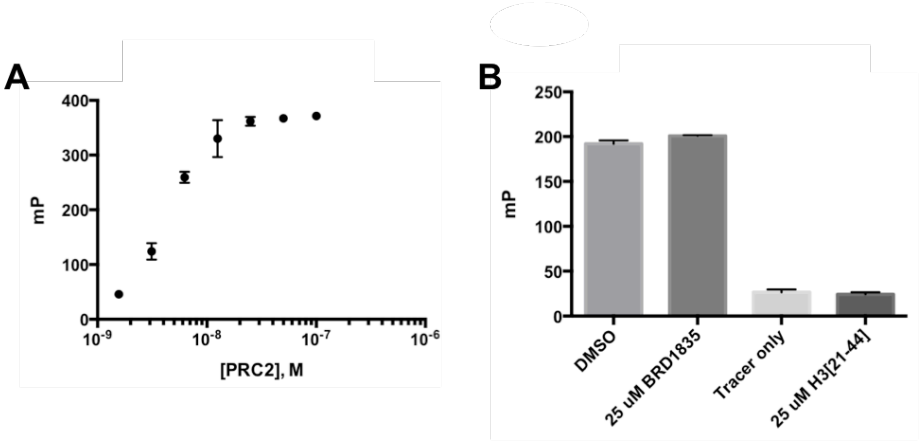

Figure 4.8 FP binding assay for PRC2 and peptide substrate interaction
(A) Titration of PRC2 in the presence of 31.25 nM H3[21-44]-HiLyte™ Fluor 488 (B) FP signal resulting from addition of DMSO, 25 uM BRD1835, or 25 uM unlabeled H3[21-44]. . Data points represent the mean and standard error of four replicate measurements in each experiment. -

4.2.5 BRD1835 is competitive with H3K27me3 peptide and destabilizes EED

As discussed in **Chapter I**, PRC2 can be allosterically activated through two known mechanisms: 1) SUZ12 binding histone H3 (residues 35-42) within nucleosomes (17) and 2) EED binding repressive histone marks, such as H3K27me3 or H3K9me3 (18,19). Given the inability of BRD1835 to directly displace peptide in FP assays, we questioned whether PRC2 inhibition was occurring through interaction with other complex members, such as SUZ12 or EED. One could imagine that apparent peptide-

competitive inhibition would be observed if BRD1835 bound the allosteric activation site of SUZ12, blocking its association with H3[21-44] (or histone H3) substrate, which happens to include the stimulating region of histone H3 (residues 35-44). Alternatively, BRD1835 could potentially disrupt the association between EED and the *product* of 5C-PRC2, H3K27me1 and H3K27me2, as even these methylation states have been shown to stimulate PRC2 activity (18). Lastly, BRD1835 could inhibit through binding an uncharacterized allosteric site—one influenced (or bound) by substrate (histone H3 or peptide) –within any of the PRC2 components.

As we were previously unable to determine a possible mode of nonspecific inhibition (i.e. assay interference, aggregation, etc), we investigated whether BRD1835 inhibits PRC2 through one of the aforementioned allosteric mechanisms. To narrow down the possible target components, we expressed, purified, and assayed the minimal catalytically active complex, EZH2-EED-SUZ12, in Sf9 cells (Figure 4.9A). After confirming activity of 3-component PRC2 (3C-PRC2) in DELFIA, we measured the IC_{50} of BRD1835 against this complex. Albeit with lower potency (~20 uM IC_{50}), BRD1835 was able to inhibit 3C-PRC2, suggesting that AEBP2 and RBBP4 were unlikely targets (Figure 4.9).

With the potential targets of BRD1835 limited to EZH2, EED, or SUZ12, we next explored whether its activity against PRC2 could be attenuated by H3K27me3 peptide. As H3K27me3 binds only the WD40 domain of EED (17-19), we suspected that if BRD1835 inhibits PRC2 through disruption of a feed-forward loop—involving EED-based PRC2 stimulation by its product —or by inducing a conformational change within EED that inhibited EZH2, H3K27me3 binding may alter its activity. Using 5C-PRC2, we

measured BRD1835 activity in the presence of increasing concentrations of an H3K27me3-modified peptide (H3[23-34], K27me3). In a dose-dependent fashion, addition of H3K27me3 peptide significantly lowered potency of BRD1835 against PRC2 (Figure 4.10), suggesting a possible connection between EED and compound activity

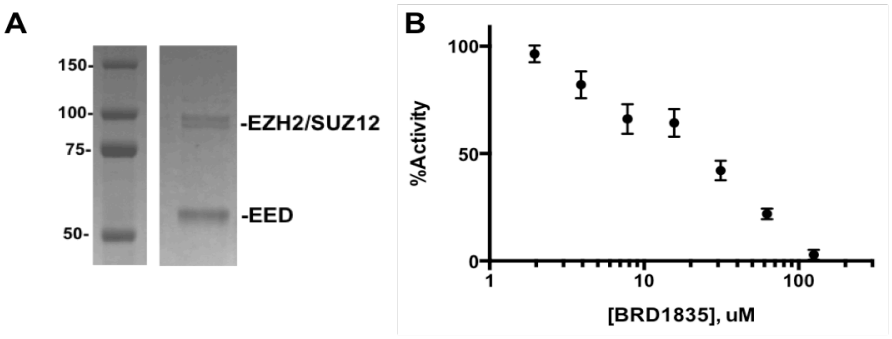

Figure 4.9 BRD1835 activity in 3-component PRC2 DELFIA
(A) 4-12% SDS-PAGE of purified 1x-FLAG-EZH2/EED/6XHIS-SUZ12 complex (3C-PRC2). Molecular weight marker shown to the left (in kDa) (B) Activity of BRD1835 on 3C-PRC2 as measured by DELFIA. Data points represent the mean and standard error of triplicate measurements.

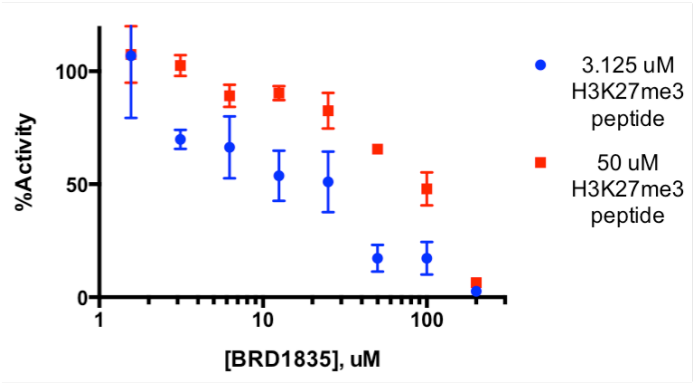

Figure 4.10 H3K27me3 peptide-induced abrogation of BRD1835 activity in DELFIA
BRD1835 activity was measured in 5C-PRC2 DELFIA in the presence of 3.125 uM and 50 uM H3K27me3-modified peptide (H3[23-34]). Data points represent the mean and standard error of triplicate measurements.

To further investigate a potential EED-BRD1835 interaction, we expressed and purified full-length 6XHIS-EED from Sf9 cells (Figure 4.11A) and evaluated direct BRD1835 binding through fluorescence-based thermal shift assays (TSA), measuring the denaturation midpoint (Tm) for EED in the presence of DMSO or 25 uM BRD1835.

While a majority of ligands are known to thermally stabilize their target protein, *increasing* the measured Tm (20), BRD1835 was found to thermally *destabilize* EED by 1.3°C (Figure 4.11B). This behavior could be suggestive of preferential binding to the unfolded state of the protein (20); however, from these results, we speculated that BRD1835 could be inducing a conformational change within EED that altered the overall enzymatic activity of EZH2 or, as mentioned earlier, disrupted a feed-forward mechanism established through EED during the course of reaction.

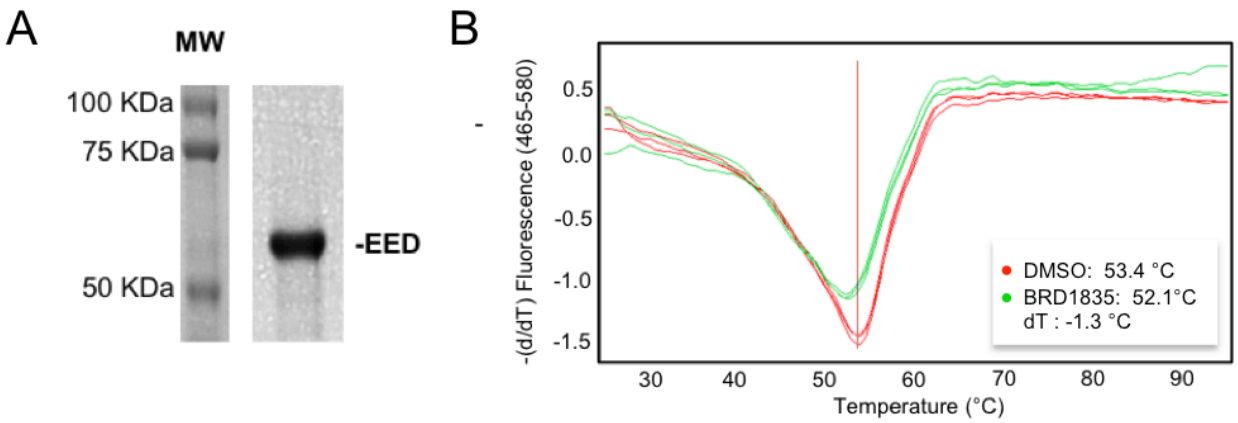

Figure 4.11 Activity of BRD1835 in EED thermal shift assay.
(A) 4-12% SDS-PAGE of purified 6XHIS-EED. (B) Derivative (d/dT) transformation of thermal melt curves for 6XHIS-EED in DMSO (red) and 25 uM BRD1835 (green) – 3 replicate wells per condition are shown. Relative to DMSO, EED is destabilized by an average of 1.3 °C in the presence of BRD1835.

4.2.6 BRD1835 disrupts interaction between EED and H3K9me3

Given that BRD1835 was found to destabilize purified EED and that its activity could be attenuated by the addition of H3K27me3 peptide, we next explored whether BRD1835 could disrupt the interaction between EED and a peptide harboring a repressive modification (e.g. H3K9me3). Since GST-EED[78-441] (WD40 domain) could be expressed in bacteria with high yields (compared to full-length EED expression in Sf9 cells) and binds peptides harboring repressive marks (18,19), we pursued

development of an AlphaLISA assay, a bead-based proximity assay commonly employed to identify inhibitors of protein-protein interactions (21,22). Using a biotinylated H3K9me3-modified peptide (H3[1-21]) and GST-EED[78-441], we developed an assay capable of measuring disruption of an EED-H3K9me3 interaction, using H3K27me3-modified and unmodified H3 peptides for assay validation (Figure 4.12A).

Consistent with data supporting an EED-binding hypothesis, BRD1835 lowered AlphaLISA signal in a dose-responsive manner, suggesting that it competes with H3K9me3 binding (Figure 4.12B). Similar to potency measured in 3C-PRC2 DELFIA, BRD1835 inhibited EED-H3K27me3 binding with an IC_{50} around 20 uM. As many compound are known to nonspecifically disrupt singlet oxygen transfer in AlphaLISA assays, we next examined whether dose-responsive loss of signal was artifactual by testing BRD1835 activity in a control assay using biotinylated-GST under similar detection conditions. BRD1835 was unable to significantly reduce AlphaLISA signal at concentrations up to 200 uM in control assays (Figure 4.12C).

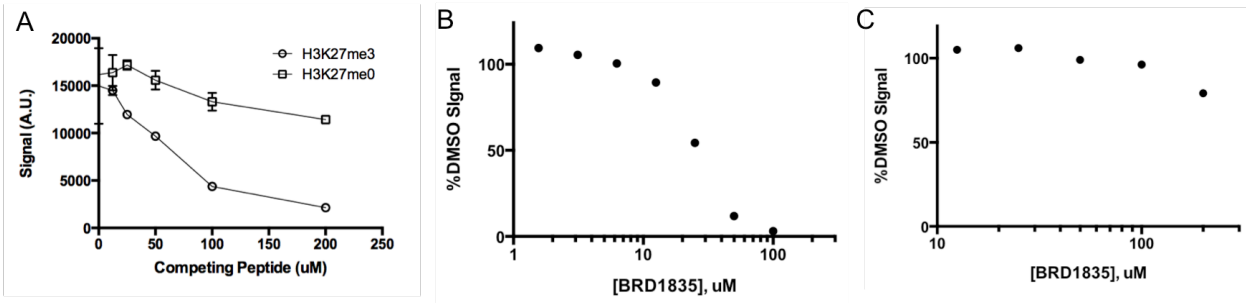

Figure 4.12 Activity of BRD1835 in EED[78-441] -H3K9m3 AlphaLISA.
(A) Activity of known competing peptide (H3[21-44], H3K27me3) versus negative control (H3[21-44]) and (B) BRD1835 activity in GST-EED[78-441]-H3K9me3 AlphaLISA and (C) biotin-GST control assay. Data points represent the mean and standard error of triplicate measurements in each assay.

4.2.7 SPR efforts to confirm binding of BRD1835 to EED

While previous experiments suggested an interaction between EED and BRD1835, we wished to confirm direct binding by SPR. As the molecular mass of GST-EED[78-441] is substantially less than that of PRC2 and its smaller size could allow immobilization at high density on an SPR surface, we expected a high probability of success in detecting a BRD1835-EED interaction (i.e. higher theoretical response levels, RU_{MAX}). We immobilized anti-GST antibody on a CM5 surface to capture GST-EED[78-441] and validated the activity of the immobilized species through kinetically monitoring binding of an H3K27me3-modified peptide at various concentrations. As shown in Figure 4.13A, we were not only able to detect H3K27me3 binding, but measured K_D values (in the 50 uM range) similar to those previously reported (18,19). We next measured SPR responses in the presence of various concentrations of BRD1835, attempting to verify direct EED binding and determine affinity (Figure 4.13B). These results suggested an interaction between EED and BRD1835 (i.e. dose-dependent SPR response); however, we were unable to reach surface saturation at higher concentrations. Moreover, these responses appeared to increase in magnitude far beyond the expected theoretical maximum (RU_{MAX}), implying super-stoichiometric binding characteristic of a nonspecific, aggregation-based interaction with the surface. T

To eliminate baseline drift, we were forced to use buffer conditions that differed significantly from those used in all previous assays (PBS-EP+ pH 7.4 versus 50 mM Tris pH 8.5 with 5mM DTT and 0.01% Tween 20). With that said, we reasoned that BRD1835 solubility could have been compromised in these studies, leading to the formation of high molecular weight aggregates or precipitate and super-stoichiometric

behavior at higher concentrations (50 and 25 uM). To explore this hypothesis, BRD1835 aggregate formation was assessed by DLS in SPR buffer conditions (PBS and PBS-EP+ at pH 7.4). While intensity autocorrelations for DMSO in PBS-EP+ buffer were slightly characteristic of aggregate presence (potentially due to the P20 Surfactant additive), BRD1835 appeared to clearly aggregate at concentrations >12.5 uM in both PBS and PBS+EP conditions (Figure S4.3), thus providing an explanation for its behavior in SPR. Interestingly, these aggregates appear to bind EED with some selectively, as all SPR responses were reference-subtracted (measuring BRD1835-GST interactions in parallel). While suggestive of BRD1835's potential to form EED-binding aggregates in a manner dependent on buffer condition, these studies were unable to confirm a classical 1:1 interaction with EED.

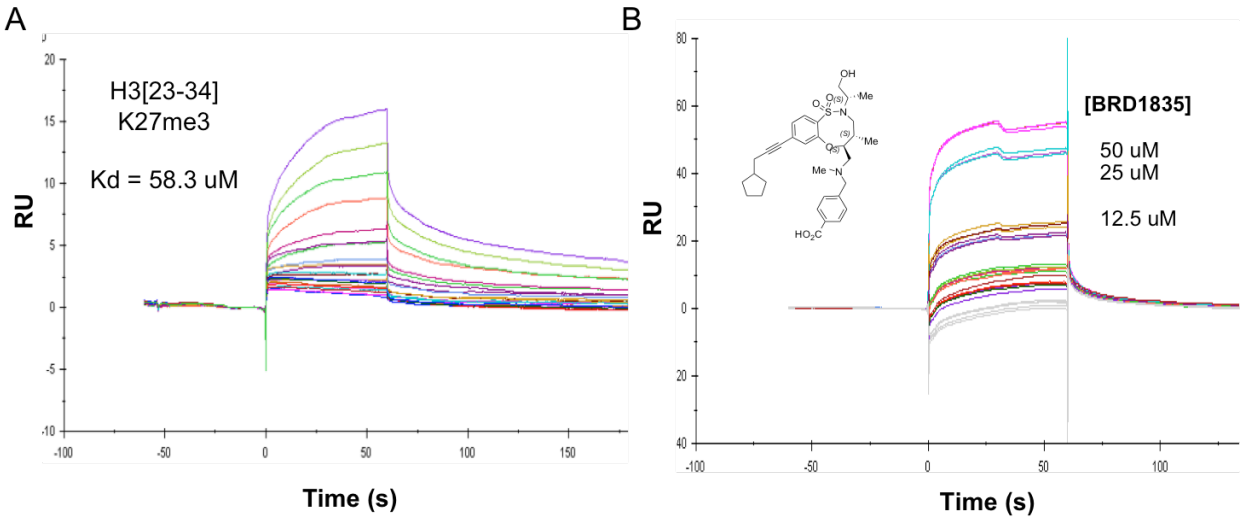

Figure 4.13 SPR studies on BRD1835 interaction with GST-EED[78-441]
(A) H3K27me3-peptide titration and K_D determination validating the activity of GST-EED[78-441] surface. (B) Titration of BRD1835 across GST-EED[78-441] surface. Super-stoichiometric binding could be detected at 25 and 50 uM BRD1835. All sensorgrams above are background-subtracted using a GST surface as a reference.

4.2.8 Photo-crosslinking as a strategy to confirm EED target engagement

As our attempts to confirm BRD1835 target engagement through SPR were inconclusive, we next explored a photo-crosslinking strategy, aiming to determine the target PRC2 component using purified 5-component complex. We synthesize an analog of BRD1835 (HU172) harboring a photoreactive benzophenone in place of the cyclopentyl propyne moiety as well as an alkyne on the northeast hydroxyl group to enable biotin attachment using click chemistry (Figure 4.14A). Prior to photo-crosslinking experiments, we characterized HU172 in PRC2 DELFIA and EED-H3K9me3 AlphaLISA to verify that its biochemical activity was similar to that of BRD1835. HU172 exhibited activity in both DELFIA and AlphaLISA assays with similar potency (~10 uM IC_{50}), although the dose-response curves appeared quite steep – a potential sign of aggregation-based inhibition (5). However, given its structural similarity to BRD1835 and biochemical activity, we proceeded with crosslinking studies, using HU172 concentrations at its IC_{50} (10 uM).

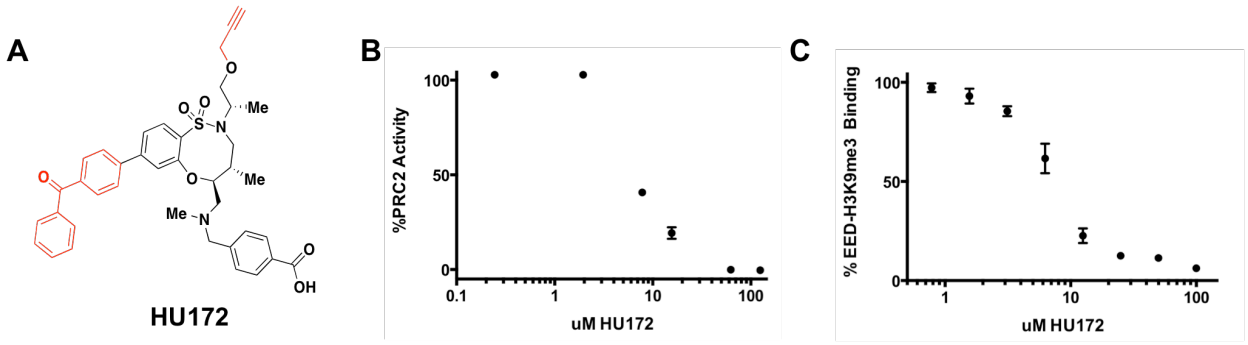

Figure 4.14 Biochemical activity of HU172 – a BRD1835 photocrosslinkable analog,
(A) Structure of HU172 with alkyne and benzophenone moieties depicted in red. Activity of HU172 in (B) PRC2 DELFIA and (C) GST-EED[78-441]-AlphaLISA. Data points represent the mean and standard error of four replicate measurements in each assay.

To identify the potential target of BRD1835, purified PRC2 and HU172 were incubated in the presence or absence of competing BRD1835 (100 uM) and photo-

crosslinking was initiated by 60 min UV exposure. After a copper-catalyzed click reaction with biotin azide, we initially identified labeled bands by western blot using streptavidin-HRP (chemiluminescence) for detection. After several attempts, no labeled bands within the molecular weight range of PRC2 components were identified and only a single band of ~25 kDa showed strong labeling and competition by BRD1835 (Figure S4.4A). When IR fluorescence detection was used in place of chemiluminescence (substituting IRDye® 800CW streptavidin for streptavidin-HRP), all PRC2 components appeared to be labeled by HU172; however, as seen previously only the 25 kDa band was competitive with BRD1835 (Figure S4.4B).

While of initial interest, this band was not identified when other active preparations of PRC2 were used. In fact, photo-crosslinking experiments using alternative batches revealed BRD1835-competitive bands within the mass range of PRC2 components, corresponding most strikingly to presumed SUZ12/EZH2 bands at ~100 kDa (Figure 4.15A). To determine whether HU172 labeling or BRD1835 competition could be influenced by the addition of peptide substrate, photo-crosslinking was repeated in the presence of 62.5 and 500 nM H3[21-44], with and without competitor. Intriguingly, HU172 labeling appeared to *increase* in a manner dependent on peptide concentration, with very strong labeling occurring in the ~100 kDa range (Figure 4.15B). Moreover, 100 uM BRD1835 was able to significantly reduce the labeling intensity of these HU172-conjugated bands in the presence of peptide, suggesting interactions between EZH2 or SUZ12, and the inhibitor. Bands corresponding to AEBP2, RBBP4, and EED were only modestly labeled in a manner weakly competitive with BRD1835.

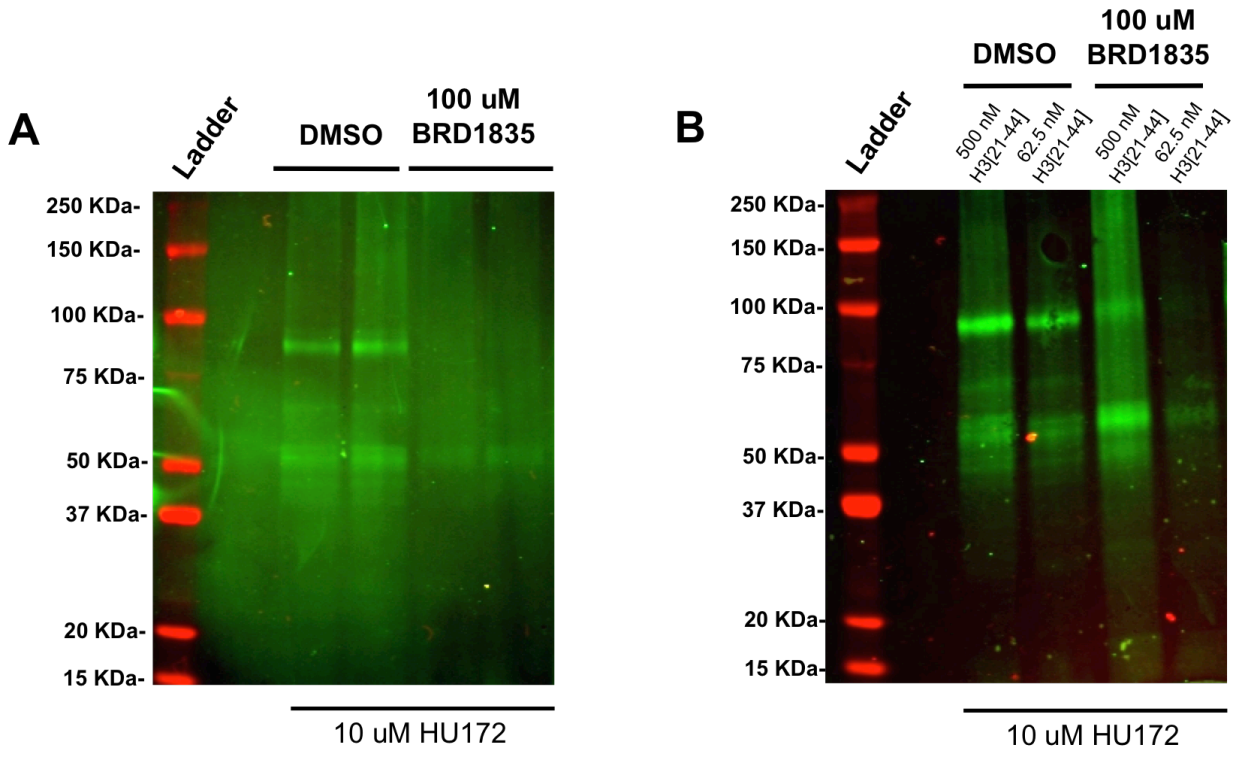

Figure 4.15 HU172 photo-crosslinking of 5C-PRC2 components
(A) Results of 5C-PRC2 photo-crosslinking studies using 10 uM HU172 in the presence of DMSO or 100 uM BRD1835. (B) HU172 photo-crosslinking and BRD1835 (100 uM) competition in the presence of 62.5 nM or 500 nM H3[21-44] peptide.

Overall, these results put into question whether BRD1835 inhibits PRC2 through engagement of EED and raises the possibility of direct interaction with EZH2 or SUZ12. Furthermore, the increased intensity of HU172 labeling in the presence of H3[21-44] implicates substrate in the mechanism of inhibition—implying that, while its inhibitory activity is substrate-competitive, the interaction between BRD1835 and PRC2 is positively influenced by substrate binding. However, the labeling of the 25 kDa species in one PRC2 preparation, likely precluding the labeling of other PRC2 components, may suggest the ability of BRD1835 to bind promiscuously. Follow-up studies revealed that this band is nonspecifically detected by both EED and EZH2 antibodies and does not emerge as a result of photo-crosslinking (Figure S4.5). Given that this species could

only be detected when mouse IgGs were used, we speculated that this band may be contaminating anti-FLAG M2 IgG light chain (mouse) that remained bound to FLAG-EZH2 throughout purification.

4.2.9 NMR studies suggest BRD1835 interaction with peptide and potential aggregation

With contradictory evidence and inconclusive results surrounding BRD1835 engagement with EED, we re-examined the possibility of aggregation. Since initial DLS and detergent-sensitivity assays were unable to convince us of significant aggregate formation, we looked for orthogonal approaches. It has been recently reported that proton NMR can provide a sensitive means to determine the critical aggregation concentrations (CACs) of organic molecules in aqueous solution (23). This is based on the observation that proton NMR spectra are sharpest when a compound is completely soluble in solution and unusually broad as they begin to form soluble aggregates or precipitates (23). In collaboration with Professor Andy Phillips, we sought to determine the CAC of BRD1835 (and two inactive analogs) by collecting proton NMR spectra at varying concentrations of compound and identifying the concentration in which peak broadening became detectable.

In an attempt to improve potency, several analogs of BRD1835 were synthesized and assayed in both PRC2 DELFIA and EED-H3K9me3 AlphaLISA. While we were unable to generate compounds of significantly greater potency, we were able to identify several inactive analogs. The structures and associated biochemical activity of these compounds are shown in Figure 4.16. To determine if the ability to form aggregates was the basis for inhibition, we performed proton NMR aggregation studies, measuring the

CACs for BRD1835, BRD5100, and BRD7301. As the results in Figure 4.17 indicate, peak broadening becomes strongly apparent for BRD1835 at concentrations of 50 uM and above, but seems to occur to some degree at 25 uM, suggesting a CAC between

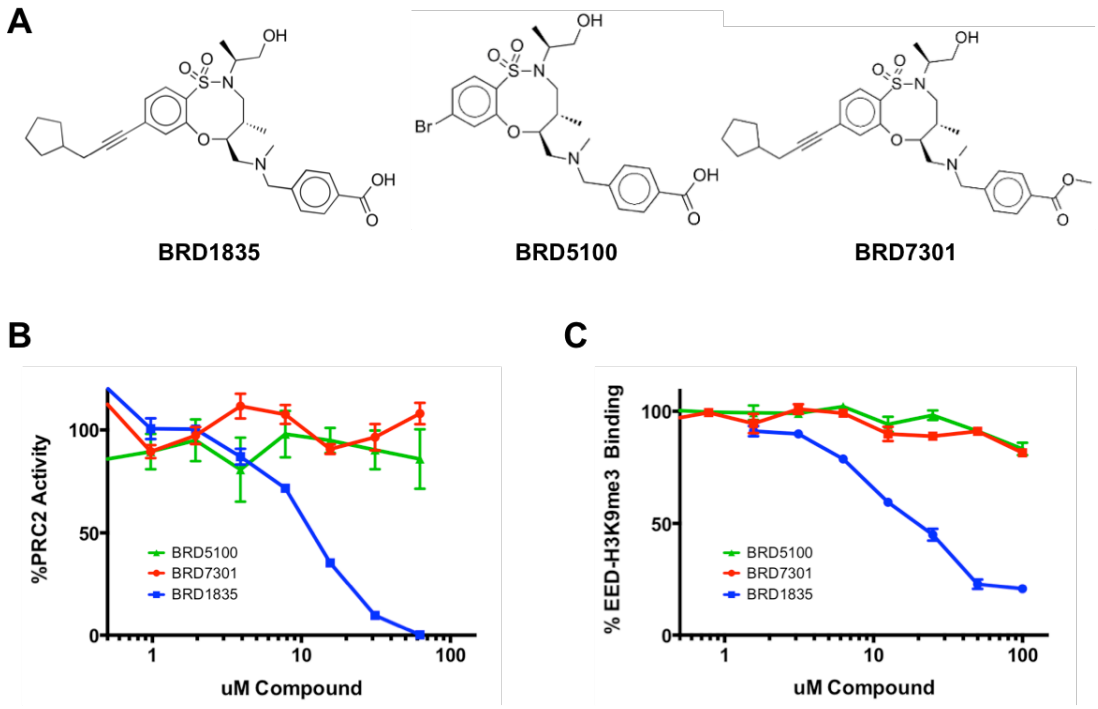

Figure 4.16 Structure and biochemical activity of Inactive BRD1835 analogs
(A) Structures of inactive analogs (BRD7301 and BRD5100) and BRD1835. (B) Activity of BRD1835, BRD7301, and BRD5100 in PRC2 DELFIA. (C) Activity of BRD1835, BRD5100, and BRD7301 in EED-H3K9me3 AlphaLISA. Data points represent the mean and standard error of triplicate measurements in each assay

25-50 uM. BRD7301, a methylester derivative of BRD1835, was completely insoluble in the sodium phosphate buffer used in these studies, while BRD5100, an analog lacking the cyclopentyl propyne moiety, exhibited no detectable aggregation up to 100 uM. As DLS was previously unable to detect particles in assay buffer (50 mM Tris pH 8.5, 5 mM DTT, 0.01% Tween 20) containing upwards of 250 uM BRD1835, we repeated these measurements in the 50 mM sodium phosphate buffer (pH 7.4) used in the NMR studies. As shown in Figure 4.17, DLS estimations were in near perfect agreement with the CACs determined by NMR, revealing significant BRD1835 aggregation at 25 uM

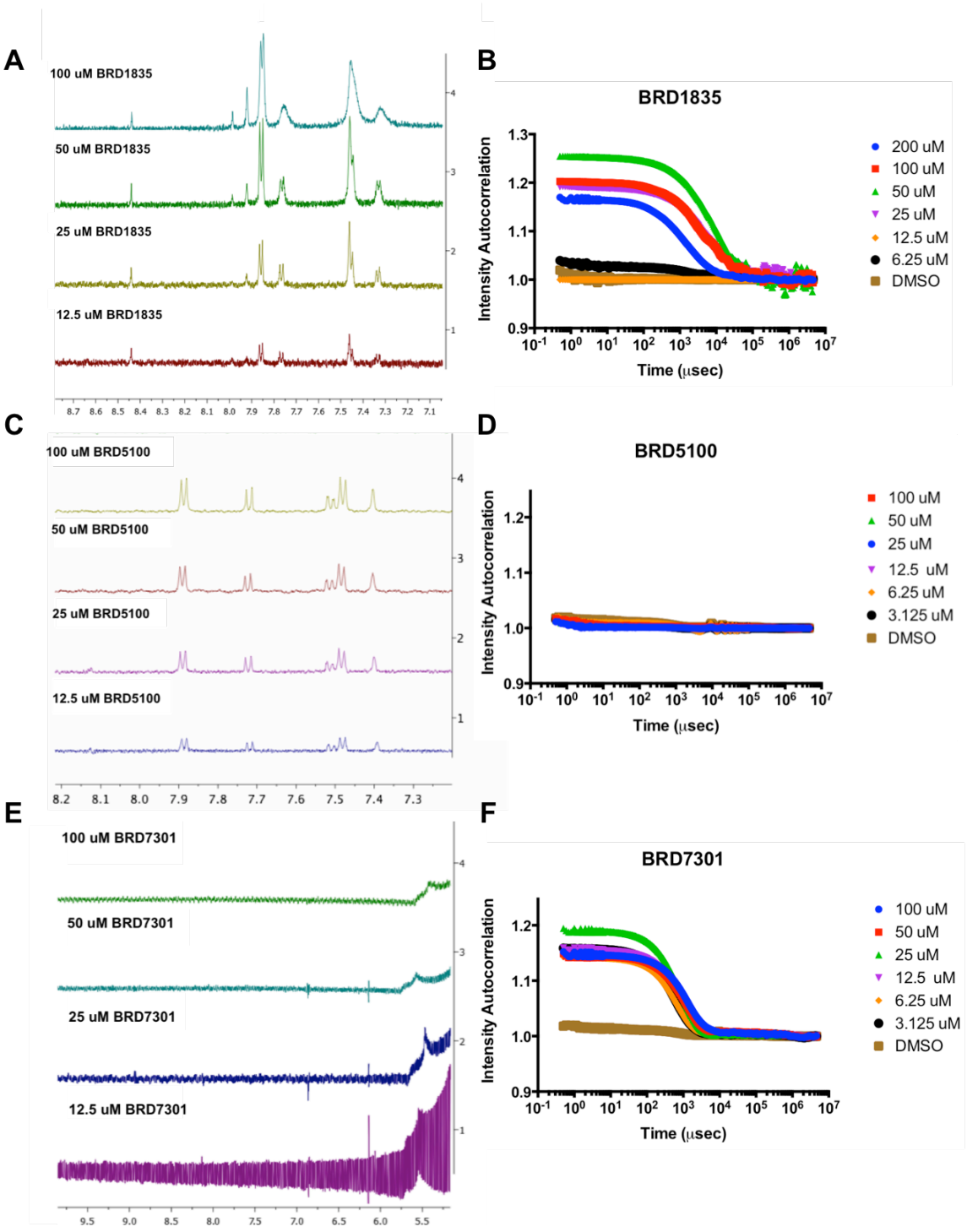

Figure 4.17 CAC determination of BRD1835 and analogs by ^{1}H NMR and DLS
^{1}H NMR spectra and DLS intensity autocorrelation curves for various concentrations of BRD1835 (A and B, resp.), BRD5100 (C and D, resp.), and BRD7301 (E and F, resp.) in 50 mM sodium phosphate, pH 7.4. Both methods confirm likely aggregation at >25 uM BRD1835 and at all concentrations of BRD7301 tested. BRD5100 showed no detectable aggregation at concentrations up to 100 uM. Each intensity autocorrelation curve represents the average of 10 single-well acquisitions for each condition.

and above, no aggregation of BRD5100 up to 100 uM, and significant aggregation formation at all BRD7301 concentrations tested (3.125 uM and above).

Small-molecule aggregation is a buffer-dependent phenomenon, however, the extreme differences in BRD1835 CAC exhibited between NMR and activity assay buffers were seemingly suspicious. The phenomenal agreement between DLS and NMR-based aggregation assays inspired us to reexamine previous DLS results and procedures to verify the CAC of BRD1835 in the buffer used to measure biochemical activity. As several compounds were profiled during our initial round of DLS, compounds were added directly to assay plates by pin tool as opposed to being manually diluted in larger volumes and dispensed accordingly. As this was the only alteration in our protocol, we revisited DLS studies, estimating the CACs for BRD1835, both inactive analogs, and the photo-affinity probe, HU172, in PRC2 assay buffer (50 mM Tris pH 8.5, 5 mM DTT, and 0.01% Tween 20). As shown in Figure 4.18, BRD1835 formed clear aggregates at 100 uM. While this CAC is still higher than those measured in NMR and SPR buffers, it does demonstrate that BRD1835 aggregates at a lower concentration than previously estimated. As expected, BRD5100 formed no detectable aggregates (up to 200 uM), while BRD7301, although soluble in PRC2 assay buffer, formed clear aggregates at 100 uM. Moreover, the photo-crosslinking analog, HU172, was found to aggregate at 25 uM, a concentration much lower than that of BRD1835.

From these studies, we determined that, while it may contribute, aggregation formation alone was unable to predict activity against PRC2, as the inactive analog, BRD7301, was found to aggregate at concentrations similar to that of BRD1835. However, it is noteworthy that HU172, an analog found to inhibit EED-H3K9me3

interaction with potency greater than that of BRD1835, was the strongest aggregator in PRC2 assay buffer. Furthermore, though the measured biochemical activity (IC_{50}) for both HU172 and BRD1835 in PRC2 DELFIA was 4-10X lower than their estimated CACs, PRC2 was potently inhibited in the presence of these aggregates. While inhibition through specific mechanisms can occur at concentrations below the CAC, these findings suggest that only specific compound aggregates can inhibit PRC2, potentially though a mechanism distinct from the enzyme sequestration or unfolding mechanisms that have been previously described (24).

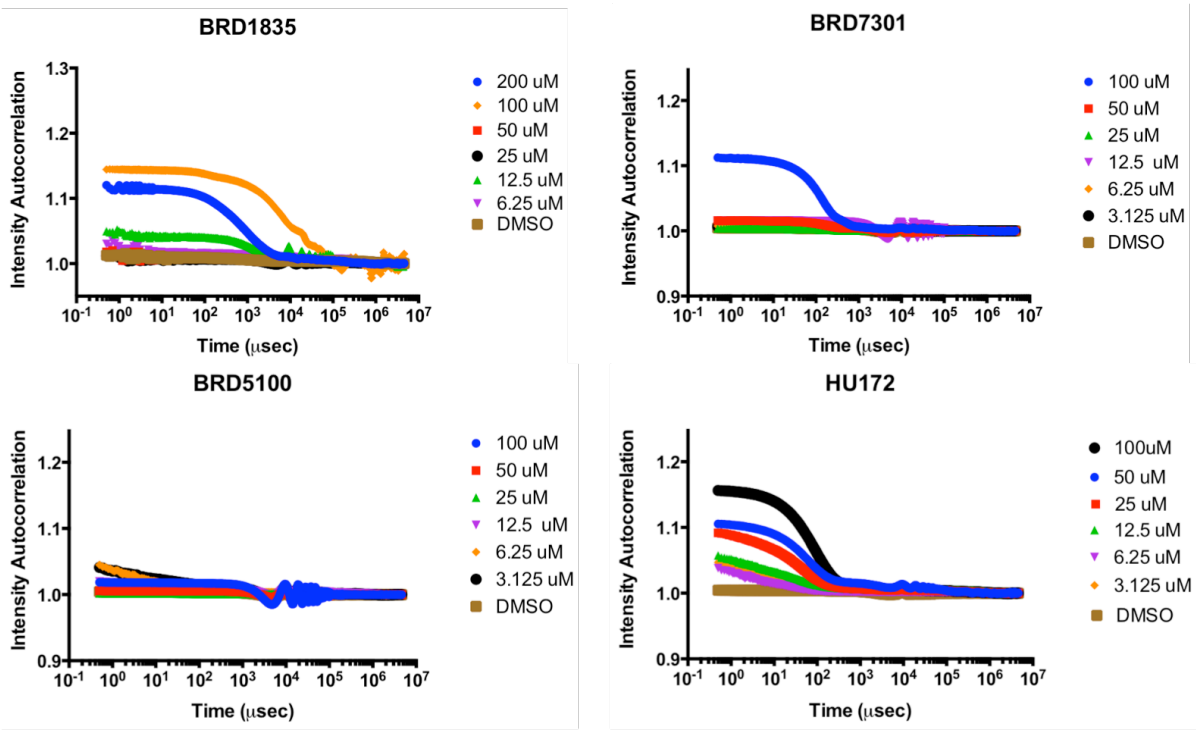

Figure 4.18 DLS analysis of BRD1835, HU172, BRD5100, and BRD7301 under activity assay buffer conditions
DLS intensity autocorrelation curves for various concentrations of BRD1835, HU172, BRD5100, and BRD7301 in activity assay buffer (50 mM Tris pH 8.5, 5 mM DTT, 0.01% Tween 20). BRD1835 and BRD7301 show large aggregate formation at >100 uM, while HU172 forms large aggregates at >25 uM. BRD5100 shows no sign of aggregation at all concentrations tested (up to 100 uM). Each intensity autocorrelation curve represents the average of 10 single-well acquisitions for each condition.

4.2.10 Exploring BRD1835 peptide-binding activity

With new knowledge regarding BRD1835 aggregation potential, we next explored whether BRD1835 aggregates could interact directly with peptide, as this might explain its peptide-competitive behavior. From our SAR studies, we learned that presence of the carboxylic acid was essential for activity and only when replaced with an isostere, such as a tetrazole, was the compound able to inhibit PRC2 activity. Given this dependence on a negatively charged group, we questioned whether this potentially promoted binding to the positively charged substrate and whether *aggregates* harboring a carboxylic acid were capable of binding in a manner that was inhibitory

To test this hypothesis, we conducted proton NMR experiments on BRD1835 (200 uM) in the presence of peptide substrate (2 uM H3[21-44]), looking for signs of interaction through changes in the BRD1835 or peptide spectra. While there were no significant changes in chemical shifts for either molecule, H3[21-44] was found to significantly lower the apparent CAC of BRD1835, suggesting an interaction between compound and substrate (Figure 4.19A). Interestingly, there appeared to be selectivity in regard to this peptide-induce deaggregation phenomenon, where only H3[21-44] peptide was able to significantly lower BRD1835 CAC, while H3[1-21] and H3[69-89] was unable to do so. Ultimately, these results suggest that BRD1835 activity on PRC2 could involve nonspecific, aggregation-based inhibition that's *reversed* by addition of peptide substrate, giving it the appearance of peptide-competitive behavior.

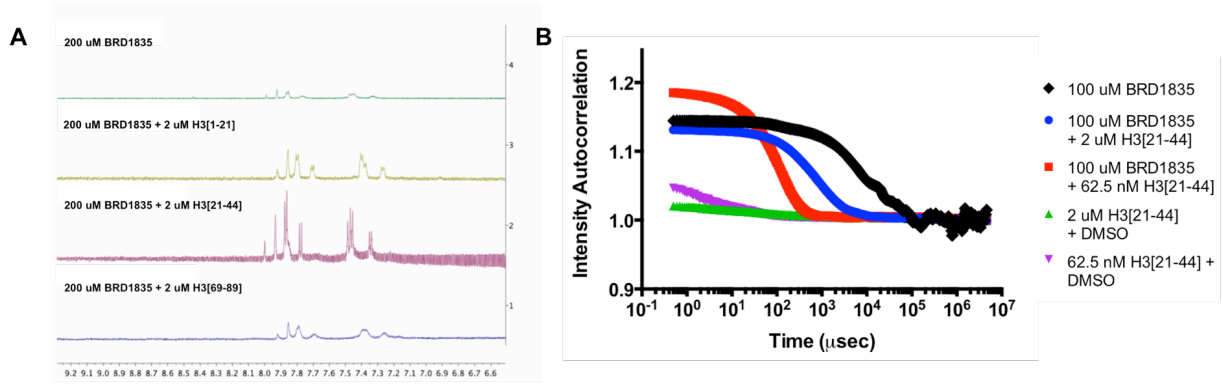

Figure 4.19 ^{1}H NMR and DLS studies on BRD1835 in the presence of histone H3-derived peptides
(A) ^{1}H NMR spectra of 200 uM BRD1835 in the presence of 2 uM H3[1-21], H3[21-44], and H3[68-89] in 50 mM sodium phosphate buffer, pH 7.4 (B) DLS intensity autocorrelation curves of 100 uM BRD1835 in the presence of various H3[21-44] concentrations in activity assay buffer (50 mM Tris pH 8.5, 5 mM DTT, and 0.01% Tween 20). While NMR studies suggest potential deaggregation of 200 uM BRD1835 the presence of H3[21-44], DLS experiments reveal that large BRD1835 particles are not diminished by H3[21-44] peptide under activity assay buffer conditions. Each intensity autocorrelation curve represents the average of 10 single-well acquisitions for each condition.

To determine whether this deaggregation phenomenon occurred in PRC2 assay buffer, we examined BRD1835 aggregation by DLS in the presence or absence of H3[21-44] peptide. As seen previously, BRD1835 appeared to aggregate at 100 uM, however, these aggregates were not eliminated by the addition of 62.5 nM or 2 uM H3[21-44] (Figure 4.19B). While peptide-induced deaggregation may only occur under specific buffer conditions or represent a phenomenon specific to these NMR studies, the interaction between BRD1835 and peptide may still occur under our assay conditions.

In earlier characterization efforts using EED-H3K9me3 AlphaLISA, we were able to demonstrate that BRD1835 disrupted the interaction between GST-EED[78-441] and H3K9me3 peptide, while H3[21-44] had no effect up to 200 uM. Considering this likely involved BRD1835 aggregation and that H3[21-44] could potentially bind and sequester these aggregates, we tested BRD1835 activity in the GST-EED[78-441]-H3K9me3 AlphaLISA in the presence or absence of 2 uM H3[21-44]. Indicative of an interaction, BRD1835 activity was abrogated by the addition of H3[21-44], implying a reduction of

activity due to peptide binding (Figure 4.19B). To explore this behavior further, we revisited our fluorescent polarization assay using HiLyte™ Fluor 488-H3[21-44]. While 25 uM BRD1835 exhibited no activity in this assay, we questioned whether aggregating concentrations of active compounds were able to increase FP signal in the presence of tracer peptide alone. At 100 uM, both HU172 and BRD1835 markedly increased FP signal, while inactive analogs (BRD7301 and BRD5100) yielded FP levels equivalent to those generated by DMSO (Figure 4.21). These results confirm that, at least at aggregating concentrations, peptide-binding behavior tracks with compound activity in both EED-H3K9me3 AlphaLISA and PRC2 DELFIA.

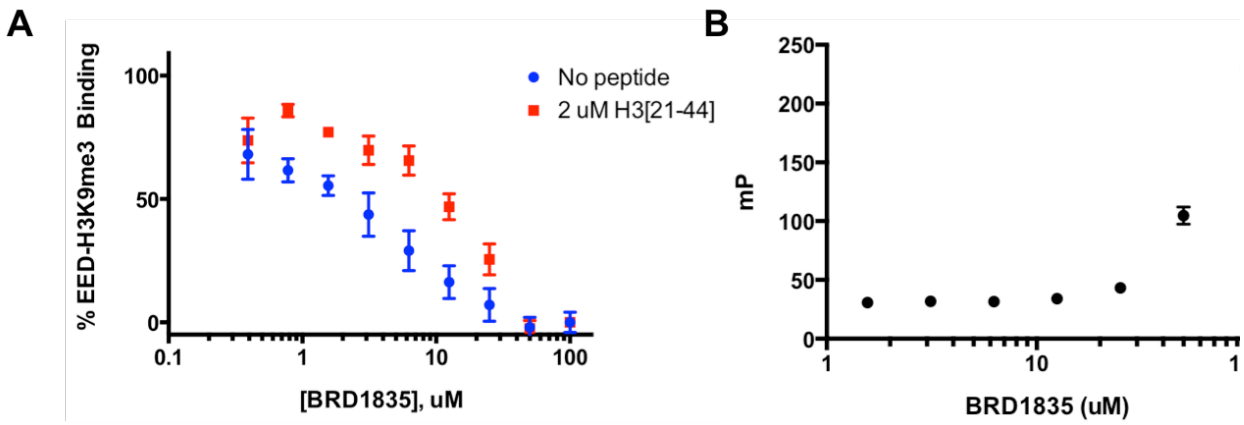

Figure 4.20 BRD1835-peptide interactions revealed by EED-H3K9me3 AlphaLISA and HiLyte™ Fluor 488-H3[21-44] FP assay.
(A) BRD1835 activity in EED-H3K9me3 AlphaLISA in the presence or absence of 2 uM H3[21-44]. (B) FP measurements of 31.25 nM HiLyte™ Fluor 488-H3[21-44] in the presence various BRD1835 concentrations. Data points represent the mean and standard error of four replicate measurements in each assay

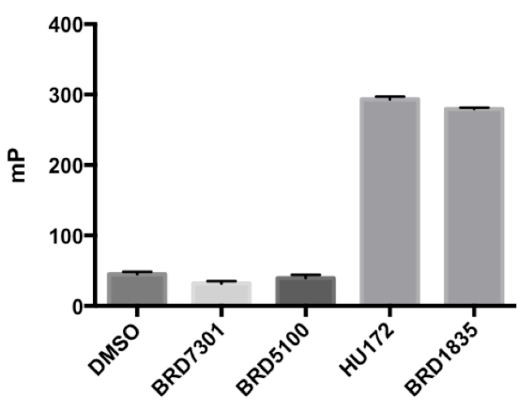

Figure 4.21 HiLyte™ Fluor 488-H3[21-44] FP assay on active and inactive BRD1835 analogs.
FP measurements of 31.25 nM HiLyte™ Fluor 488-H3[21-44] in the presence 100 uM BRD1835, HU172, and inactive analogs (BRD5100 and BRD7301). Compared to DMSO, FP signal increased in the presence of aggregating concentrations of active analogs only. Data points represent the mean and standard error of four replicate measurements in each assay.

4.2.11 Discussion and outlook

The widespread presence of aggregators in screening collections is an issue that has only quite recently been appreciated (25). As most organic molecules aggregate at some critical concentration in aqueous solution depending on the conditions, their identification and removal from screening decks has proven challenging. This challenge is underscored by the fact that many compounds can be well behaved and maintain biologically meaningful activity at concentrations below their CAC, as can be seen by the large number of drugs that can inhibit promiscuously by aggregation-based mechanisms (4). Furthermore, unlike promiscuous reactive compounds, aggregation is difficult to predict on the basis of structure alone, requiring one to empirically determine aggregation potential under their specific assay conditions. As previously mentioned, there are certain hallmarks that can be considered when determining whether a compound's activity in a biochemical assay is due to specific target engagement or promiscuous inhibition via aggregate formation. These include sensitivity to detergent,

formation of large particles detectable by DLS, sensitivity to enzyme concentration, and noncompetitive behavior (26).

In the case of BRD1835, we found this compound to be active in the presence of detergent, insensitive to enzyme concentration, and competitive for peptide substrate in PRC2 DELFIA. Along with its apparent cellular activity, no particle formation could be detected by DLS within the IC_{50} range, suggesting a mechanism that was potentially specific and on-target. While BRD1835 was unable to directly compete with labeled peptide substrate in FP experiments, the ability of H3K27me3 to attenuate activity was suggestive of an EED-based allosteric mechanism influenced by peptide concentration. EED TSA and H3K9me3-competition assays further suggested an interaction between BRD1835 and EED, prompting SPR studies that revealed an interaction, but with clear super-stoichiometric behavior at high concentrations.

As SPR results were inconclusive, we pursued PRC2 photo-crosslinking studies using a biochemically active, photoreactive analog of BRD1835, HU172. These experiments suggested EZH2 or SUZ12 (and not EED) to be the possible target and revealed, in addition to its ability to bind with some promiscuity, a positive influence of substrate on HU172 photolabeling. Consistent with this later finding, ^{1}H NMR studies uncovered a potential interaction between BRD1835 and H3[21-44]. Furthermore, NMR and follow-up DLS experiments exposed the potential of BRD1835, BRD7301, and HU172 to aggregate under different buffer conditions, with FP and EED-H3K9me3 interaction assays demonstrating the ability of only biochemically active aggregates to bind peptide substrate.

While the measured CAC of BRD1835 in our activity assay buffer exceeds its IC_{50} in PRC2 DELFIA, these results are suggestive of a novel aggregation-based mechanism of inhibition implicating the peptide substrate. Although it is an intriguing possibility, peptide sequestration by compound alone is an unlikely mechanism, as BRD1835 exhibits no activity in NSD2 DELFIA—an assay utilizing the same peptide substrate in biochemical, albeit at slightly higher concentration. Furthermore, this compound fails to displace the peptide from PRC2 in FP experiments. Lastly, photo-crosslinking experiments demonstrate a peptide-dependent *increase* in HU172 labeling and clear competition with a PRC2 component by BRD1835.

Taken together, it is likely that BRD1835 forms aggregates that engage substrate and PRC2 components nonspecifically under lower substrate conditions, with apparent peptide-competitive behavior arising from substrate-dependent sequestration of compound at higher substrate concentrations (Figure 4.22). Activity below the CAC can likely be explained by the formation of small aggregates that evade DLS detection, as differing ionic strength has been shown to impact particle size (27), but increase their number. Although it was initially assumed that differing aggregation behavior exhibited in SPR, NMR, and activity assay buffers were primarily the result of pH (given that BRD1835 harbors an ionizable tertiary amine), its possible that differences in salt concentration may have only impacted the *size* of aggregates and not their presence.

While these investigations were unsuccessful in delivering a novel small-molecule probe for PRC2, they do clearly illustrate the potential of small-molecules to behave in artifactual ways that have not previously been appreciated. BRD1835 is likely

a novel example of an aggregator, violating many of the currently established hallmarks through displaying substrate-competitive inhibition and insensitivity to protein

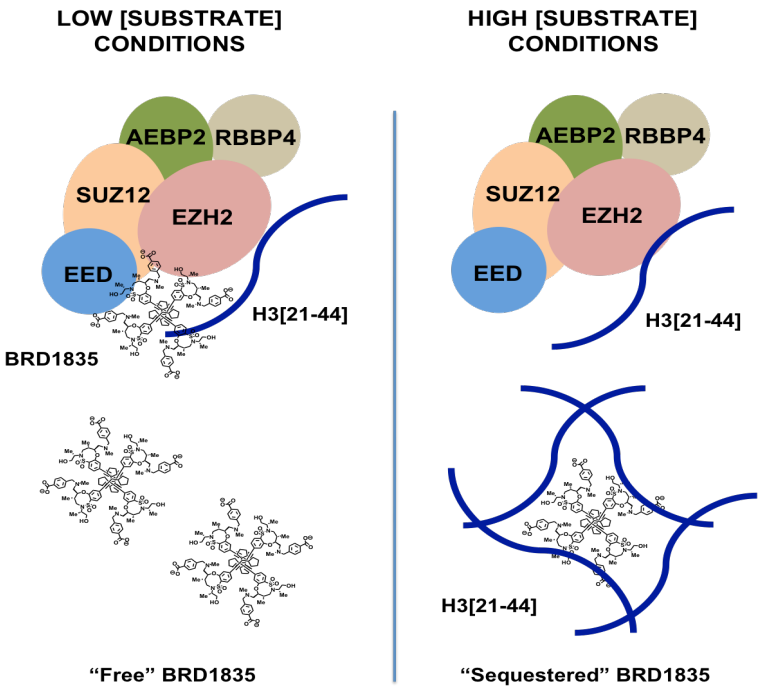

Figure 4.22 Proposed MOA for BRD1835 and active analogs
Under conditions of low substrate concentration, small negatively-charged aggregates of BRD1835 engage the substrate-bound complex in the vicinity of SUZ12, EED, and SUZ12, blocking activity (*left)*. With increased concentrations of substrate, BRD1835 is effectively sequestered by excess peptide enabling PRC2 to freely methylate available substrate.

concentration. Moreover, the aggregates formed are potentially of a nature that evades detection by DLS under low ionic conditions. Although these small aggregates appear to inhibit through a nonspecific mechanism (i.e. lacking classical 1:1 target engagement), they are not entirely promiscuous, given that no activity was measured in G9a and NSD2 assays. Moreover, it is yet undetermined whether the apparent cellular activity exhibited by BRD1835 is a result of direct PRC2 engagement or nonspecific interactions with the H3K27 region of histone H3 or other proteins. Confirmation of the later possibility would underline the issue of confirming intracellular target engagement using

broad target-connected phenotypes. With that said, the use of mass spectrometry-based target ID methods (28) or mutagenesis and resistance studies to identify dominant drug-resistant alleles (29) should always be considered, as these methods provide the most substantial proof for intracellular activity.

Lastly, it should be noted that other molecules likely share the novel inhibitory mechanism exhibited by BRD1835. As discussed in the previous chapter, three additional, distinct structural classes of putative PRC2 inhibitors were found to be strongly peptide-competitive, selective for PRC2, and able to bind peptide at high concentrations (as inferred by FP). Furthermore, all were active in the presence of detergent and lacked the ability to form large aggregates detectable by DLS. Taken together, these familiar properties are highly suggestive of nonspecific activity against PRC2 and may perhaps be predictive of artifactual behavior occurring in other HMT assays. Whether this phenomenon is specific to assays using highly charged peptides or those derived from histones remains to be determined. In any case, upfront assessment of peptide-binding activity may provide a means to rapidly and cost-effectively identify undesirable molecules in large screening collections or to avoid their pursuit if identified in future HTS campaigns.

4.3 Experimental methods

PRC2 DELFIA. PRC2 activity was measured using DELFIA performed on 384-well, white, streptavidin-coated plates (PerkinElmer). In short, PRC2 was diluted in 20 uL 2X Enzyme Buffer (50mM Tris HCl pH 8.5, 10 mM DTT, 0.02% Tween 20), 100 nL compound was pinned, reactions were initiated with 20 uL of a SAM (NEB) solution containing H3[21-44]-GK-biotin (Anaspec). Plates were incubated at room temperature for 1 hr and then washed three times with 100 uL of wash buffer (50mM Tris pH 7.4, 150 mM NaCl, 0.05% Tween 20, 0.2% BSA). Fluoroimmunoassay (FI) Buffer (50 mM Tris HCl pH 7.8, 150 mM NaCl, 0.05% Tween 40, 25 µM DTPA, 0.2% BSA, 0.05% BGG) containing a anti-H3K27me2 rabbit IgG (Cell Signaling, #9728) with 691 ng/mL Eu-N1-anti-rabbit IgG (PerkinElmer) was added at 50 uL per well. Following 1 hr incubation at room temperature, the plates were washed three times with wash buffer and 50 uL of Enhancement Solution (PerkinElmer) was added to each well. Plates were incubated for 30 min at room temperature and time-resolved fluorescence (TRF) was measured on Wallac Envision 2104 Multilabel Reader (400 us window, 400 us delay, 320 excitation, 615 emission).

PRC2 radiometric assays. PRC2 was diluted to final concentration in 2X enzyme buffer (50mM Tris HCl pH 8.5, 10 mM DTT, 0.01% Tween 20). Reactions were initiated with an equal volume of an SAM solution (NEB) containing ^{3}H-SAM (at 25% total SAM concentration; NET155001MC; PerkinElmer) and H3[21-44]-GK-biotin (AnaSpec) or histone H3.1 (NEB) and incubated at room temperature. For kinetic analysis, 100 uL aliquots were quenched in an equal volume of 3.2 mM SAM at various time points in a 96-well plate. After all time points were collected, quenched reactions were transferred

to a streptavidin-coated 96-well DELFIA plates (PerkinElmer) and incubated at RT for 1 hr. Unreacted ^{3}H-SAM was removed by washing plates three times with 200 uL of wash buffer (50mM Tris pH 7.4, 150 mM NaCl, 0.05% Tween 20, 0.2% BSA) per well. Modified peptide was then eluted by a 1 hr RT incubation with 100 uL/ well elution buffer (70% ACN, 5% formic acid, 1 mM biotin) and ^{3}H incorporation was measured by LSC (TriCarb 2910; PerkinElmer). For histone H3 assays, 50 mM histone H3.1 was substituted for peptide and reactions were filtered through an Immobilon (Bio-Rad) membrane using the 96-well Miniblot I Spot-Blot System (Sigma). Membranes were subsequently washed 3X with PBS and incubated in Ponceau S for protein visualization. Individual spots were excised and transferred to scintillation fluid for ON incubation before LSC.

DLBCL cell culture and RT-qPCR. DLBCL lines (Pfeiffer, WSU-DLCL2, HT, and OCI-LY-19) were cultured using conditions described in (10). Primer sequences for TXNIP, TNFRS21, and GAPDH used in RT-qPCR were identical to those described in (10) and obtained through Integrated DNA Technologies. DLBCL cells were seeded in 6-well plates at a density of 4E5 cells per well and treated with compound or DMSO. After 96 hours, cells were collected by centrifugation, washed with PBS, and RNA was extracted using RNeasy Mini Kit columns and QIAshredder homogenization (Qiagen). RNA was quantified by NanoDrop 2000 spectrophotometer and cDNA was synthesized from 5 ug RNA on a 100 uL scale using the High-Capacity cDNA Reverse Transcription Kit (Life Technologies) and random primers. RT-qPCR was conducted in 384-well ABI- plates with the Applied Biosystems 7900HT default protocol using 1 uL cDNA per well in 10 uL reactions containing 2X Power SYBR® Green Master Mix (Life Technologies) and 1 uM

concentrations of each primer. Ct values for each primer set, treatment condition, and cell line were measured in quadruplicate and fold-change over DMSO was calculated using GAPDH normalization of mean Ct values.

Surface plasmon resonance. SPR was performed using a Biacore T200 instrument using CM5 chips (GE Healthcare) to immobilize anti-FLAG M2 antibody (Sigma) in 50 mM acetate, pH 4.5. or anti-GST antibody provided by GST Capture Kit (GE) using the Amine Coupling Kit (GE). For 5C-PRC2 capture, 6 nM PRC2 was injected at a flow rate of 2 uL/min over anti-FLAG surface until saturation. For GST-EED[78-441], 30 ng/uL protein solution was injected at 10 uL/min over anti-GST surface to saturation. BRD1835 DMSO stock was diluted in PBS+EP Buffer (GE) to a final DMSO concentration of 5% in PBS+EP Buffer (GE) and injected for 60s at a flow rate of 60 uL/min.

Thermal shift assay. 6XHIS-EED (500 ng/uL in Assay Buffer) was mixed with SYPRO® Orange 5000X DMSO stock (Sigma) diluted 100X. To each well of a 384-well LightCycler® 480 multiwell plate Compounds were pinned at 100 nL per well and fluorescence was measured over a 25 °C – 95 °C temperature ramp using a Roche 480 LightCycler.

GST-EED[78-441] AlphaLISA. GST-EED[78-441] and biotinylated H3K9me3 peptide (H3[1-21]-GK-biotin) were diluted to 140 ng/uL and 2 uM in assay buffer (50 mM Tris, pH 8.5, 150 mM NaCl, 5 mM DTT, 0.01% Tween 20), respectively, and added to 384-well AlphaPlates (PerkinElmer) at 10 uL per well. Compounds and competing peptides were diluted in assay buffer to 2X final concentration and 10 uL stocks were mixed with GST-EED and H3K9me3 peptide. After 1 hr incubation, AlphaLISA Streptavidin Donor

Beads (PerkinElmer) and AlphaLISA anti-GST Acceptor Beads (PerkinElmer) were diluted in 1X Epigenetics Buffer (PerkinElmer) to 20 ug/mL each and added to plates at 20 uL per well. Alpha signal was detected using the Wallac Envision 2104 Multilabel Reader after 1 hr incubation.

Detergent and DELFIA-interference assays DELFIA assays were conducted as above with the following modifications. Detergent screening was performed using assay buffer with and without 0.01% Tween 20. For DELFIA-disruption assays, compounds were either pinned 1 hr post-reaction initiation and washed after 10 min or pinned into 2X Enzyme Buffer without enzyme, substituting H3K27me2-modified H3[21-44]-GK-biotin (AnaSpec) for unmodified H3[21-44]-GK-biotin.

^{1}H-NMR CAC determination ^{1}H NMR spectra were recorded on a 600 MHz Agilent spectrometer equipped with an automatic sample changer and a C{H} cold probe. 1680 scans with a relaxation plus acquisition time of 2 seconds were used for each spectrum. The residual solvent peak (H_2O) was referenced to 4.79 ppm and a Bernstein polynomial fit (order =3) baseline correction was applied along f1. Dilution series was carried out in 50 mM sodium phosphate, pH 7.4 formulated in D_2O following procedures outlined in (23). Data were collected by Michal Hallside, a graduate student in the laboratory of Professor Andy Phillips at Yale University.

HU172 photo-crosslinking. 0.5 uL of DMSO or BRD1835 was added to 24 uL of 5C-PRC2 diluted to 300 ng/uL in storage buffer (50 mM Tris, pH 8, 150 mM NaCl, 10% glycerol) and incubated for 15 minutes on ice. HU172 was diluted in DMSO to 500 uM and 0.5 uL was then added for a final concentration of 10 uM. After 15 min incubation on ice, mixture was transferred to a 96-well PP plate and irradiated by UV lamp (ENF-

260C) or 60 min at 365 nM. After crosslinking, 19.5 uL of sample was transferred to an eppendorf tube and 2.5 uL of 10% SDS, 0.5 uL of 5 mM biotin-PEG-azide (Life Technologies), and click catalyst (4 mM TBTA, 40 mM TCEP, and 40 mM $CuSO_4$) were added. After 60 min incubation at 50 °C, 1X LDS Sample Buffer (Life Technologies) was added and samples were immediately separated by SDS-PAGE; Precision Plus Protein Kaleidoscope standards (Bio-Rad) were used for downstream molecular weight estimation. Proteins were transferred to Immobilon PVDF membrane (Bio-Rad) at 30V for 1 hr and membranes were blocked with 5% BSA in TBST. Biotin was detected by ON incubation with 1:1000 dilution of streptavidin-HRP (Thermo) or IRDye® 800CW Streptavidin (LI-COR) followed by TBST washes and development using SuperSignal West Pico Chemiluminescent Substrate (Thermo) or high-sensitivity imaging (84 um resolution; 700/800 nm dual scan) on Odyssey® CLx Infrared Imaging System.

Histone Extraction and Western Blotting 293T cells (ATCC) were cultured in DMEM supplemented 10%(v/v) FBS and 100 U mL^{-1} penicillin-streptomycin. Cells were plated at 2e5 cells/well in 6-well dishes and treated with compound or DMSO vehicle on the following day. After 48 hr incubation, cells were rinsed with PBS, scraped into ice-cold PBS, and collected via centrifugation at 200 x g for 10 minutes. Pellets were resuspended in 0.2 volumes of 0.4 N HCl and incubated for at least 30 minutes on ice to extract histones. Cellular debris was then cleared by centrifugation at 10,000 x g for 10 minutes. Supernatant containing extracted histones was then neutralized with 0.4 volumes of 1 M sodium phosphate (pH 12.5) and concentration was determined via Bradford assay. 1 ug of acid-extracted histones from each treatment was separated on a precast 12% NuPAGE Bis-Tris SDS-PAGE gel (Life Technologies) and transferred to

a PVDF membrane. After blocking in 5% (w/v) non-fat dry milk dissolved in TBST for 1hr at RT, membranes were incubated overnight in blocking buffer containing primary antibody at 4°C. Membranes were then washed with TBST, incubated in blocking buffer containing a 1:2500 dilution of HRP-linked anti-rabbit IgG (GE Healthcare), and developed using chemiluminescence detection (SuperSignal, Thermo Fisher Scientific; Image Station 4000MM Pro, Kodak). For loading normalization, membranes were stripped using Restore Plus (Thermo) and re-probed with total H3 antibody (#9715, Cell Signaling).

Dynamic light scattering. DLS experiments as described in (7) with modifications. DMSO stock solutions were pinned at 250 nL in black 384-well clear bottom plates (Corning) containing 40 uL of assay buffer (50 mM Tris, pH 8.5, 5 mM DTT, 0.01%Tween 20). Alternatively, compounds were diluted manually into 100 uL of assay buffer, 50mM Sodium Phosphate (pH 7.4), PBS (pH 7.4), or 1X PBS-EP+ (pH 7.4; GE Healthcare). Autocorrelation functions were collected using DynaPro Plate Reader II using default settings.

Fluorescence polarization. Compound, DMSO, or competitor peptide was diluted to 2X final concentration in 1X Enzyme Buffer and added at 20 uL per well in black 384-well plates. H3[21-44] -HiLyte488 peptide (62.5 nM) and PRC2 (12.5 nM) were diluted in 1X Enzyme Buffer and added at 20 uL per well. Following 10 min incubation, fluorescence polarization (mP) was measured using Wallac Envision 2104 Multilabel Reader (FP FITC dual optical module; Excitation: 480 nm, Emission: 535 nm for both S- and P-channels).

4.4 References

1. Heidebrecht RW, Mulrooney C, Austin CP, Barker RH, Beaudoin JA, Cheng KC-C, et al. Diversity-Oriented Synthesis Yields a Novel Lead for the Treatment of Malaria. ACS Med Chem Lett. 2012 Feb 9;3(2):112–7.

2. Schreiber SL. Target-oriented and diversity-oriented organic synthesis in drug discovery. Science. 2000 Mar 17;287(5460):1964–9.

3. Doak AK, Wille H, Prusiner SB, Shoichet BK. Colloid formation by drugs in simulated intestinal fluid. J Med Chem. 2010 May 27;53(10):4259–65.

4. Seidler J, McGovern SL, Doman TN, Shoichet BK. Identification and prediction of promiscuous aggregating inhibitors among known drugs. J Med Chem. 2003 Oct 9;46(21):4477–86.

5. Shoichet BK. Interpreting steep dose-response curves in early inhibitor discovery. J Med Chem. 2006 Dec 14;49(25):7274–7.

6. Vedadi M, Barsyte-Lovejoy D, Liu F, Rival-Gervier S, Allali-Hassani A, Labrie V, et al. A chemical probe selectively inhibits G9a and GLP methyltransferase activity in cells. Nat Chem Biol. 2011 Aug;7(8):566–74.

7. McCabe MT, Ott HM, Ganji G, Korenchuk S, Thompson C, Van Aller GS, et al. EZH2 inhibition as a therapeutic strategy for lymphoma with EZH2-activating mutations. Nature. 2012 Dec 6;492(7427):108–12.

8. Sneeringer CJ, Scott MP, Kuntz KW, Knutson SK, Pollock RM, Richon VM, et al. Coordinated activities of wild-type plus mutant EZH2 drive tumor-associated hypertrimethylation of lysine 27 on histone H3 (H3K27) in human B-cell lymphomas. Proc Natl Acad Sci USA. National Acad Sciences; 2010 Dec 7;107(49):20980–5.

9. Cheng Y, Prusoff WH. Relationship between the inhibition constant (K1) and the concentration of inhibitor which causes 50 per cent inhibition (I50) of an enzymatic reaction. Biochemical Pharmacology. 1973 Dec 1;22(23):3099–108.

10. McCabe MT, Ott HM, Ganji G, Korenchuk S. EZH2 inhibition as a therapeutic strategy for lymphoma with EZH2-activating mutations. Nature. 2012.

11. Knutson SK, Wigle TJ, Warholic NM, Sneeringer CJ, Allain CJ, Klaus CR, et al. A selective inhibitor of EZH2 blocks H3K27 methylation and kills mutant lymphoma cells. Nat Chem Biol. 2012 Nov;8(11):890–6.

12. Konze KD, Ma A, Li F, Barsyte-Lovejoy D, Parton T, Macnevin CJ, et al. An orally bioavailable chemical probe of the Lysine Methyltransferases EZH2 and EZH1. ACS Chem Biol. 2013 Jun 21;8(6):1324–34.

13. Garapaty-Rao S, Nasveschuk C, Gagnon A, Chan EY, Sandy P, Busby J, et al. Identification of EZH2 and EZH1 small molecule inhibitors with selective impact on diffuse large B cell lymphoma cell growth. Chem Biol. 2013 Nov 21;20(11):1329–39.

14. Damian L. Isothermal titration calorimetry for studying protein-ligand interactions. Methods Mol Biol. Totowa, NJ: Humana Press; 2013;1008(Chapter 4):103–18.

15. De Simone A, Mancini F, Real Fernàndez F, Rovero P, Bertucci C, Andrisano V. Surface plasmon resonance, fluorescence, and circular dichroism studies for the characterization of the binding of BACE-1 inhibitors. Anal Bioanal Chem. Springer-Verlag; 2013 Jan;405(2-3):827–35.

16. Huber W, Mueller F. Biomolecular interaction analysis in drug discovery using surface plasmon resonance technology. Curr Pharm Des. 2006;12(31):3999–4021.

17. Yuan W, Wu T, Fu H, Dai C, Wu H, Liu N, et al. Dense chromatin activates Polycomb repressive complex 2 to regulate H3 lysine 27 methylation. Science. American Association for the Advancement of Science; 2012 Aug 24;337(6097):971–5.

18. Margueron R, Justin N, Ohno K, Sharpe ML, Son J, DruryIII WJ, et al. Role of the polycomb protein EED in the propagation of repressive histone marks. Nature. Nature Publishing Group; 2009 Aug 10;461(7265):762–7.

19. Xu C, Bian C, Yang W, Galka M, Ouyang H, Chen C, et al. Binding of different histone marks differentially regulates the activity and specificity of polycomb repressive complex 2 (PRC2). Proc Natl Acad Sci USA. National Acad Sciences; 2010 Nov 9;107(45):19266–71.

20. Lo M-C, Aulabaugh A, Jin G, Cowling R, Bard J, Malamas M, et al. Evaluation of fluorescence-based thermal shift assays for hit identification in drug discovery. Analytical Biochemistry. 2004 Sep 1;332(1):153–9.

21. Ullman EF, Kirakossian H, Switchenko AC, Ishkanian J, Ericson M, Wartchow CA, et al. Luminescent oxygen channeling assay (LOCI): sensitive, broadly applicable homogeneous immunoassay method. Clin Chem. 1996 Sep;42(9):1518–26.

22. Wigle TJ, Herold JM, Senisterra GA, Vedadi M, Kireev DB, Arrowsmith CH, et al. Screening for inhibitors of low-affinity epigenetic peptide-protein interactions: an AlphaScreen-based assay for antagonists of methyl-lysine binding proteins. J Biomol Screen. 2010 Jan;15(1):62–71.

23. LaPlante SR, Carson R, Gillard J, Aubry N, Coulombe R, Bordeleau S, et al. Compound aggregation in drug discovery: implementing a practical NMR assay for medicinal chemists. J Med Chem. 2013 Jun 27;56(12):5142–50.

24. McGovern SL, Helfand BT, Feng B, Shoichet BK. A specific mechanism of nonspecific inhibition. J Med Chem. 2003 Sep 25;46(20):4265–72.

25. Thorne N, Auld DS, Inglese J. Apparent activity in high-throughput screening: origins of compound-dependent assay interference. Curr Opin Chem Biol. 2010 Jun;14(3):315–24.

26. Shoichet BK. Screening in a spirit haunted world. Drug Discov Today. 2006 Jul;11(13-14):607–15.

27. McGovern SL, Caselli E, Grigorieff N, Shoichet BK. A common mechanism underlying promiscuous inhibitors from virtual and high-throughput screening. J Med Chem. 2002 Apr 11;45(8):1712–22.

28. Schenone M, Dančík V, Wagner BK, Clemons PA. Target identification and mechanism of action in chemical biology and drug discovery. Nat Chem Biol. 2013 Apr;9(4):232–40.

29. Wacker SA, Houghtaling BR, Elemento O, Kapoor TM. Using transcriptome sequencing to identify mechanisms of drug action and resistance. Nat Chem Biol. 2012 Mar;8(3):235–7.

Chapter V

Characterization of putative PRC2 activators, BRD8284 and BRD3934

Collaborator Contributions

- **Dr. Fumika Hirobe Yakushiji and Mengfei Zhang** resynthesized BRD8284 and BRD3934.
- **Dr. Fumika Hirobe Yakushiji** performed H3.1 assays (radiometric and western blot) for biochemical evaluation of BRD8284 and BRD3934 activity on PRC2.

5.1 Introduction

In contrast to the overwhelming number of identified chemical probes and drugs that inhibit their protein targets, very few synthetic, small-molecule activators of enzyme function have been identified to date (1). Some examples include activators of glucokinase (RO281675; ref. 2), PDK1 (PS48; refs. 3,4), RNase L (C1; ref. 5) , AMPK (A769662; refs. 6,7), and most famously, SIRT1 (resveratrol and SRT1720; refs. 8,9)—although the ability of SIRT1 probes to *directly* activate enzyme activity has generated debate (10,11). Biochemical activation of a given target can occur through a small molecule binding an allosteric site within the catalytic domain (RO281675; ref. 12) or regulatory subunit (A769662; ref.13) to stabilize the active enzyme conformation or induce activating multimerization (C1; ref 5). The therapeutic utility of small-molecule activators varies from target to target. However, regardless of therapeutic impact, elucidating the MOA of small-molecule activators often can lead to advances in biological understanding by illuminating previously unknown and/or underappreciated mechanisms of allosteric regulation (1).

In **Chapter III**, we described the use of DELFIA to assay, over two rounds of screening, >120,000 diverse small molecules for their ability to modulate PRC2 activity. In the second round, among a set of 58,917 DOS compounds screen, we discovered a large number of high signal outliers that were potential PRC2 activators. In total, we identified 274 compounds that increased DELFIA signal by >50% relative to DMSO. Among these initial hits, 23 compounds increased apparent PRC2 activity in a dose-responsive manner (Figure 5.1A). These putative activators clustered into five major structural categories (with AC_{50}s in the 3-25 uM range); however, two chemotypes,

azocane and bridged bicyclic, were overrepresented (Figure 5.1B). Since the most potent activators were bridged bicyclic compounds, we chose members of this structural class for further study. This chapter describes the identification and characterization of two such bridged bicyclic activators, BRD8284 and BRD3934.

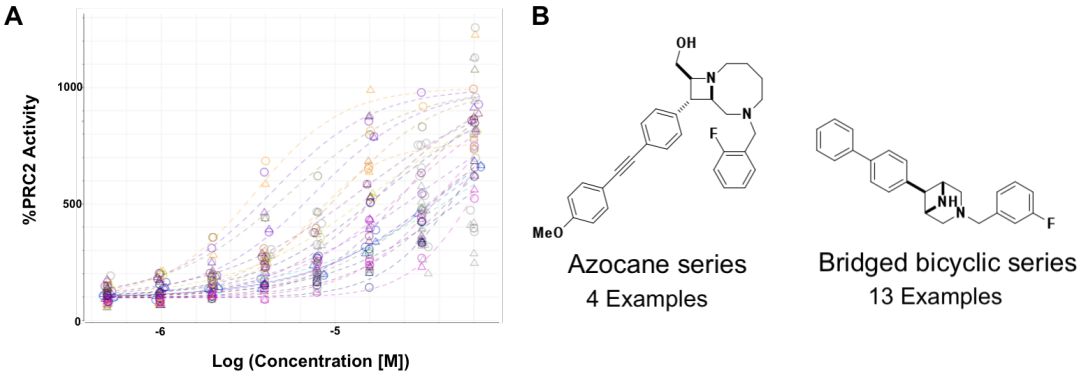

Figure 5.1 Activity and structures of identified PRC2 activator candidates
(A) Dose-response curves for 23 activator hits identified. (B) Major structural classes of clustered activator candidates. A majority of activator candidates were of the bridged bicyclic DOS series (13/24).

5.2 Results and discussion

5.2.1 Initial SAR studies and the identification of BRD8284 and BRD3934

The Broad Institute's unique DOS compound libraries, which contain a large number of stereoisomers and analogs for any given DOS molecule, are designed to facilitate rapid identification of both structure-activity relationships (SAR) and stereochemical structure-activity relationships (SSAR) (14). As the bridge bicyclic PRC2 activator candidates were derived from DOS, we were able to establish preliminary SAR and identify analogs of improved potency by obtaining compounds of interest directly from internal compound management services at the Broad Institute. For subsequent SAR studies, we selected the most potent activator identified by hit retest in PRC2 DELFIA, BRD-K51079083 (Figure 5.2A).

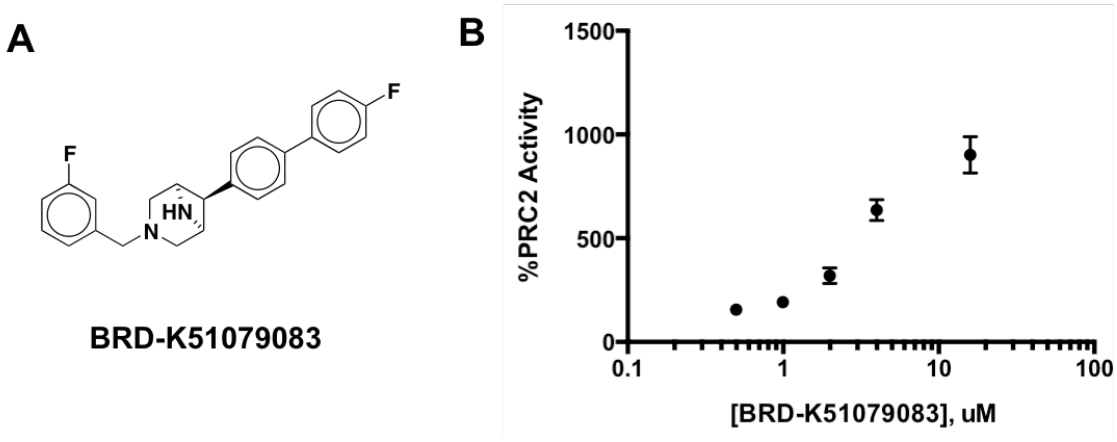

Figure 5.2 Structure and activity of BRD-K51079083
(A) Structure of BRD-K51079083 and (B) its activity in PRC2 DELFIA. Data points represent mean and standard error of triplicate measurements.

In DELFIA format, BRD-K51079083 increased apparent PRC2 activity by ~10-fold in a dose-responsive manner, exhibiting an AC_{50} in the ~2 uM range (Figure 5.2B). For initial SAR studies, we obtained nine analogs harboring different phenyl substituents (meta-, ortho-, and para-fluoro phenyl, meta-methyl phenyl, etc.) and varying in their stereochemical configurations (Figure 5.3A). Upon evaluating these analogs in PRC2 DELFIA, we discovered, while BRD-K51079083 increased PRC2 DELFIA signal by only 2-fold over DMSO, BRD-K31198284 (BRD8284) was able to increase signal to a greater degree (a 3-fold increase over DMSO). In contrast to BRD-K51079083, BRD8284 contains a phenyl substituent in place of the para-fluoro phenyl group and differed in configuration at all stereocenters (Figure 5.3B). Interestingly, BRD-K68443934 (BRD3934), differing from BRD8284 in configuration at the C7 (pseudo)stereocenter, appeared to activate PRC2 to a lesser degree (~1.5 fold activation over DMSO) with lower potency (Figure 5.3B,C).

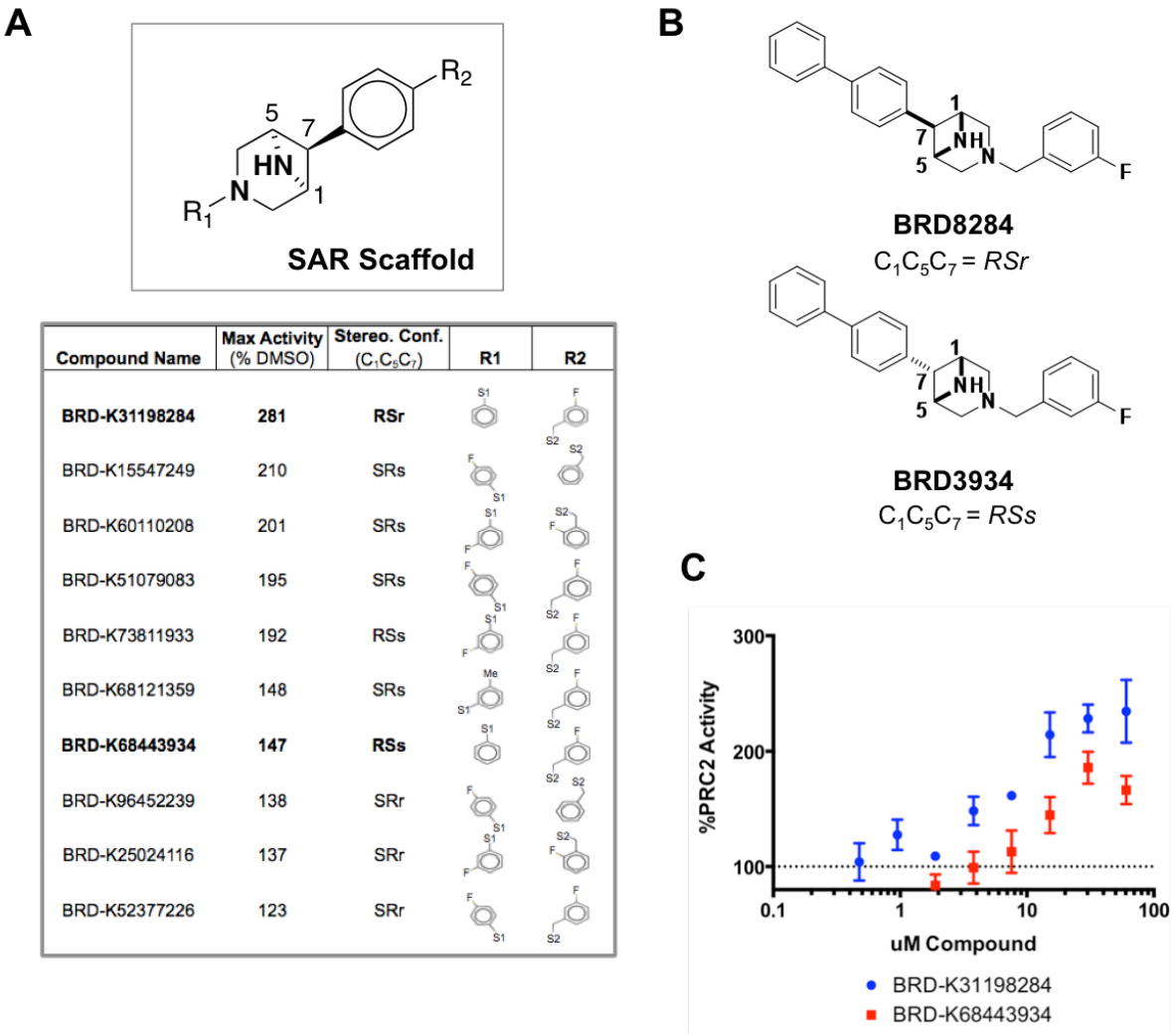

Compound Name	Max Activity (% DMSO)	Stereo. Conf. ($C_1C_5C_7$)	R1	R2
BRD-K31198284	**281**	**RSr**		
BRD-K15547249	210	SRs		
BRD-K60110208	201	SRs		
BRD-K51079083	195	SRs		
BRD-K73811933	192	RSs		
BRD-K68121359	148	SRs		
BRD-K68443934	**147**	**RSs**		
BRD-K96452239	138	SRr		
BRD-K25024116	137	SRr		
BRD-K52377226	123	SRr		

Figure 5.3 SAR summary of BRD-K51079083 analogs and identification of BRD8284 and BRD3934
(A) SAR summary of BRD-K51079083 analogs and their maximum activity relative to DMSO in PRC2 DELFIA, representing the mean of triplicate measurements (B) Structures of BRD-K31198284 (BRD8284) and BRD-K68553934 (BRD3934). (C) Activity of BRD-K31198284 (BRD8284) and BRD-K68553934 (BRD3934) in PRC2 DELFIA. Data points represent the mean and standard error of triplicate measurements,

While no striking SAR could be established within the series tested, we were able to identify an analog with activity superior to that of our initial activator candidate. We selected both BRD8284 and BRD3934 for resynthesis and further study, given that their differing stereochemistry appeared to influence their ability to activate in PRC2 DELFIA—a potentially useful feature that could be exploited to gauge the validity and specificity of their activity in downstream characterization efforts (e.g. orthogonal

biochemical and cellular assays). Since probe discovery efforts have yielded few examples of small-molecule activators of enzyme activity (1) and no synthetic molecules capable of activating PRC2 are known, we were attracted by the possibility of developing first-in-class PRC2 activators.

5.2.2 Investigating the substrate dependency of BRD8284 and BRD3934

After resynthesis of BRD8284 and BRD3934, we retested their activity in PRC2 DELFIA. Unexpectedly, resynthesized BRD8284 was unable to significantly increase signal, while BRD3934, a stereoisomer previously shown to exhibit weaker activity, was able to increase apparent PRC2 activity by >2-fold at the highest concentration tested (100 uM; Figure 5.4A). Moreover, the potency (AC_{50}) of these resynthesized analogs appeared comparatively weaker (no dose-response curve convergence up to 100 uM) than those obtained through internal compound management services (2-10 uM AC_{50}). While the exact reasons for this difference in activity were never uncovered, BRD3934 displayed reproducible activation in PRC2 DELFIA, thus we pursued further study.

To determine whether activation by BRD3934 and BRD8284 were artifacts of DELFIA or, similar to SIRT1 activators (10,11), dependent on use of peptide substrate, we tested the activity of these candidates in an orthogonal radiometric assay using full-length histone H3.1 and ^{3}H-SAM, measuring ^{3}H incorporation over time by LSC. To ensure that reaction conditions were such that activation of PRC2 could be measured, we included, as a positive control, an H3K27me3-modified peptide (H3[23-34], K27me3; 25 uM) previously shown to allosterically increase PRC2 activity (V_{MAX}) (15). Compared to DMSO, BRD3934 (at 50 uM) was able to effectively increase PRC2 reaction velocity in this orthogonal assay, while BRD8284 displayed little activity, consistent with PRC2

DELFIA (Figure 5.4B). These results suggest that the apparent activation of PRC2 measured in DELFIA can occur independently of peptide substrate and is not an artifact of assay readout.

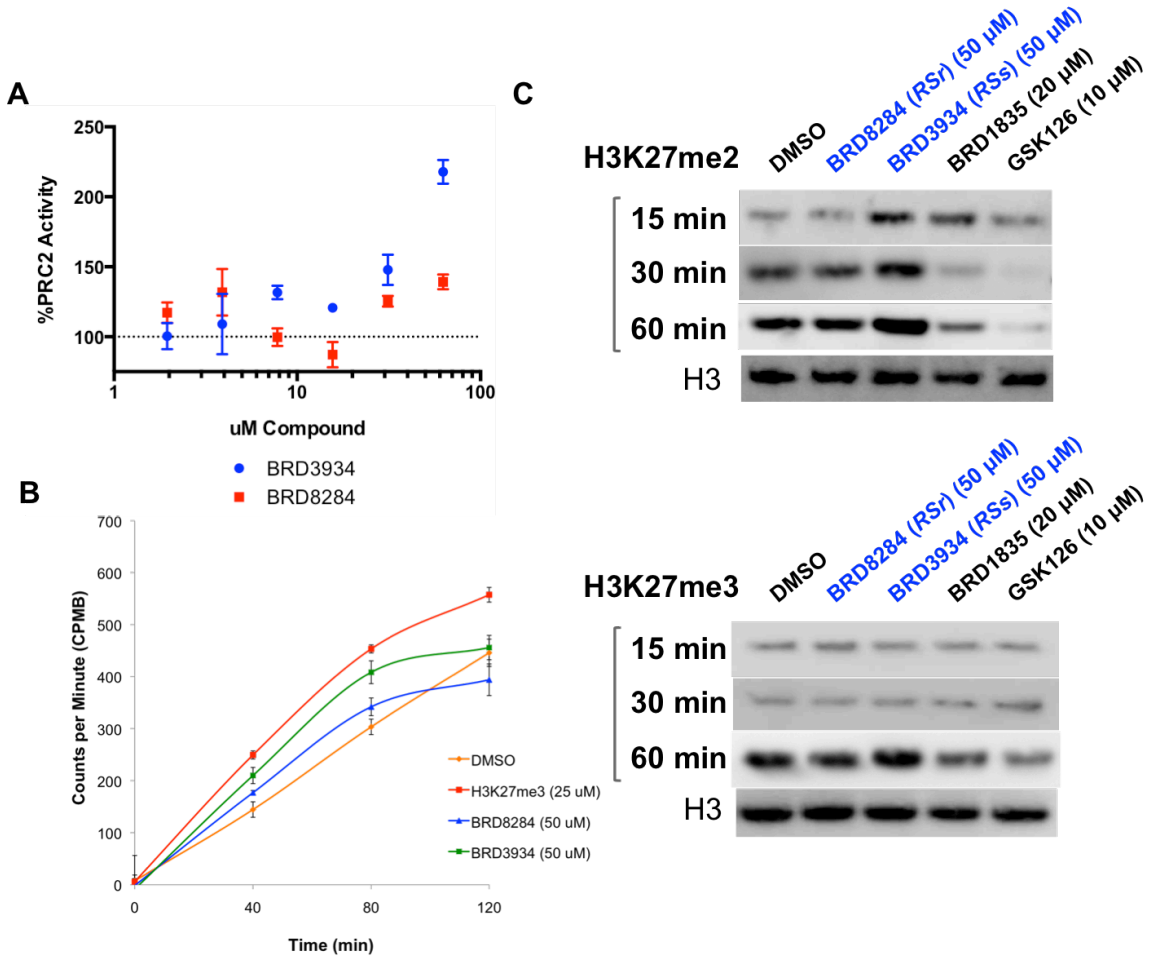

Figure 5.4 Activity of resynthesized activators in DELFIA and histone H3.1 assays
(A) Activity of resynthesized BRD8284 and BRD3934 in PRC2 DELFIA. Data points represent the mean and standard error of triplicate measurements. (B) Activity of 50 uM BRD8284, 50 uM BRD3934, and 25 uM H3[23-34]-K27me3 peptide in a PRC2 radiometric time-course assay using histone H3.1 substrate. Data points represent the mean and standard deviation of triplicate measurements. (C) Western blot detection of H3K27me2-and H3K27me3-modified H3.1 substrate, at various reaction time points, generated in the presence of BRD8284 and BRD3934 at 50 uM. Samples from each PRC2 reaction were quenched with LDS loading buffer at the times indicated and separated by SDS-PAGE (12% BT gel). BRD1835 and GSK126 were used as inhibitor controls.

We next aimed to explore whether BRD3934 or BRD8284 influenced the degree of methylation (i.e. H3K27me2 or H3K27me3) achieved by PRC2. *In vitro*, 5-component PRC2 (EED, SUZ12, AEBP2, and RBBP4) is able to catalyze H3K27 mono- and

dimethylation, yet it is unable to achieve efficient H3K27 trimethylation (16,17). By way of EZH2 mutation (e.g. Y641 and A677 alterations) or PHF1/PCL1 binding, PRC2 can adopt conformations that enable trimethylation of its substrate (17-20). As most known small-molecule activators stabilize a specific enzyme states (1), we questioned whether PRC2 activators could endow trimethylation activity *in vitro* by way of stabilizing PRC2 conformations resulting typically from PCL1 binding or activating mutation.

Using histone H3.1 as a substrate, we conducted a PRC2 time course assay in the presence of BRD8284 or BRD3934 (both at 50 uM) and measured specific changes in H3K27me2 and H3K37me3 levels by western blot to assess the degree of methylation achieved under each condition. Compared with DMSO and BRD8284, BRD3934 increase H3K27me2 levels by >2-fold at 50 uM, while neither activator candidate induced substantial differences in H3K27me3 (Figure 5.4C). Interestingly, an apparent increase in H3K27me3 could be detected under DMSO conditions. While the use of full-length histone H3.1 (rather than peptide fragment) may endow greater H3K27me3 activity *in vitro*, these findings were likely the result of nonspecific antibody binding.

5.2.3 Exploring BRD8284 and BRD3934 mechanism-of-action (MOA)

Endogenous and biochemical PRC2 activation has been previously shown to occur through several mechanisms. In addition to PCL1 regulation discussed in the previous section (19), PRC2 can be allosterically activated by SUZ12 binding histone H3 (residues 35-42) within nucleosomes (21) and EED binding repressive histone marks, such as H3K27me3 or H3K9me3 (15,22). As these mechanisms could provide a

basis for small-molecule activation, we questioned whether BRD3934 activated PRC2 through engagement of SUZ12, EED, or a previously uncharacterized allosteric site.

As we were unable to obtain sufficient quantities of pure SUZ12 protein to support assay development, we were limited to studies on EED. As GST-EED[78-441] (WD40 domain) could be expressed in bacteria with high yields and binds H3K9me3 with reasonable affinity (~10 uM K_D) (15,22), we developed an AlphaLISA assay (23,24) using a biotinylated H3K9me3-modified peptide (H3[1-21]) and GST-EED[78-441] to measure potential disruption of EED-H3K9me3 interaction. We speculated that if BRD3934 were modulating PRC2 activity through an interaction with EED, it might bind the same allosteric site as its known ligands and thus compete with H3K9me3 peptide binding. With this in mind, we evaluated the activity of BRD8284 and BRD3934 in an EED-H3K9me3 AlphaLISA, expecting potential reductions in signal corresponding to displacement of H3K9me3 from EED (Figure 5.5A). Interestingly, BRD8284 showed modest dose-responsive activity, while BRD3934 was essentially inactive. Given that resynthesized BRD8284 failed to exhibit significant activation of PRC2 in previous assays, we suspected that its apparent activity on EED was likely the result of nonspecific inhibition.

While BRD8284 and BRD3934 were unlikely binding the known allosteric site on EED, interaction with EED at another site remained a possibility. To investigate any potential interaction between EED and our activator candidates, we obtained full-length 6XHIS-EED (purified from Sf9 cells) and evaluated direct binding through fluorescence-based thermal shift assays (TSA) by measuring the denaturation midpoint (Tm) for EED in the presence of DMSO or high concentrations of BRD8284 and BRD3934 (125 uM).

As ligand binding is often exemplified by thermal stabilization of target proteins (25), we expected BRD3934 (and to a lesser degree, BRD8284), if the compound bound EED, to increase the Tm of EED. However, neither BRD8284 nor BRD3934 was able to alter the thermal stability of EED relative to DMSO (Figure 5.5B), suggesting their activation of PRC2 does not involve EED binding.

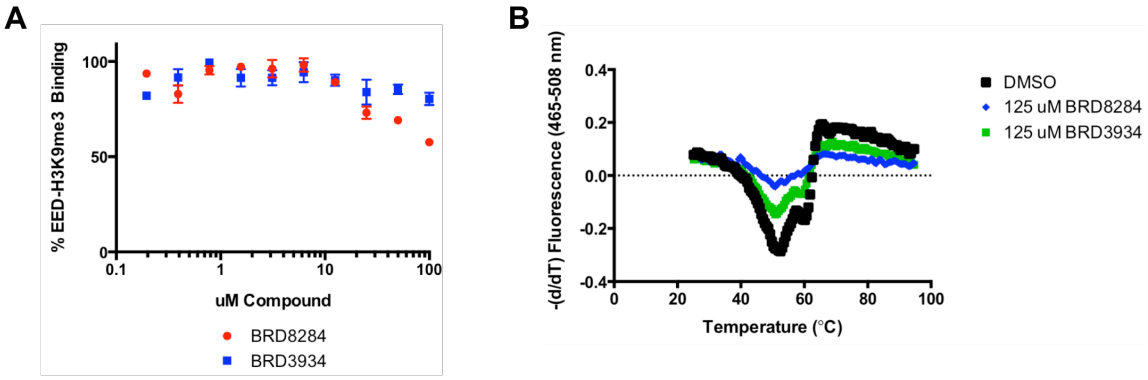

Figure 5.5 Activity of BRD8284 in EED-H3K9me3 AlphaLISA and EED TSA
(A) Activity of BRD8284 and BRD3934 in GST-EED[78-441]-H3K9me3 AlphaLISA. Data points represent the mean and standard error of four replicate measurements. (B) 6X-EED thermal shift assay (TSA) with 125 uM BRD8284 and 125 uM BRD3934. The curve minima are representative of Tm. Each curve represents a single sample.

While aggregation-based inhibition is excepted as a widespread phenomenon, aggregation-induced activation has only recently been demonstrated and its mechanism remains poorly understood (26). Regardless, as we had identified a large number of aggregator hits from our PRC2 HTS campaign, we sought to rule out such an aggregation-based activation mechanism. As dynamic light scattering (DLS) successfully enabled identification of large aggregates in past studies, we used this method to estimate the critical aggregation concentrations (CACs) of BRD8284 and BRD3934. By measuring intensity autocorrelation functions to detect the presence of particles, we found that BRD3934 exhibited no sign of large aggregate formation (up to

200 uM), while BRD8284 clearly aggregated at 25 uM (and above) in activity assay buffer (50 mM Tris pH 8.5, 5 mM DTT, 0.01% Tween 20; Figure 5.6).

Although BRD8284 does not inhibit PRC2 activity at concentrations above its CAC, the ability of BRD8284 to form large aggregates may explain its activity in EED-H3K9me3 AlphaLISA, as apparent disruption could occur through an aggregation-based mechanism. Furthermore, since BRD3934 formed no detectable aggregates in activity assay buffer (up to 200 uM), differing aggregation behavior might underlie the ability to activate PRC2 and relate to activity discrepancies between compound preparations. In other words, varying purity could influence aggregation, while the formation of large particles impedes activation. Future studies will aim to explore this hypothesis through synthesis and biochemical evaluation of analogs with improved solubility.

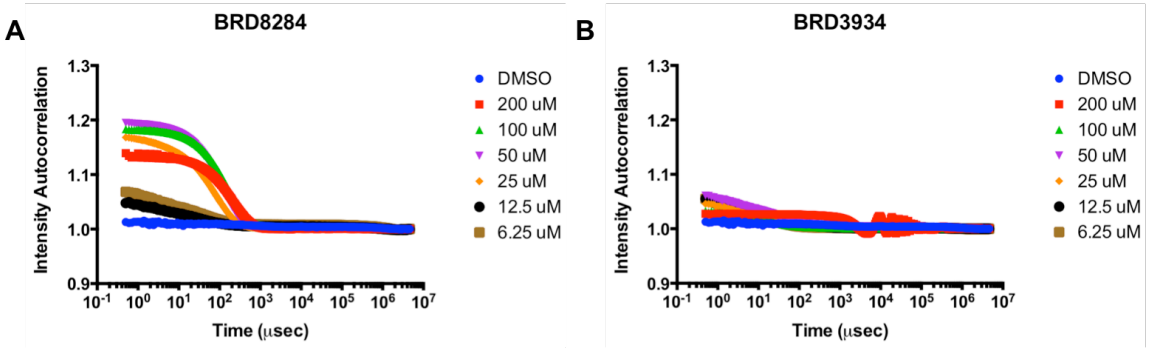

Figure 5.6 DLS evaluation of BRD8284 and BRD3934 in activity assay buffer
DLS intensity autocorrelation functions for BRD8284(A) and BRD3934(B) in activity assay buffer. While no aggregation could be detected for BRD3934 (up to 200 uM), BRD8284 exhibited clear aggregation at 25 uM and above. Data represent the average of 10 acquisitions of single samples.

5.2.4 Evaluating cellular activity of putative activators

To determine whether BRD8284 or BRD3934 were able to activate PRC2 in cells, we evaluated their activity in an H3K27me3 HCA, treating HeLa cells with DMSO

or compound in 10-point dose. Following 72 hr incubation, cells were stained for H3K27me3 and imaged by automated microscope (IX Micro), using an optimized immunofluorescence protocol described in **Chapter II**. Average nuclear fluorescence (presumed H3K27me3 levels) and total cell number were determined by image analysis

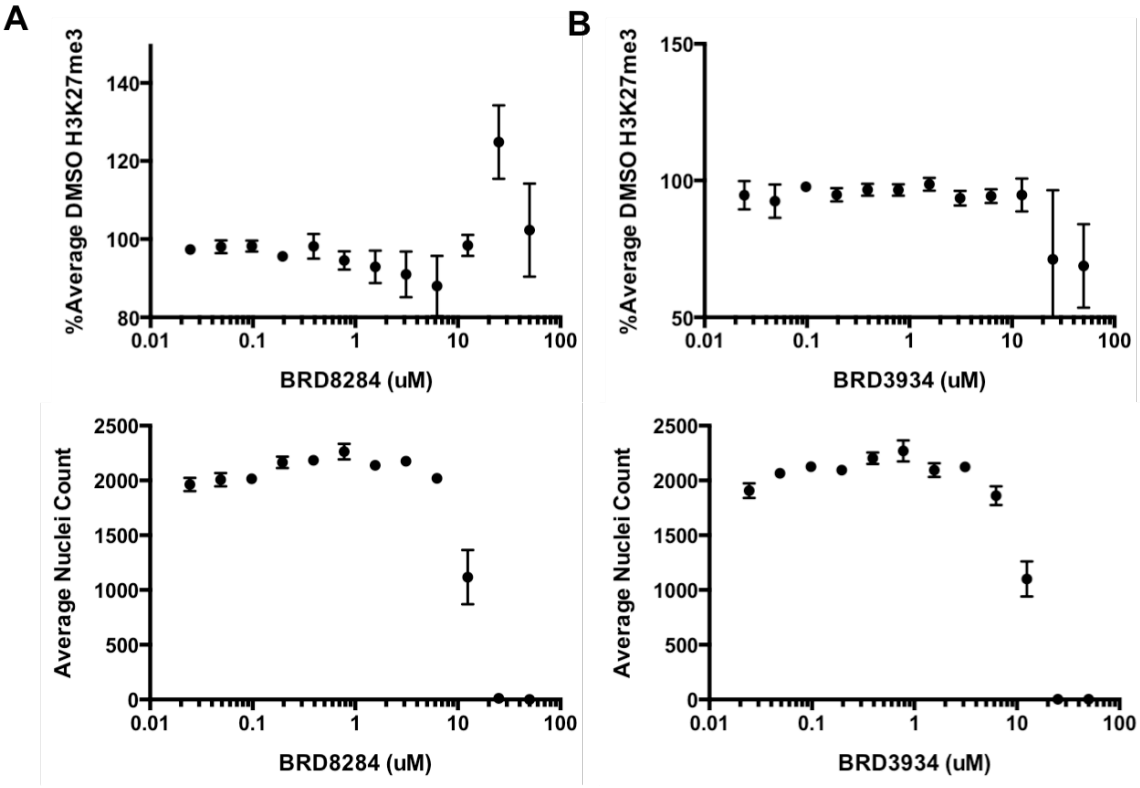

Figure 5.7 Cellular activity of BRD8284 and BRD3934 in H3K27me3 HCA following 72 treatment
DMSO-normalized average nuclear fluorescence (*top panels*) and average nuclei counts (*bottom panels*) per well following 72 hr treatment with (A) BRD8284 and (B) BRD3934. Data points represent mean and standard error of six replicates across two assay plates.

for each treatment condition. As seen in Figure 5.7, BRD3934 (at concentrations above 50 uM) *decreased* average nuclear fluorescent signal, while similar concentrations of BRD8284 lead to an apparent increase. However, both BRD8284 and BRD3934 significantly decreased cell number at these concentrations, suggesting that apparent changes in global H3K27me3 levels were likely artifacts of immunostaining, as dead or

dying cells typically display autofluorescence and can effectively skew estimates of average nuclear fluorescence (often though erroneous detection of nuclei).

Given their apparent toxicity at biochemically active concentrations, we were unable to determine the cellular activity of BRD8284 or BRD3934. Moreover, *both* BRD8284 and BRD3934 impacted cell number with steep dose-response curves at concentrations above 10 uM, suggesting that solubility (or aggregation) may underlie cellular toxicity. Whether this finding can be extrapolated to biochemical assays, suggesting potential formation of small BRD3934 aggregates that were less readily detected than BRD8284 aggregates but that may still underlie apparent PRC2 activation, is yet to be determined. In any case, these results reveal future challenges in developing BRD3934 into a cell-active probe, as significant improvements in potency and/or solubility will be required to avoid nonspecific toxicity. However, before such medicinal chemistry efforts are undertaken, additional work toward establishing SAR and verifying target engagement should be conducted.

5.2.5 Discussion and future studies

In contrast to the development of PRC2 inhibitors (27-31), efforts to discover small-molecule activators of PRC2 have not been described—undoubtedly a consequence of their perceived lack of therapeutic utility. The motivation to develop potent EZH2 inhibitors is clear, stemming from the assumed oncogenic role of PRC2 (20,32-34) and the strong evidence of EZH2 dependencies in several human cancers, including DLBCL (35) and aggressive rhabdoid sarcomas (36). While EZH2 does appear to function as a tumor suppressor in different cancer contexts (e.g. MDS/MPN and T-ALL; refs. 37,38), the presumed scenario in which PRC2 activation would provide

therapeutic benefit, small-molecules that stimulate PRC2 activity in an in vitro setting may also, while seemingly contradictory, provide benefit in EZH2-dependent cancers. For instance, small molecules binding SUZ12 or EED in cells could potentially block effective H3K27me3 propagation necessary to establish repressive chromatin domains, leading to a global loss of H327me3 and derepression of PRC2 target genes, functioning as an effective inhibitor. PRC2 activators may also prove useful in H3.3-K27M-driven pediatric glioblastoma, as H3.3-K27M-sequestered PRC2 may be freed upon small-molecule binding (40,41)

Regardless of therapeutic utility, small-molecule PRC2 activators may reveal previously unknown mechanisms through which the complex is allosterically regulated, contributing to our understanding of PRC2 biology. Further study of BRD3934 may provide a route to the development of such activators, as these candidates were able to activate PRC2 in a substrate-independent manner and through a mechanism distinct from those involving EED. While mechanism-of-action studies will be required to confirm target engagement and rule out an aggregation-based mechanism, continued exploration of BRD3934 may demonstrate the feasibility of small-molecule PRC2 activator development, uncover novel PRC2 regulatory mechanisms, or, at the very least, contribute to our understanding of nonspecific activation mechanisms.

5.3 Experimental methods

PRC2 DELFIA. PRC2 activity was measured using DELFIA performed on 384-well, white, streptavidin-coated plates (PerkinElmer). In short, PRC2 was diluted in 20 uL 2X Enzyme Buffer (50mM Tris HCl pH 8.5, 10 mM DTT, 0.02% Tween 20), 100 nL compound was pinned, reactions were initiated with 20 uL of a SAM (NEB) solution containing H3[21-44]-GK-biotin (Anaspec). Plates were incubated at room temperature for 1 hr and then washed three times with 100 uL of wash buffer (50mM Tris pH 7.4, 150 mM NaCl, 0.05% Tween 20, 0.2% BSA). Fluoroimmunoassay (FI) Buffer (50 mM Tris HCl pH 7.8, 150 mM NaCl, 0.05% Tween 40, 25 µM DTPA, 0.2% BSA, 0.05% BGG) containing a anti-H3K27me2 rabbit IgG (Cell Signaling, #9728) with 691 ng/mL Eu-N1-anti-rabbit IgG (PerkinElmer) was added at 50 uL per well. Following 1 hr incubation at room temperature, the plates were washed three times with wash buffer and 50 uL of Enhancement Solution (PerkinElmer) was added to each well. Plates were incubated for 30 min at room temperature and time-resolved fluorescence (TRF) was measured on Wallac Envision 2104 Multilabel Reader (400 us window, 400 us delay, 320 excitation, 615 emission).

PRC2 radiometric assays PRC2 was diluted to final concentration in 2X enzyme buffer (50mM Tris HCl pH 8.5, 10 mM DTT, 0.01% Tween 20). Reactions were initiated with an equal volume of an SAM solution (NEB) containing ^{3}H-SAM (at 25% total SAM concentration; NET155001MC; PerkinElmer) and H3[21-44]-GK-biotin (AnaSpec) or histone H3.1 (NEB) and incubated at room temperature. For kinetic analysis, 100 uL aliquots were quenched in an equal volume of 3.2 mM SAM at various time points in a 96-well plate. After all time points were collected, quenched reactions were transferred

to a streptavidin-coated 96-well DELFIA plates (PerkinElmer) and incubated at RT for 1 hr. Unreacted ^{3}H-SAM was removed by washing plates three times with 200 uL of wash buffer (50mM Tris pH 7.4, 150 mM NaCl, 0.05% Tween 20, 0.2% BSA) per well. Modified peptide was then eluted by a 1 hr RT incubation with 100 uL/ well elution buffer (70% ACN, 5% formic acid, 1 mM biotin) and ^{3}H incorporation was measured by LSC (TriCarb 2910; PerkinElmer). For H3.1 filter binding assay, reaction volume was scaled to 100 uL per well and 50 nM histone H3.1 (NEB) was substituted for peptide. Reactions were quenched with equal volumes of cold SAM (3.2 mM) and filtered through 96-well HA filter plates (Millipore) after 1 hr incubation. Wells were washed 3X with PBS pH 7.4 and membranes were dried. 50 uL MicroScint (PerkinElmer) was added per well before reading on TopCount NTX.

Thermal shift assay. 6XHIS-EED (500 ng/uL in Assay Buffer) was mixed with SYPRO® Orange 5000X DMSO stock (Sigma) diluted 100X. To each well of a 384-well LightCycler® 480 multiwell plate Compounds were pinned at 100 nL per well and fluorescence was measured over a 25 °C – 95 °C temperature ramp using a Roche 480 LightCycler.

GST-EED[78-441] AlphaLISA. GST-EED[78-441] and biotinylated H3K9me3 peptide (H3[1-21]-GK-biotin) were diluted to 140 ng/uL and 2 uM in assay buffer (50 mM Tris, pH 8.5, 150 mM NaCl, 5 mM DTT, 0.01% Tween 20), respectively, and added to 384-well AlphaPlates (PerkinElmer) at 10 uL per well. Compounds and competing peptides were diluted in assay buffer to 2X final concentration and 10 uL stocks were mixed with GST-EED and H3K9me3 peptide. After 1 hr incubation, AlphaLISA Streptavidin Donor Beads (PerkinElmer) and AlphaLISA anti-GST Acceptor Beads (PerkinElmer) were

diluted in 1X Epigenetics Buffer (PerkinElmer) to 20 ug/mL each and added to plates at 20 uL per well. Alpha signal was detected using the Wallac Envision 2104 Multilabel Reader after 1 hr incubation.

Fluorescence polarization. Compound or DMSO was diluted to 2X final concentration in 1X Enzyme Buffer and added at 20 uL per well in black 384-well plates. H3[21-44] - HiLyte488 peptide was then diluted to 62.5 nM in 1X Enyzme Buffer and added at 20 uL per well. Following 10 min incubation, fluorescence polarization (mP) was measured using Wallac Envision 2104 Multilabel Reader (FP FITC dual optical module; Excitation: 480 nm, Emission: 535 nm for both S- and P-channels).

Immunofluorescence. HeLa cells (ATCC) were cultured in DMEM supplemented 10%(v/v) FBS, 1 mM sodium pyruvate, and 100 U mL-1 penicillin-streptomycin. Cells were diluted in culture medium at 5e4 cells/mL and plated in black clear-bottom 96-well plates (Corning, 3904) at 100 uL/well. After 24 hr incubation at 37°C/5% CO2, 100 nL of compound or DMSO vehicle was pinned into each well and cells were incubated for an additional 48 hrs. Treated cells were fixed with 4% paraformaldhyde for 10 min, permeabilized with 0.3% Triton X-100 in PBS for 20 min, and blocked with 3% BSA in PBST for 1 hr at room temperature. Cells were then incubated with primary antibody (anti-H3K27me3; Cell Signaling, #9733) diluted in blocking buffer overnight at 4°C. A mixture of 1 nM Hoechst 33342 (Life Technologies) and 2 ug/mL Alexa Fluor 488 goat anti-rabbit IgG (Life Technologies, A11008) in blocking buffer was then added. Following a 1 hr incubation at RT, cells were then imaged on an ImageXpress Micro automated microscope (Molecular Devices) using a 10X objective with laser-based focusing. Image analysis was performed using the Cell Scoring module in the

MetaXpress software (Molecular Devices) to determine average nuclear fluorescence and nuclei counts per well. Mean and standard deviation (STDEV) were calculated for all DMSO wells within each assay plate.

Data analysis and curve fitting (AC_{50}). For AC_{50} determination, DMSO-normalized, background-subtracted activity values (see equation below) for each compound at varying concentration were fit using Condoseo GeneData Screener (Smart Fit Strategy using default settings with no restrictions and no requirement for convergence).

$$\%Activity = 100 \times \frac{Signal_{Compound} - MEAN(Signal_{PosCon\ wells})}{MEAN(Signal_{DMSO\ wells}) - MEAN(Signal_{PosCon\ wells})}$$

Dynamic light scattering. DLS experiments as described in (7) with modifications. DMSO stock solutions were pinned at 250 nL in black 384-well clear bottom plates (Corning) containing 40 uL of assay buffer (50 mM Tris, pH 8.5, 5 mM DTT, 0.01%Tween 20). Alternatively, compounds were diluted manually into 100 uL of assay buffer, 50mM Sodium Phosphate (pH 7.4), PBS (pH 7.4), or 1X PBS-EP+ (pH 7.4; GE Healthcare). Autocorrelation functions were collected using DynaPro Plate Reader II using default settings.

5.4 References

1. Zorn JA, Wells JA. Turning enzymes ON with small molecules. Nat Chem Biol. 2010 Mar;6(3):179–88.

2. Grimsby J, Sarabu R, Corbett WL, Haynes N-E, Bizzarro FT, Coffey JW, et al. Allosteric activators of glucokinase: potential role in diabetes therapy. Science. American Association for the Advancement of Science; 2003 Jul 18;301(5631):370–3.

3. Stroba A, Schaeffer F, Hindie V, Lopez-Garcia L, Adrian I, Fröhner W, et al. 3,5-Diphenylpent-2-enoic acids as allosteric activators of the protein kinase PDK1: structure-activity relationships and thermodynamic characterization of binding as paradigms for PIF-binding pocket-targeting compounds. J Med Chem. 2009 Aug 13;52(15):4683–93.

4. Engel M, Hindie V, Lopez-Garcia LA, Stroba A, Schaeffer F, Adrian I, et al. Allosteric activation of the protein kinase PDK1 with low molecular weight compounds. EMBO J. 2006 Nov 29;25(23):5469–80.

5. Thakur CS, Jha BK, Dong B, Gupta Das J, Silverman KM, Mao H, et al. Small-molecule activators of RNase L with broad-spectrum antiviral activity. Proc Natl Acad Sci USA. National Acad Sciences; 2007 Jun 5;104(23):9585–90.

6. Cool B, Zinker B, Chiou W, Kifle L, Cao N, Perham M, et al. Identification and characterization of a small molecule AMPK activator that treats key components of type 2 diabetes and the metabolic syndrome. Cell Metab. 2006 Jun;3(6):403–16.

7. Zhao G, Iyengar RR, Judd AS, Cool B, Chiou W, Kifle L, et al. Discovery and SAR development of thienopyridones: a class of small molecule AMPK activators. Bioorg Med Chem Lett. 2007 Jun 15;17(12):3254–7.

8. Howitz KT, Bitterman KJ, Cohen HY, Lamming DW, Lavu S, Wood JG, et al. Small molecule activators of sirtuins extend Saccharomyces cerevisiae lifespan. Nature. 2003 Sep 11;425(6954):191–6.

9. Milne JC, Lambert PD, Schenk S, Carney DP, Smith JJ, Gagne DJ, et al. Small molecule activators of SIRT1 as therapeutics for the treatment of type 2 diabetes. Nature. 2007 Nov 29;450(7170):712–6.

10. Kaeberlein M, McDonagh T, Heltweg B, Hixon J, Westman EA, Caldwell SD, et al. Substrate-specific activation of sirtuins by resveratrol. J Biol Chem. American Society for Biochemistry and Molecular Biology; 2005 Apr 29;280(17):17038–45.

11. Pacholec M, Bleasdale JE, Chrunyk B, Cunningham D, Flynn D, Garofalo RS, et al. SRT1720, SRT2183, SRT1460, and resveratrol are not direct activators of SIRT1. Journal of Biological Chemistry. American Society for Biochemistry and Molecular Biology; 2010 Mar 12;285(11):8340–51.

12. Kamata K, Mitsuya M, Nishimura T, Eiki J-I, Nagata Y. Structural basis for allosteric regulation of the monomeric allosteric enzyme human glucokinase. Structure. 2004 Mar;12(3):429–38.

13. Göransson O, McBride A, Hawley SA, Ross FA, Shpiro N, Foretz M, et al. Mechanism of action of A-769662, a valuable tool for activation of AMP-activated protein kinase. J Biol Chem. American Society for Biochemistry and Molecular Biology; 2007 Nov 9;282(45):32549–60.

14. Heidebrecht RW, Mulrooney C, Austin CP, Barker RH, Beaudoin JA, Cheng KC-C, et al. Diversity-Oriented Synthesis Yields a Novel Lead for the Treatment of Malaria. ACS Med Chem Lett. 2012 Feb 9;3(2):112–7.

15. Margueron R, Justin N, Ohno K, Sharpe ML, Son J, DruryIII WJ, et al. Role of the polycomb protein EED in the propagation of repressive histone marks. Nature. Nature Publishing Group; 2009 Aug 10;461(7265):762–7.

16. Sneeringer CJ, Scott MP, Kuntz KW, Knutson SK, Pollock RM, Richon VM, et al. Coordinated activities of wild-type plus mutant EZH2 drive tumor-associated hypertrimethylation of lysine 27 on histone H3 (H3K27) in human B-cell lymphomas. Proc Natl Acad Sci USA. National Acad Sciences; 2010 Dec 7;107(49):20980–5.

17. Yap DB, Chu J, Berg T, Schapira M, Cheng S-WG, Moradian A, et al. Somatic mutations at EZH2 Y641 act dominantly through a mechanism of selectively altered PRC2 catalytic activity, to increase H3K27 trimethylation. Blood. 2011 Feb 24;117(8):2451–9.

18. Sarma K, Margueron R, Ivanov A, Pirrotta V, Reinberg D. Ezh2 requires PHF1 to efficiently catalyze H3 lysine 27 trimethylation in vivo. Molecular and Cellular Biology. 2008 Apr;28(8):2718–31.

19. Nekrasov M, Klymenko T, Fraterman S, Papp B, Oktaba K, Köcher T, et al. Pcl-PRC2 is needed to generate high levels of H3-K27 trimethylation at Polycomb target genes. EMBO J. 2007 Sep 19;26(18):4078–88.

20. Sneeringer CJ, Scott MP, Kuntz KW, Knutson SK, Pollock RM, Richon VM, et al. Coordinated activities of wild-type plus mutant EZH2 drive tumor-associated hypertrimethylation of lysine 27 on histone H3 (H3K27) in human B-cell lymphomas. Proc Natl Acad Sci USA. 2010 Dec 7;107(49):20980–5.

21. Yuan W, Wu T, Fu H, Dai C, Wu H, Liu N, et al. Dense chromatin activates Polycomb repressive complex 2 to regulate H3 lysine 27 methylation. Science. American Association for the Advancement of Science; 2012 Aug 24;337(6097):971–5.

22. Xu C, Bian C, Yang W, Galka M, Ouyang H, Chen C, et al. Binding of different histone marks differentially regulates the activity and specificity of polycomb repressive complex 2 (PRC2). Proc Natl Acad Sci USA. National Acad Sciences; 2010 Nov 9;107(45):19266–71.

23. Ullman EF, Kirakossian H, Switchenko AC, Ishkanian J, Ericson M, Wartchow CA, et al. Luminescent oxygen channeling assay (LOCI): sensitive, broadly applicable homogeneous immunoassay method. Clin Chem. 1996 Sep;42(9):1518–26.

24. Wigle TJ, Herold JM, Senisterra GA, Vedadi M, Kireev DB, Arrowsmith CH, et al. Screening for inhibitors of low-affinity epigenetic peptide-protein interactions: an AlphaScreen-based assay for antagonists of methyl-lysine binding proteins. J Biomol Screen. 2010 Jan;15(1):62–71.

25. Lo M-C, Aulabaugh A, Jin G, Cowling R, Bard J, Malamas M, et al. Evaluation of fluorescence-based thermal shift assays for hit identification in drug discovery. Analytical Biochemistry. 2004 Sep 1;332(1):153–9.

26. Goode DR, Totten RK, Heeres JT, Hergenrother PJ. Identification of promiscuous small molecule activators in high-throughput enzyme activation screens. J Med Chem. 2008 Apr 24;51(8):2346–9.

27. Knutson SK, Wigle TJ, Warholic NM, Sneeringer CJ, Allain CJ, Klaus CR, et al. A selective inhibitor of EZH2 blocks H3K27 methylation and kills mutant lymphoma cells. Nat Chem Biol. 2012 Nov;8(11):890–6.

28. Konze KD, Ma A, Li F, Barsyte-Lovejoy D, Parton T, Macnevin CJ, et al. An orally bioavailable chemical probe of the Lysine Methyltransferases EZH2 and EZH1. ACS Chem Biol. 2013 Jun 21;8(6):1324–34.

29. Qi W, Chan H, Teng L, Li L, Chuai S, Zhang R, et al. Selective inhibition of Ezh2 by a small molecule inhibitor blocks tumor cells proliferation. Proc Natl Acad Sci USA. 2012 Dec 26;109(52):21360–5.

30. McCabe MT, Ott HM, Ganji G, Korenchuk S. EZH2 inhibition as a therapeutic strategy for lymphoma with EZH2-activating mutations. Nature. 2012.

31. Garapaty-Rao S, Nasveschuk C, Gagnon A, Chan EY, Sandy P, Busby J, et al. Identification of EZH2 and EZH1 small molecule inhibitors with selective impact on diffuse large B cell lymphoma cell growth. Chem Biol. 2013 Nov 21;20(11):1329–39.

32. Lund K, Adams PD, Copland M. EZH2 in normal and malignant hematopoiesis. Leukemia. 2014 Jan;28(1):44–9.

33. Xu K, Wu ZJ, Groner AC, He HH, Cai C, Lis RT, et al. EZH2 oncogenic activity in castration-resistant prostate cancer cells is Polycomb-independent. Science. 2012 Dec 14;338(6113):1465–9.

34. Chase A, Cross NCP. Aberrations of EZH2 in cancer. Clin Cancer Res. 2011 May 1;17(9):2613–8.

35. McCabe MT, Ott HM, Ganji G, Korenchuk S, Thompson C, Van Aller GS, et al. EZH2 inhibition as a therapeutic strategy for lymphoma with EZH2-activating mutations. Nature. 2012 Dec 6;492(7427):108–12.

36. Knutson SK, Warholic NM, Wigle TJ, Klaus CR, Allain CJ, Raimondi A, et al. Durable tumor regression in genetically altered malignant rhabdoid tumors by inhibition of methyltransferase EZH2. Proc Natl Acad Sci USA. 2013 May 7;110(19):7922–7.

37. Ernst T, Chase AJ, Score J, Hidalgo-Curtis CE, Bryant C, Jones AV, et al. Inactivating mutations of the histone methyltransferase gene EZH2 in myeloid disorders. Nat Genet. 2010 Aug;42(8):722–6.

38. Ntziachristos P, Tsirigos A, Van Vlierberghe P, Nedjic J, Trimarchi T, Flaherty MS, et al. Genetic inactivation of the polycomb repressive complex 2 in T cell acute lymphoblastic leukemia. Nat Med. 2012 Feb;18(2):298–301.

39. Score J, Hidalgo-Curtis C, Jones AV, Winkelmann N, Skinner A, Ward D, et al. Inactivation of polycomb repressive complex 2 components in myeloproliferative and myelodysplastic/myeloproliferative neoplasms. Blood. 2012 Feb 2;119(5):1208–13.

40. Schwartzentruber J, Korshunov A, Liu X-Y, Jones DTW, Pfaff E, Jacob K, et al. Driver mutations in histone H3.3 and chromatin remodelling genes in paediatric glioblastoma. Nature. 2012 Feb 9;482(7384):226–31.

41. Lewis PW, Müller MM, Koletsky MS, Cordero F, Lin S, Banaszynski LA, et al. Inhibition of PRC2 activity by a gain-of-function H3 mutation found in pediatric glioblastoma. Science. 2013 May 17;340(6134):857–61.

Chapter VI

High-content screening for small-molecule modulators of global H3K27me3 levels

Collaborator Contributions

- **Dr. Patrick Faloon** developed MDA-MB-231 H3K27me3 HCA automation protocol and collected all initial HCA screening data for bioactive compounds.
- **Dr Fumika Hirobe Yakushiji** synthesized miconazole (and associated stereoisomers) and performed radiometric H3.1 assays to evaluate miconazole activity on PRC2 and PRC2-EED(Y365A).

6.1 Introduction

Dysregulation of H3K27me3 is a common occurrence in many cancers, often driven by the altered expression or mutation of cellular factors governing H3K27 methylation—most frequently, the components of PRC2 and H3K27me3 demethylases (1,2). While much attention has been given to the development and evaluation of direct EZH2 inhibitors (3-8), efforts towards the identification and therapeutic investigation of compounds that target upstream regulators of PRC2 or those that engage EZH2 co-regulatory components (e.g. SUZ12, EED) have not been described. Inhibitors of UTX and JMJD3 have been recently disclosed (9), but their potential therapeutic utility is only beginning to be explored (10).

Phenotypic screening of compound libraries offers several key advantages over biochemical target-based approaches, enabling the *direct* discovery of cell-active small molecules that modulate a desired phenotype (11-13). In addition, subsequent target identification can yield insights into the regulatory mechanisms underlying the chosen phenotype and uncover novel therapeutic targets (14,15). With that said, phenotypic screening efforts to identify small molecules altering global H3K27me3 levels may be of great value for discovering small-molecule probes and also for revealing novel mechanisms underlying the regulation and dysregulation of H3K27 levels.

In a recent study, a method coined CROSS (Chromatin Regulation Ontology SiRNA Screening) was used to identify known histone regulators that influence levels of H3K27me3 by measuring the mark upon siRNA-mediated knockdown of >500 distinct chromatin factors (16). While they identified few novel regulators, PRC2 regulatory factors undoubtedly extend beyond those explored in this study, as many new

regulatory mechanisms have recently surfaced. For example, EZH2 activity is regulated by CDK1- and AKT1-mediated phosphorylation (17-20) and glycosylation by OGT (21). As further discussed in **Chapter VII**, PRC2 activity is also regulated through substrate level 'crosstalk; for example, H3S28 phosphorylation by MSK1(22) and H3K36 (or H3K4) methylation by their associated HMTs (23,24) render PRC2 unable to methylate H3K27, thus implicating these CMEs in PRC2 regulation. A small-molecule phenotypic screen may uncover targets and mechanisms undetected by the siRNA screen, as they could inhibit PRC2-regulatory factors beyond those associated with chromatin.

This chapter describes the use of an HCS assay to identify known bioactive compounds that alter global H3K27me3 levels, aiming to identify compounds that target novel H3K27me3-connected regulatory nodes or target PRC2 (or opposing demethylases) directly. This screen ultimately led to the discovery of an antifungal agent, miconazole, capable of *activating* PRC2 activity in vitro, as well as a mucolytic agent, bromhexine, that selectively ablates cellular H3K27me3 levels through targeting an activity distinct from PRC2.

6.2 Results and discussion

6.2.1 Screening 2,230 bioactives identifies bromhexine as a potential, selective H3K27me3 modulator.

To identify compounds that modulate cellular nodes influencing H3K27 methylation, we initially screened 2,230 bioactive compounds in a cell-based high-content assay (HCA) measuring H3K27me3 levels by immunofluorescence (IF) staining. Here, we implemented, with minor modifications, an HCA protocol developed by Bayer

HealthCare and used to screen the BHC internal compound library and the Broad's DOS library in collaboration with the Broad Institute's Center for the Science of Therapeutics. While similar to our previously described H3K27me3 HCS assay (**Chapter II**), notable differences included the substitution of MDA-MB-231 (breast adenocarcinoma) cells for HeLa and the use of higher concentrations of both primary and secondary antibodies (6- and 10-fold increase, respectively). As before, cells were treated with compound for 72 hrs in 384-well plates and global H3K27me3 levels were inferred by measuring average nuclear fluorescence after staining and imaging. A reported EZH2 inhibitor, GSK343 (7), was used at 1 uM as a positive control. For each assay plate, average nuclear fluorescence signals from DMSO- and GSK343-treated wells were used for normalization in Genedata Assay Analyzer, setting their respective value distribution medians to 0% and -100%. Compounds that reduced normalized average nuclear fluorescence to -40% or less were considered potential hits. However, those that lowered cell number by >25% (compared with DMSO) were rejected, as toxic compounds can nonspecifically influence staining intensity.

Out of the 2,230 bioactives screened (Figure 6.1), 91 unique compounds met our selection criteria (4.1% hit rate), 50 of which were immediately available from internal compound management services and obtained for single-dose retest. Referencing the signal distribution of DMSO wells, compounds reducing average nuclear fluorescence by >2 standard deviations (Z-score <-2) in both replicates were considered for further study. As shown in Figure 6.2, only five bioactive compounds were able to reduce presumed H3K27me3 levels by these standards—bromhexine (a mucolytic agent; ref. 25), papaverine (an antispasmodic; ref. 26), pentamidine (an antimicrobial; ref.27),

ketoconazole (an antifungal; ref. 28)), and chlorpromazine (a typical anti-psychotic; ref. 29). Of these compounds, bromhexine exhibited an apparent reduction in H3K27me3 closest to that of EPZ005687, an inhibitor of EZH2 (4) and positive control used in retest assays.

While activities of the remaining compounds were not explored further, the most potent compound, bromhexine, was assayed by HCA in dose, revealing apparent dose-responsive reduction of global H3K27me3 in MDA-MB-231 cells with an IC_{50} of 10 uM (Figure 6.3B). Given these findings, we next tested bromhexine activity in HEK293T cells, treating for 96 hrs and extracting histones for western blot analysis of global levels of various histone marks. While bromhexine exhibited little effect on H3K4me3, H3K9me3, and H3K36me2 at the concentrations tested, the compound potently reduced global levels of H3K27me3 (<2.5 uM EC_{50}; Figure 6.2C). The increased potency exhibited by bromhexine in this assay may reflect differences between cell lines or the extended treatment period (30). Interestingly, no reduction of H3K27me2 levels was observed suggesting that this compound does not directly target EZH2 (which results in similar levels of reduction of H3K27 di and tri methylation; ref. 30,31) and may instead target (through direct or indirect means) a specific regulator of H3K27 trimethylation—for example, PHF1 (32). Furthermore, bromhexine (up to 50 uM) exhibited no activity in a PRC2 biochemical assay, suggesting that its cellular effects occurred through a mechanism distinct from direct PRC2 inhibition (Figure S6.1).

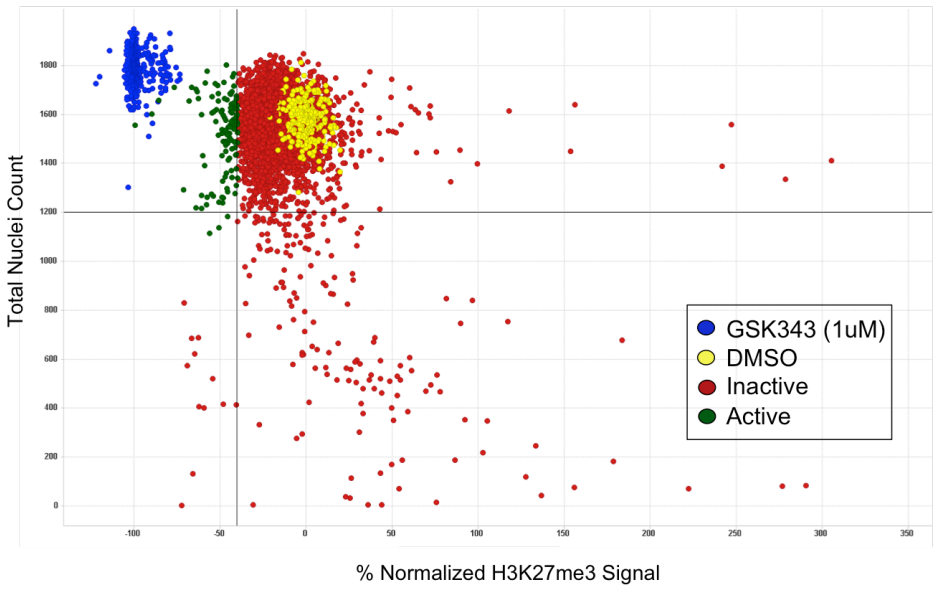

Figure 6.1 Summary 2,230 bioactive compounds screened in H3K27me3 HCA
Scatter plot of total nuclei count versus normalized H3K27me3 signal for all assay wells. Of the 2,230 bioactives screened, those with < -40% normalized H3K27me3 signal and <25 % reduction in cell number (relative to DMSO; >1200 cells per well) were considered 'active' hits (*shown in green*). Data for positive control (1 uM GSK343; *Blue*) and DMSO (*Yellow*) wells are included above. 'Inactive' compounds are shown in red.

A

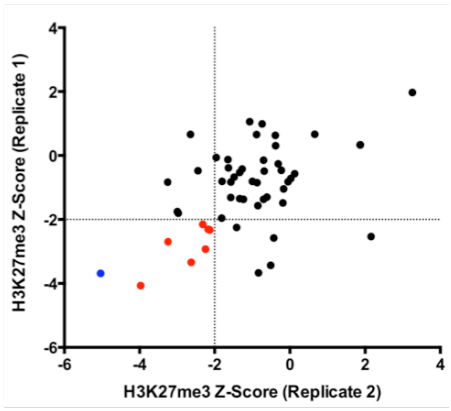

B

Compound Name	Conc. (uM)	Z-score (rep 1)	Z-score (rep 2)
EPZ005687	2.5	-5.0	-3.7
Bromhexine	25	-4.0	-4.1
Ketoconazole	25	-3.2	-2.7
Chlorpromazine	25	-2.6	-3.3
Pentamidine	25	-2.3	-2.2
Papaverine	25	-2.2	-2.9

C

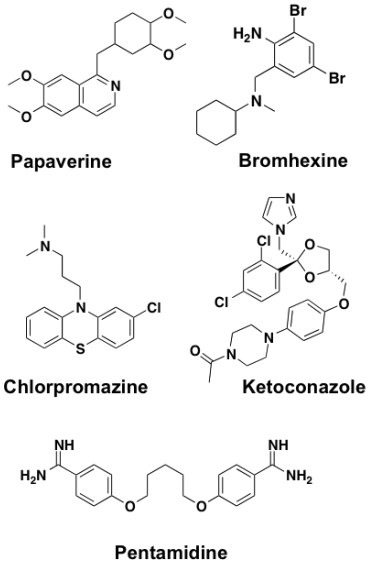

Figure 6.2 Retest of 50 bioactive hit compounds in H3K27me3 HCA.
(A) Z-score scatter plot (replicate 1 versus replicate 2) for 50 bioactive hits. Those with a z-score below -2 in both replicates were considered for further study (shown in red). Data for positive control, EPZ005687, is shown in blue. (B) Selected bioactive compounds and their associated activity in H3K27me3 HCA. (C) Structures of selected bioactive hit compounds. Z-scores were calculate as described in **Experimental methods**

Currently, bromhexine (also known as ambroxol) is administered as an expectorant and mucoactive agent, increasing cough effectiveness through stimulation of sufactant secretion within the lung (25). The exact mechanism by which this is accomplished is unknown, providing little insight into the potential cellular targets of bromhexine in cells. Further study will be required to understand the exact mechanism by which bromhexine alters H3K27me3 levels; however, success in identifying its target may reveal novel mechanisms of H3K27me3 regulation or provide a useful starting point for the development of a new cell-active chemical probe. However, before such undertaking, these findings should be confirmed by orthogonal approaches, such as mass spectrometry-based global chromatin profiling (33).

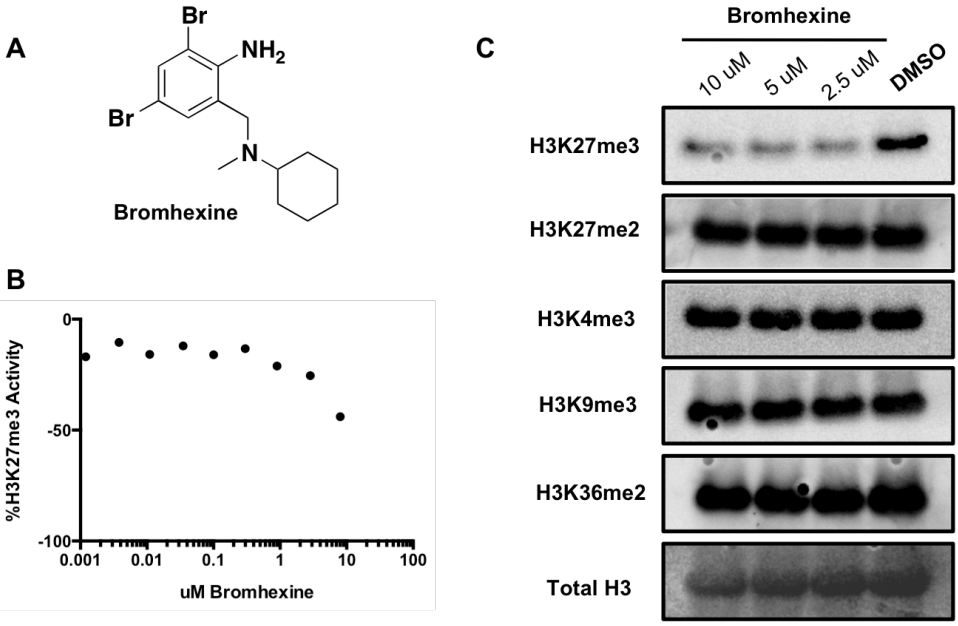

Figure 6.3 Activity of bromhexine in cellular assays measuring global H3K27me3 levels
(A) Structure of bromhexine. (B) Activity of bromhexine in H3K27me3 HCA after 72 hr treatment of MDA-MB-231 cells. Data points represent the mean of duplicate measurements. (C) Global levels of histone marks measured by western blot of histones extracted from HEK293T cells following 96 hr treatment with various concentrations of bromhexine or DMSO. Total histone H3 was used as a loading control.

6.2.2 Miconazole as an activator of PRC2 activity

In parallel to retesting in a cellular assay, all 50 bioactive hit compounds identified in our H3K27me3 HCA screen were assayed for their ability to inhibit PRC2 biochemical activity, as their observed cellular effects could result from direct PRC2 engagement. For this purpose, we measured PRC2 activity on a peptide substrate (H3[21-44]) by scintillation proximity assay (SPA)— a radiometric approach using streptavidin-coated, scintillant-containing beads which luminesce upon capture of biotinylated ^{3}H-labeled product (34). While no compounds exhibited PRC2 inhibition, one compound, miconazole, *increase*d apparent PRC2 biochemical activity in a dose-responsive manner (Figure 6.4A,C). To confirm that activation was not dependent on peptide or an artifact of SPA, we tested miconazole activity in an orthogonal filter-binding assay that uses histone H3.1 as a substrate and measures ^{3}H-incorporation over time. At 25 uM, miconazole increased PRC2 reaction velocity by >40% compared with DMSO control, suggesting that apparent activation was unlikely to be an artifact of assay format (Figure 6.4D).

As the PRC2 SPA enabled well-controlled enzyme kinetic studies in high-throughput, we next performed mechanistic kinetic analysis of PRC2 activation by miconazole, determining V_{MAX} and K_M for both SAM and peptide under varying concentrations of compound (Figure 6.5). From these results, we determined that, while K_M values for SAM and peptide were not significantly altered, miconazole induced a clear dose-responsive increase in V_{MAX} (by up to ~50% compared with DMSO; Figure 6.5C,D), suggesting an allosteric activation mechanism.

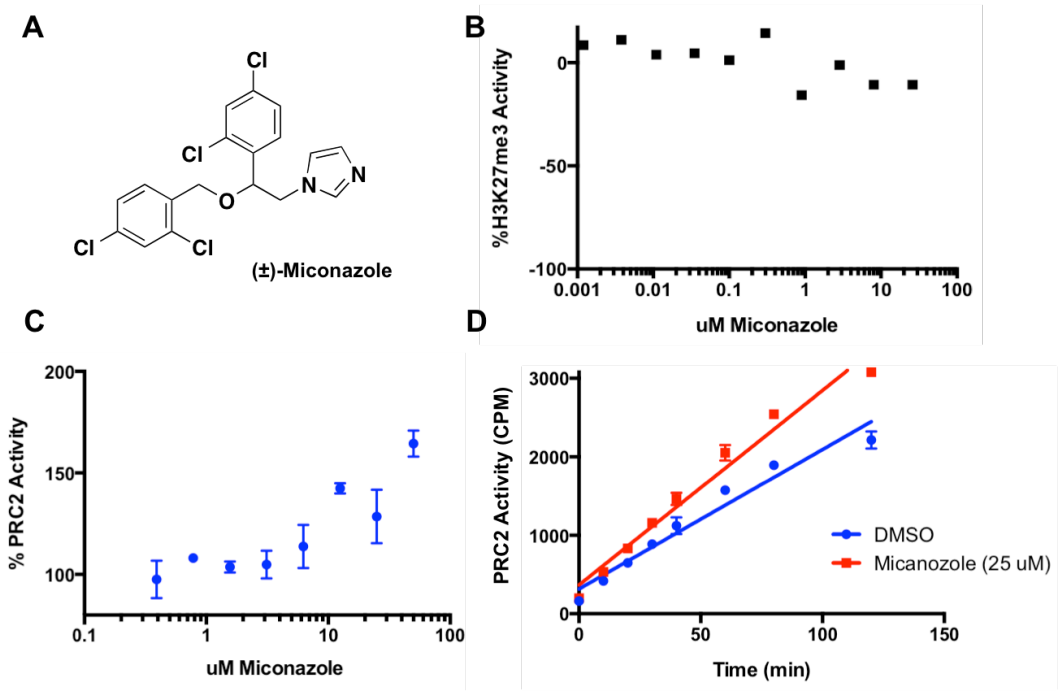

Figure 6.4 Biochemical and cellular activity of miconazole
(A) Structure of miconazole. (B) Cellular activity of miconazole determined by H3K27me3 HCA. Data represent mean of duplicate wells. (C) Biochemical activity of miconazole in PRC2 SPA and (D) PRC2 filter-binding assay using histone H3.1. Data points represent the mean and standard error of duplicate measurements in each assay.

While it might at first appear contradictory that a compound that inhibits H3K27 methylation levels in cells could be a PRC2 activator in vitro, PRC2 is a multi-protein complex that is highly regulated in cells and a compound that binds PRC2 to potentiate activity in an in vitro context may, depending on the mechanism of in vitro activation, have a net impact of reducing global cellular H3K27me3. For instance, as there are known allosteric activation sites within two PRC2 components, EED or SUZ12 (35,36), it is possible that miconazole activates the complex through binding these components or a yet uncharacterized site (within any of the five). In cells, small molecules that bind EED (or other regulatory domains) and disrupt PRC2 histone localization could potentially block effective H3K27me3 propagation necessary to establish repressive

chromatin domains, leading to a global loss of H327me3 and derepression of PRC2 target genes, regardless of their ability to stimulate PRC2 biochemical activity *in vitro*.

6.2.3 Investigating the MOA for PRC2 activation by miconazole

Intrigued by this possibility, we pursued further mechanistic characterization of miconazole. To further investigate the basis of miconazole-induced alterations of V_{MAX} measured by PRC2 SPA, we first aimed to rule out potential nonspecific mechanisms of activation. As V_{MAX} is dependent on the total enzyme concentration (37,38), miconazole may activate in an artifactual manner involving nonspecific PRC2 stabilization or effects on adsorption to the assay plate, as each scenario could influence total active enzyme concentration. Unfortunately, the prevalence of these effects are unknown and additional mechanisms for nonspecific activation have not been described (39).

As miconazole is a known bioactive (an antifungal agent) included in many screening collections, we explored whether there were any previous reports describing its nonspecific activation of enzyme activity or its aggregation. While we were unable to find precedence of *in vitro* activation, one study, reported by Shoichet and colleagues, describes miconazole as a strong aggregator (>25 uM CAC) in 50 mM sodium phosphate buffer (pH 7.4) and capable of inhibiting several enzymes by nonspecific mechanisms (40). To corroborate these findings, we assessed aggregation potential by DLS at various concentrations of miconazole under buffer conditions identical to those used in the study. As Figure 6.6A indicates, miconazole exhibited clear aggregation under the reported conditions (at concentrations above 12.5 uM), suggesting that an aggregation-based mechanism could potentially underlie its activity. To explore this possibility, we repeated these experiments under our activity assay buffer conditions

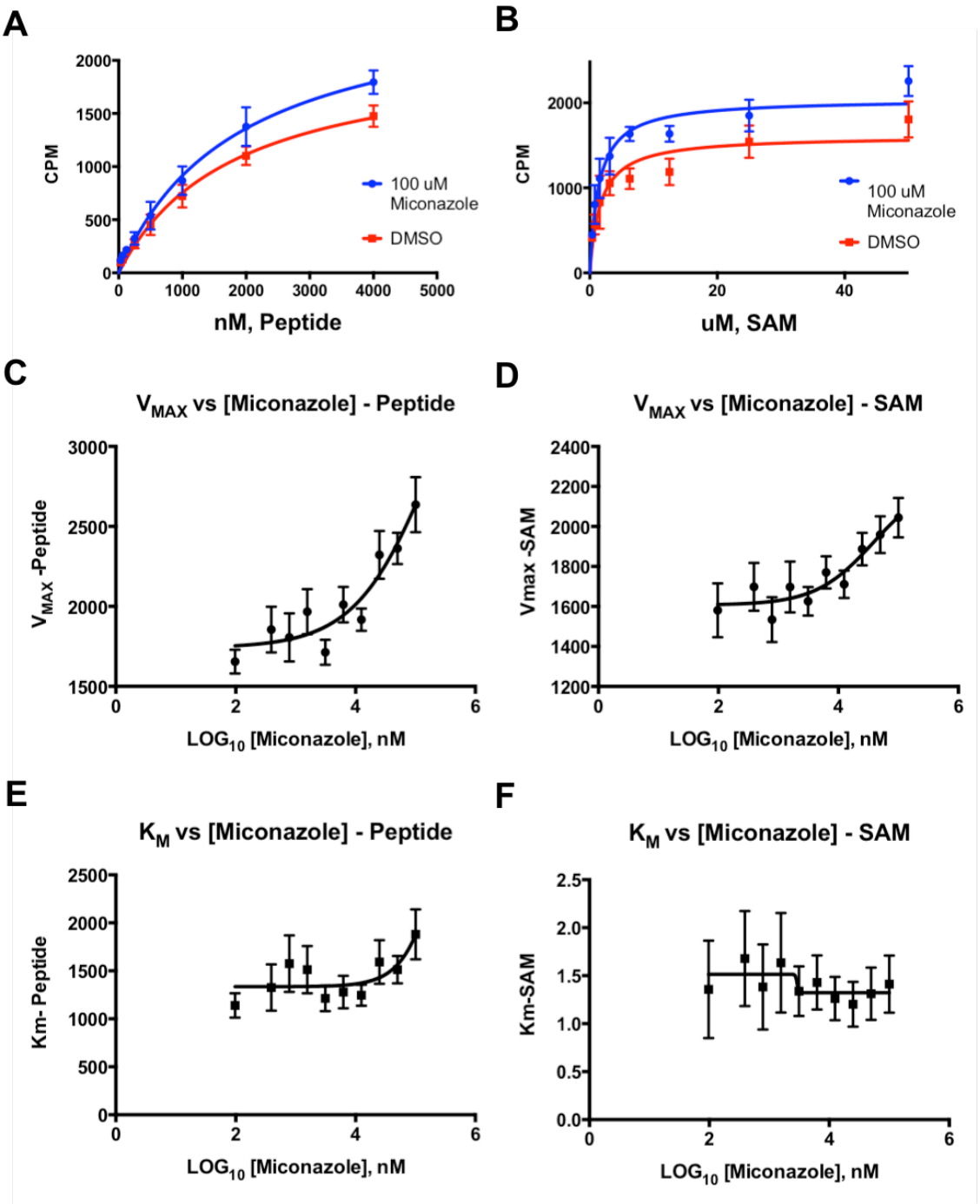

Figure 6.5 Miconazole activity in mechanistic PRC2 kinetic studies
Kinetic studies were performed using H3[21-44] peptide as a substrate in radiometric PRC2 SPA. Initial velocities were estimated by measuring activity (CPM) at a single time point (t=120 min) within the linear range of reaction. (A) Estimated initial velocities versus H3[21-44] or (B) SAM concentration in the presence of DMSO or 100 uM miconazole. Data points represent the mean and standard error of four replicate measurements. Miconazole exhibited clear effects on V_{MAX}, increasing its apparent values by ~1.4X under at the highest concentration tested (100 uM). (C,D) V_{MAX} and (E, F) K_M values for H3[21-44] and SAM, respectively, versus miconazole concentration Nonlinear regression fits were performed using the Michaelis-Menten model in PRISM 6.0 to obtain and plot best-fit V_{MAX} and K_M values and their associated standard errors.

(50 mM Tris pH 8.5, 5 mM DTT, and 0.01% Tween 20), detecting no large aggregates at all concentrations tested (up to 200 uM; Figure 6.6B). Still, this may be the result of the low ionic strength of our activity assay buffer and suggest the potential of miconazole to form small, undetectable aggregates under these conditions as previously described (**Chapter IV**). However, unlike other nonspecific PRC2 modulators found in earlier studies, we were unable to detect miconazole-substrate binding or its influence on PRC2-peptide interaction by a FP assay (Figure 6.6C). Moreover, given that nonspecific activation is likely promiscuous (39), we measured miconazole activity in a G9a SPA, but detected no apparent activation at concentrations up to 100 uM (Figure 6.6D).

Absence of miconazole aggregation under PRC2 assay conditions and its nonpromiscuous behavior might alternatively suggest a mechanism involving *specific* engagement of PRC2. Given this possibility, we next sought to determine which PRC2 component might be the target of miconazole. To investigate whether AEBP2 or RBBP4 were required for activation, we evaluated miconazole activity on 5-component and 3-component PRC2 (EZH2/EED/SUZ12) in the histone H3.1 filter binding assay. As shown in Figure 6.7A, miconazole exhibited dose-responsive activation (~2-fold compared with DMSO) of 3-component PRC2 with an apparent AC_{50} of ~10 uM, suggesting AEBP2 and RBBP4 to be unlikely targets.

As these data suggested engagement with EZH2, SUZ12, or EED, we chose to first explore the possibility of miconazole binding EED, as this factor harbors a known allosteric site that, upon ligand binding, can influence V_{MAX} (k_{cat}) in PRC2 kinetic assays We previously described (**Chapter IV**) development of an AlphaLISA assay (41,42),

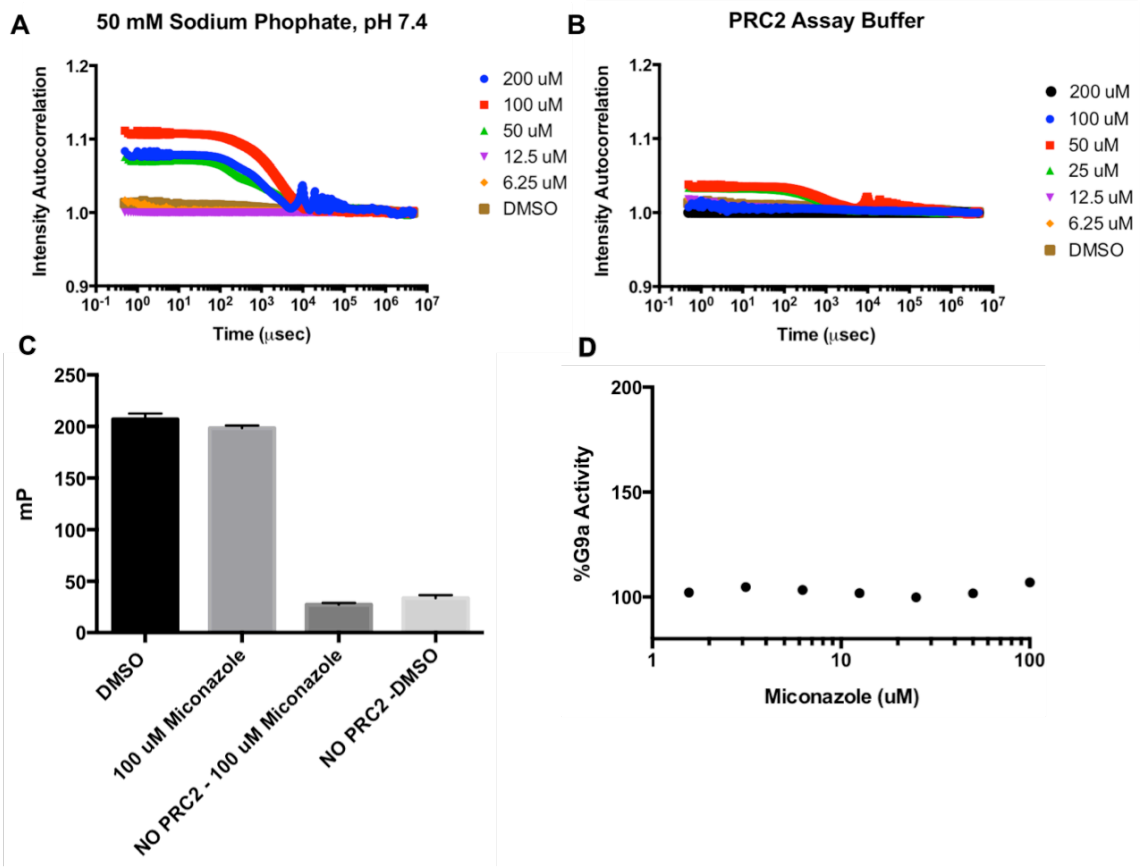

Figure 6.6 Exploring potential nonspecific mechanisms of miconazole through aggregation (DLS), peptide-binding (FP), and G9a activation studies.
(A) DLS intensity autocorrelation curves for various concentrations of miconazole in 50 mM sodium phosphate pH 7.4 and (B) activity assay buffer (50 mM Tris pH 8.5, 5 mM DTT, 0.01% Tween 20). Each intensity autocorrelation curve represents the average of 10 single-well acquisitions for each condition. (C) Activity of 100 uM miconazole in of H3[21-44]-HiLyte™ Fluor 488 FP assay in the presence (left pair of columns) or absence (right pair of columns) of 10 nM PRC2. Data represent mean and standard error of four replicate measurements. As indicated by resulting FP signal, miconazole is unable to disrupt PRC2-tracer interaction nor able to bind tracer alone. (D) Activity of G9a in radiometric SPA at various concentrations of miconazole.

using a biotinylated H3K9me3-modified peptide (H3[1-21]) and GST-EED[78-441] capable of measuring EED-H3K9me3 interaction. We speculated that if miconazole were modulating PRC2 activity through an interaction with EED, it might bind the same allosteric site as its known ligands and compete in their binding. With this in mind, we evaluated the activity of miconazole in an EED-H3K9me3 AlphaLISA, expecting potential reductions in signal corresponding to displacement of H3K9me3 from EED (Figure 6.7B). Interestingly, miconazole was able to exhibit modest dose-responsive

activity in this assay, suggesting that miconazole may activate PRC2 through bind a known allosteric site on EED.

Crystallographic studies have revealed that the interaction between EED and repressive trimethyllysine marks, H3K9me3 and H3K27me3, requires an ‘aromatic cage’ consisting of F97, Y148, and Y365 residues within the EED WD40 domain (35,43). Substitution of these residues by alanine renders EED incapable of binding trimethyllysine and PRC2 harboring EED(Y365A) cannot be allosterically activated by either H3K27me3 or H3K9me3 (35). To investigate further whether miconazole stimulates PRC2 through binding EED at its allosteric site, we expressed and purified PRC2-EED(Y365A) (Figure S6.2A), assuming that mechanistic insights might be gained if miconazole activity differed between mutant and wild-type EED complexes.

After confirming the inability PRC2-EED(Y365A) to be allosterically activated by an H3K27me3-modified peptide (Figure S6.2B), we evaluated miconazole activity on mutant complex in a radiometric assay using histone H3.1. Interestingly, miconazole was unable to stimulate PRC2-EED(Y365A) activity at the concentrations tested (up to 50 uM), demonstrating miconazole-induced PRC2 activation be EED-dependent. Furthermore, these results suggest potential engagement with EED through its trimethyllyine-binding pocket. It should be noted, however, that PRC2-EED(Y365A) has demonstrated reduced binding affinity for chromatin (35), raising the possibility that miconazole activity may instead be influenced by conformational changes related to this phenomenon.

While additional effort will be required to confirm target engagement and rule out aggregation-based mechanisms, the continued exploration of miconazole may provide a

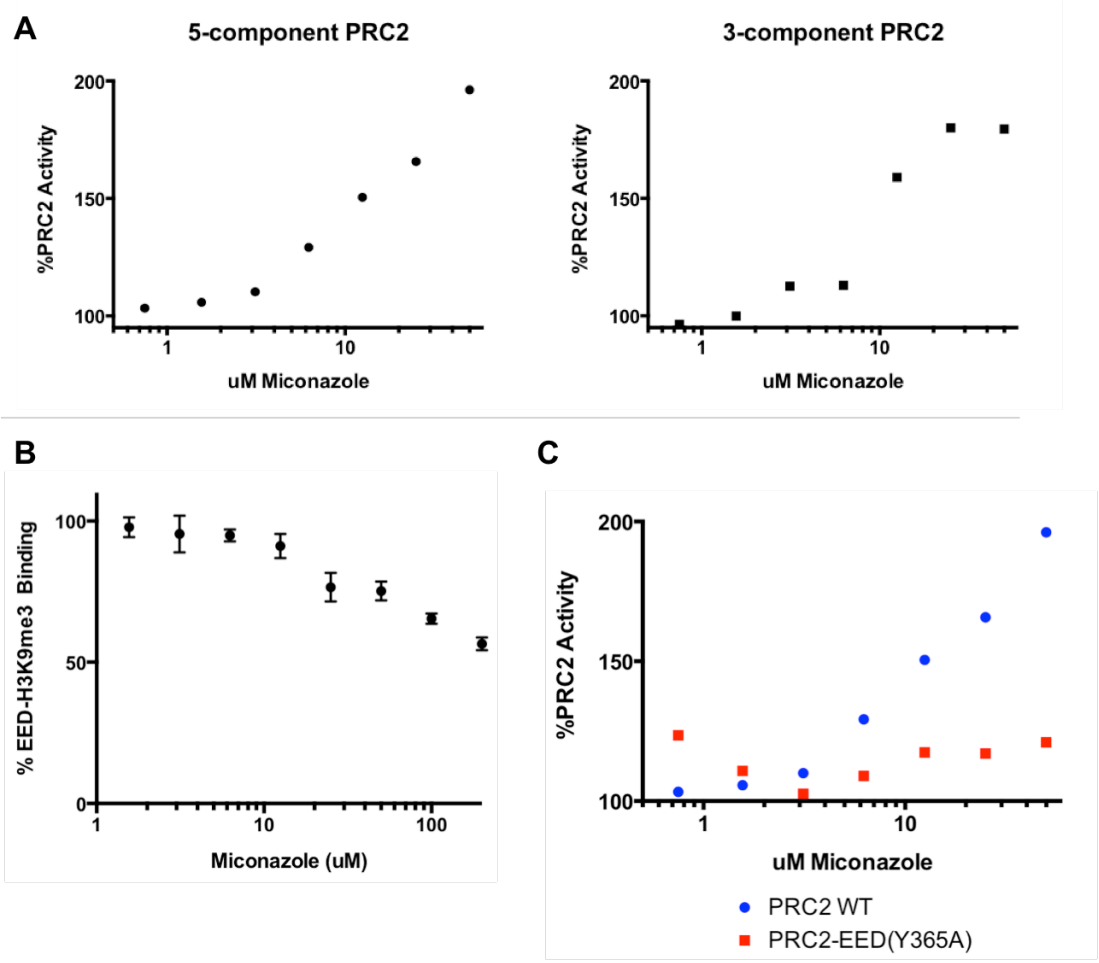

Figure 6.7 Biochemical studies on the mechanism of PRC2 activation by miconazole.
(A) Activity of 5C-PRC2 and (B) 3C-PRC2 in a radiometric histone H3.1 filter-binding assay at various concentrations of miconazole. (C) Activity of miconazole in GST-EED[78-441]-H3K9me3 AlphaLISA. (D) Activity of 5C-PRC2-EED(Y365A) compared with 5C-PRC2 activity in histone H3.1 filter-binding assay at various concentrations of miconazole. Filter-binding assay data points represent the mean of duplicate measurements, while AlphaLISA data points represent the mean and standard error of four replicate measurements.

useful starting point in the development of EED chemical probes. While the therapeutic utility of EZH2 activation seems unclear in principle, given its oncogenic role in several cancers (2,44-46), the impact of biochemical PRC2 activators in a cellular context may prove to yield novel strategies for its inhibition. Although miconazole exhibited only weak apparent activity on H3K27me3 levels upon retest, it is intriguing that such an activator emerged from a screen for compounds reducing H3K27me3 levels. Whether

this is exemplary of target inhibition through engagement of EED will have to be confirmed in future studies.

6.3 Experimental methods

Histone extraction and western blotting. Cells were rinsed with PBS, scraped into ice-cold PBS, and collected via centrifugation at 200 x g for 10 minutes. Pellets were resuspended in 0.2 volumes of 0.4 N HCl and incubated for at least 30 minutes on ice to extract histones. Cellular debris was then cleared by centrifugation at 10,000 x g for 10 minutes. Supernatant containing extracted histones was then neutralized with 0.4 volumes of 1 M sodium phosphate (pH 12.5) and concentration was determined via Bradford assay. After normalization, extracts were diluted in 1X LDS Sample Buffer containing 1X Reducing Agent (Life Technologies) and separated on 12% Bis-Tris NuPAGE gels (Life Technologies) prior to 1 hr transfer (30V at RT) onto Immobilon PVDF membranes (Bio-Rad). Primary antibodies were diluted in 5% non-fat milk or 5% BSA in TBST to manufacturer's specification for overnight primary antibody incubations. Anti-mouse IgG or anti-rabbit IgG HRP conjugates (GE) diluted 1:2500 in primary antibody diluent (incubated at RT for 1hr) was used for chemiluminescence detection with SuperSignal West Pico Chemiluminescent Substrate (Pierce) following TBST washes

Immunofluorescence – H3K27me3 HCA. MDA-MB-231 cells (ATCC) were cultured in F12K media supplemented 10%(v/v) FBS and 100 U mL-1 penicillin-streptomycin. Cells were diluted in culture medium at 3E3 cells/well and plated in black clear-bottom 384-well plates (Aurora) at 40 uL/well. After 24 hr incubation at 37°C/5% CO2, 100 nL of compound or DMSO vehicle was pinned into each well and cells were incubated for an additional 72 hrs. Treated cells were fixed with 4% paraformaldhyde for 10 min, permeabilized with 0.3% Triton X-100 in PBS for 20 min, and blocked with 3% BSA in

PBST for 1 hr at room temperature. Cells were then incubated with primary antibody (anti-H3K27me3; Cell Signaling, #9733) diluted in blocking buffer overnight at 4°C. A mixture of 1 nM Hoechst 33342 (Life Technologies) and 2 ug/mL Alexa Fluor 488 goat anti-rabbit IgG (Life Technologies, A11008) in blocking buffer was then added. Following 1 hr incubation at RT, cells were then imaged on an ImageXpress Micro automated microscope (Molecular Devices) using a 10X objective with laser-based focusing. Image analysis was performed using the Multi Wavelength Cell Scoring module in MetaXpress (Molecular Devices) to determine average nuclear fluorescence and nuclei counts per well. Z-scores were calculated as indicated below. Mean and standard deviation (STDEV) were calculated for all DMSO wells within each assay plate.

$$Z-score = \frac{Average\ Nuclear\ Fluorescence_{Compound} - MEAN(Average\ Nuclear\ Fluorescence_{DMSO\ Wells})}{STDEV(Average\ Nuclear\ Fluorescence_{DMSO\ Wells})}$$

PRC2 and G9a radiometric assays. PRC2 and G9a were diluted to their final concentration in 2X enzyme buffer (50mM Tris HCl pH 8.5, 10 mM DTT, 0.01% Tween 20). 20 uL reactions were initiated with an equal volume of an SAM solution (NEB) containing 3H-SAM (at 25% total SAM concentration; NET155001MC; PerkinElmer) and H3[21-44]-GK-biotin (Anaspec; PRC2) or biotin-H3[1-21] (G9a) and incubated at room temperature for 2 hrs. Methylation levels were detected by SPA as previously described (34) on a TopCount NTX (PerkinElmer). For H3.1 filter binding assay, reaction volume was scaled to 100 uL per well and 50 nM histone H3.1 (NEB) was substituted for peptide. Reactions were quenched with equal volumes of cold SAM (3.2 mM) and filtered through 96-well HA filter plates (Millipore) after 1 hr incubation. Wells were

washed 3X with PBS pH 7.4 and membranes were dried. 50 uL MicroScint (PerkinElmer) was added per well before reading on TopCount NTX.

GST-EED[78-441] AlphaLISA. GST-EED[78-441] and biotinylated H3K9me3 peptide (H3[1-21]-GK-biotin) were diluted to 140 ng/uL and 2 uM in assay buffer (50 mM Tris, pH 8.5, 150 mM NaCl, 5 mM DTT, 0.01% Tween 20), respectively, and added to 384-well AlphaPlates (PerkinElmer) at 10 uL per well. Compounds and competing peptides were diluted in assay buffer to 2X final concentration and 10 uL stocks were mixed with GST-EED and H3K9me3 peptide. After 1 hr incubation, AlphaLISA Streptavidin Donor Beads (PerkinElmer) and AlphaLISA anti-GST Acceptor Beads (PerkinElmer) were diluted in 1X Epigenetics Buffer (PerkinElmer) to 20 ug/mL each and added to plates at 20 uL per well. Alpha signal was detected using the Wallac Envision 2104 Multilabel Reader after 1 hr incubation.

Dynamic light scattering. DLS experiments as described in (7) with modifications. DMSO stock solutions were pinned at 250 nL in black 384-well clear bottom plates (Corning) containing 40 uL of assay buffer (50 mM Tris, pH 8.5, 5 mM DTT, 0.01%Tween 20). Alternatively, compounds were diluted manually into 100 uL of assay buffer, 50mM Sodium Phosphate (pH 7.4), PBS (pH 7.4), or 1X PBS-EP+ (pH 7.4; GE Healthcare). Autocorrelation functions were collected using DynaPro Plate Reader II using default settings.

6.4 References

1. Lim S, Metzger E, Schuele R, Kirfel J, Buettner R. Epigenetic regulation of cancer growth by histone demethylases. International Journal of Cancer. Wiley Subscription Services, Inc., A Wiley Company; 2010;127(9):1991–8.

2. Chase A, Cross NCP. Aberrations of EZH2 in cancer. Clin Cancer Res. American Association for Cancer Research; 2011 May 1;17(9):2613–8.

3. McCabe MT, Ott HM, Ganji G, Korenchuk S. EZH2 inhibition as a therapeutic strategy for lymphoma with EZH2-activating mutations. Nature. 2012.

4. Knutson SK, Wigle TJ, Warholic NM, Sneeringer CJ, Allain CJ, Klaus CR, et al. A selective inhibitor of EZH2 blocks H3K27 methylation and kills mutant lymphoma cells. Nat Chem Biol. 2012 Nov;8(11):890–6.

5. Qi W, Chan H, Teng L, Li L, Chuai S, Zhang R, et al. Selective inhibition of Ezh2 by a small molecule inhibitor blocks tumor cells proliferation. Proc Natl Acad Sci USA. 2012 Dec 26;109(52):21360–5.

6. Garapaty-Rao S, Nasveschuk C, Gagnon A, Chan EY, Sandy P, Busby J, et al. Identification of EZH2 and EZH1 small molecule inhibitors with selective impact on diffuse large B cell lymphoma cell growth. Chem Biol. 2013 Nov 21;20(11):1329–39.

7. Verma SK, Tian X, LaFrance LV, Duquenne C, Suarez DP, Newlander KA, et al. Identification of Potent, Selective, Cell-Active Inhibitors of the Histone Lysine Methyltransferase EZH2. ACS Med Chem Lett. 2012 Dec 13;3(12):1091–6.

8. Konze KD, Ma A, Li F, Barsyte-Lovejoy D, Parton T, Macnevin CJ, et al. An orally bioavailable chemical probe of the Lysine Methyltransferases EZH2 and EZH1. ACS Chem Biol. 2013 Jun 21;8(6):1324–34.

9. Kruidenier L, Chung C-W, Cheng Z, Liddle J, Che K, Joberty G, et al. A selective jumonji H3K27 demethylase inhibitor modulates the proinflammatory macrophage response. Nature. 2012 Aug 16;488(7411):404–8.

10. Ntziachristos P, Tsirigos A, Welstead GG, Trimarchi T, Bakogianni S, Xu L, et al. Contrasting roles of histone 3 lysine 27 demethylases in acute lymphoblastic leukaemia. Nature. 2014 Aug 17.

11. Mayr LM, Bojanic D. Novel trends in high-throughput screening. Curr Opin Pharmacol. 2009 Oct;9(5):580–8.

12. Moffat JG, Rudolph J, Bailey D. Phenotypic screening in cancer drug discovery - past, present and future. Nat Rev Drug Discov. 2014 Aug;13(8):588–602.

13. Prior M, Chiruta C, Currais A, Goldberg J, Ramsey J, Dargusch R, et al. Back to the future with phenotypic screening. ACS Chem Neurosci. 2014 Jul 16;5(7):503–13.

14. Schenone M, Dančík V, Wagner BK, Clemons PA. Target identification and mechanism of action in chemical biology and drug discovery. Nat Chem Biol. 2013 Apr;9(4):232–40.

15. Cong F, Cheung AK, Huang S-MA. Chemical genetics-based target identification in drug discovery. Annu Rev Pharmacol Toxicol. 2012;52(1):57–78.

16. Baas R, Lelieveld D, van Teeffelen H, Lijnzaad P, Castelijns B, van Schaik FM, et al. A novel microscopy-based high-throughput screening method to identify proteins that regulate global histone modification levels. J Biomol Screen. SAGE Publications; 2014 Feb;19(2):287–96.

17. Kaneko S, Li G, Son J, Xu CF, Margueron R, Neubert TA, et al. Phosphorylation of the PRC2 component Ezh2 is cell cycle-regulated and up-regulates its binding to ncRNA. Genes & Development. 2010 Dec 1;24(23):2615–20.

18. Chen S, Bohrer LR, Rai AN, Pan Y, Gan L, Zhou X, et al. Cyclin-dependent kinases regulate epigenetic gene silencing through phosphorylation of EZH2. Nature Publishing Group. Nature Publishing Group; 2010 Oct 10;12(11):1108–14.

19. Wei Y, Chen Y-H, Li L-Y, Lang J, Yeh S-P, Bin Shi, et al. CDK1-dependent phosphorylation of EZH2 suppresses methylation of H3K27 and promotes osteogenic differentiation of human mesenchymal stem cells. Nature Publishing Group. Nature Publishing Group; 2010 Dec 5;13(1):87–94.

20. Kim E, Kim M, Woo D-H, Shin Y, Shin J, Chang N, et al. Phosphorylation of EZH2 activates STAT3 signaling via STAT3 methylation and promotes tumorigenicity of glioblastoma stem-like cells. Cancer Cell. 2013 Jun 10;23(6):839–52.

21. Chu C-S, Lo P-W, Yeh Y-H, Hsu P-H, Peng S-H, Teng Y-C, et al. O-GlcNAcylation regulates EZH2 protein stability and function. Proc Natl Acad Sci USA. 2014 Jan 28;111(4):1355–60.

22. Lau PNI, Cheung P. Histone code pathway involving H3 S28 phosphorylation and K27 acetylation activates transcription and antagonizes polycomb silencing. Proc Natl Acad Sci USA. 2011 Feb 15;108(7):2801–6.

23. Yuan W, Xu M, Huang C, Liu N, Chen S, Zhu B. H3K36 methylation antagonizes PRC2-mediated H3K27 methylation. Journal of Biological Chemistry. 2011 Mar 11;286(10):7983–9.

24. Schmitges FW, Prusty AB, Faty M, Stützer A, Lingaraju GM, Aiwazian J, et al. Histone methylation by PRC2 is inhibited by active chromatin marks. Molecular Cell. 2011 May 6;42(3):330–41.

25. Rogers DF. Mucoactive agents for airway mucus hypersecretory diseases. Respir Care. 2007 Sep;52(9):1176–93–discussion1193–7.

26. Labrid C, Dureng G, Bert H, Duchene-Marullaz P. Different membrane mechanisms of action for tiemonium; a comparison with atropine and papaverine. Arch Int Pharmacodyn Ther. 1976 Oct;223(2):231–45.

27. Barrett MP, Gemmell CG, Suckling CJ. Minor groove binders as anti-infective agents. Pharmacol Ther. 2013 Jul;139(1):12–23.

28. Rojas FD, Sosa M de LA, Fernández MS, Cattana ME, Córdoba SB, Giusiano GE. Antifungal susceptibility of Malassezia furfur, Malassezia sympodialis, and Malassezia globosa to azole drugs and amphotericin B evaluated using a broth microdilution method. Med Mycol. Oxford University Press; 2014 Aug;52(6):641–6.

29. Hettige NC, Zai C, Hazra M, Borlido C, Kennedy JL, Strauss J, et al. Use of candidate gene markers to guide antipsychotic dosage adjustment. Prog Neuropsychopharmacol Biol Psychiatry. 2014 Oct 3;54:315–20.

30. McCabe MT, Ott HM, Ganji G, Korenchuk S, Thompson C, Van Aller GS, et al. EZH2 inhibition as a therapeutic strategy for lymphoma with EZH2-activating mutations. Nature. 2012 Dec 6;492(7427):108–12.

31. Knutson SK, Kawano S, Minoshima Y, Warholic NM, Huang K-C, Xiao Y, et al. Selective Inhibition of EZH2 by EPZ-6438 Leads to Potent Antitumor Activity in EZH2 Mutant Non-Hodgkin Lymphoma. Mol Cancer Ther. 2014 Feb 21.

32. Sarma K, Margueron R, Ivanov A, Pirrotta V, Reinberg D. Ezh2 requires PHF1 to efficiently catalyze H3 lysine 27 trimethylation in vivo. Molecular and Cellular Biology. 2008 Apr;28(8):2718–31.

33. Jaffe JD, Wang Y, Chan HM, Zhang J, Huether R, Kryukov GV, et al. Global chromatin profiling reveals NSD2 mutations in pediatric acute lymphoblastic leukemia. Nat Genet. 2013 Nov;45(11):1386–91.

34. Horiuchi KY, Eason MM, Ferry JJ, Planck JL, Walsh CP, Smith RF, et al. Assay development for histone methyltransferases. Assay Drug Dev Technol. 2013 May;11(4):227–36.

35. Margueron R, Justin N, Ohno K, Sharpe ML, Son J, DruryIII WJ, et al. Role of the polycomb protein EED in the propagation of repressive histone marks. Nature. Nature Publishing Group; 2009 Aug 10;461(7265):762–7.

36. Yuan W, Wu T, Fu H, Dai C, Wu H, Liu N, et al. Dense chromatin activates Polycomb repressive complex 2 to regulate H3 lysine 27 methylation. Science. American Association for the Advancement of Science; 2012 Aug 24;337(6097):971–5.

37. Yang J, Copeland RA, Lai Z. Defining balanced conditions for inhibitor screening assays that target bisubstrate enzymes. J Biomol Screen. SAGE Publications; 2009 Feb;14(2):111–20.

38. Michaelis L, Menten ML, Johnson KA, Goody RS. The original Michaelis constant: translation of the 1913 Michaelis-Menten paper. Biochemistry. 2011. 6 p.

39. Goode DR, Totten RK, Heeres JT, Hergenrother PJ. Identification of promiscuous small molecule activators in high-throughput enzyme activation screens. J Med Chem. 2008 Apr 24;51(8):2346–9.

40. Seidler J, McGovern SL, Doman TN, Shoichet BK. Identification and prediction of promiscuous aggregating inhibitors among known drugs. J Med Chem. 2003 Oct 9;46(21):4477–86.

41. Ullman EF, Kirakossian H, Switchenko AC, Ishkanian J, Ericson M, Wartchow CA, et al. Luminescent oxygen channeling assay (LOCI): sensitive, broadly applicable homogeneous immunoassay method. Clin Chem. 1996 Sep;42(9):1518–26.

42. Wigle TJ, Herold JM, Senisterra GA, Vedadi M, Kireev DB, Arrowsmith CH, et al. Screening for inhibitors of low-affinity epigenetic peptide-protein interactions: an AlphaScreen-based assay for antagonists of methyl-lysine binding proteins. J Biomol Screen. 2010 Jan;15(1):62–71.

43. Xu C, Bian C, Yang W, Galka M, Ouyang H, Chen C, et al. Binding of different histone marks differentially regulates the activity and specificity of polycomb repressive complex 2 (PRC2). Proc Natl Acad Sci USA. National Acad Sciences; 2010 Nov 9;107(45):19266–71.

44. Lund K, Adams PD, Copland M. EZH2 in normal and malignant hematopoiesis. Leukemia. 2014 Jan;28(1):44–9.

45. Xu K, Wu ZJ, Groner AC, He HH, Cai C, Lis RT, et al. EZH2 oncogenic activity in castration-resistant prostate cancer cells is Polycomb-independent. Science. 2012 Dec 14;338(6113):1465–9.

46. Sneeringer CJ, Scott MP, Kuntz KW, Knutson SK, Pollock RM, Richon VM, et al. Coordinated activities of wild-type plus mutant EZH2 drive tumor-associated hypertrimethylation of lysine 27 on histone H3 (H3K27) in human B-cell lymphomas. Proc Natl Acad Sci USA. 2010 Dec 7;107(49):20980–5.

Chapter VII

Identification of novel crosstalk mechanisms regulating PRC2 biochemical activity

7.1 Introduction

Crosstalk between chromatin-modifying enzymes (CMEs) and their modifications comprises an important facet of regulation occurring on the level of chromatin (1-3). Some chromatin marks (in cis or trans) may facilitate CME recruitment to its substrate or allosterically stimulate its activity, while others may block substrate recognition or directly inhibit CME activity (4-6). Several of these crosstalk mechanisms have been implicated in the regulation of PRC2—for example, binding H3K4me3 or H3K27me3 allosterically inhibits (7) or stimulates its activity (8,9), respectively. Beyond these allosteric mechanisms, PRC2 substrate recognition is disrupted by the presence of H3S28 phosphorylation (10), H3K36 methylation (7,11), or H327ac (10).

As dysregulation of H3K27me3 is a common occurrence in many cancers (12), identification and elucidation of PRC2-regulatory crosstalk mechanisms may implicate additional CMEs in supporting tumorigenesis and reveal new drug targets within these cancer contexts. This chapter discusses our efforts to identify novel PRC2-connected crosstalk mechanisms. Through screening libraries of uniquely modified histone peptides for their ability to bind to PRC2 or act as substrates for PRC2 H3K27 methylation, we uncovered a role for H3R26 methylation in suppressing PRC2 activity, implicating CARM1 in PRC2 regulation. Furthermore, we find further evidence to support a role for H3K23me1, a mark only recently reported in humans (13,14), in repressing PRC2 activity.

7.2 Results and discussion

7.2.1 Identification of histone modifications regulating PRC2 binding and activity.

As we were able to express and purify active 5-component PRC2, we sought to use this and other biochemical assays to further explore the biochemical regulation of this key HMT. The commercial availability of histones and histone-derived peptides harboring known modifications found in chromatin provides opportunities to study the impact of these modifications on the binding and enzymatic activity of chromatin-associated factors, including readers, writers and erasers (15-17). Using an array containing 384 uniquely modified histone peptides (Celluspots peptide array), we aimed to identify histone modifications that modulated PRC2 binding. We incubated the peptide arrays with PRC2 containing 1XFLAG-EZH2 and, after several washes, detected PRC2 binding by subsequent incubations with anti-FLAG M2 antibody and HRP-conjugated secondary antibody..

Figure 7.1A shows the raw data obtained following chemiluminescence detection of an array incubated with recombinant PRC2. To quantify the levels of PRC2 bound to each peptide, we measured chemiluminescence intensity of corresponding peptide ‘spots’ by densitometry. With these data, we could then examine the relative degrees to which PRC2 binding occurred on unmodified peptides derived from different histones and different histone regions (Figure 7.1B). We found that, out of the 8 unique unmodified peptides, PRC2 bound most strongly to H3[16-35], a peptide containing H3K27 and the ARKS motif (8), while other H3 peptides, H3[7-26] and H3[26-45],

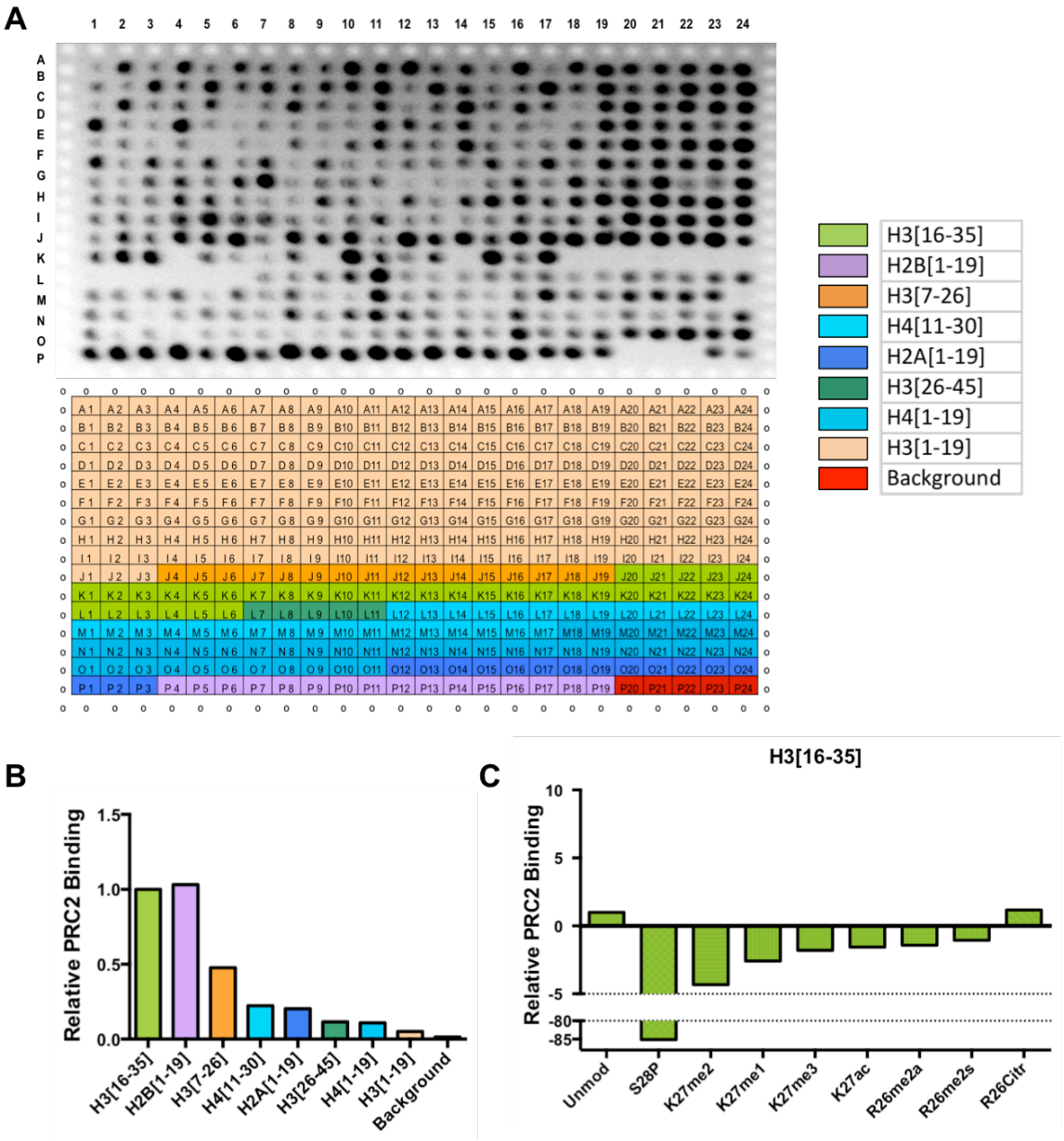

Figure 7.1 5C-PRC2 peptide-binding explored using MODified Histone Peptide Array
(A) Raw chemiluminescence signal from PRC2 bound to spotted peptides on MODified Histone Peptide Array. Map indicates locations of modified-peptides of the same histone and regions from which they were derived. (B) Relative chemiluminescence signal from each unmodified histone peptide spot. Data are normalized to H3[16-35] and represent ratios derived from mean signal from duplicate arrays. (C) Relative chemiluminescence signal from various H3[16-35]-derived modified peptides spots. Data are normalized to H3[16-35] signal, with ratios <1 transformed [=1-1/(mod/unmod)] and represent ratios derived from the mean signal from duplicate arrays.

lacking the full motif bound to a lesser degree. Interestingly, H3[7-26] exhibited much higher PRC2 binding than H3[26-45], suggesting necessary engagement with residues

upstream of H3K27. Of note, PRC2 bound H2B[1-19] with near equal affinity to the top H3-derived peptide; a finding potentially consistent with recent evidence suggesting H2B (H2BK120) methylation by PRC2 (18).

Given that PRC2 bound most strongly to H3[16-35], we examined the extent of PRC2 binding to singly-modified H3[16-35] peptides present on the array. All modifications, with the exception of H3R26Cit, reduced PRC2 binding compared with H3[16-35] (Figure 7.1C). As expected, H3S28 phosphorylation completely ablated PRC2 binding, consistent with previous findings (10). Interestingly, H3R26 methylation was among the peptide modifications that reduced binding – an observation that we explored further in PRC2 activity assays (see below). The effects of single modifications on PRC2 interaction with additional histone-derived peptides (e.g. H2B[1-19] and H3[7-26]) are included in Figure S7.1.

Following these studies, large sets of modified histone peptides in 'unbound' formats (i.e. free in solution) became available from a number companies (Alta Biosciences, JPT peptide, etc), enabling additional efforts to profile the influence of specific histone modifications on PRC2 activity, to complement our binding studies described above. As these sets often comprise biotinylated peptides, PRC2 biochemical assays developed over the course of our earlier HTS and hit characterization efforts were implemented to measure activity on various modified substrates —the Histone H3 (Set 1), Histone H3/N-terminal H4 (Set 3), and Histone phosphorylation and Arginine methylation (Set 5) collections available from Alta Biosciences. Each of these sets contained 94 distinct histone peptides harboring various modifications, including acetylation, phosphorylation, and methylation in multiple combinations. To measure

PRC2 activity on each peptide, we arrayed peptide sets in 384-well source plates and, after pin transfer into PRC2-containing assay wells, we initiated reactions with ^{3}H-SAM and measured ^{3}H incorporation by scintillation proximity assay (SPA)— a radiometric approach using streptavidin-coated, scintillant-containing beads which luminesce upon capture of biotinylated ^{3}H-labeled product (19).

PRC2 activity (CPM) on each unmodified histone peptide is shown in Figure 7.2A. As expected, PRC2 methylated H3[14-34] (and other H3K27-containing peptides) to the most significant degree; however, activity was also detected on H3[1-21], a likely result of low H3K9 methyltransferase activity that has previously been suggested (20). No significant methylation was detected on histone H2A, H2B, or H4-derived peptides. As PRC2 exhibited the highest activity on H3[14-34], which is consistent with our prior observation that PRC2 bound H3[16-35] most strongly, we next compared methylation levels exhibited between singly-modified H3[14-34] peptides present in the collection. We observed weaker activity on peptides harboring previously described inhibitory modification, such as H3S28 phosphorylation (10); PRC2 exhibited no activity on H3K27me3, little activity on H3K27me2, and reasonable activity on H3K27me1 as expected from wild-type EZH2 complexes (21).

In addition to these expected results, novel findings did emerge. Notably, H3K23 methylation appeared to *increase* PRC2 activity, while peptides methylated at R26, were not viable substrates for PRC2 (Figure 7.1). As the impact of these modifications on PRC2 activity had not previously reported, we further evaluated their biochemical and cellular impact in preliminary follow-up studies.

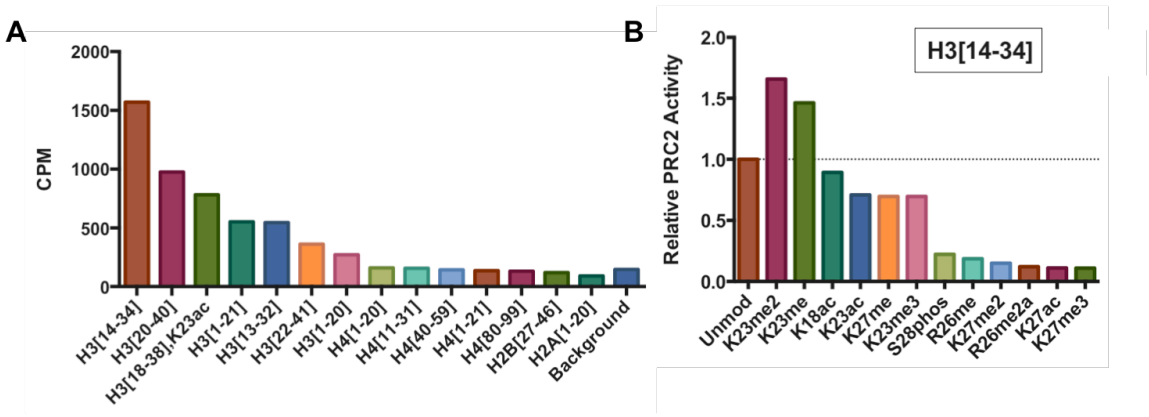

Figure 7.2 PRC2 activity screen on 282 modified histone peptides from Alta Biosciences
(A) Raw PRC2 activity (CPM) on unmodied peptides (5 uM) from Alta Biosciences. SPA data represent the mean of four replicate measurements. (B) Relative PRC2 activity on various H3[14-34]-derived modified peptides. Data are normalized to H3[14-34] and represent ratios derived from the means of four replicate measurements

7.2.2 Characterizing H3K23me1 modulation of PRC2 biochemical activity

As substrate profiling suggested increased PRC2 activity on H3K23 methylated peptides, we next kinetically characterized the activity of PRC2 on an H3K23me1-modified peptide (H3[21-44], K23me1) in SPA, measuring V_{MAX} and K_M. We focused specifically on the monomethylated H3K23 peptide, as the presence of H3K23me2/3 in humans is unclear (14,22). As shown in Figure 7.3A, PRC2 exhibits both an increase in V_{MAX} (~1.6 fold) and a decrease in K_M (~2-fold) when H3K23me1 is present on its substrate. These findings suggest that H3K23me1 stimulates PRC2 activity (in cis or in trans) and that PRC2 also has higher binding affinity for H3K23me1. To explore the latter, we used a fluorescence polarization (FP) assay to compare the ability of H3K23me1-modified (H3[21-44]-H3K23me1) and unmodified (H3[21-44]) peptides to disrupt the interaction between PRC2 and fluorescently-labeled H3[21-44] tracer. Consistent with the suggestion of higher binding affinity, H3[21-44]-H3K23me1 exhibited

greater potency (0.3 uM vs. 1.7 uM) in disrupting PRC2-H3[21-44] tracer compared with H3[21-44] unmethylated at H3K23 (Figure 7.3B).

How H3K23me1 modification impacts PRC2 V_{MAX} remains to be determined. While this enhanced affinity could result from H3K23me1-induced stabilization of the enzyme-substrate complex (regulation in cis), it also is possible that conformational changes in the EZH2 substrate-binding pocket, related to trans H323me1 stimulation, can alter PRC2 affinity for the peptide substrate. If this is the case, one might expect to see synergistic behavior between H3[21-44]-H3K23me1 and H3[21-44] in the previously described competitive FP assay. Furthermore, if H3K23me1 stimulation does occurs in trans, it raises the question as to which PRC2 component harbors the allosteric site. Additional studies will be required to decipher the exact mechanism of H3K23me1 stimulation and could uncover previously unknown allosteric regulatory sites within PRC2, expanding our understanding of the scope of its regulation.

The role of H3K23 methylation in chromatin regulation remains poorly understood and the CMEs involved in its deposition and removal have not been identified. Recent studies, however, are beginning to reveal connections between H3K23me1 and heterochromatin, including biochemical and cellular evidence of an association between H3K23me1 and HP1ß, a heterochromatin-associated factor (13). Most interestingly, focused H3K23me1 ChIP studies have revealed evidence of enrichment of the mark on genes within heterochromatin, as well as known Polycomb targets (23). Future studies characterizing the genome-wide localization of H3K23me1 (ChIP-seq) may reveal stronger connections between H3K23 methylation and

heterochromatin, as well as its potential involvement in PRC2 localization and regulation.

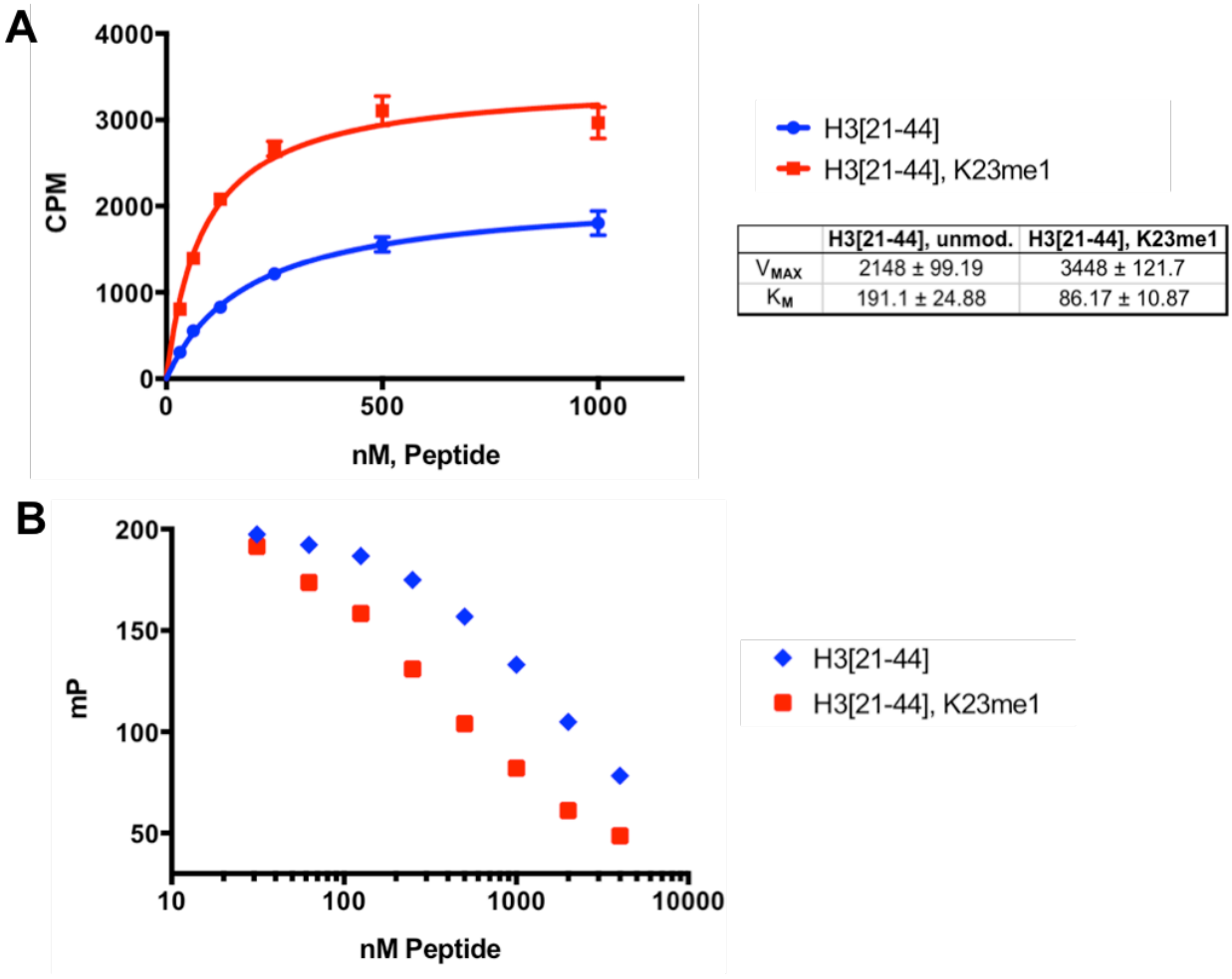

	H3[21-44], unmod.	H3[21-44], K23me1
V_{MAX}	2148 ± 99.19	3448 ± 121.7
K_M	191.1 ± 24.88	86.17 ± 10.87

Figure 7.3 PRC2 kinetic and FP studies on H3[21-44]-K23me1 peptide
Kinetic studies were performed using indicated peptides as a substrates in radiometric PRC2 SPA. Initial velocities were estimated by measuring activity (CPM) at a single time point (t=120 min) within the linear range of reaction. (A) Estimated initial velocities versus H3[21-44] or H3[21-44]-K23me1. Data points represent the mean and standard error of four replicate measurements. Nonlinear regression fits were performed using the Michaelis-Menten model in PRISM 6.0 to obtain and plot best-fit VMAX and KM values and their associated standard errors. (B) FP measurements of 31.25 nM HiLyteTM Fluor 488-H3[21-44] in the presence various concentrations of peptide. H3K23me1 and unmodified peptides exhibited apparent IC_{50} values of 0.3 and 1.7 uM, respectively. Data points represent the mean and standard error of four replicate measurements in each assay. Nonlinear regression fits were performed using the 'log(inhibitor) vs response—variable slope (four parameter)' module in PRISM 6.0 to obtain IC_{50} values.

7.2.3 Investigating the impact of H3R26 methylation on PRC2 biochemical and cellular activity

In addition to H3K23me1, our substrate profiling also revealed a role for H3R26 methylation in regulating PRC2 activity, as both monomethylation (H3R26me) and asymmetric dimethylation (H3R26me2a) rendered PRC2 unable to methylate H3K27 within the same peptide substrate. In parallel to H3K23me1 studies, we examined PRC2 kinetic behavior on peptide substrates harboring H3R26me and H3R26me2a modifications, as well as peptides asymmetrically methylated and citrullinated (H3R26me2s and H3R26Cit) at the same position. In contrast to unmodified substrates (H3[21-44] and H3[15-36]), all R26-methylated peptides supported no significant PRC2 activity relative to background at all concentrations tested (Figure 7.4). These data suggest that H3R26me and H3R26Cit strongly antagonize H3K27 in vitro, potentially implicating their associated CMEs in PRC2 regulation. Whether this effect is the result of cis or trans interactions remains to be determined.

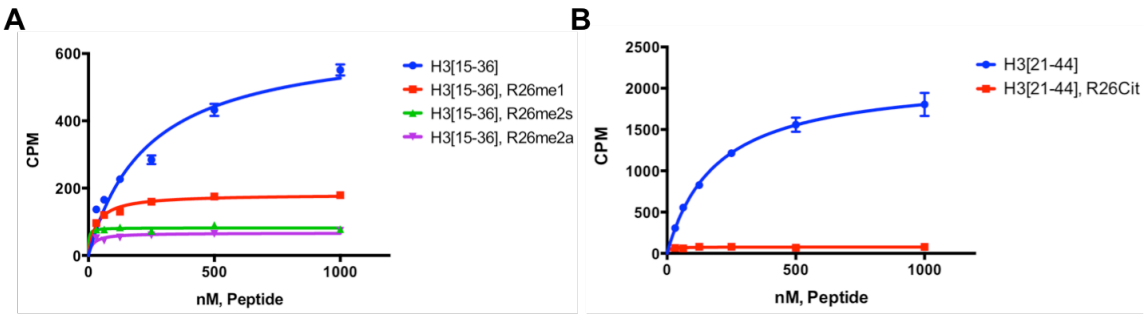

Figure 7.4 PRC2 kinetic studies on various H3R26-modified peptides
Kinetic studies were performed using indicated peptides as a substrates in radiometric PRC2 SPA. Initial velocities were estimated by measuring activity (CPM) at a single time point (t=120 min) within the linear range of reaction. (A) Estimated initial velocities versus H3[15-36] and R26me-, R26me2s-, and R26me2a-modified H3[15-36]. (B) Estimated initial velocities versus H3[21-44] and H3[21-44]-R26Cit. Data points represent the mean and standard error of four replicate measurements. Nonlinear regression fits were performed using the Michaelis-Menten model in PRISM 6.0 to obtain and plot best-fit VMAX and KM values and their associated standard errors

CARM1/PRMT4 and PAD2 mediate H3R26 methylation(24) and citrullination(25), respectively. Given the ability of both of these modifications to block subsequent H3K27 methylation *in vitro*, we questioned whether alterations in CARM1 or PAD2 expression in cells could influence the expression of PRC2 target genes. To investigate this possibility, we searched publically available data through Gene Expression Omnibus (GEO) in an effort to find gene expression profiles associated with PAD2 or CARM1 perturbation. While we were unable to find any data associated with PAD2, we located a record for a study that investigated the impact of CARM1 knockdown and overexpression on estrogen receptor α (ERα) target gene expression(26) in MCF7 cells. In this study, DOX-inducible CARM1 expression or shRNA-mediated knockdown proceeded for five days prior to gene expression profiling by microarray – a length of time that should be sufficient for any expected alterations in H3K27me3 to occur (27,28).

As we hypothesized based on our in vitro data that increasing CARM1 activity would effectively block PRC2 activity at a given loci, we focused on gene expression profiles obtained for MCF7 cells overexpressing CARM1. We analyzed data from these samples using the GEO2R web tool (29), comparing the replicate gene expression profiles from CARM1-overexpressing cells (DOX-induced) to those obtained from DOX-untreated controls (three biological replicates per conditions). From this analysis, we selected the most significantly upregulated (96 total; p-value <0.01) and downregulated (91 total; p-value <0.02) genes resulting from CARM1 overexpression.

Each of these lists were investigated using the 'Compute Overlaps' function on the Molecular Signatures Database (MSigDB) website to explore whether the identified

Table 7-1 Summary of the top overlapping gene sets (FDR q-value <0.05) for most significant 96 upregulated genes (black) and 91 downregulated genes (red) after 5-day CARM1 overexpression in MCF7 (GEO accession: GSE26454). PRC2-connected gene sets are emphasized in bold.

Gene Set Name	# Genes in Gene Set (K)	# Genes in Overlap (k)	k/K	p-value	FDR q-value
ZWANG_TRANSIENTLY_UP_BY_2ND_EGF_PULSE_ONLY	1725	19	0.011	2.66E-09	7.62E-06
MARTENS_TRETINOIN_RESPONSE_UP	857	14	0.0163	3.23E-09	7.62E-06
BENPORATH_EED_TARGETS	**1062**	**14**	**0.0132**	**4.69E-08**	**7.39E-05**
YOSHIMURA_MAPK8_TARGETS_UP	1305	15	0.0115	8.85E-08	1.04E-04
KONDO_PROSTATE_CANCER_WITH_H3K27ME3	**196**	**7**	**0.0357**	**1.99E-07**	**1.88E-04**
BENPORATH_ES_WITH_H3K27ME3	**1118**	**13**	**0.0116**	**6.10E-07**	**4.80E-04**
REACTOME_GPCR_DOWNSTREAM_SIGNALING	805	11	0.0137	1.02E-06	6.86E-04
BENPORATH_PRC2_TARGETS	**652**	**10**	**0.0153**	**1.16E-06**	**6.87E-04**
BENPORATH_SUZ12_TARGETS	**1038**	**12**	**0.0116**	**1.81E-06**	**9.52E-04**
REACTOME_SIGNALING_BY_GPCR	920	11	0.012	3.66E-06	1.66E-03
MIKKELSEN_MCV6_HCP_WITH_H3K27ME3	**435**	**8**	**0.0184**	**3.87E-06**	**1.66E-03**
MIKKELSEN_MEF_HCP_WITH_H3K27ME3	**590**	**9**	**0.0153**	**4.29E-06**	**1.69E-03**
PID_SMAD2_3NUCLEARPATHWAY	82	4	0.0488	2.76E-05	1.00E-02
ZHOU_INFLAMMATORY_RESPONSE_LPS_UP	431	7	0.0162	3.53E-05	1.19E-02
SHEN_SMARCA2_TARGETS_DN	357	6	0.0168	1.09E-04	3.42E-02
DODD_NASOPHARYNGEAL_CARCINOMA_UP	1821	18	0.0099	1.61E-08	7.58E-05
MEISSNER_NPC_HCP_WITH_H3_UNMETHYLATED	536	10	0.0187	1.18E-07	2.79E-04
RICKMAN_HEAD_AND_NECK_CANCER_C	113	5	0.0442	3.23E-06	5.08E-03
LIU_PROSTATE_CANCER_DN	481	8	0.0166	5.40E-06	6.38E-03
CHICAS_RB1_TARGETS_CONFLUENT	567	8	0.0141	1.77E-05	1.67E-02
FARMER_BREAST_CANCER_APOCRINE_VS_LUMINAL	326	6	0.0184	4.89E-05	3.01E-02
MEISSNER_BRAIN_HCP_WITH_H3K4ME3_AND_H3K27ME3	1069	10	0.0094	5.21E-05	3.01E-02
LIM_MAMMARY_STEM_CELL_UP	489	7	0.0143	5.54E-05	3.01E-02
PICCALUGA_ANGIOIMMUNOBLASTIC_LYMPHOMA_UP	205	5	0.0244	5.73E-05	3.01E-02
SENGUPTA_NASOPHARYNGEAL_CARCINOMA_DN	349	6	0.0172	7.12E-05	3.21E-02
BRUINS_UVC_RESPONSE_VIA_TP53_GROUP_A	898	9	0.01	7.49E-05	3.21E-02
RODRIGUES_THYROID_CARCINOMA_ANAPLASTIC_DN	537	7	0.013	9.93E-05	3.91E-02
ZHAN_MULTIPLE_MYELOMA_MF_UP	47	3	0.0638	1.14E-04	4.15E-02
CHICAS_RB1_TARGETS_GROWING	243	5	0.0206	1.27E-04	4.30E-02
DOUGLAS_BMI1_TARGETS_UP	566	7	0.0124	1.37E-04	4.32E-02
ROVERSI_GLIOMA_COPY_NUMBER_DN	54	3	0.0556	1.73E-04	4.97E-02
ONDER_CDH1_TARGETS_1_UP	140	4	0.0286	1.80E-04	4.97E-02
MEISSNER_NPC_HCP_WITH_H3K4ME3_AND_H3K27ME3	142	4	0.0282	1.90E-04	4.97E-02

genes shared statistically significant overlap with any curated gene sets (C2 category) (30,31). As shown in Table 7-1, of the top gene sets overlapping with genes *upregulated* by CARM1 overexpression (FDR q-value <0.05), nearly half (7/15) appear to be PRC2 connected. In fact, three of the gene sets comprise genes bound by individual PRC2 components (EZH2, EED, and SUZ12) and the remaining four comprise those enriched in H3K27me3 (32-34). No PRC2-connected gene sets were found to overlap significantly with genes *downregulated* by CARM1 overexpression. While preliminary, these results suggest that CARM1 might oppose PRC2 activity in a cellular context, lowering H3K27me3 levels through increased H3R26 methylation.

Taken together, the preliminary results presented here and in **Chapter VI,** suggest that more remains to be uncovered regarding how PRC2 activity is regulated in a cellular context and whether this regulation is altered in disease. If so, efforts toward

the identification of novel PRC2-regulatory nodes and mechanisms may reveal new drug targets with different impact compared with direct EZH2 inhibition. While it remains to be determined whether CARM1, PAD2, or the yet-to-be-identified H3K23 methyltransferase represent such nodes, their further study in the context of PRC2 regulation may yield novel insights leading to discovery of impactful therapeutics.

7.3 Experimental methods

PRC2 radiometric assays. PRC2 was diluted to final concentration in 2X enzyme buffer (50mM Tris HCl pH 8.5, 10 mM DTT, 0.01% Tween 20). 20 uL reactions were initiated with an equal volume of an SAM solution (NEB) containing ^{3}H-SAM (at 25% total SAM concentration; NET155001MC; PerkinElmer) and indicated peptide (AnaSpec/Alta) and incubated at room temperature for 2 hrs. Methylation levels were detected by SPA as previously described (19) on a TopCount NTX (PerkinElmer)

MODified™ Histone Peptide Array. Histone peptide arrays (ActiveMotif) were blocked with %5 non-fat milk in TBST for 1 hr at RT prior to antibody incubation. Was diluted in activity assay buffer (50 mM Tris pH 8.5, 5 mM DTT, 0.01% Tween 20) and incubated on individual arrays for 1 hr at RT. Arrays were washed with TBST and incubated with anti-FLAG M2 antibody diluted 1:1000 in blocking buffer for 1 hr. After TBST washes, anti-rabbit IgG-HRP (GE) diluted 1:2500 in blocking buffer for 1 hr at RT and washed in TBST prior to chemiluminescence detection with SuperSignal West Pico Chemiluminescent Substrate (Pierce). Arrays were imaged on an Image Station 4000MM Pro (Kodak) and densitometry was performed using included Carestream software.

Fluorescence polarization. Competing peptide or DMSO was diluted to 2X final concentration in 1X Enzyme Buffer and added at 20 uL per well in black 384-well plates. H3[21-44] - HiLyte488 peptide was then diluted to 62.5 nM in 1X Enzyme Buffer and added at 20 uL per well. Following 10 min incubation, fluorescence polarization (mP) was measured using Wallac Envision 2104 Multilabel Reader (FP FITC dual optical module; Excitation: 480 nm, Emission: 535 nm for both S- and P-channels).

7.4 References

1. Schreiber SL, Bernstein BE. Signaling network model of chromatin. Cell. 2002 Dec 13;111(6):771–8.

2. Smith E, Shilatifard A. The Chromatin Signaling Pathway: Diverse Mechanisms of Recruitment of Histone-Modifying Enzymes and Varied Biological Outcomes. Molecular Cell. Elsevier Inc; 2010 Dec 10;40(5):689–701.

3. Arzate-Mejía RG, Valle-García D, Recillas-Targa F. Signaling epigenetics: novel insights on cell signaling and epigenetic regulation. López-Casillas F, Vázquez-Prado J, editors. IUBMB Life. 2011 Oct;63(10):881–95.

4. Molina-Serrano D, Schiza V, Kirmizis A. Cross-talk among epigenetic modifications: lessons from histone arginine methylation. Biochem Soc Trans. 2013 Jun;41(3):751–9.

5. Lee J-S, Shukla A, Schneider J, Swanson SK, Washburn MP, Florens L, et al. Histone Crosstalk between H2B Monoubiquitination and H3 Methylation Mediated by COMPASS. Cell. 2007 Dec;131(6):1084–96.

6. Lee J-S, Smith E, Shilatifard A. The language of histone crosstalk. Cell. 2010 Sep 3;142(5):682–5.

7. Schmitges FW, Prusty AB, Faty M, Stützer A, Lingaraju GM, Aiwazian J, et al. Histone methylation by PRC2 is inhibited by active chromatin marks. Molecular Cell. 2011 May 6;42(3):330–41.

8. Xu C, Bian C, Yang W, Galka M, Ouyang H, Chen C, et al. Binding of different histone marks differentially regulates the activity and specificity of polycomb repressive complex 2 (PRC2). Proc Natl Acad Sci USA. National Acad Sciences; 2010 Nov 9;107(45):19266–71.

9. Margueron R, Justin N, Ohno K, Sharpe ML, Son J, DruryIII WJ, et al. Role of the polycomb protein EED in the propagation of repressive histone marks. Nature. Nature Publishing Group; 2009 Aug 10;461(7265):762–7.

10. Lau PNI, Cheung P. Histone code pathway involving H3 S28 phosphorylation and K27 acetylation activates transcription and antagonizes polycomb silencing. Proc Natl Acad Sci USA. 2011 Feb 15;108(7):2801–6.

11. Yuan W, Xu M, Huang C, Liu N, Chen S, Zhu B. H3K36 methylation antagonizes PRC2-mediated H3K27 methylation. Journal of Biological Chemistry. 2011 Mar 11;286(10):7983–9.

12. Chase A, Cross NCP. Aberrations of EZH2 in cancer. Clin Cancer Res. American Association for Cancer Research; 2011 May 1;17(9):2613–8.

13. Liu H, Galka M, Iberg A, Wang Z, Li L, Voss C, et al. Systematic Identification of Methyllysine-Driven Interactions for Histone and Nonhistone Targets. J Proteome Res. 2010 Nov;9(11):5827–36.

14. Tan M, Luo H, Lee S, Jin F, Yang JS, Montellier E, et al. Identification of 67 histone marks and histone lysine crotonylation as a new type of histone modification. Cell. 2011 Sep 16;146(6):1016–28.

15. Nady N, Min J, Kareta MS, Chedin F, Arrowsmith CH. A SPOT on the chromatin landscape? Histone peptide arrays as a tool for epigenetic research. Trends Biochem Sci. 2008 Jul;33(7):305–13.

16. Thiele A, Stangl GI, Schutkowski M. Deciphering Enzyme Function Using Peptide Arrays. Molecular Biotechnology. Humana Press Inc; 2011 Nov;49(3):283–305.

17. Gurard-Levin ZA, Kilian KA, Kim J, Baehr K, Mrksich M. Peptide Arrays Identify Isoform-Selective Substrates for Profiling Endogenous Lysine Deacetylase Activity. ACS Chem Biol. 2010 Sep;5(9):863–73.

18. Kogure M, Takawa M, Saloura V, Sone K, Piao L, Ueda K, et al. The Oncogenic Polycomb Histone Methyltransferase EZH2 Methylates Lysine 120 on Histone H2B and Competes Ubiquitination. Neoplasia. 2013 Nov;15(11):1251–.

19. Horiuchi KY, Eason MM, Ferry JJ, Planck JL, Walsh CP, Smith RF, et al. Assay development for histone methyltransferases. Assay Drug Dev Technol. 2013 May;11(4):227–36.

20. Cao R, Wang L, Wang H, Xia L, Erdjument-Bromage H, Tempst P, et al. Role of histone H3 lysine 27 methylation in Polycomb-group silencing. Science. 2002 Nov 1;298(5595):1039–43.

21. Sneeringer CJ, Scott MP, Kuntz KW, Knutson SK, Pollock RM, Richon VM, et al. Coordinated activities of wild-type plus mutant EZH2 drive tumor-associated hypertrimethylation of lysine 27 on histone H3 (H3K27) in human B-cell lymphomas. Proc Natl Acad Sci USA. National Acad Sciences; 2010 Dec 7;107(49):20980–5.

22. Papazyan R, Voronina E, Chapman JR, Luperchio TR, Gilbert TM, Meier E, et al. Methylation of histone H3K23 blocks DNA damage in pericentric heterochromatin during meiosis. Elife. 2014;3:e02996.

23. Mahrez W. HISTONE MODIFICATIONS AND TRANSCRIPT PROCESSING DURING ARABIDOPSIS DEVELOPMENT. e-collection.library.ethz.ch.

24. Bedford MT, Clarke SG. Protein arginine methylation in mammals: who, what, and why. Molecular Cell. 2009 Jan 16;33(1):1–13.

25. Zhang X, Bolt M, Guertin MJ, Chen W, Zhang S, Cherrington BD, et al. Peptidylarginine deiminase 2-catalyzed histone H3 arginine 26 citrullination facilitates estrogen receptor α target gene activation. Proc Natl Acad Sci USA. 2012 Aug 14;109(33):13331–6.

26. Al-Dhaheri M, Wu J, Skliris GP, Li J, Higashimato K, Wang Y, et al. CARM1 is an important determinant of ERα-dependent breast cancer cell differentiation and proliferation in breast cancer cells. Cancer Research. American Association for Cancer Research; 2011 Mar 15;71(6):2118–28.

27. McCabe MT, Ott HM, Ganji G, Korenchuk S, Thompson C, Van Aller GS, et al. EZH2 inhibition as a therapeutic strategy for lymphoma with EZH2-activating mutations. Nature. 2012 Dec 6;492(7427):108–12.

28. Knutson SK, Wigle TJ, Warholic NM, Sneeringer CJ, Allain CJ, Klaus CR, et al. A selective inhibitor of EZH2 blocks H3K27 methylation and kills mutant lymphoma cells. Nat Chem Biol. 2012 Nov;8(11):890–6.

29. Barrett T, Wilhite SE, Ledoux P, Evangelista C, Kim IF, Tomashevsky M, et al. NCBI GEO: archive for functional genomics data sets-update. Nucleic Acids Research. Oxford University Press; 2013 Jan;41(D1):D991–5.

30. Subramanian A, Tamayo P, Mootha VK, Mukherjee S, Ebert BL, Gillette MA, et al. Gene set enrichment analysis: A knowledge-based approach for interpreting genome-wide expression profiles. Proc Natl Acad Sci USA. National Acad Sciences; 2005;102(43):15545–50.

31. Liberzon A. A description of the Molecular Signatures Database (MSigDB) Web site. Methods Mol Biol. New York, NY: Springer New York; 2014;1150(Chapter 9):153–60.

32. Mikkelsen TS, Ku M, Jaffe DB, Issac B, Lieberman E, Giannoukos G, et al. Genome-wide maps of chromatin state in pluripotent and lineage-committed cells. Nature. 2007 Aug 2;448(7153):553–60.

33. Kondo Y, Shen L, Cheng AS, Ahmed S, Boumber Y, Charo C, et al. Gene silencing in cancer by histone H3 lysine 27 trimethylation independent of promoter DNA methylation. Nat Genet. 2008 Jun;40(6):741–50.

34. Ben-Porath I, Thomson MW, Carey VJ, Ge R, Bell GW, Regev A, et al. An embryonic stem cell-like gene expression signature in poorly differentiated aggressive human tumors. Nat Genet. 2008 May;40(5):499–507.

Appendix (Supplementary information)

Chapter 3 Supplementary information:

Table S3 1 Potency (IC_{50}) and selectivity of PRC2 hits exhibiting activity on G9a

Compound Name (BRD number)	PRC2 IC50 (M)	PRC2 Selectivity over G9a
BRD-A70967617	1.70E-05	0.00
BRD-A77349281	2.60E-05	0.55
BRD-A19326847	3.00E-05	0.63
BRD-K05016999	2.02E-05	0.81
BRD-K56369987	2.60E-05	1.20
BRD-A09320301	1.27E-05	1.35
BRD-A87845306	8.92E-06	2.11
BRD-K04557493	1.68E-05	2.53
BRD-K43833768	2.24E-05	2.56
BRD-K14221570	2.50E-06	3.32
BRD-K74901416	2.60E-05	3.45
BRD-K93380348	2.60E-05	3.45
BRD-K55448425	2.60E-05	3.75
BRD-K83241810	7.58E-06	3.82
BRD-K01238973	1.65E-05	3.94
BRD-K29824954	4.42E-06	4.72
BRD-A62772571	2.60E-05	5.16
BRD-K42692167	4.30E-06	5.55
BRD-K97810414	1.34E-05	6.33
BRD-K97550475	4.16E-06	6.38
BRD-K15016198	7.68E-06	6.64
BRD-K65337188	2.60E-05	7.00
BRD-K79498992	7.02E-06	7.01
BRD-K68670732	1.42E-05	7.25
BRD-K06024458	5.13E-06	7.37
BRD-K54708045	3.03E-06	7.79
BRD-K21667562	7.20E-06	8.26
BRD-K49348342	6.44E-06	8.32
BRD-A65671304	4.03E-06	9.04
BRD-K47012829	1.33E-05	10.13
BRD-K08794464	6.40E-06	11.79
BRD-A59033029	1.83E-05	12.59
BRD-K39855928	2.67E-06	12.76
BRD-K09917719	5.03E-06	12.87
BRD-A15415227	4.17E-06	13.56
BRD-K04181155	1.39E-05	15.30
BRD-A54029483	2.29E-06	15.79
BRD-K30414341	2.10E-06	17.07
BRD-A43003619	2.60E-05	17.21
BRD-K82700792	7.80E-06	18.28
BRD-K57579529	3.90E-06	18.37
BRD-K91393021	2.39E-05	20.20
BRD-K44673118	5.84E-06	20.69
BRD-K23759596	2.83E-06	25.34
BRD-K39733634	2.41E-06	25.88
BRD-A39255369	7.53E-06	27.59
BRD-K50736931	1.82E-05	28.04
BRD-K77817104	3.47E-06	29.66
BRD-K00050226	8.06E-06	38.89
BRD-A39747742	1.54E-05	41.58
BRD-K88544581	7.95E-06	44.41
BRD-K88267207	4.36E-06	59.39
BRD-K44436874	1.30E-05	60.74
BRD-K37746737	6.97E-06	81.16
BRD-K65897442	1.78E-06	90.32
BRD-K39120595	1.88E-06	134.19

Table S3 2 Potency (IC_{50}) and selectivity of PRC2 hits exhibiting activity on NSD2

Compound Name (BRD number)	PRC2 IC50 (M)	PRC2 Selectivity over NSD2
BRD-A01439145	2.60E-05	0.15
BRD-K29073714	2.10E-05	0.30
BRD-K43149758	2.06E-06	0.52
BRD-K26401136	2.60E-05	0.56
BRD-K73991644	2.60E-05	0.61
BRD-K24344555	2.31E-05	0.91
BRD-K56460189	3.72E-06	1.23
BRD-A99091156	1.75E-06	1.31
BRD-K48459082	6.44E-07	1.47
BRD-K86695309	1.50E-06	1.83
BRD-K78515374	7.84E-06	1.93
BRD-K73348788	1.90E-05	1.99
BRD-A22721917	1.09E-05	2.38
BRD-K54142860	1.89E-06	2.64
BRD-A82952413	8.71E-06	2.69
BRD-K12807006	7.72E-06	2.85
BRD-K75748852	1.33E-05	2.94
BRD-K58086828	1.61E-05	2.97
BRD-K51517422	1.03E-05	3.80
BRD-K65223912	3.33E-06	3.98
BRD-A51820102	9.40E-06	4.03
BRD-A14615658	7.99E-06	4.07
BRD-A16665823	6.63E-06	4.21
BRD-A75299426	2.62E-06	4.33
BRD-A01024162	2.60E-05	4.37
BRD-A60384554	3.35E-06	4.47
BRD-K32402716	6.48E-06	4.55
BRD-A25705184	4.70E-06	4.65
BRD-K30788832	2.57E-06	4.72
BRD-K62494373	1.85E-06	4.85
BRD-K10211066	2.73E-06	4.89
BRD-K40416271	1.02E-05	4.97
BRD-K29673530	1.11E-06	5.23
BRD-A11943179	8.71E-06	5.38
BRD-A28579486	2.66E-06	5.74
BRD-K27529556	7.55E-07	5.94
BRD-A70649075	1.32E-05	6.50
BRD-A62832076	8.72E-07	6.71
BRD-A06421966	3.25E-06	7.27
BRD-A08304061	5.79E-06	7.75
BRD-K07888196	6.49E-07	8.98
BRD-A80217729	7.60E-06	9.02
BRD-K90261553	2.12E-05	9.08
BRD-A08261539	1.90E-06	9.44
BRD-A24859907	1.65E-06	10.39
BRD-K76169033	2.39E-06	11.84
BRD-A77705379	8.12E-07	15.04
BRD-K18584477	6.71E-07	15.11
BRD-A53909391	1.93E-06	15.91
BRD-A38331280	8.88E-06	19.15
BRD-K07325606	3.20E-06	30.86
BRD-K80384954	2.65E-06	87.44
BRD-K30620592	2.50E-06	92.85
BRD-K02331976	1.53E-06	171.71

Table S3 3 Results of detergent screening to eliminate aggregators

Completely Sensitive (Inactive)	Extreme Shifts (>0.5 LOG)	Weak Shifts (<0.5 LOG)	No Shift
BRD-A07380652	BRD-K65897442	BRD-K97550475	BRD-K80384954
BRD-A11943179	BRD-K64245000	BRD-K93176058	BRD-K79498992
BRD-A16665823	BRD-K59869584	BRD-K86695309	BRD-K77817104
BRD-A97603968	BRD-K30929673	BRD-K84010935	BRD-K76169033
BRD-K07888196	BRD-K08794464	BRD-K83241810	BRD-K63514750
BRD-K09917719	BRD-K07746328	BRD-K82700792	BRD-K62494373
BRD-K21667562	BRD-K02331976	BRD-K79366068	BRD-K56460189
BRD-K23291942	BRD-K00050226	BRD-K72430479	BRD-K54142860
BRD-K39598593	BRD-A87845306	BRD-K64589645	BRD-K49348342
BRD-K44673118	BRD-A65671304	BRD-K58324927	BRD-K43149758
BRD-K55548239	BRD-A33065105	BRD-K57579529	BRD-K42261139
BRD-K55980412		BRD-K48459082	BRD-K38434480
BRD-K58502057		BRD-K45085681	BRD-K12807006
BRD-K88267207		BRD-K42692167	BRD-K07033348
BRD-K99293846		BRD-K40888903	BRD-K06877872
		BRD-K39733634	BRD-A39255369
		BRD-K34200762	BRD-A25705184
		BRD-K30414341	
		BRD-K29824954	
		BRD-K23759596	
		BRD-K15016198	
		BRD-K10256279	
		BRD-K07325606	
		BRD-A99091156	
		BRD-A88029023	
		BRD-A80217729	
		BRD-A77449281	
		BRD-A69976679	
		BRD-A56964404	
		BRD-A54029483	
		BRD-A45976312	
		BRD-A34935857	
		BRD-A33734112	
		BRD-A15415227	

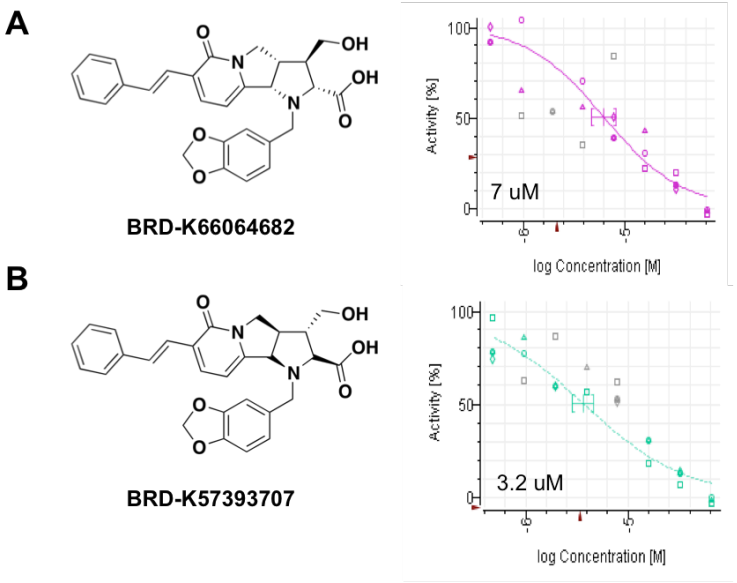

Figure S3 1 Activity of BRD-K66064682 and its enantiomer in PRC2 DELFIA
Activity (PRC2 DELFIA) and structure of (A) the top Pyridone PRC2 inhibitor candidate, BRD-K660664682, and (B) its enantiomer, BRD-K57393707. All data points for triplicate measurements are shown. IC_{50} values were calculated as described in **Experimental methods (3.3)** and are indicated above.

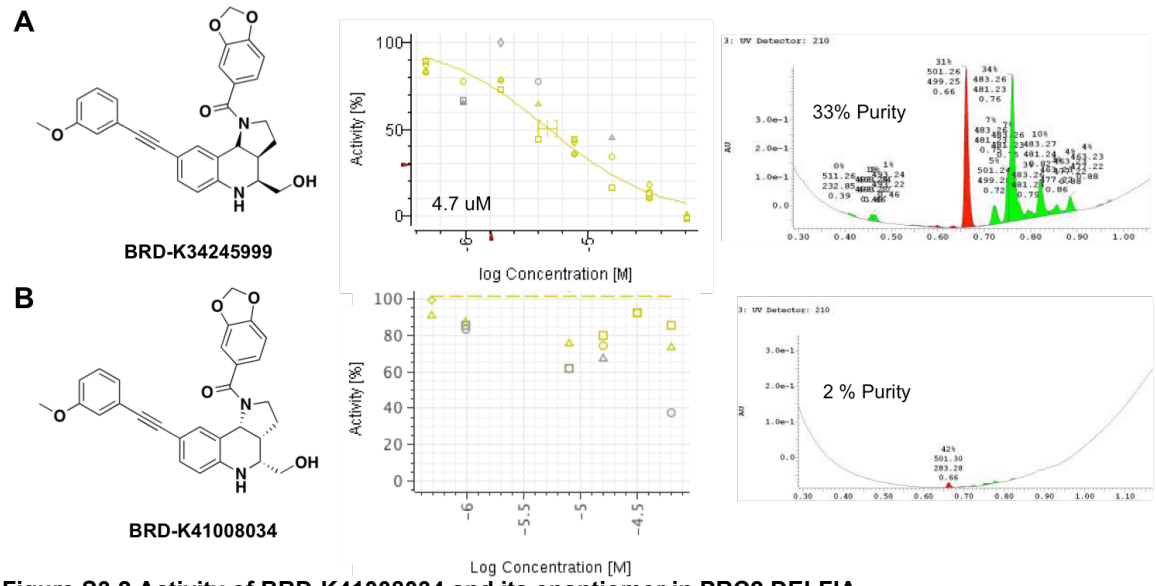

Figure S3 2 Activity of BRD-K41008034 and its enantiomer in PRC2 DELFIA
Structural, activity (PRC2 DELFIA), and HPLC data for (B) the top Povarov PRC2 inhibitor candidate, BRD-K41008034, and (A) its enantiomer, BRD-K34245999. BRD-K41008034 exhibited no activity in this assay due to its remarkably low purity. All data points for triplicate measurements are shown. IC_{50} values were calculated as described in **Experimental methods (3.3)** and are indicated above. HPLC traces were generated by the Broad Institute's Therapeutics Platform analytical chemistry team and obtained through compound management services.

A

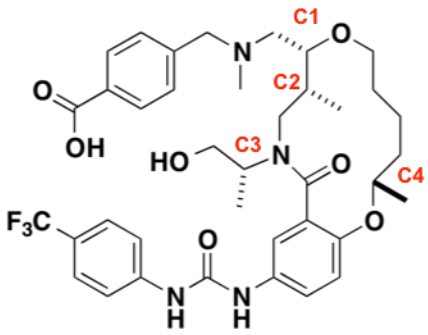

BRD-K55066668

B

Compound ID	Stereoconfiguration (C1,C2,C3,C4)	IC50 (M)
BRD-K03439427-001-01-5	R,S,R,S	6.31E-07
BRD-K19375124-001-01-9	S,R,R,R	7.38E-06
BRD-K26212172-001-01-6	S,S,R,S	1.90E-06
BRD-K32699388-001-01-6	S,S,S,S	1.64E-05
BRD-K40205849-001-01-5	R,S,R,R	2.62E-06
BRD-K47915252-001-01-2	S,S,R,R	8.26E-06
BRD-K49201483-001-01-6	R,S,S,S	3.07E-05
BRD-K49846214-001-01-4	S,R,R,S	3.19E-05
BRD-K55066668-001-01-1	**S,R,S,S**	**9.63E-07**
BRD-K63607172-001-01-1	R,R,S,S	5.35E-06
BRD-K73431244-001-01-8	R,R,S,R	2.76E-06
BRD-K73490331-001-01-8	R,S,S,R	7.41E-06
BRD-K78596368-001-01-3	R,R,R,R	2.54E-05
BRD-K93000977-001-01-0	R,R,R,S	1.51E-05
BRD-K99429365-001-01-5	S,R,S,R	1.17E-06

Figure S3 3 Potency (IC_{50}) of BRD-K5506668 stereoisomers in PRC2 DELFIA
(A) Structure of the top RCM PRC2 inhibitor candidate, BRD-K55066668, with labeled stereocenters (B) SSAR summary table with potency (IC_{50}) data for all BRD-K55066668 stereoisomers tested in PRC2 DELFIA. IC_{50} values were calculated as described in **Experimental methods (3.3)**

Chapter 4 Supplementary information:

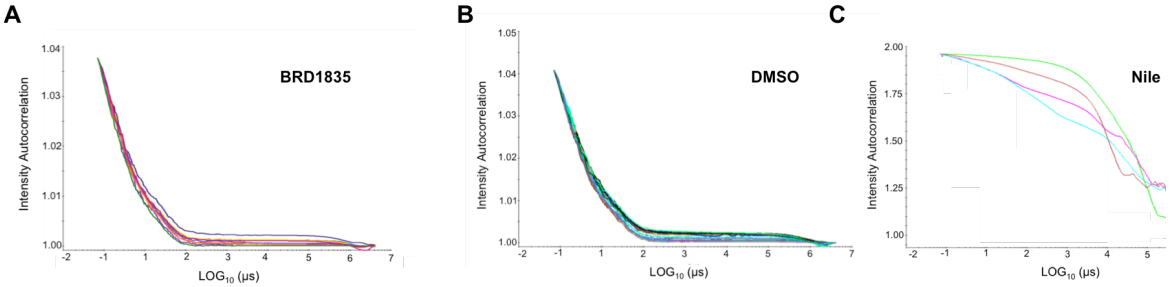

Figure S4.1 Initial DLS studies on BRD1835 in activity assay buffer
DLS intensity autocorrelation curves for (A) various concentrations of BRD1835 (overlay of 2-fold dilution series from 2- 250 uM), DMSO replicates (15 samples shown), and 10 uM Nile Red (3 samples shown) in activity assay buffer (50 mM Tris pH 8.5, 5 mM DTT, 0.01% Tween 20. Compounds were pinned at 250 nL per well (into 40 uL of buffer). Each intensity autocorrelation curve represents the average of 10 single-well acquisitions.

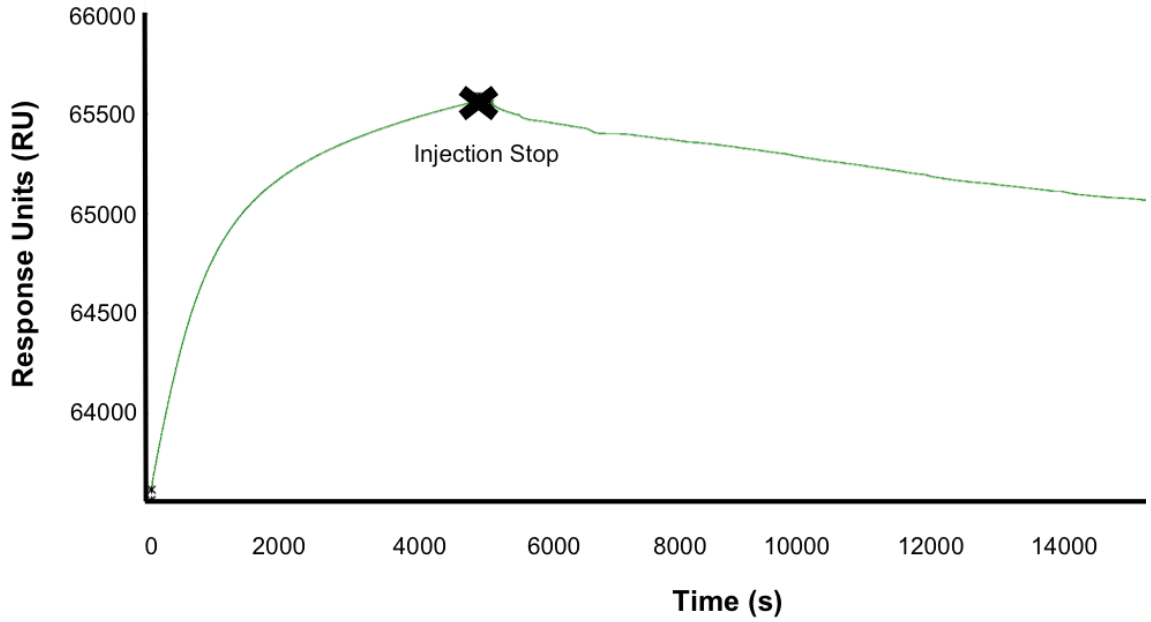

Figure S4.2 Anti-FLAG capture of 5-component PRC2 on Biacore CM5 chip.
5C-PRC2 (6 nM) was injected (2 uL/min) over an anti-FLAG antibody-coated CM5 surface on a Biacore T200. After 5000s, injection was stopped and wash continued over the course of 3.5 hours to estimate drift.

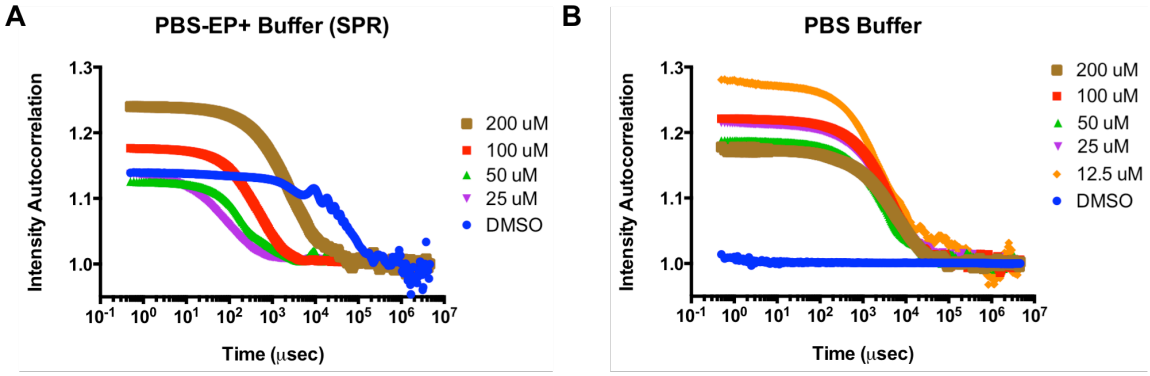

Figure S4.3 DLS intensity autocorrelation functions of BRD1835 in SPR buffer conditions
DLS intensity autocorrelation curves for various concentrations of BRD1835 in (A) 1X PBS-EP+ (GE) and (B) PBS (both at pH 7.4). Each intensity autocorrelation curve represents the average of 10 single-well acquisitions.

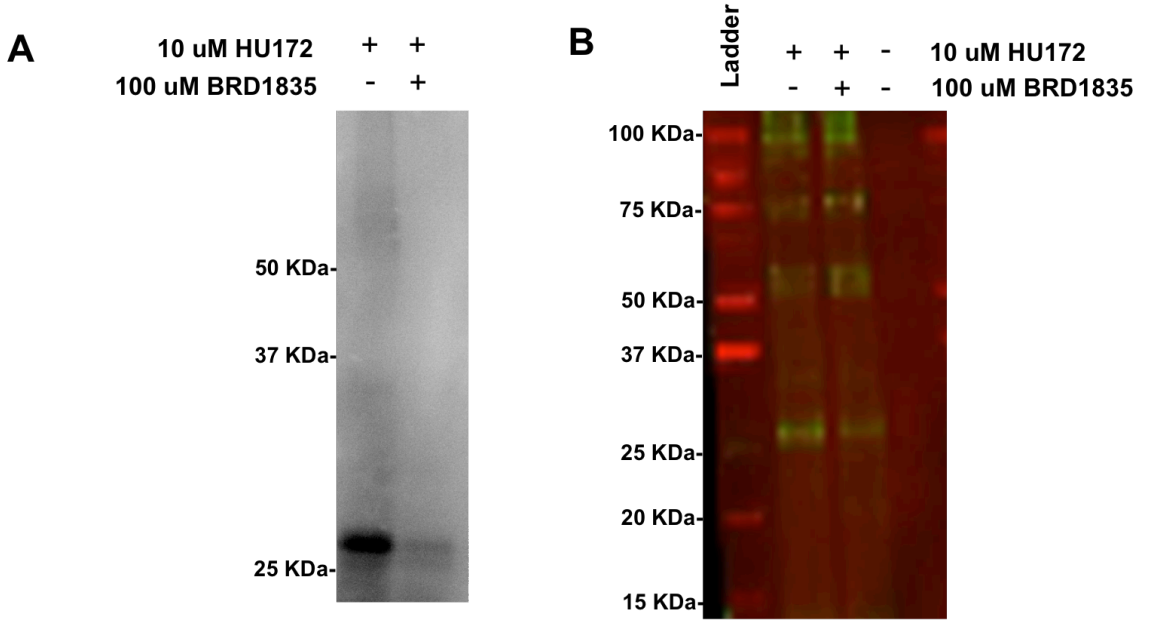

Figure S4.4 Initial HU172 photo-crosslinking studies on PRC2 showing BRD1835-competitive band at 25 kDa.
(A) Initial HU172 photo-crosslinking studies revealing a BRD1835-competitive band at 25kDa and no apparent labeling of bands in the molecular weight range of PRC2 components. Streptavidin-HRP was used to detect biotin-linked HU172 by chemiluminescence (B) Using IRDye-streptavidin and infrared fluorescence detection, HU172 was found to label bands in the molecular weight range of PRC2 components; however, unlike the previously identified 25 kDa band, labeling was not competitive with BRD1835. Detection of this band was unique to a single PRC2 prep.

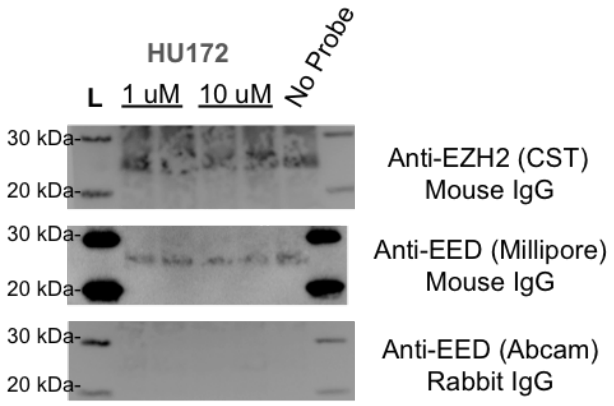

Figure S4.5 EZH2 and EED western blot revealing non-specific detection with mouse IgG antibodies
SDS-PAGE separation and western blot analysis of HU172-crosslinked and mock-treated 5C-PRC2 reveal the presence of a 25 KD detected by both anti-EZH2 and anti-EED antibodies. Interestingly, anti-EED antibodies derived from rabbit were unable to detect this band. (L = M.W. standards)

Chapter 5 Supplementary information:

Investigating potential BRD8284 and BRD3934 peptide-binding activity

A described earlier in this chapter, DLS detected significant aggregation of BRD8284 in activity assay buffer (Figure 5.6A) and cellular studies revealed potential BRD3934 solubility issues in cell culture media (Figure 5.7B). We explored whether aggregation-induced substrate binding could be detected, providing some clue to potential nonspecific mechanisms of activation, as several supposed PRC2 modulators identified by HTS had exhibited this phenomenon (**Chapter III** and **Chapter IV**).

Using a HiLyte-Fluor 488-H3[21-44] FP assay, we were unable to detect binding of BRD8284 or BRD3934 to the peptide tracer, suggesting no interaction between compound aggregates and substrate. However, an interaction between peptide and small aggregates or monomeric compound is still possible, as the mass of this compound-peptide complex may be too small to significantly alter the FP signal.

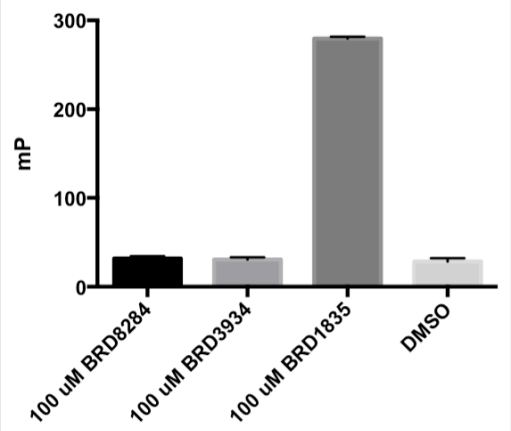

Figure S5.1 Activity of BRD8284 and BRD3934 in HiLyte-Fluor 488-H3[21-44] FP assay.
HiLyte-Fluor 488-H3[21-44] (31.23 nM) FP signal was measured in the presence of 100 uM BRD8284, 100 uM BRD3934, 100 uM BRD1835, and DMSO. Data represent mean and standard error for four replicate measurement.

Chapter 6 Supplementary information:

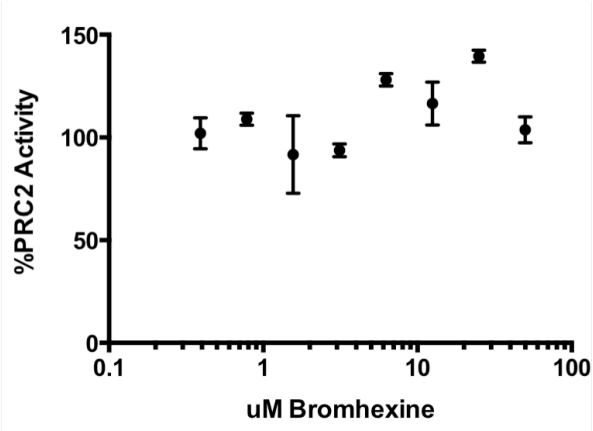

Figure S6.1 Biochemical activity of bromhexine in PRC2 SPA
Bromhexine activity in a radiometric biochemical PRC2 assay (SPA) using peptide H3[21-44] as a substrate. Data points represent the mean and standard error of duplicate measurements.

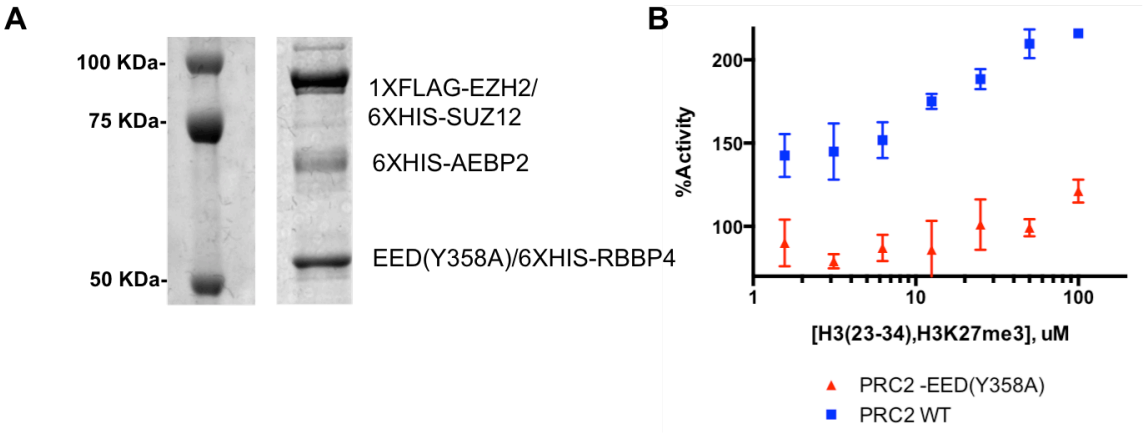

Figure S6.2 Expression, purification, and validation of 5C-PRC2-EED(Y365A) in SPA
(A) 4-12% SDS-PAGE separation of purified 5C-PRC2-EED(Y365A). (B) Activity of 5C-PRC2 and 5C-PRC2-EED(Y365A) in radiometric SPA assay at various concentrations of stimulating peptide (H3[23-34], K27me3). Unlike PRC2-EED(Y365A), PRC2-WT exhibits dose-responsive activation by stimulating peptide, corroborating previous findings.

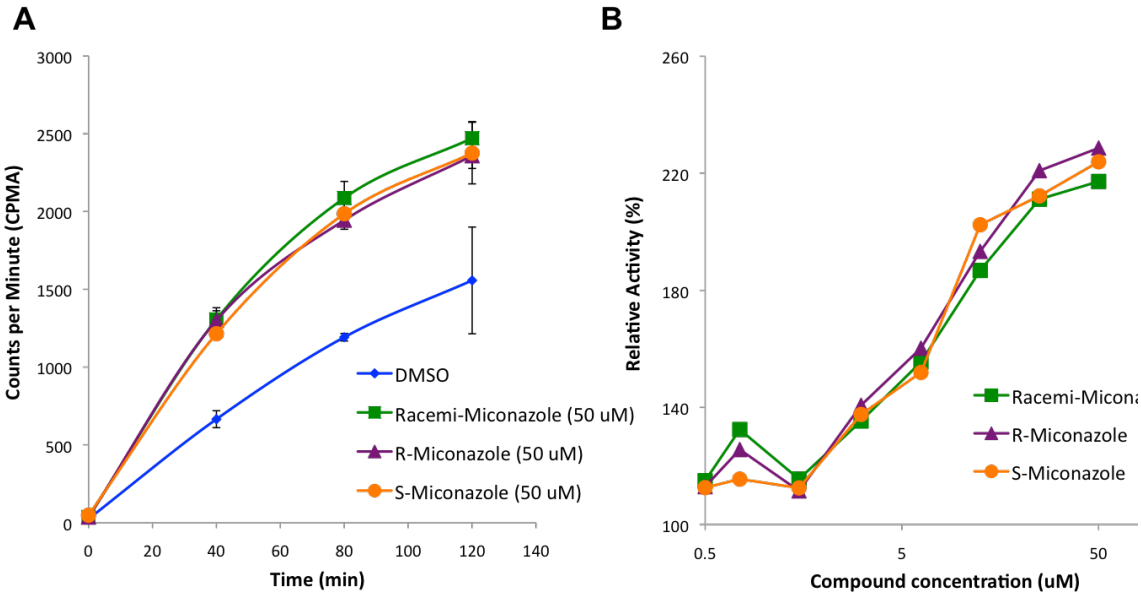

Figure S6.3 Biochemical activity of R-miconazole, S-miconazole, and its racemate
(A) PRC2 activity in histone H3.1 filter-binding assay time course in the presence of 50 uM R-miconazole, S-miconazole, and miconazole racemate. (B) Dose-response of R-miconazole, S-miconazole, and miconazole racemate in histone H3.1 filter-binding PRC2 assay. Both stereoisomers appear to exhibit similar activity--a lack of stereochemical preference which may signify nonspecific activity.

Chapter 7 Supplementary information:

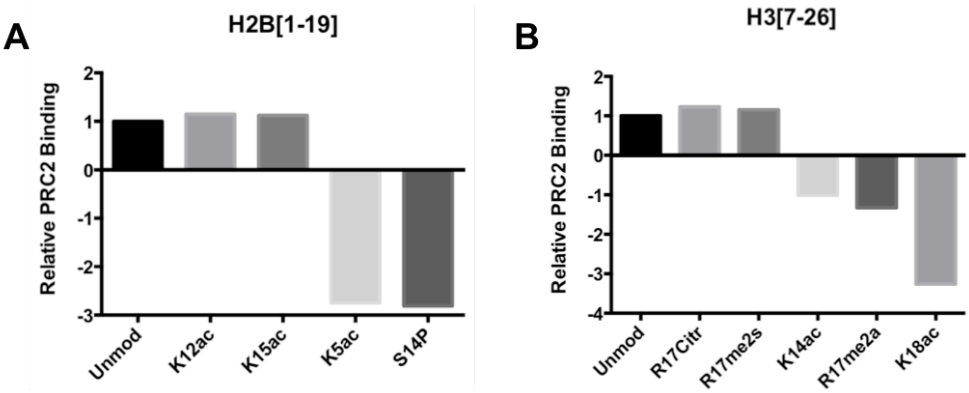

Figure S7.1 PRC2 binding data for H2B[1-19] and H3[7-26] peptides harboring various modifications
Relative chemiluminescence signal from various (A) H2B[1-19]-derived and (B) H3[7-26]-derived modified peptides spots. Data are normalized to H3[16-35] signal, with ratios <1 transformed [=1-1/(mod./unmod.)] and represent ratios derived from the mean signal from duplicate arrays.

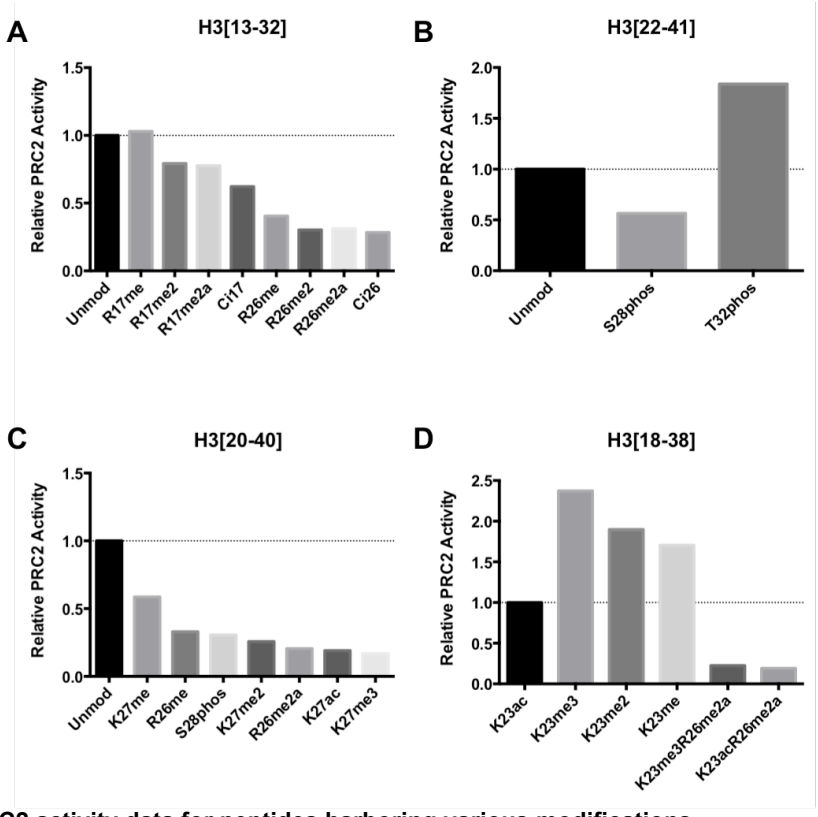

Figure S7.2 PRC2 activity data for peptides harboring various modifications
Relative PRC2 activity on various (A) H3[13-32]-, (B) H3[22-41]-, (C) H3[20-40]-, and (D) H3[13-32]-derived modified peptides. Data are normalized to respective unmodified peptides and represent ratios derived from the means of four replicate measurements